THE EFFECT OF MANUFACTURING VARIABLES ON SHORT FATIGUE CRACK GROWTH IN WASPALOY

BY

JORGE SALOMÃO BOABAID

A Dissertation Submitted to the University of Sheffield for the Degree of Doctor of Philosophy in the Faculty of Engineering

Department of Mechanical and Process Engineering
University of Sheffield

September 1994

Preface

This dissertation is based on the work and findings of research carried out in the Department of Mechanichal and Process Engineering of the University of Sheffield.

The content of this thesis is original, except where specific reference is made to other works. The research reported in this thesis has not been submitted to any other University for a degree.

J.S. Boabaid

September, 1994

Acknowledgements

I wish to thank the Head of the Departament of Mechanical and Process Engineering, University of Sheffield, for the provision of laboratory and departmental facilities; CAPES, Ministry of Education, Brazilian Government, for the financial support given during this project through a PhD Research Studentship; Rolls-Royce plc, Derby, for financial support and supply of material for the experiments; and EMBRACO, Empresa Brasileira de Compressores S.A., Joinville, Brazil, for giving me a period of leave to carry out this study.

I am extremely grateful to my supervisor Dr. J.R. Yates for his help, guidance and continuous encouragement during this project. Special thanks are due to the research and academic staff of the department, in particular to Prof. K.J. Miller, Dr. E.R. de los Rios and Dr. M.W. Brown for their assistance, advice and many helpful discussions throughout this project. Discussions with Dr. L. Grabowski, Rolls-Royce plc, Derby, are also gratefully acknowledged as well as his assistance with residual stress measurements.

I would also like to express my gratitude to all technical staff of SIRIUS for their time and assistance during my experimental work.

Last but not least the encouragement and considerable support, both moral and practical, of my parents and my wife for her patience and care throughout my stay in Sheffield.

Contents

Summary

The importance of short fatigue crack growth has been emphasized in a number of recent experimental works. Most have been concerned with the natural initiation of cracks from smooth surfaces, such as those produced by mechanical and electrolytical polishing, their early propagation and interaction with the material microstructure.

It is, however, recognized that manufacturing operations, such as those involved in the production and finishing of engineering components, can have a strong effect on short fatigue crack growth. In many cases fatigue crack growth data generated by testing smooth surface laboratory specimens may not be directly applied to predict short crack growth in the surface of real components.

In the present work the effect of manufacturing operations on short fatigue crack growth has been studied on a nickel base superalloy, Waspaloy, at room temperature, using four-point-bend square section beam specimens.

Surface preparation procedures were systematically varied in order to obtain different grades of surface finish which ranged from polished (electropolished) to ground finish. Constant amplitude load controlled fatigue tests were performed using material in two different treatment conditions. Fatigue crack growth was monitored by a plastic replication technique, and surface crack measurements were performed by means of a computer image analysis system.

Short fatigue crack growth was observed to be not only of intermittent nature but also to follow two distinct patterns of behaviour which appear to be related to the surface condition produced by the finishing operations.

It was also observed that short crack growth behaviour in ground surfaces cannot be related with any conventional surface texture parameters, e.g. R_a or R_v, since crack growth in the early stages is affected not only by the depth of manufacturing defects, such as grinding marks, but also by their length and orientation. Moreover, residual stress patterns induced by grinding operations were also observed to play an important role in the early stages of fatigue crack

growth in engineering surfaces.

Based on the experimental observations and theoretical analyses carried out in the present study, an attempt was made to quantify the contribution of three inherent parameters, namely material microstructure, surface topography and residual stresses, at the early stages of fatigue crack growth in a mechanically prepared surface.

Nomenclature

a	half surface crack length
a_0	initial crack length
a_{mean}	mean crack length
a_f	crack length at failure
a_{th}	threshold crack length
a_{tr}	transition crack length
b	crack depth
C	material constant
C_1	short crack parameter
C_2, C_2'	long crack constants
d	distance between the crack initiation site and a microstructural barrier
da/dN	crack growth rate
D	distance between crack initiation sites
E	Young's modulus
$EPFM$	elastic plastic fracture mechanics
F	applied load
G	shear modulus
K	linear elastic stress intensity factor
K_I, K_{II}, K_{III}	stress intensity factors in mode I, mode II and mode III crack tip deformation
K_c	fracture toughness
K_{max}, K_{min}	maximum and minimum values of applied stress intensity factor
l	critical length below which LEFM cannot be applied
$LEFM$	linear elastic fracture mechanics
L_a	average length of grinding marks
M	bending moment

n	material constant; sample size
n_i	number of crack initiation sites
N_f	mean lifetime to failure
N_l	number of cycles spent in stage II crack growth
N_{mean}	mean number of cycles required for the observed cracks to reach a given length
N_{model}	predicted number of cycles for a given crack length
N_{+1sd}, N_{-1sd}	mean number of cycles plus or minus one standard deviation required for the observed cracks to reach a given length
N_s	number of cycles spent in stage I crack growth
r	distance ahead of crack tip
r_p	plastic zone size
R	applied stress or load ratio
R_a	arithmetic mean of the departures of the roughness profile from the mean line
R_p	maximum height of the profile above the mean line within the assessment length
R_v	maximum depth of the profile below the mean line within the assessment length
R_y	maximum peak-to-valley height of the profile within the assessment length
R_zDIN	mean value of the maximum peak-to-valley heights obtained within the assessment length
t	Specimen thickness; Student's t statistics
Y	geometry factor
$\triangle\epsilon_e$	applied elastic strain range
$\triangle K$	applied range of stress intensity factor
$\triangle K_{eff}$	effective value of stress intensity range
$\triangle K_{th}$	threshold value of stress intensity range
$\triangle\sigma$	applied stress range

σ	applied stress; standard deviation
σ_{cy}	cyclic yield stress
σ_r	surface residual stress
σ_{th}	plain specimen fatigue limit
σ_y	yield strength of the material
ν	Poisson's modulus

Chapter 1

Introduction

It is widely recognized that manufacturing operations have a strong effect on the fatigue performance of aeroengine components and that variations in manufacturing procedures can give rise to a wide range of fatigue crack growth behaviour. Since fatigue crack initiation usually occurs at the free surface of a component, the condition of the surface can be considered to be critical with regard to the initiation of a crack and its subsequent propagation to failure.

Machine grinding ranks amongst the most widely used metal finishing processes in the aerospace industry. Fatigue strength and precision are common requirements for satisfactory performance of critical aeroengine components.

From the fatigue point of view low stress grinding (fine grinding) procedures are usually preferred to high stress grinding (conventional or abusive grinding) procedures, since the latter produce more surface alterations e.g. rehardening, overtempering or softening and generate poorer surface finishes.

Surface roughness has long been a prime criterion to define the quality of a ground surface and is an accepted guide to the fatigue performance of highly stressed components. The influence of the surface roughness on high cycle fatigue performance has been addressed by a number of workers, e.g. references [1][2][3][4][5], who recognized the beneficial effect of low surface roughness, which is obtained as a general rule through low stress grinding procedures. In spite of the extensive number of works on the role of the surface finish in fatigue a quantitative description of the short crack behaviour in mechanically prepared

surfaces has not yet been provided.

Moreover, there is some evidence [2][6][7][8] that in some instances the surface roughness is not a critical criterion in the control of fatigue crack growth in ground surfaces, and that conventional grinding procedures, in spite of producing poorer surface finishes, can give rise to a better fatigue response when compared with fine grinding operations in a number of structural materials.

The beneficial effect of conventional grinding procedures on the fatigue performance of such materials appears to be related with the nature of the residual stresses developed by the machining or grinding process. During the grinding operation, residual surface stresses are induced. Variations in the grinding conditions of the surface can produce a wide range of residual stress patterns, which strongly affect the fatigue response of the ground surface.

The purpose of this work is to provide an improved understanding of the role of the defects introduced in the surface of an engineering component by common manufacturing procedures such as machine grinding. In particular, it is intended to be able to offer a quantitative description of the contribution of the three inherent parameters affecting fatigue crack initiation in a mechanically prepared surface, namely material microstructure, surface topography and residual stresses.

Results obtained in this research refer to a nickel-base superalloy, Waspaloy, which is used in aeroengine turbine discs. A literature review on fatigue is presented in chapter 2 of this thesis. Details on the experimental work, material, specimens and testing programme are presented in chapter 3. Results obtained from this study are presented in chapter 4, analysed in chapter 5 and discussed in chapter 6. Conclusions drawn from this study as well as suggestions for future research in this area are presented in chapter 7.

Chapter 2

Literature Survey

2.1 Introduction

Fatigue is the progressive fracture of a material by the growth of cracks under cyclically varying stresses. Metal fatigue is known to be the primary cause of a wide range of failures in structures and components. It is often stated [9] that fatigue failures account for more than ninety percent of all mechanical failures in industrial plants and machinery.

Research into fatigue was long concerned with the production of S-N curves [10], as well as with a great deal of experimental data about the effect of surface finish, mean stresses, notches, etc., for a range of engineering materials.

Extensive development in the field of fatigue was made during the fifties, mainly through the use of new research tools, such as electron microscopy, which was applied for the first time in fractography studies to observe fatigue striations in fracture surfaces [11]. The introduction of the concept of *Stress Intensity Factor* [12] and the development of the theory of *Linear Elastic Fracture Mechanics* in the following decades gave a further boost to the research of metal fatigue and still provide to date a more rigorous framework for the analysis of fatigue crack growth.

In spite of its extensive use in a wide range of fatigue crack growth problems it is now widely recognized [13][14][15][16][17][18] that the use of linear elastic fracture mechanics methods can present serious limitations in many fatigue de-

sign situations, particularly when the size of initial defects present in the material become as small as the scale of the material microstructure, as occurs in most highly stressed components, e.g. turbine discs. The short crack growth problem has been extensively addressed in the recent years with many important contributions, some of them will be reviewed in this literature survey.

2.2 Fatigue Crack Growth Mechanisms

Fatigue failure occurs as a result of the initiation and propagation of one or more cracks across the cross-section of the part until its remaining ligament is unable to support an additional cycle of load. The fatigue fracture process is generally considered (see e.g. reference [16]) to involve the following phenomena:

- Initial cyclic damage in the form of cyclic hardening or softening
- Nucleation of initial microscopic flaws (microcrack initiation)
- Coalescence of these microcracks to form an initial 'fatal' flaw (microcrack growth)
- Subsequent macroscopic propagation of this flaw (macrocrack growth)
- Final catastrophic failure or instability.

The first three stages involving cyclic deformation, microcrack initiation and growth are usually referred together as crack initiation or crack nucleation period (see e.g. reference [16][19]), implying the formation of an 'engineering size' detectable crack (e.g. having a length corresponding to several grain diameters), and the fourth stage is referred to as crack propagation period.

It is clear that the definition of an 'engineering size' detectable crack has continuously changed over the time [20], since it has always been subjected to the increasing ability of engineers to locate and monitor very small cracks. As a result of this increasing ability the arbitrary division between crack initiation and crack propagation periods has been forced back further and further in time towards the origin of the fatigue damage process.

In support of a more rational division which could bear some physical meaning Forsyth [21] argued that, if we accept that the common mode of crack formation is by the deepening of a slip band groove by an atomic process of dislocation movement, then the continued use of this division presents certain difficulties, and leads to the absurdity of trying to specify a minimum crack size in a process starting on an atomic scale. Based on this argument and on extensive fractographic evidence for the early initiation of fatigue cracks in aluminium alloys, Forsyth [21] defined fatigue fracture as a two-stage crack growth process, showing that rather than being an arbitrary division the change from Stage I to Stage II mechanisms is a natural division in behaviour.

Evidence of fatigue as a two-stage crack growth process continues to accumulate in recent years and is becoming increasingly accepted by scientists and engineers.

It must be noted that although the term crack initiation has been used extensively in this work, as it has been in the literature, it is understood that the demarkation between the initiation and propagation phases is totally arbitrary and does not have any physical basis. In order to avoid such an arbitrary demarkation in the present work the number of cycles to initiate a crack was considered to be zero in all fatigue lifetime calculations. However, the mechanisms of fatigue crack initiation and growth will be described in the following sections.

2.2.1 Crack Initiation

A large number of experimental observations have shown that fatigue cracks start predominantly at the free surface of a metal. The main reasons why this happens are:

- Surface grains are the only ones which are not completely surrounded by neighbouring grains, making it easier for them to deform plastically at a lower stress.
- The surface of a metal is a natural site of manufacturing defects, e.g. machining marks, burrs and scratches, as well as notch-like discontinuities, which can be both particularly effective as stress raising features.

- The metal surface can also be subjected to a range of corrosive and environmental action giving rise, for example, to corrosion fatigue.

In the absence of stress raising effects, such as in the smooth surface of a laboratory specimen, crack initiation can be considered to involve a sequence of events which start with localized plastic deformation [22] along planes of maximum shear stress. Because of the absence of constraint, dislocation substructures can be more easily activated in surface grains. Extension of these substructures out of the free surface of the metal will produce microscopic changes, which are known as slip bands. Although the development of slip bands can be observed within many surface grains, in some of them they will become particularly prominent. These are termed persistent slip bands (PSB), (after Thomson, Wadsworth and Louat [23]). As cycling continues (persistent) slip bands will become more accentuated giving rise to extrusions and intrusions [24]. It is from the deepening of the intrusions that cracks will eventually form.

The definition of when a slip band or an intrusion becomes a crack is still object of much discussion among scientists with no satisfactory answer up to date. The question is considered to be purely an academic one and it appears to have no practical implications in terms of engineering design.

The process of slip band formation was investigated by a number of workers, see e.g. references [23][24][25]. A simple model for the formation of intrusions and extrusions was proposed by Cottrell and Hull [25], who suggested that the formation of an intrusion-extrusion pair is the consequence of the operation of two dislocation sources acting in two neighbouring slip planes.

Extensive evidence of slip band cracking has been provided over the last twenty years by many studies of fatigue crack growth in nickel base superalloys, see e.g. [26][27][28][29]. In most of these works crack initiation was observed to occur predominantly along (persistent) slip bands, although initiation from twin boundaries, carbides, voids and inclusions have also been reported.

Exceptions to the rule of slip band cracking are fairly well understood and can be attributed to subsidiary effects, some of them are described as follows:

In some metals, see e.g. reference [30], grain boundaries can be weaker than the grains themselves due to segregation of second phase particles to boundary regions, making them more prone to crack initiation. Nucleation at grain boundaries is also observed to occur due to environmental effects and in high strain fatigue, especially at higher temperatures [31]. It was observed by Shaikh [32] that as temperature increases into the creep range grain boundaries become the dominant weak paths and the prime initiation sites in the material change from transgranular to intergranular initiation.

Evidence of crack initiation from inclusions has also been provided by a number of workers [14][33][34][35], who observed three distinct sites of nucleation, namely, cracking of the matrix close to the inclusion, cracking of the inclusion itself, and debonding of the inclusion/matrix interface. However, this type of nucleation is known to occur only in some commercial alloys containing large enough particles [31].

2.2.2 Stage I Crack Growth

This stage was considered by Forsyth [21] as an extension of the crack initiation process involving the deepening of a slip band or intrusion. Because Stage I cracking is a shear stress dependent process Stage I cracks grow by a predominantly Mode II mechanism [36]. During this process a growing crack can extend crystallographically across many grains deviating from its fracture path as it crosses grain boundaries. This mechanism of growth proceeds until the slip band crack changes from a plane of maximum shear stress and start to propagate along a plane perpendicular to the maximum tensile stress (see figure 2.1). This transition from a crystallographic growth to a non-crystallographic growth is often called Stage I - Stage II transition and is supposed to occur as a result of the decrease in the ratio of shear stress to tensile stress with depth in the specimen. The changeover to Stage II growth is not necessarily sudden. It can occur gradually as the crack extends over a number of grains. The crack length at which the Stage I to Stage II transition occurs seldom exceeds the length of a few grains, although in some nickel base superalloys the transition can take place

for much longer cracks (of the order of millimeters) [31].

The fractions of fatigue lifetime spent in Stage I and Stage II will vary with the applied stress or strain range. In high strain (low cycle) fatigue Stage II crack growth dominates whilst in low stress (high cycle) fatigue Stage I crack growth can take a significant (if not the largest) proportion of the fatigue lifetime of the specimen or component.

2.2.3 Stage II Crack Growth

The criterion for Stage II crack growth is the value of the maximum principal tensile stress operating in the specimen or component in the region of the crack tip. During Stage II the crack grows under Mode I opening conditions in a direction normal to the maximum principal tensile stress (see figure 2.1). Unlike Stage I, the crack path in Stage II is not much affected by local variations in the microstructure and crack extension appears to be controlled by the continuum response of the material.

This mechanism of crack growth is often characterized by the appearance of striations, which can be observed on fracture surfaces of ductile metals. The effect of striation was studied by a number of workers [21][37][38]. Forsyth [21] observed that the spacing of striations represents the advance of the crack front during a stress cycle. Although there is some dispute as to the precise mechanism of striation formation it is generally accepted that it involves successive blunting and resharpening operations at the crack tip. Striation mechanisms were proposed by Laird and Smith [37] and by McMillan and Pelloux [38].

Examination of striations in fracture surfaces can provide valuable information on Stage II crack growth. However, the attempt to quantify crack growth rates from direct measurements and countings of striations can be misleading [36][39].

2.2.4 Stage III Crack Growth

This is the final stage of the fatigue fracture process leading to the failure of the specimen or component. Stage III can be considered as an approach to

unstable fracture due to the increasing length of the growing crack and involves a combination of the Stage II Mode I opening with a process of microvoid formation (see figures 2.1).

Stage III crack growth is always a rapid process taking only a small fraction of the total lifetime of the component. It is therefore of limited interest in terms of fatigue design.

2.3 Fracture Mechanics Characterization of Fatigue Crack Growth

The introduction of a crack-like defect in a structure or component causes a redistribution of stress with the highest stresses developing around the tip of the crack. The crack behaviour, including the growth rate and the conditions for non-propagation of the crack, can only be quantified provided an adequate parameter is known to describe the local stress and strain field at the crack tip.

Exact calculation of the crack tip stress and strain fields is only possible for the elastic case, which occurs for example in engineering structures. Because most large structures contain initial crack-like defects (e.g. in weldments), which can be at least several milimeters long, applied stress amplitudes must be well below the cyclic yield stress of the material. A fracture mechanics description of these 'long cracks' can be made by using the traditional approach of Linear Elastic Fracture Mechanics (LEFM). As a practical consequence crack growth results obtained from laboratory specimens can be used to predict crack growth in engineering structures, provided the local crack tip stress and strain fields are the same in both cases.

Linear Elastic Fracture Mechanics can be successfully applied to a number of 'long crack' problems and still represents the major tool in fatigue design of engineering structures. However, application of LEFM concepts to 'small crack' problems has been shown to fail [10][16].

Because most engineering components are subject to much higher stress levels, which approach in some cases (e.g. in turbine discs) the cyclic yield stress of

the material, initial crack-like defects can only be tolerated as long as they do not exceed much smaller sizes, typically in the range of the material microstructure. A number of studies (see e.g. [13][14][40][41]) have shown that these 'short cracks' grow much faster than the LEFM equivalent long ones, experiencing also transient retardation and sometimes permanent arrest. This anomalous behaviour suggests that the similitude concept generally accepted for the LEFM characterization of 'long cracks' is not fully obeyed by 'short' fatigue cracks. The fracture mechanics procedures used to describe the growth of 'short' and 'long cracks' will be reviewed in the following subsections.

2.3.1 Linear Elastic Fracture Mechanics

The extension of a crack in an elastic body is a local crack tip phenomenon caused by the cyclic stress and strain which develops in the vicinity of the crack tip. Crack extension can occur by one of the following crack tip deformation modes [42][43], namely, Mode I (opening mode), Mode II (in-plane shear mode) and Mode III (anti-plane shear mode). These modes of crack tip deformation are illustrated in figure 2.2.

The nature of the stress and strain field near the tip of a crack was examined by Irwin [12] who observed that, for a number of cracked plate configurations, the magnitudes of the local stress components at any given distance from the crack tip are proportional to the term $\sigma\sqrt{\pi a}$, which is a simple function of the remote applied stress σ and the half crack length a. The term $\sigma\sqrt{\pi a}$ was defined by Irwin [12] as the *Stress Intensity Factor.*

In order to extend the applicability of Irwin's concept to the most general case, the stress intensity factor can be expressed as:

$$K = Y\sigma\sqrt{\pi a} \tag{2.1}$$

where Y is a dimensionless geometry factor which depends on the shape of the body containing the crack, the crack geometry and the type of loading to which it is subjected. Actual values of Y for most usual engineering structures can be found in a number of handbooks, see e.g. references [44][45][46]. The importance of K parameter lies in the fact that it enables local conditions in the vicinity of

the crack tip to be fully described in terms of easily measured quantities remote from the complicated crack tip area [47].

Stress intensity factors K_I, K_{II} and K_{III}, can be defined for each mode of crack tip deformation. The crack tip stresses (see figure 2.3), for example in Mode I, can be expressed by:

$$\sigma_x = \frac{K_I}{\sqrt{2\pi r}} cos\left(\frac{\theta}{2}\right)\left[1 - sin\left(\frac{\theta}{2}\right) sin\left(\frac{3\theta}{2}\right)\right] \tag{2.2}$$

$$\sigma_y = \frac{K_I}{\sqrt{2\pi r}} cos\left(\frac{\theta}{2}\right)\left[1 + sin\left(\frac{\theta}{2}\right) sin\left(\frac{3\theta}{2}\right)\right] \tag{2.3}$$

$$\tau_{xy} = \frac{K_I}{\sqrt{2\pi r}} sin\left(\frac{\theta}{2}\right) cos\left(\frac{\theta}{2}\right) cos\left(\frac{3\theta}{2}\right) \tag{2.4}$$

and for plane strain

$$\sigma_z = \nu(\sigma_x + \sigma_y) \tag{2.5}$$

where K_I is the Mode I stress intensity factor, r is the distance ahead of the crack tip, θ is the polar angle measured from the crack plane (see e.g. reference [48]).

One of the limitations underlying the LEFM approach is that a state of small scale yielding must exist in order to use K_I as a valid parameter to describe the crack tip stress field. From equations (2.2), (2.3) and (2.4) it is apparent that, as the tip of the crack is approached ($r = 0$), the local stress components tend to infinity. In a real component such stresses are limited by the yield strength of the material. Local yielding takes place over a distance ahead of the crack tip known as the plastic zone. The approximate size r_p of this plastic zone for a monotonically loaded crack in state of plane stress is given by:

$$r_p = \frac{1}{2\pi}\left(\frac{K_I}{\sigma_y}\right)^2 \tag{2.6}$$

where σ_y is the yield strength of the material. Provided the extent of the plastic zone is much smaller compared to the extent of the K_I-field, which is itself small compared to the overall dimensions of the cracked body (including the crack length), the plastic zone can be considered as a small perturbation in the linear elastic stress field, and the K_I-field can be assumed to control the region surrounding the crack tip. This situation, known as small scale yielding, occurs only

when the size of the plastic zone is at most one-fiftieth of the in-plane dimensions of the crack length and the depth of remaining ligament (see references [47][49]).

Paris and Erdogan [50] reasoned that because the stress intensity factor K fully characterizes the stress field around the crack tip, the range in stress intensity $\triangle K$ should also control the rate of fatigue crack growth. Based on this argument they suggested that fatigue crack growth rate could be correlated by a power law relationship, known as *Paris' law*:

$$\frac{da}{dN} = C(\triangle K)^n \tag{2.7}$$

where C and n are material constants and $\triangle K$ is the difference between the maximum and minimum values of the stress intensity factor during a fatigue cycle, as in the expression below:

$$\triangle K = K_{max} - K_{min} \tag{2.8}$$

Although this basic assumption has been confirmed by a large amount of experimental data, it is clear that Paris' equation does not fully describe the relationship between da/dN and $\triangle K$ for the whole range of crack growth rates [39][51][52], being valid only for the middle linear portion of the *log* da/dN versus *log* $\triangle K$ plot (see e.g. figure 2.4 from reference [53]). This intermediate linear portion is also referred to as the 'long crack' growth regime. It was in fact observed by a number of workers, e.g. [39][51] that the variation of da/dN with $\triangle K$ tends to be sigmoidal rather than linear.

Over the intermediate region of $\triangle K$, (region 2 in figure 2.4), where Paris relationship is valid, fatigue crack growth is known to be controlled by the continuum response of the material (see section 2.2.3). Effects of microstructure, mean stress and environment on crack growth rate in this region were found to be small for most materials, see e.g. reference [54].

At high values of $\triangle K$ (region 3 in figure 2.4), when the maximum value of stress intensity factor K_{max} approaches the fracture toughness K_c, crack growth rate deviates from the linear behaviour and tends to infinity [51]. In this region, fatigue crack growth was observed to be largely dependent on the microstructure and mean stress. However, as explained in section 2.2.3, this region is of little interest in terms of fatigue design.

Of more interest is the fatigue crack growth in region 1 of figure 2.4. Fatigue crack growth in this region is dominated by non-continuum mechanisms being strongly influenced by microstructural variations. It has been observed [14] that, under low ΔK values, cracks can experience transient retardation and sometimes permanent arrest. As ΔK value is progressively lowered crack growth rate is reduced until a threshold value ($\Delta K = \Delta K_{th}$) is reached below which no crack growth will take place. Effects of mean stress and environment are also stronger in this region. Due to the strong influence of microstructure fatigue crack growth in this region deviates considerably from the linear behaviour, and Paris law can no longer be expected to be a good model to describe fatigue crack growth.

2.3.2 Elastic Plastic Fracture Mechanics - Short Crack Growth Behaviour

One of the conditions for the use of ΔK as a valid correlation parameter to fatigue crack growth rate is that the plastic-zone size, r_p, ahead of the crack tip is small compared to the stress intensification field surrounding the crack tip. It has been shown (see e.g. reference [20]) that when these small scale yielding conditions are violated K is no longer sufficiently accurate to describe the crack tip stresses and LEFM can no longer be used to describe fatigue crack growth.

Fatigue crack growth situations in which LEFM small scale yielding conditions are violated have become an important field in fatigue crack growth studies, especially when fatigue design of engineering components is concerned. Moreover, because engineering components are often subject to much higher operating stresses, which can approach in some cases (e.g. in turbine discs) the cyclic yield stress of the material, initial crack-like defects can only be tolerated as long as they do not exceed the scale of the material microstructure. A number of studies (see e.g. [13][14][40][41]) have shown that most of these initial defects, known as 'short cracks', grow at projected ΔK levels below the long crack threshold ΔK_{th} and experience also higher growth rates when subjected to the same nominal driving force.

There are many ways of defining 'short cracks' and a number of definitions

have been proposed in the last ten years. Suresh and Ritchie [16], for example, defined short cracks as the following:

- Cracks having a length which is small compared to the scale of the microstructure (e.g. of the order of the grain size)
- Cracks which are of a length comparable to the scale of local plasticity (e.g. small cracks embedded in the plastic zone of a notch or of a length comparable with their own crack tip plastic zones, typically $\leq 0.01mm$ in ultrahigh strength materials and $\leq 0.1 - 1mm$ in low strength materials)
- Cracks which are simply physically small (e.g. $\leq 0.5 - 1mm$).

where the first definition represents a limitation in terms of continuum mechanics, while the second represents a limitation in terms of applicability of LEFM.

In a more recent review on short cracks Miller [55] defined three different regimes of short crack growth, which are described below with reference to figure 2.5:

- Microstructurally short cracks (MSC): In this regime crack lengths a are smaller than the dominant microstructural barrier, e.g. d_3. Continuum mechanics is not applicable in this regime and crack growth rates can only be characterized in terms of microstructural parameters like grain size, etc.. More generally these cracks can also be called Stage I Mode II cracks, since they grow on shear planes.
- Physically small cracks (PSC): In this regime crack lengths a are bigger than d_3 but smaller than a critical length l bellow which LEFM is no longer applicable. Crack growth behaviour in this regime can, however, be represented by a continuum mechanics approach as these cracks are not strongly affected by microstructural features, but because these cracks are still physically small and require high stress levels to grow, considerable macro-plasticity can be involved. Since their direction of growth is normal to the applied maximum principal stress these cracks are also designated as Stage II Mode I cracks.

- Highly stressed cracks: In this regime crack lengths a are bigger than the critical length l and experience an applied stress range greater than two thirds of the cyclic yield stress. These cracks are typical only of high strain fatigue, and can also be termed as highly stressed Stage II Mode I (EPFM type) cracks.

Due to the high stress levels required and macro-plasticity involved in both physically small (PSC) and highly stressed (EPFM) crack growth regimes, elastic-plastic fracture mechanics (EPFM) must be used to describe the behaviour of these short cracks, since erroneous use of ΔK can often result in overestimates of fatigue lifetimes.

Regarding the prediction of the extent of the short crack behaviour and the minimum crack length suitable for LEFM analysis, different approaches [41][56][57] have been used. Kitagawa and Takahashi [56], for example, studying the fatigue thresholds of steels, proposed a diagram in which the threshold stress range is related with the size of crack-like defects pre-existent in the specimen. They observed that for cracks longer than $500\mu m$ ΔK_{th} was constant, whereas for cracks shorter than $500\mu m$ the threshold stress range $\Delta\sigma_{th}$ was found to deviate gradually from the ΔK_{th} threshold straight line and assymptotically approach the plain specimen fatigue limit $\Delta\sigma_{th}$.

Kitagawa and Takahashi type plots are still a very convenient way to represent fatigue threshold results and have been widely used in a number of studies. One of such diagrams is reproduced from reference [20] in figure 2.6. It shows that LEFM can only be applied for crack lengths a bigger than the critical crack length a_1. Two important limiting lines are drawn to describe the fatigue crack behaviour. The line given by ΔK_{th} represents the threshold condition below which a crack should not grow if LEFM assumptions are valid. These assumptions are contravened if the applied stress range exceeds one-third of the cyclic yield stress σ_{cy}. The second line denotes the stress range corresponding to the plain specimen fatigue limit, which is sometimes approximately related to the cyclic yield stress of the material. Above this line cracks will initiate and grow to failure, while below this line Stage I cracks may initiate, but they do not propa-

gate beyond a depth a_2 corresponding to some microstructural barriers, such as grain boundaries.

Taylor and Knott [41], who also used a Kitagawa and Takahashi plot [56] to describe the extent of the microstructural influence in fatigue crack growth, have proposed a correlation between the critical crack length for short crack growth behaviour and the scale of microstructure. For a wide range of materials they found the following approximate correlation to be valid:

$$l_2 \approx 10d \tag{2.9}$$

where l_2 represents the crack length below which the use of the stress intensity approach becomes non-conservative, and d is a characteristic microstructural dimension, which is defined as the grain size for mild steels and aluminium bronze or the spacing of martensitic laths for quenched and tempered steels.

In a later work [58] the same author expressed the same limiting condition in terms of reversed plastic zone size, r_p. This condition can be approximated by:

$$l_2 \approx 10r_p \tag{2.10}$$

It must be observed that equations (2.9) and (2.10) represent two independent conditions on the value of l_2. The critical crack length, l_2, for any given material is therefore given by whichever is the larger of $10d$ and $10r_p$. Other values were quoted in the literature for the critical crack length at which LEFM can be applied. Smith [57], for example, indicated a value of $0.025mm$ as a minimum crack length suitable for a stress intensity approach. It appears, however, that this limiting value of $0.025mm$ is too small when compared to those proposed by Taylor and Knott [41][58]. It can, therefore, be concluded that this value is rather a lower bound crack size below which LEFM can never be used for short crack growth predictions.

In a more recent work by Brown [18] Kitagawa-Takahashi diagram was expanded and replotted as shown in figure 2.7. In this diagram the boundary conditions between short, long and non-propagating cracks are represented together with their operating crack tip deformation modes. By including the contours of constant crack growth rate for a particular material, in this case medium carbon

steel, he produced a fatigue fracture-mode map in which six different regimes of fatigue crack behaviour are identified in terms of stress level and crack length. The boundary conditions between each regime of crack growth can be moved considerably depending upon changes in material properties, such as yield stress, fracture ductility, microstructure, etc., but these six regimes remain in general being observed for any other materials.

2.4 The Metal Surface Condition - Effect of Surface Finishing Operations on Fatigue Crack Growth

It is widely recognized that manufacturing operations have a strong effect on the fatigue performance of engineering components and that variations in manufacturing procedures can give rise to a wide range of fatigue crack growth behaviour. Since fatigue crack initiation usually occurs at the free surface of a component, the condition of the surface can be considered to be critical with regard to the initiation of a crack and its subsequent propagation to failure.

The role of the manufacture and surface condition in fatigue limit has been given a lot of attention in the past, see e.g. references [6] [59]. More recently the influence of the surface condition on high cycle fatigue has been addressed in a number of studies, see e.g. references [1][2][3][4][5][7] using the conventional S-N curves and LEFM threshold (e.g. Kitagawa-Takahashi type) diagrams.

In spite of the extensive literature on this subject the role of the surface condition in fatigue crack growth is still not well understood. Fatigue crack growth in the surface of a real component is controlled by geometrical and metallurgical properties, whose inherent effects on fatigue crack growth cannot be satisfactorily separated. Moreover, it is apparent that most of the present studies on the effect of surface finish still ignore that any metal removal process will always introduce additional residual stresses, whose effects on fatigue crack growth will invariably interfere with those of the surface texture produced by the particular process. The role of the surface condition in fatigue is essentially a short crack growth

problem involving the interaction of inherent surface manufacturing defects (in the form of surface roughness) with a highly disturbed (residual stress) layer and the material microstructure.

The role of the surface condition in fatigue crack growth must be therefore resolved in three main effects, namely of surface topography, residual stress and microstructure. These three effects will be reviewed in the following subsections.

2.4.1 Material Microstructure

A number of experimental studies [14][26][28][29][41] on the initiation and growth of fatigue cracks in a wide range of materials have shown that short cracks, particularly those having a length comparable with the grain diameter, are strongly influenced by variations in the material microstructure. The initially higher growth rates of short cracks have been shown [14][29][41][60] to decelerate progressively (and even arrest in some cases) before merging with long crack data.

Evidence of grain or phase boundaries interacting with the growth of short cracks has been reported for a number of structural materials, including aluminium alloys [14][40], medium carbon steel [30][61], titanium alloy [62] and nickel-base superalloys [29][60]. In all cases retardation or arrest of cracks at the grain or phase boundaries was observed.

Lankford [14], for example, working on an aluminium alloy observed that short cracks were subject to growth rate perturbations and experienced retardation at a depth corresponding approximately to the grain size (15 to 20μm). Results obtained by Lankford [14] are shown in figure 2.8 and indicate that different growth rates can be observed for cracks growing in grains of different sizes (d_{g1} and d_{g2}). The minimum crack growth rate appears to correspond to a crack length roughly equal to the smallest grain size (i.e. $a \approx d_{g1}$).

De los Rios *et al.* [30][61], working on a medium carbon steel observed cracks propagating initially at a high growth rate while growing through ferrite grains, but slowing down as they approached microstructural obstructions, i.e. at pearlite/ferrite interfaces. Once the pearlite band was overcome, the crack continued to grow at an increasing growth rate.

Brown and Hicks [62] studying the short crack behaviour in the titanium alloy IMI685 observed that the amount of crack retardation and acceleration was a function of the difference in orientation between grains ahead of a growing crack. Similar orientation between the grain containing the crack and the neighbouring grain would cause little deceleration in growth rates at the boundary, whereas bad orientation would cause the crack to be slowed down or even arrest.

Navarro and de los Rios [63] suggested that the intermittent decelerating and accelerating behaviour of short crack growth is caused by the successive blocking of the plastic zone by slip barriers such as grain boundaries and subsequent initiation of localized slip in the adjacent grains. The interaction of cracks with grain boundaries was found to cease only when the plastic zone size is of the order of the average grain size at which point the short to long crack growth transition occurs.

It is apparent from the above references that microstructural aspects play an important role in the initiation and growth of short fatigue cracks and that microstructure effects must be incorporated into the analysis of fatigue crack growth of structural components.

Pertinent remarks were made by Miller [20][64] regarding the effect of grain size on the limiting conditions for crack growth. He pointed out that increasing the grain size can increase the LEFM threshold value ΔK, thereby increasing the fatigue limit for structures containing long cracks, presumably because more deformation can be accommodated prior to fracture. However, the reverse would apply to the fatigue limit of a plain specimen, *i.e.* an increasing grain size can lower the fatigue limit, presumably because short cracks can soon be retarded by grain boundaries. These effects are schematically illustrated in figures 2.9. From the above remarks it follows that the fatigue strength of a specimen or component can be improved by 'making' the grains on the surface smaller and the grains in the core larger [64].

On the other hand, Suresh and Ritchie [16] in their study on the propagation of short fatigue cracks have expressed the view that the interaction of short cracks with microstructural features, which leads to progressive crack retardation

below the long cracks threshold $\triangle K_{th}$, results mainly from crack deflection and associated crack closure.

Since the crack can not propagate while it is closed, the effect of closure is to reduce the nominal stress intensity range $\triangle K$ to some lower effective value $\triangle K_{eff}$ actually experienced at the crack tip, i.e. $\triangle K_{eff} = K_{max} - K_{cl}$, where K_{cl} is the stress intensity factor at closure ($\geq K_{min}$). Figure 2.10 illustrates the different mechanisms that can induce closure, e.g. cyclic plasticity, corrosion deposits and rough fracture surfaces.

The closure aspect of short crack behaviour is very much complicated by the difficulty in obtaining reliable measurements of this effect. However, closure arguments have often been used [65][66][67] to explain the anomalous behaviour of short cracks, although it is generally recognized that short cracks are likely to be less influenced by closure than long cracks.

Evidence that the extent of crack closure is smaller for short cracks was provided by James and Morris [67], in studying short crack growth in titanium alloys. By examining the effect of crack closure for cracks from 50 to $500\mu m$ they concluded that, for cracks smaller than approximately $160\mu m$ long, roughness induced crack closure decreased with decreasing crack length.

Similar conclusions were drawn by McCarver and Ritchie [65] regarding the influence of closure in short cracks. Studying the growth of long and physically small cracks in the nickel base alloy René 95, they observed differences in closure between long and short cracks. At lower stress ratios ($R = 0.1$), the $\triangle K_{th}$ for short cracks ($a \approx 0.1 - 0.2mm$) was 60% lower than that for longer cracks ($a \approx 25mm$) while at higher stress ratios ($R = 0.7$), where the closure effects are minimal, the $\triangle K_{th}$'s were virtually the same. The differences between long and short crack behavior were rationalised in terms of roughness induced closure. As crack closure can be caused by residual stresses in the crack wake it was proposed that a short crack will experience less closure as there is insufficient length behind the crack tip for the wake to develop fully.

2.4.2 Surface Topography

Surface roughness has long been used as a prime criterion to define the quality of an engineering surface and to some extent has been an accepted guide to the fatigue performance of highly stressed components. It is generally accepted that exceedingly smooth surfaces will provide the maximum in terms of fatigue strength for most structural materials.

A measure of the surface roughness introduced by a particular surface preparation procedure can be obtained by means of a stylus-type measuring instrument and is often expressed as the roughness average (R_a or CLA). For common manufacturing processes, such as polishing, grinding, milling and turning, the R_a value is usually in the range of $0.10\mu m$ for a highly polished or electropolished finish to $1.6\mu m$ for a coarse ground finish, and $0.80\mu m$ for a fine milled finish to $6.3\mu m$ for a coarse milled or coarse turned finish (see e.g. reference [8]). One of the main criticisms of the R_a parameter is that it cannot distinguish between profiles of different shapes. Figure 2.11, reproduced from reference [68], shows that surfaces having entirely different profiles can, in effect, have identical R_a values.

Other surface texture parameters are also used to characterize measurements of surface profiles, however, most of them do not describe adequately the physical character of the surface, but give only a measure of its amplitude.

It has been suggested [1][2][5] that the most significant parameter describing the quality of a machined surface from the fatigue point of view is the maximum depth of the surface irregularities which can be obtained from the surface profile scan. However, as mentioned before, it has not been generally appreciated that any metal removal process will always produce surface alterations, either to a larger or smaller extent, and introduce additional residual stresses, whose effects on fatigue crack growth will invariably interfere with the evaluation of surface roughness effects. It follows that a full understanding of the effect of surface roughness on fatigue crack growth can only be achieved providing that this effect is examined in isolation from residual stress effects on stress-free specimens [2]. However, this may not always be practical since stress relief treatments may produce changes in the metallurgical condition of the material.

The influence of the surface roughness on high cycle fatigue has been addressed in a number of studies, see e.g. references [1][2][3][4][5][7], some of them are reviewed below.

An experimental study of the influences of surface roughness and residual stress on the fatigue properties of ground EN31 steel was conducted by El-Helieby and Rowe [7], who performed reversed-bending fatigue tests on flat bar specimens in as-ground condition (no stress relief treatment took place after grinding). Surface grinding of the bending specimens was grouped into three classes which were labelled as abusive, conventional and gentle according to the individual grinding parameters (wheel types and speed, feed, dressing, and lubricant) used in this process. Fatigue life results obtained in this study (see S-N results in figure 2.12) have shown that variations in surface finish within the normal range of the grinding process have no consistent effect on fatigue behaviour.

Suhr [1] examined the effect of surface finish on the high cycle fatigue life of a low alloy steel. Fatigue life results were compared for a variety of ground finished and shallow grooved surfaces in which residual stress effects were eliminated by prior heat treatment. By examining the fracture surfaces of the fatigued specimens Suhr [1] observed that fatigue cracks initiated from some form of surface irregularity resulting either from the surface finishing process or inherent in the material, such as (a) grinding or emery marks transverse to the direction of loading, (b) particles of the grinding wheel becoming detached and either embedding or leaving sharp notches in the ground surface, (c) MnS inclusions inherent to the material, and (d) closed or partially closed pores. It was also observed in this study that an increase in the depth of the defect or surface roughness as indicated by a Talysurf scan is accompanied by a decrease in fatigue limit in both bending and push-pull fatigue.

Greenfield and Allen [2] compared the fatigue lives to failure of a low alloy engineering steel (EN19) for different grades of surface finish, namely fine ground, coarse ground, $0.05mm$ and $0.5mm$ grooved. They found in their study that although surface roughness has a marked effect on the fatigue life of the material tested there is no significant difference in fatigue strength between the fine and

coarse ground specimens. From their results, which are shown in the form of S-N curves in figure 2.13, it can be observed that the fatigue strength for coarse ground specimens is actually slightly higher than the fine ground specimens. This might suggest that higher magnitude residual compressive stresses, such as those measured in the coarse ground specimens, may have played some role in high cycle fatigue strength, especially by counteracting the detrimental effects of the rougher surface finish produced by coarse grinding.

Recent work by Taylor and Clancy [5] on the fatigue performance of the alloy steel EN19 compared the fatigue limits for polished, ground, milled and shaped surfaces using three-point-bend specimens in stress relieved condition. S-N results obtained in this study show that surface roughness is clearly effective in reducing fatigue life in this material, and that even relatively low roughness produced by moderate grinding and milling operations is significant. Based on these results they showed that for relatively low roughness values, such as those obtained through normal grinding and milling operations, data can be described in terms of Kitagawa-Takahashi diagram in which the crack length axis is replaced by the maximum amplitude of the surface profile scan (R_{max}), whereas for higher roughness levels, fracture mechanics predictions become too conservative, and a notch-based approach which allows for notch size effects is required.

It is apparent from the above studies that surface roughness is not always the critical criterion in the control of fatigue crack growth in engineering surfaces (see e.g. references [2][7][8]) and that variations in surface roughness within the normal range of grinding processes only have a consistent effect on fatigue properties in cases where the material is subjected to a stress relief treatment after the surface grinding operation (see e.g. references [1][5]).

2.4.3 Residual Stresses

The effect of residual stresses on the fatigue performance of a structure or component can be often more important than is usually realized (see e.g. reference [69]). Locked-in stresses are set up by common manufacturing operations, such as casting, welding, machining, heat treating, etc., and are known to be the

predominant factor contributing to a number of fatigue failures. Most of the processes that induce residual stresses also harden the surface, however it is difficult to determine their separate effects on fatigue strength. Virtually all manufacturing processes introduce residual stresses. These can result from a combination of mechanical and thermal effects, or from surface diffusion treatments such as carburising and nitriding. Whatever the nature of the residual stresses introduced in the surface of a metal, their effect on the fatigue properties are the same as if mean stresses of the same magnitude were superimposed on the cyclic operating stresses. Figure 2.14, reproduced from reference [70], shows that the resultant stress at any depth will be equal to the algebraic sum of the residual stress and the stress due to the applied load at that depth.

The effect of residual stresses may be either beneficial or detrimental, see e.g. figure 2.15 [69], depending upon the following factors:

- Residual stress magnitude, sign and direction with respect to the operating stresses
- In-depth distribution of the residual stresses
- Stability of the residual stresses with respect to time and temperature during cyclic stressing

Some surface treatment processes, e.g. mechanical polishing, skin rolling, shot peening and flame hardening, are known to induce compressive residual stresses, which are regarded as beneficial to fatigue strength. Skin rolling and shot peening are considered [39] as particularly effective treatments to eliminate the stress-raising effects of machining and grinding marks whilst setting up a compressive residual stress layer which considerably improves the fatigue properties of various components.

Comprehensive reviews of the effect of residual stresses introduced by different surface treatments have been made by Almen and Black [71], and Frost *et al.* [48].

Residual stresses are also introduced into the surface by metal removal processes such as machining and grinding, however the nature of these internal

stresses will largely depend upon the material and machining procedures employed. It has been generally observed (see e.g. references [2][7]) that when metal removal rates are low and efficient cooling is used, compressive residual stresses are usually induced, whereas with high metal removal rates such as those obtained by dry turning with carbide tools or coarse dry grinding, a state of tensile residual stresses may result in the metal surface.

The role of residual stress and work hardening produced on alloy steels by machining operations was studied by Hyler [6], who observed that rough machining can set up high residual surface stresses to an appreciable depth, whereas efficient metal removal by fine machining produces very little work hardening and a very shallow residual stress layer. It has been shown in his study that, despite the detrimental effects of a rougher surface, the former condition may still produce better results in terms of fatigue. Hyler [6] argues that it may be preferable to stop growing cracks by introducing sub-surface compressive stresses rather than to retard the initiation of the crack by machining a smooth surface.

The same study [6] has shown that a combination of deep surface deformation by rough machining or shot peening followed by mechanical polishing gives the best in terms of fatigue endurance. Fatigue endurance results obtained in this study are compared in figure 2.16 by means of S-N curves for 'as heat treated', polished, shot-peened, and shot-peened and polished conditions.

It has been found that residual tensile stresses induced by severe grinding operations can approach the ultimate tensile strength of the material itself. Koster [72], by studying the effect of peak residual stress on fatigue strength of ground parts observed that as the peak residual stress shifts from compression to increasing tension, the fatigue strength is dramatically reduced. Results of this study is shown in figure 2.17 for a ground steel AISI 4340 (RC50).

It has long become clear that residual stresses can exist as both macrostresses and microstresses (see e.g. references [69][73][74]). Macrostresses are caused by differential deformation of one region of the material with respect to another. They are usually balanced over macroscopic portions of the unit and vary on a scale that is large compared with the material microstructure. In contrast,

microstresses are the result of structural heterogeneities, e.g., the hard and soft constituent in a two-phase alloy. They vary on the scale of the material microstructure and must balance between the phases. Microstresses have not often been measured and their effect on fatigue is still not clear. Forsyth [73] observed that local peak microstresses may play an important role in the early stages of crack formation and growth. However, it is likely that macrostresses have an overriding influence on fatigue behaviour, since any previous local deformation would thoroughly relax the microstresses in the vicinity of the crack initiation site.

The distinction between macrostresses and microstresses is important especially when considering the method of measuring residual stresses. Residual stresses can be obtained using X-ray diffraction techniques [69][71], which consists in measuring the changes in lattice spacing in different directions in the specimen. These techniques permit the measurement of the total stress in each phase of a material, which is the sum of the macrostress and microstress tensors.

Recent work [74] on low cycle fatigue of steel showed that residual stresses initially present in the surface of a component as a result, for example, of shot peening fade under the application of cyclic stresses. It is known that this effect of stress relaxation will be stronger in a soft material; on the other hand, the process of cyclic deformation is likely to produce a deeper work-hardened layer in a soft material than in a hard one. This suggests that surface hardening may be the dominant beneficial effect in soft materials whereas the induced residual stresses may have a dominant effect in hard ones.

2.5 Short Fatigue Crack Growth Models

A typical fatigue diagram used to represent short crack growth behaviour is illustrated in figure 2.18 [18]. Crack growth rates for different levels of applied stress (or strain) are shown in this plot to be strongly dependent on the microstructural barrier d, which is shown to correspond to a nominal value of $100\mu m$ for this specific material.

Although this 'microstructural effect' on short cracks has been recognized for

many years (see e.g. references [13][14])[40][41]), attempts to model it have only been made more recently. Short fatigue crack growth in most of these models is described on the basis of either grain boundary blocking or crack closure, or a combination of these two effects.

By examining the published literature in this field it can be noted that most of the models presented over the last fifteen years incorporate some type of continuum mechanics parameter, such as ΔK or ΔK_{eff}, to describe microstructurally short crack growth (see e.g. [75][76][77]). Since crack growth in the microstructural region is dominated by non-continuum mechanisms, application of continuum mechanics to Stage I crack growth appears to be questionable. Therefore, most of these models cannot be used in fatigue lifetime predictions, and therefore are limited in terms of fatigue design.

This review will concentrate on the category of models which incorporate microstructural effects into the analysis of fatigue crack growth. Moreover, more attention will be given to those models which are also able to give lifetime predictions.

A number of such models have been developed over the last ten years (see e.g. [30][61][63][78] based on the blocking effect of the plastic zone by microstructural barriers, such as grain boundaries.

De los Rios *et al.* [30], for example, presented a model to describe short crack growth in a medium carbon steel subject to high cycle torsional fatigue. Crack growth rate in this model is given by the following expression:

$$\frac{da}{dN} = f_s \frac{\tau_s (L_s - a)}{G} \tag{2.11}$$

where L_s is the length of the slip band formed, G is the shear modulus and f_s is the fraction of dislocations on the slip band taking part in the crack growth process. The shear stress τ_s acting on a slip band of length L_s was given by the following expression:

$$\tau_s = \frac{G n_s b}{L_s} \tag{2.12}$$

where n_s is the number of dislocations in the slip band and b is the Burger's vector.

This model gives an initial high growth rate for large L_s which then decreases to zero as the crack grows. Although the model was successful in predicting the crack growth rates for individual cracks fatigue lifetime predictions had to rely upon statistical methods.

Hobson *et al.* [78][79] developed a model to describe the growth of Stage I and Stage II cracks using two different equations. The equation for Stage I crack growth is microstructurally dependent and is expressed as:

$$\frac{da}{dN} = C_1(d - a_s) \tag{2.13}$$

where C_1 is a constant which depends upon the applied stress/strain, d is the length of some dominant microstructural barrier like grain size, and a_s is the surface crack length. This equation predicts a decreasing growth rate with increasing crack length, with crack growth rate eventually becoming zero when $a_s = d$. Stage II crack growth is assumed to be a continuum mechanics dependent process with growth rate in this regime being expressed as:

$$\frac{da}{dN} = Ga_s - D \tag{2.14}$$

where G is also a constant which depends upon the applied stress/strain and D is a threshold constant. This equation predicts increasing crack growth rate with increasing crack length, a_s.

Fatigue lifetime calculations can be estimated by integrating these two equations within the limits of three different zones, namely, (*i*) a microstructural zone, in which the crack grows from its initial length a_0 (assumed to be the peak to trough surface roughness measurement) to the threshold crack length, a_{th}; (*ii*) an interactive zone, in which the crack extends from a length a_{th} to a length d, and in which both mechanisms represented by equations (2.13) and (2.14) may operate; and (*iii*) a continuum fracture mechanics zone, in which the crack grows from a length $a = d$ to the crack length at failure, a_f.

Fatigue lifetime predictions using this model have been shown to be in good agreement with the experimental lifetime results obtained from fatigue tests.

Navarro and de los Rios [63][80], based on two previous works [30][61], presented a unified model consisting of a single fracture mechanics-controlled crack

growth law to describe both microstructurally short (Stage I) and elastic-plastic (Stage II) crack growth. Crack growth rate in this model is dependent on the plastic displacement ϕ_3 at the crack tip as in the following expression:

$$\frac{da}{dN} = f\phi_3 \tag{2.15}$$

where f, is the fraction of dislocations taking part in the process of crack extension, as defined in reference [30]. Both f and ϕ_3 depend upon the applied stress level. The plastic displacement ϕ_3 at the tip of a crack is determined for values of stresses much higher than the friction stress given by the following expression:

$$\phi_3 = \frac{2\kappa}{G}\frac{\sqrt{1-n_2^2}}{n_2}\sigma\, a \tag{2.16}$$

where G is the shear modulus, σ is the applied stress and n_2 is a dimensionless parameter taken as equal to a/c, wherein a is half of surface crack length, and c is a segment length which incorporates both crack length and the plastic zone. The value of κ is taken equal to one for screw dislocations and $1-\nu$ for edge dislocations.

Fatigue lifetime predictions can be made by integrating equation (2.15) which describes the whole fatigue process, including Stage I and Stage II crack growth. Predictions can be used to obtain theoretical S-N curves for a given material.

In an attempt to simplify the existing fatigue prediction methods Yates and Grabowski [81] proposed a two stage crack growth model where a minimum of experimentally fitted parameters could be derived, wherever possible, from conventional linear elastic fracture mechanics. The model was applied to short crack growth data obtained from tension/tension tests (see reference [82]) and four point bend tests (see References [29][83]) on Waspaloy, both subjected to the same applied maximum stress.

The model developed by Yates and Grabowski [81] consists of two parts. The first, which describes the microstructurally short crack growth regime, is based on the model of Hobson and Brown [78][79]; and the second, which describes long crack growth regime, adopts a traditional linear elastic fracture mechanics (LEFM) approach. Microstructurally short crack growth is assumed to occur by a Stage I Mode II process in which the growth rate is proportional to the slip

band length. It is also assumed that slip bands extend right across the grains and are blocked by successive grain boundaries along the crack path [84][85]. A general form of the equation proposed by Yates and Grabowski [81] for Stage I crack growth is:

$$\frac{da}{dN} = C_1(d_i - a) \tag{2.17}$$

where C_1 is a function of the applied stress range $\Delta\sigma$ and applied stress ratio R, d_i is the slip band length and a is half the surface crack length, both extended to include the crack growth from the initiation site to subsequent grains.

The model assumes that on approaching each grain boundary the crack growth rate decreases continuously in response to the diminishing plasticity ahead of the crack tip, reaching a minimum at the grain boundary. If crack propagation is to continue then the crack must have sufficient driving force to overcome the microstructural barrier. It has been suggested [86] that a crack overcomes a barrier when the stress ahead of the crack tip attains a critical value such that a dislocation source can be operated and plastic slip initiated in the next grain. In the present model it is proposed that a crack can reach a length of $0.95d_i$ before a dislocation source is unlocked and propagation is continued in the next grain.

Based on the observation that cracks initiated in larger than average grains Yates and Grabowski [81] assumed the initiation grain to be one standard deviation larger than the mean value of grain size. According to the model growth proceeds by a Stage I mechanism until more favourable growth kinetics lead to a transition to a Stage II mechanism (after Hourlier and Pineau [87]). It is proposed that the Stage I to Stage II transition will occur when the long crack growth rate exceeds that of the short crack growth mechanism.

In the long crack growth regime propagation is assumed to occur by a Stage II Mode I process. For this crack growth regime the model adopts a traditional linear elastic fracture mechanics (LEFM) approach and can be represented by the following 'Paris' type equation:

$$\frac{da}{dN} = C_2\Delta K^m \tag{2.18}$$

where C_2 and m are material constants.

Fatigue lifetime predictions can be made by integrating equations (2.17) and (2.18) which describe Stage I and Stage II crack growth. Integration procedures for this model are explained in detail in chapter 5 where the analysis of the results of the present investigation was carried out. As in Hobson's model, predictions can be used to obtain theoretical S-N curves for a given material.

Chapter 3

Experimental Work

3.1 Introduction

A test programme was planned to investigate the influence of the manufacturing procedures on short fatigue crack growth in Waspaloy. In order to achieve this aim the following experimental work was performed:

- Characterisation of the material and microstructure.
- Systematic variation of surface preparation procedures.
- Heat treatment of the material (option).
- Characterization of the surface finish and residual stresses.
- Fatigue four-point-bend tests.
- Short crack growth monitoring and measurements.

Details of the experimental work performed in this project are presented in this chapter.

3.2 Material

The material used in this project was a cast and wrought nickel base superalloy, Waspaloy. This is one of a group of alloys developed for use at high

temperatures and high cyclic stresses. A typical application of Waspaloy has been, to date, in aeroengines for critical components such as turbine discs. Temperature conditions in turbine discs can vary from around 150°C at the hub to about 550°C at the rim, and, during certain periods of the aeroengine operation, the discs may be loaded in excess of 80% of the yield strength. In addition to the high temperatures and corrosive environments, temperature gradients and load variations arise as operating conditions change, giving rise to thermomechanical fatigue problems. Because of its thermomechanical and fatigue properties Waspaloy stands as a material of prime importance in modern design of aeroengines.

The nominal chemical composition in weight percentage of the material used in the tests is shown in table 3.1 and its mechanical properties are shown in table 3.2. In the final disc condition the material was subject to the following heat treatments:

1. 1115°C for four hours and then oil quenched,
2. 800°C for four hours and then air cooled,
3. 760°C for sixteen hours and then air cooled.

The microstructure found in Waspaloy consists of an FCC γ matrix which is solid solution strengthened by the gamma prime (γ') precipitate. The alloys also contain carbides and other phases which may be distributed throughout the matrix and/or located at grain boundaries.

Grain size measurements have been conducted on the test material and results are presented in chapter 4. Measurements have been performed in three different locations and in both direction, i.e. along and across the surface of the specimens. All measurements of grain size have been conducted according to the Mean Linear Intercept method.

3.3 Specimen Design

A four-point-bend square section beam specimen with dimensions shown in figure 3.1(a) was used in the test programme. Loading points on the specimen

are illustrated by the arrows in figure 3.1(b). Although there is no standard specimen geometry universally accepted for collection of short crack growth data, the geometry chosen is becoming widely accepted in some research institutes and in the aerospace industry. Recent studies [88] on the influence of the specimen geometry on short crack growth in Waspaloy have shown that this particular geometry is adequate for collection of short crack growth data and provides reliable results when compared with other specimen geometries currently used in the industry. Some advantages of this specimen geometry are listed below and are mainly related with the surface replication procedure.

- Square section beam specimens are easier to machine and to polish compared to conventional hour glass shaped specimens.
- Crack growth detection and monitoring is made easier since crack growth occurs in the central region of the specimen, thus restricting the area of the specimen to be replicated and studied under the microscope.
- The replication procedure is made easier compared to that used for hour glass specimens, since only the top surface of the specimen needs to be replicated.
- As the surface to be replicated is flat, replicas do not come off wavy like those taken from hour glass specimens, which make crack measurements more time consuming due to the difficulty of focusing the whole length of a crack or a particular area of the replica.

3.4 Specimen Preparation

Specimens were machined from the material cut from the central bore section of the disc and were supplied with a longitudinal ground finish. Specimens were oriented in both directions tangential and transversal to the rim of the disc.

In order to study and compare the effect of the surface finish on the short crack behaviour two methods of surface preparation have been used. The first method involved grinding of the top surface of a series of specimens. The second

involved the mechanical polishing of the surfaces. These two procedures are described in the following sections.

3.4.1 Grinding Procedure

Machine grinding was performed on the top surface of four-point-bend specimens in a direction transversal to the longitudinal axis of the specimen. In order to obtain the same grade of surface finish in a number of specimens and to ensure good repeatibility of fatigue crack growth results, specimens were ground in four different batches.

Specimens were tightly held, side by side, in the jaws of a small vice, which was fixed to the magnetic table of the grinding machine. The use of this device was necessary because of the nonmagnetic properties of the material to be worked on, which could not be directly fixed to the table. Dressing of the grinding wheel was performed in some instances before the grinding operation in order to ensure a better finish. Grinding parameters e.g. wheel speed, table speed, downfeed rate, crossfeed per pass and grinding wheel, were carefully checked and the necessary adjustments were made before starting the grinding. These parameters have been kept constant for each batch of specimens except for the infeed rate, which was varied during the grinding process. A roughening operation was then performed on the top surface of the specimens taking not more than 10μm per pass in depth. The roughening operation continued until the top surface of the whole batch of specimens was flat and levelled. An additional dressing of the grinding wheel was then performed and the finishing operation took place. Grinding procedures for the finishing operation were systematically varied in order to produce batches of specimens with different surface conditions. Grinding parameters which were used in each batch of specimens are shown in table 3.3.

A final polishing operation was carried out on the ground specimens in order to round the sharp edges of the top ground surfaces. This operation was performed to reduce the effect of stress concentration of the sharp edges of the specimens, thus preventing crack initiation from the edges.

3.4.2 Polishing Procedure

Mechanical polishing was carried out on the top surface of the specimens and involved two successive stages. Polishing in both stages was performed using polishing wheels of the conventional type. In the first stage a coarse polishing was performed to remove grinding marks with a 400 grit emery paper. A succession of polishing operations was also accomplished using progressively finer grit papers, e.g. 600, 800, 1000 and 1200. Polishing operations were performed alternately in the longitudinal and transversal directions to ensure the complete removal of all marks and scratches resulting of the previous operation. Specimens were washed and dried with acetone after each polishing operation to avoid contamination of finer grit papers with coarser particles. Polished surfaces were carefully examined under the microscope to make sure that all polishing marks were in a single direction.

In the second stage, polishing was completed by cloth polishing the surfaces with a succession of progressively finer diamond pastes, e.g. 6, 3 and $1\mu m$. This operation was continued until a "mirror finish" surface was obtained, thus enabling the surface microstructure to be examined after electropolishing.

3.4.3 Electropolishing

Electropolishing was carried out as a final finishing operation following the mechanical polishing of the surfaces. Electropolishing was performed with the main purpose of revealing the microstructure of the metal, thus allowing crack - grain boundary interactions to be observed under the microscope.

It is well established that polishing and abrasive finishing operations produce a thin hard highly disturbed layer below the surface of a metal and that this hardened and disturbed layer accounts for a major source of scatter in fatigue crack growth data. It has also been observed by some workers (see e.g. reference [89]), that much less scatter of fatigue test data occurs by electropolishing surfaces that have undergone work hardening operations such as grinding, polishing and abrasive finishing. This decrease in fatigue test data scatter of electropolished surfaces can be ascribed to the removal of the work hardened layer of surface

metal caused by the finishing operation, and can be regarded as a beneficial effect of the electropolishing process.

A solution of 65% methanol, 32% butoxyetanol and 3% perchloric acid was used as electrolyte. The electrolyte was first cooled down to a temperature of aproximately -50°C using liquid nitrogen. The specimen to be electropolished was made the anode and a stainless steel container was made the cathode of the cell. A potential difference of $50V$ was then applied by means of a d.c. power supply. This process was interrupted at every three or four minutes for surface inspection. The specimen was then thoroughly rinsed in warm water and dried, and the surface was examined under the microscope. The electropolishing process went on for five to ten minutes until the grain boundaries became clearly visible. During the electropolishing the temperature of the electrolyte was carefully controlled and nitrogen was constantly added with agitation to ensure most constant and uniform electropolishing conditions.

3.4.4 Heat Treatment

The material was tested in both as-received and annealed condition. Annealing took place after surface preparation with the purpose of removing residual stresses from the surface of the specimen. Stress relieved specimens are required if the effect of surface roughness is to be investigated in complete separation from those of residual machining stresses. The heat treatment was conducted at 1010°C for two hours, according to procedure described in reference [90]. A heating rate of 3°C/min was used and the material was naturally cooled in the furnace. The treatment was conducted in argon atmosphere to prevent surface contamination.

3.5 Analysis and Description of Surface Condition

3.5.1 Quantification of Surface Finish

In order to relate fatigue crack growth behaviour with the surface condition produced by different manufacturing procedures, e.g. polishing and grinding, surface measurements were conducted on each grade of surface finish obtained. Measurements have been taken at random locations on the surface of the specimens using a computer controlled Talysurf-type measuring device. Surface profile readouts were taken on five consecutive sampling lengths of $0.95mm$ (filter cut-off lengths), and averaged over an assessment length of $4.8mm$. Surface profile readouts were computer processed and surface texture parameters, i.e. R_a, R_p, R_v, R_y and R_zDIN, were calculated by means of appropriate software. Results of the measurements are presented in chapter 4.

3.5.2 Quantification of Surface Residual Stresses

Residual machining stresses introduced by grinding procedures were measured by X-ray diffraction technique. Due to the penetration of X-rays into the metal being very small, e.g. up to a depth of $25\mu m$, this technique can only be applied non-destructively to measure residual stresses at the surface of the specimen, but since machining stresses are induced in a very thin layer, e.g. $15-50\mu m$ (see e.g. references [2][71]), the technique was considered to be satisfactory for the measurements required in this case. Results of the measurements are presented in chapter 4.

3.6 Fatigue Crack Growth Monitoring and Measurement Technique

3.6.1 Replication Technique

Fatigue crack growth was monitored by means of a replication technique. The replication method has been one of the most widely used in short fatigue crack growth studies, see for example references [14][26][91][92][93][94][95][96]. Some advantages of this method as a crack growth monitoring tool are listed as follows:

- Plastic replicas provide a simple and reliable method for keeping a permanent record of the crack growth history, including crack length, orientation, and neighbouring cracks.
- The behaviour of short cracks can be studied, as there is no need to locate the cracks before they have grown to an easily detectable size.
- Replicas can be taken from specimens of various geometrical configurations, e.g. cylindrical, hourglass-shaped, notched and flat.
- Multiple crack growth on a single specimen can be easily monitored and information about crack spacing and density can be made available.
- Crack initiation mechanisms and the interaction of the cracks with the microstructure can be derived.
- Equipment required for the analysis of replica data is not very sophisticated and expensive.

The replication technique which was used involved the following steps and procedures:

Pieces of the replica material of a size suitable to cover the central area of the specimen, e.g. $25mm$ long and $12mm$ wide, were cut from the sheets. Cellulose acetate sheets of a thickness 35μm were used as replication material.

A few drops of acetone were placed on to the specimen surface and the replica film immediately applied allowing surface tension forces to pull it down. The film

was left to dry for about five minutes after which it could be easily removed by simply peeling it off from the surface of the specimen. The replica film was then stretched and attached, replication side upwards, to the surface of a microscope slide with two pieces of adhesive tape for easy handling and examination in the microscope.

Care must be taken during the replication procedure to ensure that the replica film is laid in such a way to cover the whole area of the surface to be reproduced, moving the replica film when necessary towards the central area of the specimen before the acetone dries out. Care has also to be taken not to moisten the outer surface of the replica film with acetone since the replica can be dissolved and damaged. Moistening of the edge of the replica film which is held by the tweezers is also to be avoided, otherwise the replica film becomes attached to them and can be damaged.

A common problem that arises during the replication procedure is concerned with the air bubbles which can be trapped below the replica film causing partial deletion of the area reproduced on the replica. This problem was prevented by gradually laying down the replica film on the surface of the specimen after it was sprayed with acetone. Air bubbles that might be trapped were easily removed by gradually lifting and lowering the edge of the replica film, so allowing the air bubbles to escape.

Monitoring the fatigue crack growth by replication means is a discontinuous process. Fatigue tests must be periodically interrupted and the specimen must be loaded under tension to keep the surface cracks open during the replication. The cyclic interval at which the replicas are to be taken depends upon the expected fatigue life of the specimen and must be determined from previous fatigue life tests performed on the same specimen geometry and test conditions. In the present programme replicas were taken at least at twenty stages of the fatigue life of the specimen but as the main interest was the growth of short cracks, replicas were taken more frequently in the early stages of lifetime.

In spite of being a suitable tool for monitoring the growth of short fatigue cracks the replication method has a number of weak points which can in some

instances limit its application. Some of these limitations are summarized below:

- Fatigue tests have to be periodically stopped so that replicas can be taken. Some materials, such as 7076-T6 under certain loading conditions have been shown (see reference [96]) to exhibit different total fatigue life when rest periods are introduced in comparison to a continuous fatigue life test.
- Replicas do not give a continuous record of the crack growth history of a test.
- Taking and analysing replicas is a very time consuming process and can not be automated.
- Replicas do not provide information about the depth of cracks.
- Replication method is not very suitable for high temperature tests, since specimens have to be cooled down to room temperature before the replicas can be taken.

3.6.2 Crack Measurement Technique

Acetate replicas were examined directly under an optical microscope. In each of the replicas crack lengths were found by measuring the total surface length of each major crack, i.e. by taking into account the complex path followed by these cracks up to that stage.

Crack length measurements were accomplished using a computer controlled image analysis system. This system consists of a high resolution optical microscope which is connected through a video camera to a video monitor screen. The system also includes a personal computer fitted with an image capturing board which allows the image of the microscope to be captured on to the monitor screen. The whole system is operated by a purpose written piece of software which offers a number of options in terms of measurements, such as crack lengths, angles, areas and contours. The process of measurement is entirely menu driven and cracks can be followed on the video monitor screen with the help of a mouse

controlled cursor. The results of the measurements performed are displayed on the computer screen and can be permanently stored on a hard or floppy disc.

Replica analysis begins with the last replica taken during the test, for example near the fracture. The first step in the analysis is to locate the dominant crack which led the specimen to failure. On the last replica the identity of the failure crack or cracks is obvious, since it spans over the whole width of the specimen. The crack length can be directly measured from the replica with the help of the image analysis system. This procedure is repeated going backwards in the series of replicas to the early stages of the fatigue life of the specimen. As the replicas of an earlier stage are examined crack lengths become smaller and more difficult to locate. Attention should then be paid to the microstructural features which are reproduced on the replicas, such as grain boundaries, inclusion particles and scratches. These features can be used as references on the area where the crack initiated making its location easier.

Despite the use of this technique crack measurements in most of the coarse ground specimens could not be performed in the early stages of fatigue lifetime due to the difficulty in locating the tips of cracks that grew along the grinding marks.

3.7 Fatigue Tests

3.7.1 Test Machine

A Mayes servohydraulic testing machine with a $250kN$ nominal static load capacity was used for the four-point-bend tests. The main loading frame of the testing machine is a vertical two-column type with a movable crosshead. The upper crosshead is clamped on to the columns using clamping screws which can be released so allowing the crosshead to move upwards and downwards. The crosshead can be moved by action of two symmetrical hydraulic actuators, and can be positioned at any desired height within the range of the columns in order to suit different sizes of specimens and testing fixtures.

Three modes of control are available for testing, i.e. position, load and strain

control. A waveform generator is able to generate periodic waveform signals either of sinusoidal, triangular or square form, with any frequency in the range from $0.02Hz$ to $180Hz$.

3.7.2 Test Procedure

Four-point-bend load controlled fatigue tests were performed using the Mayes $250kN$ servohydraulic testing machine. Tests were conducted at room temperature at a frequency of $15Hz$.

The conventional four-point-bend loading fixture (see figures 3.2 and 3.3) available in the SIRIUS laboratory, Department of Mechanical and Process Engineering, University of Sheffield, was used to perform the tests.

Applied loads were calculated for each specimen so that the maximum surface stress did not exceed $880MPa$. The dimensions of the cross-section of each specimen were measured with a micrometer after surface preparation, so that the required test loading could be precisely determined and applied in each test. The applied stress, σ, was calculated using the standard formula for an elastic beam with a rectangular cross-sectional area subjected to bending:

$$\sigma = \frac{6M}{bt^2} \tag{3.1}$$

where M is the bending moment, and b and t are the width and height of the cross-section of the specimen.

For the particular four-point-bend geometry tested, the relationship between the applied bending stress σ and the applied load F can be obtained by substituting M in equation (3.1) with $F(l-s)/4$, where l is the distance between the upper loading points ($50mm$) and s is the distance between the lower loading points ($10mm$) as shown in figure 3.1(b). After making the necessary corrections for the units this relationship can be expressed by the following formula:

$$\sigma = \frac{6 \times 10^{-2} F}{bt^2} \tag{3.2}$$

In order to investigate the effect of the applied stress range on the short fatigue crack growth, tests were carried out at three different stress levels. Applied

stress ranges ($\Delta\sigma$), stress ratios ($\sigma_{min}/\sigma_{max}$) and peak surface stresses (σ_{max}) are shown in table 3.4.

Fatigue tests were performed according to the following procedures:

- Four-point-bend grips were assembled after adjusting the height of the crosshead.
- The lower grip of the four-point-bend fixture was raised to hold the specimen in the required position. The hydraulic actuator was kept in position control mode during this operation.
- Balance of the pressure in the servo-valve was accomplished by setting the servo-valve current to zero, and the hydraulic actuator was switched over from position to load control mode.
- Required mean static load (or maximum load for ground surfaces) was applied and the first replica was taken. In order to have a reproduction of the undamaged surface, i.e. before any fatigue cracks had initiated, the first replica was taken before the cyclic load was applied on the specimen.
- Required cyclic load range and test frequency were set. Cycle counter was pre-set and test started.
- Further surface replication followed at different stages (pre-set number of cycles) of the fatigue test.
- Test continued until the specimen broke open or reached a stage close to fracture.

3.7.3 Test Programme

Four sets of tests were carried out as a test programme which is described below:

Set 1

- A series of 7 four-point-bend load controlled fatigue tests was performed on polished, as-received, Waspaloy specimens to investigate the influence of the microstructure on short fatigue crack growth. In order to investigate the effect of the applied stress range on the short fatigue crack growth, tests were carried out at three different stress levels. Applied stress ranges ($\Delta\sigma$), stress ratios ($\sigma_{min}/\sigma_{max}$) and peak surface stresses (σ_{max}) are shown in table 3.4.

Set 2

- An additional series of 7 four-point-bend load controlled fatigue tests was performed on polished, heat-treated, Waspaloy specimens to investigate the influence of the microstructure on short fatigue crack growth in the stress-relieved material condition. Tests were conducted under the same loading conditions described in set 1.

Set 3

- A series of 4 four-point-bend load controlled fatigue tests was performed on ground, heat-treated, Waspaloy specimens to investigate the effect of increased surface roughness, caused by surface grinding, on short fatigue crack growth. In order to be able to describe the effect of the surface roughness in complete isolation from those caused by residual stresses all specimens were stress relieved. Specimens with two different grades of surface finish, named condition 1 and condition 2, were tested. Tests were conducted under one stress level.

Set 4

- A series of 4 four-point-bend load controlled fatigue tests was performed on ground, as-received, Waspaloy specimens to investigate the combined effect of surface roughness and residual stresses, caused by the surface grinding procedure, on short fatigue crack growth. Specimens with two different grades of surface finish, named condition 3 and condition 4, were tested. Tests were conducted under one stress level.

Chapter 4

Results

4.1 Introduction

This chapter presents the results obtained from the test programme and experimental work described in chapter 3. Preliminary information is presented on the material microstructure, surface condition and residual stresses. In the following sections results of fatigue endurance and fatigue crack growth are presented for both polished and ground finish, in both as-received and stress relieved condition.

4.2 Characterization of the Material Microstructure

A micrograph of the material tested are shown in figure 4.1. The mean grain size of the material has been used to characterize the material microstructure. Grain size measurements were performed in two perpendicular directions, i.e. along and across the surface of the specimens, according to the Mean Linear Intercept method, and indicated that the grains of the material tested are aproximately equiaxed. The mean grain size has been averaged from individual measurements in both directions, i.e. along and across the surface of the specimens. Results of 169 individual grain size measurements taken on the material in untreated condition indicated a mean grain size of 59μm with a standard de-

viation of 35μm. Measurements performed after heat-treating the material did not to reveal any significant changes in grain size.

4.3 Characterization of the Surface Topography

Surface topographies were characterized according to the procedure described in chapter 3, section 3.5. Results of measurements of surface texture parameters, i.e. R_a, R_p, R_v, R_y, and R_zDIN, are presented in table 4.1 and surface profiles are shown in figure 4.2, 4.3, 4.4, 4.5 and 4.6.

4.4 Characterization of Surface Residual Stresses

Residual stress patterns introduced by grinding operations were characterized by means of X-ray diffraction measurements, as described in chapter 3, section 3.5. Due to the shallow penetration of the X-rays used, this technique was only applied to the surface of the specimens.

Results of the measurements showed residual stresses in the range of $+52MPa$ and $+106MPa$ for polished stress relieved specimens and in the range of $-69MPa$ and $-104MPa$ for ground (condition 2) stress relieved specimens. Results of these measurements were of the same order of accuracy of the X-ray method employed, indicating that full stress relief was achieved.

Surface residual stresses for ground specimens tested in as-received condition were in the range of $+33MPa$ and $-2MPa$ (grinding condition 3), and $-117MPa$ and $-136MPa$ (grinding condition 4). Results of the measurements in grinding condition 3 were also in the range of accuracy of the X-ray equipment employed, suggesting that residual stresses induced by grinding condition 3 are negligible.

4.5 Fatigue Endurance Results

Fatigue lifetimes to failure were recorded for each specimen tested. An attempt was made in each test to take the last replica of the surface just before the complete fracture of the specimen. It was noticed that complete fracture occurred rapidly once the major crack or cracks had extended across the surface of the specimen, and that the number of cycles spent between these two events did not exceed a few thousands in any case. The fatigue lifetime to failure of a specimen was then considered to occur either when the specimen broke open or when the major cracks spanned all over across the surface of the specimen.

4.5.1 Fatigue Endurance Results for Polished Finish Condition

Fatigue lifetimes to failure from four-point-bend fatigue tests performed on polished finish surface specimens in both as-received and stress relieved condition are shown in table 4.2. Mean lifetimes to failure, N_f, are shown in the same table for each stress range, $\triangle\sigma$, and material treatment conditions.

Fatigue endurance results for both material treatment conditions were plotted as applied stress range versus number of cycles to failure, in figure 4.7(a) and (b).

A best fit analysis was performed on the endurance curves, and the following relationships of the type 'Basquin Law' were derived. These can be expressed by the following equations:

As-Received Condition

$$\triangle\sigma(N_f)^{0.08} = 2220 \tag{4.1}$$

Stress Relieved Condition

$$\triangle\sigma(N_f)^{0.17} = 7510 \tag{4.2}$$

where $\triangle\sigma$ is the applied stress range in *MPa*.

4.5.2 Fatigue Endurance Results for Ground Finish Condition

Fatigue lifetimes to failure from four-point-bend fatigue tests performed on ground surface specimens in both stress relieved and as-received condition are shown in table 4.3. Mean lifetimes to failure are shown in the same table for each of the grinding and material treatment conditions.

4.6 Fatigue Crack Growth Results

Fatigue crack growth data were obtained from direct measurements on the series of acetate replicas taken during the fatigue tests. All major surface cracks which led the specimen to failure were observed and had their length measured. It was noted that in many instances failure cracks developed as a result of the coalescence of individual cracks. In such instances, crack length measurements were taken on each of the subsidiary cracks that contributed to the failure crack.

The half measured surface crack lengths and the corresponding elapsed number of cycles data were used to derive the growth rate of each crack. Crack growth rates, (da/dN), were estimated by dividing the variation in crack length by the variation in the elapsed number of cycles for two successive stages of lifetime, as expressed by the following formula:

$$\left(\frac{da}{dN}\right)_{i+1} = \frac{a_{i+1} - a_i}{N_{i+1} - N_i} \tag{4.3}$$

where a_i is the half surface crack length at N_i number of cycles, and a_{i+1} is the half surface crack length at N_{i+1} number of cycles.

Because this crack growth rate is more representative of the speed of the crack at a crack length halfway between two successive stages of lifetime a mean value of crack length was also estimated by using the following expression:

$$(a_{mean})_{i+1} = \frac{a_i + a_{i+1}}{2} \tag{4.4}$$

Experimental crack growth data referring to each of the cracks measured are presented in Appendix A. In each table of Appendix A, column 1 represents

the number of cycles N completed before the test was stopped for replication. Column 2 represents half the measured surface crack length a at each stage in the fatigue test. Column 3 represents the mean growth rate of the crack between two successive stages in the fatigue test, which was calculated by using formula 4.3; and column 4 represents the mean value of crack length between two successive stages in the fatigue test, which was calculated by using formula 4.4.

In order to identify each set of crack growth data in the tables the following convention has been adopted.

Example: F1/2A3

- F Four-point-bend geometry
- 1 Specimen number
- 2 Number of a particular crack
- A Refers to one of the subsidiary cracks which joined to form a major failure crack, e.g. F1/2
- 3 Refers to one of the subsidiary cracks which joined to form a given subsidiary crack, e.g. F1/2A

The experimental crack growth data from each complete set of tests, performed under the same conditions, e.g. same surface finish, heat treatment and stress range, were plotted in a series of graphs of the type 'Half Surface Crack Length' versus 'Number of Cycles' and 'Crack Growth Rate' versus 'Mean Crack Length', which are presented in the next sections.

It was noticed from these plots that a wide variation exists in the number of cycles required for each crack to reach a given length and for each specimen to fail. In order to apply normal statistics to the study of short cracks a simple logarithmic transformation, described in reference [97], was applied to the number of cycles data of each major and subsidiary crack investigated. The logarithm of the fatigue lifetimes was found to be approximately normally distributed allowing the statistical properties of each set of data to be determined by normal statistics.

Results of the mean number of cycles to different crack lengths ranging from 12 to 800μm, and their corresponding standard deviation are presented in the following sections for each complete set of crack growth data.

4.6.1 Short Crack Growth in Polished Finish Condition

The experimental crack growth data from the complete set of tests, performed on polished surface specimens, are shown in figures 4.8(a), (b) and (c) for specimens in as-received condition, and in figures 4.9(a), (b) and (c) for specimens in stress relieved condition. The figures represent the 'Half Surface Crack Length' versus 'Number of Cycles' plots referring to some 31 cracks obtained from tests in the as-received material, and 20 cracks obtained from tests in the stress relieved material. Plots are presented according to the stress range applied in the tests.

Results of the mean number of cycles to crack lengths ranging from 12 to 800μm and to the failure are presented in tables 1, 2 and 3, Appendix B, for the material in as-received condition, and in tables 4, 5 and 6, Appendix B, for the material in stress relieved condition. The number of cycles taken for each crack to reach the required length was calculated by linear interpolation between the available crack growth data. Results presented in the tables refer respectively to the stress ranges of 850, 792 and 750MPa.

4.6.2 Short Crack Growth in Ground Finish Condition

The experimental crack growth data from the complete set of tests, performed on ground surface specimens in stress relieved condition, were plotted in figure 4.10(a) for grinding condition 1, and in figure 4.10(b) for grinding condition 2, as 'Half Surface Crack Length' versus 'Number of Cycles'. The plots represent the growth data of some 10 cracks obtained from tests on ground/stress relieved specimens.

The experimental crack growth data from the complete set of tests, performed on ground surface specimens in as-received condition, were plotted in figure 4.11(a) for grinding condition 3 and in figure 4.11(b) for grinding condition 4. The plots represent the growth data of some 11 cracks obtained from tests on ground/as-received specimens.

Results of the mean number of cycles to crack lengths ranging from 12 to 800μm and to the failure are presented in tables 7 and 8, Appendix B, for ground surface specimens in stress relieved condition, and in tables 9 and 10, Appendix B,

for the ground surface specimens in as-received condition. The number of cycles taken for each crack to reach the required length was calculated by linear interpolation as explained in the previous section. Results presented in the tables refer to four different grinding conditions and were obtained from tests performed at the same stress range, namely 792MPa.

A comparison between the mean crack growth results obtained from polished and ground surface specimens is shown in figures 4.12(a) and (b) for both stress relieved and as-received condition.

Chapter 5

Analysis of Short Fatigue Crack Growth Results

5.1 Introduction

This chapter is concerned with the analysis of the short crack growth results obtained from four point bend fatigue tests on Waspaloy.

A number of models are in use to date to predict the effect of the material microstructure on short fatigue crack growth, see e.g. references [27][63][78], however, none of them is able to account for the effect of the surface condition on fatigue crack growth.

A major concern of this chapter is the application and development of suitable mathematical models to describe the short crack growth behaviour of the material subjected to different finishing operations, namely polishing and grinding, in both stress relieved and as-received conditions.

A two stage crack growth model, presented by Yates and Grabowski [81], has been used to predict the effect of the microstructure on Waspaloy. This model has been modified to take into account three inherent parameters affecting the short crack growth in ground surfaces, i.e. surface microstructure, surface roughness and residual stresses.

5.2 Analysis of Short Crack Growth Behaviour

Fatigue crack growth behaviour was observed to follow two distinct patterns which appear to be related to the surface condition produced by the finishing operations such as polishing or grinding. Polished and fine ground surfaces gave rise to a pattern 'A' of crack behaviour, whereas coarse ground surfaces gave rise to a pattern 'B' of crack behaviour. These two patterns of crack behaviour are described in the following sections.

5.2.1 Short Crack Growth Behaviour in Polished Surface Condition

Fatigue crack initiation in smooth surfaces has been considered by a number of workers as a Stage I Mode II cracking process.

Previous studies conducted on nickel base alloys have shown that crack initiation is predominantly associated with the occurrence of persistent slip bands (PSB) [26][27][29]. In the present study four different sites of crack initiation were observed in the replicas:

1. Crack initiation occurred along slip bands as shown in figure 5.1.
2. Crack initiation occurred along twin boundaries as shown in figure 5.2.
3. Crack initiation occurred in grains showing no signs of slip bands, as shown in figure 5.3.
4. Crack initiation occurred at grain boundaries, as shown in figures 5.4(a) and (b).

Irrespective of the initiation site in the microstructure, cracks showed an initial orientation of approximately 45° with the principal axis of the specimen, suggesting that crack initiation in bending specimens occurs by a Stage I Mode II (shear mode) process.

Examination of the fracture surfaces revealed that crack initiation and stage I propagation in four point bend specimens are characterized by crystallographic

cracking as shown in figures 5.5(a). Fractographs show that the initial crystallographic appearence of the fracture surfaces gradually changes as cracks grow, giving rise to a much flatter mode of fracture, as shown in figures 5.5 (b), and eventually to striation marks, as shown in figures 5.5(c), which characterize a Stage II crack growth.

Examination of the plastic replicas reveals the intermittent nature of short fatigue crack growth. Acceleration and deceleration periods are observed at crack lengths approximately multiples of the grain size. Cracks showed a decreasing growth rate on approaching grain boundaries, slowing down to a minimum and even arresting (see e.g. figure 5.6(a), (b) and (c)) at or near grain boundaries. Replicas showed that, after reaching the first grain boundary, cracks changed their initial path and experienced a period of increasing growth rate. Crack speed continued to rise until the crack tip approached the next grain, when a further retardation period took place. This discontinuous pattern of behaviour was noted for crack lengths equivalent to several grain diameters.

In a previous work, Zhang [83] noted that the grain boundary blocking effect occurred over a distance of several grain diameters, though the first boundary was the strongest barrier to crack growth. In the present work, however, this did not appear to be always the case. Stronger retardation effects were noted in some instances after the crack had overcome the first or even the second grain boundary.

5.2.2 Short Crack Growth Behaviour in Ground Surface Condition

In spite of the fine surface finish obtained in most ground surfaces, marked differences in mean lifetimes were observed in some instances, between the polished and ground specimens, or between different grades of ground finish (see e.g. figure 4.12(a)). These differences appeared to be related to two different patterns of crack behaviour observed in ground surfaces (see figures 5.7 and 5.8).

Fine ground surfaces gave rise to the same pattern 'A' of crack behaviour observed in polished surfaces, see e.g. figure 5.7). Cracks developing this pattern

of behaviour appeared to be deflected from their initial path as a result of the surface microstructure and not to be affected by the depth and orientation of the grinding marks produced in the surface of the specimens.

Coarse ground surfaces gave rise to a pattern 'B' of crack behaviour, see e.g. figure 5.8. In this second pattern of behaviour crack initiation and propagation were observed to occur along the grinding marks, showing that pattern 'B' cracks strongly interact with the depth and orientation of surface defects. Faster growth rates were observed in pattern 'B' cracks (see e.g. table B.8, Appendix B) compared to pattern 'A' cracks (see e.g. table B.7, Appendix B). Replicas and SEM fracture observations showed that the faster crack growth and failure of these specimens were due to multiple crack initiation and coalescence of individual microcracks along single grinding marks.

Pattern 'B' of behaviour would suggest that crack initiation occurs according to a Stage II Mode I process. Examination of the fracture surfaces of ground specimens showed, however, that initial cracking occurs in a crystallographic mode in both fine and coarse ground surfaces, as shown in figures 5.9(a) and (b), characterizing a Stage I Mode II fracture process.

Crack initiation in pattern 'A' observed in fine ground surfaces is identical to the one observed in polished surface specimens and can be associated with the crack orientation described by Brown and Miller [22][98] as case A, whereas crack initiation in pattern 'B' observed in coarse ground surfaces can be associated with the crack orientation described as case B. In case B the planes of maximum shear are oriented at 45° to the cross section plane of the specimen.

5.3 Fatigue Crack Growth Modelling

A short crack growth model first presented by Yates and Grabowski [81], described in chapter 2, was used in the present study. This model was previously used in fatigue lifetime predictions of short crack growth data obtained from tension/tension tests (see reference [82]) and four point bend tests (see references [29][83]) on Waspaloy.

The model developed by Yates and Grabowski [81] consists of two parts. The

first, which describes the microstructurally short crack growth regime, is based on the model of Hobson and Brown [78][79] and can be represented by the following equation:

$$\frac{da}{dN} = C_1(d_i - a) \tag{5.1}$$

where C_1 is an empirical constant which depends upon the applied stress (or strain) range $\Delta\sigma$ and stress (or strain) ratio R; d_i is the slip band length and a is half the surface crack length, both extended to include the crack growth from the initiation site to subsequent grains.

Fatigue crack growth was assumed to proceed by a Stage I mechanism until more favourable growth kinetics leads to a transition to a Stage II mechanism (after [87]). The Stage I to Stage II transition was assumed by Yates and Grabowski [81] to occur when the long crack growth rate exceeded the short crack growth rate with the additional requirement that the short crack growth rate would never exceed the long crack growth rate as the crack grew.

The second part of the model, which describes Stage II crack growth, adopts a traditional linear elastic fracture mechanics (LEFM) approach and can be represented by the following 'Paris' type equation:

$$\frac{da}{dN} = C_2\Delta K^m \tag{5.2}$$

where C_2 and m are material constants.

It must be noted that this model assumes that crack growth beyond the transition point is no longer affected by the microstructural features of the material and that therefore Stage II crack growth can be described in terms of the range in linear elastic stress intensity factor ΔK.

5.4 Application of the Model to Four Point Bend in Polished Surface Condition

5.4.1 Stage I Crack Growth Equation

Stage I crack growth in Waspaloy was described by equation 5.1. The formulation of this equation involved the determination of the empirical constant

C_1 and the slip band lengths d_i in successive grains.

A method for determination of the constant C_1 has been described, see e.g. references [78] and [99], and consisted in plotting a regression line through each successive pair of data points $(da/dN, a_{mean})$ showing a decreasing growth rate, but only for crack lenghts smaller than the distance d corresponding to the first microstructural barrier observed.

In the present work a slightly different procedure was used to determine the value of C_1 in equation 5.1. Based on experimental evidence (see e.g. [27][82][83]) that cracks growing in Waspaloy experience a succession of retardation periods on approaching grain boundaries, a least squares best-fit line was applied to each pair of data points $(da/dN, a_{mean})$, corresponding to the first and to the second microstructural barriers, where this retardation effect was more evident.

Values of C_1 were calculated for each individual crack observed from tests at different stress levels and on different material treatment conditions.

An attempt has been made to fit a powerlaw relationship of the type shown in a number of previous works [32][35][78], to the values of C_1 calculated for each different stress level (available from the tests). It was noted, however, that better correlations would be obtained by excluding from the regression analysis the values of C_1 corresponding to the highest stress level of the test programme, i.e. $850MPa$.

The reason why this happened can be attributed to the effect of the mean stress on short fatigue crack growth. This effect was observed by Wang and Miller [100] in their study on the short fatigue crack growth of an alloy steel subject to various combinations of mean and alternating shear stress. By plotting the short crack parameter C_1 as a function of mean shear stress they observed an increasing value of C_1 with the applied mean stress when the shear stress range was kept constant.

Since the value of C_1 depends on the applied mean stress it is apparent that better correlations between C_1 and $\Delta\sigma$ would be obtained at all stress levels if all tests had been performed at the same applied mean stress. However, in the present programme tests conducted at $850MPa$ were performed under a lower

mean stress, i.e. $R = 0.03$, as described in section 3.7.2, so that maximum surface stresses did not exceed the material yield stress, i.e. $880MPa$. It was also observed that such a correlation would be poorer for values of C_1 obtained from tests performed on the stress relieved specimens, showing that the effect of mean stress was more pronounced in heat treated condition.

Because of this effect it was decided that power law relationships would be fitted only to those values of C_1 obtained from tests performed at the same stress ratio, i.e. $R = 0.1$, and that a mean value of C_1 would be used for the highest stress level, i.e. $850MPa$, in the case of heat treated material.

Values of C_1 from tests performed at the same stress ratio, i.e. $R = 0.1$, were plotted in figures 5.10 and 5.11 in terms of applied stress range $\Delta\sigma$. The following regression power law relationships were then derived for each material treatment condition:

Material in As-Received Condition

$$C_1 = 1.54 \times 10^{-45}(\Delta\sigma)^{14.01} \tag{5.3}$$

Material in Stress Relieved Condition

$$C_1 = 1.36 \times 10^{-38}(\Delta\sigma)^{11.52} \tag{5.4}$$

where the units for $\Delta\sigma$ and C_1 are respectively MPa and $cycle^{-1}$.

Since some of the cracks initiated and propagated much faster than others a lot of scatter was observed in the plots of C_1 against the applied stress range $\Delta\sigma$ (see figure 5.10 and 5.11). Such large scatter in the values of C_1 was reported by a number of workers, see e.g. references [32][35][79], and is to be attributed to local variations in metallurgical properties, such as grain size and orientation of the slip planes with respect to the maximum shear stress direction for those particular grains in which the cracks initiated.

It was also observed that a regression power law relationship representing simply the average values of C_1 led in some cases to non-conservative predictions of fatigue lifetime. The reason why this happened can be ascribed to the fact that the fatigue failure of a specimen or machine component is more likely to be caused by the fast growing cracks than by the 'average' growing cracks. It is

also to be noted that the final fracture of a specimen or machine component is a process which will involve in most cases the coalescence of two or more cracks.

In order to incorporate these probabilistic factors into the analysis of short crack growth a standard statistical method [102] was used to establish a confidence band around the regression line fitted to the experimental data of the constant C_1, which was plotted against the values of applied stress range $\Delta\sigma$ in the form of conventional 'X' and 'Y' graphs. According to this statistical method [102] the confidence interval for a mean value of 'Y', and for a given value of 'X' can be calculated by the following formula:

$$Y = \hat{A}_0 + \hat{A}_1 X_0 \pm T_{\frac{1}{2}\alpha,N-2} \times S_{Y|X} \sqrt{\frac{1}{N} + \frac{(X_0 - X_{mean})^2}{\sum (X_i - X_{mean})^2}} \qquad (5.5)$$

where $\hat{A}_0 + \hat{A}_1 X_0$ is the linear regression equation obtained from the power law expressions 5.3 and 5.4, X_0 is a given value of X for which the average value of Y is to be predicted, X_{mean} is the mean value of X data points, N is the number of data points, $T_{\frac{1}{2}\alpha,N-2}$ is a one-sided Student's t-distribution (see e.g [102][103]) with $N - 2$ degrees of freedom, and $S_{Y|X}$ is the standard error of the estimate which is given by the following expression:

$$S_{Y|X} = \sqrt{\frac{\sum (Y_i - \hat{A}_0 - \hat{A}_1 X_i)^2}{N - 2}} \qquad (5.6)$$

It must be noted that before applying formulas 5.5 and 5.6 a standard logarithmic transformation was performed on the regression power law equations 5.3 and 5.4 and on the values of X_0, X_{mean}, X_i and Y_i. This transformation was performed in order to enter these values in a form compatible with the linear regression $\hat{A}_0 + \hat{A}_1 X_0$ mentioned before.

In a first attempt to predict the behaviour of the fast growing cracks a Student's t-distribution [102][103] giving 60% confidence interval was used. Application of equation 5.5 to the values of C_1 produces two curves which represent the upper and lower bounds of the confidence band. The curve representing the upper bound of the confidence band is shown in figures 5.10 and 5.11. It is apparent from these curves (see reference [103]) that the most reliable estimates of Y (represented in the figures by the values of C_1) are obtained for values of X

(represented in the figures by the values of $\Delta\sigma$) which are close to X_{mean}, and further X is from X_{mean} the larger the possible error in the estimates of Y.

In order to express the upper bound values of C_1 in terms of applied stress range $\Delta\sigma$, for each material treatment conditions a best fit line was passed through the upper bound values corresponding to the maximum and minimum stress ranges shown in figures 5.10 and 5.11. This regression equations are expressed by the following powerlaw relationships:

Material in As-Received Condition

$$(C_{1_{U60\%}}) = 2.71 \times 10^{-43}(\Delta\sigma)^{13.25} \tag{5.7}$$

Material in Stress Relieved Condition

$$(C_{1_{U60\%}}) = 1.61 \times 10^{-33}(\Delta\sigma)^{9.79} \tag{5.8}$$

where $C_{1_{U60\%}}$ is the upper bound value of C_1 for a confidence interval of 60%. The units for $\Delta\sigma$ and $C_{1_{U60\%}}$ in equations 5.7 and 5.8 are respectively MPa and $cycle^{-1}$.

In order to apply Yates-Grabowski model to Stage I crack growth the distances between the microstructural barriers, e.g. d_1, d_2, etc., must also be known.

Forsyth [89] has shown that, plastic deformation is not uniform all over the surface grains of a polycrystalline material, and that, due to less constraint, large surface grains will be more prone to irreversible plastic deformation than small ones. In a recent work, Zhang [83] observed that cracks in Waspaloy were most likely to initiate in grains whose sizes were about the upper bound of the average grain size. Based on similar observations Yates and Grabowski [81] have assumed the initiation grain to be one standard deviation larger than the average grain size, and took the distance from the initiation site, in the centre of the grain, to the first barrier as half the diameter of the initiation grain. Subsequent barriers were assumed to arise at multiple distances of the mean grain size.

In the present study a method proposed by Hobson et al. [79] [99] was used to calculate the value of the first microstructural barrier d_1. This method consisted in plotting on linear scale the data points of crack growth rate da/dN against the mean values of half crack length a_{mean}, and then to fit a least squares line

through the data points showing a decreasing crack growth rate with increasing crack length. The intersection of the abscissa by this best fit line gave the value of d_1 for each crack. Some variation was observed in the calculated value of d_1 but this is to be expected due to variations in the microstructure of this material. A mean value of $d_1 = 51.39\mu m$ was found for the material in as-received condition, and $d_1 = 42.37\mu m$ was found for the material in stress relieved condition. A fair agreement was observed between these results and the value of d_1 proposed by Yates and Grabowski [81], of $47\mu m$. According to their criterium the initiation grain would have $94\mu m$ diameter (considering an average grain size of $59\mu m$ plus $35\mu m$ standard deviation), and the distance from the initiation site in the centre of the grain to the first grain boundary would be half this diameter, which is $d_1 = 47\mu m$. In view of the close agreement (less than 10% difference) between these values of d_1 the latter was eventually adopted in the short crack growth equation. Further microstructural barriers d_i were assumed to arise at multiple distances of the average grain size such as $d_2 = 106\mu m$, $d_3 = 165\mu m$, $d_4 = 224\mu m$, etc..

Substitution of the values of C_1 from equations 5.7 and 5.8 in equation 5.1 gives the final expression to describe Stage I crack growth in Waspaloy. As there are two material treatment conditions two different equations were formulated:
Material in As-Received Condition

$$\frac{da}{dN} = 2.71 \times 10^{-43}(\triangle\sigma)^{13.25}(d_i - a) \tag{5.9}$$

Material in Stress Relieved Condition

$$\frac{da}{dN} = 1.61 \times 10^{-33}(\triangle\sigma)^{9.79}(d_i - a) \tag{5.10}$$

where i stands for the grain number, i.e. 1, 2, 3, etc., and $d_i = 47\mu m$, $106\mu m$, $165\mu m$, etc.. The units of (da/dN) in these equations are $\mu m/cycle$ for $\triangle\sigma$ expressed in MPa and d_i and a expressed in μm.

Equations 5.9 and 5.10 can be expressed in terms of strain range by simply substituting the stress range $\triangle\sigma$ by $E\triangle\epsilon_e$ for linear elastic conditions, with $E = 215000MPa$. The final expressions to describe Stage I crack growth in terms of strain range will then be:

Material in As-Received Condition

$$\frac{da}{dN} = 1.16 \times 10^{28}(\triangle\epsilon_e)^{13.25}(d_i - a) \tag{5.11}$$

Material in Stress Relieved Condition

$$\frac{da}{dN} = 2.44 \times 10^{19}(\triangle\epsilon_e)^{9.79}(d_i - a) \tag{5.12}$$

Based on these equations short crack growth rate calculations were made. Results of these calculations are presented with experimental growth rates in section 5.4.3.

5.4.2 Stage II Crack Growth Equation

Stage II crack growth in Waspaloy was described by the 'Paris' type equation 5.2. The coefficients C_2 and m were obtained by Yates and Grabowski [81] from test results of Tagahani and Powell [104] for combined corner notch and compact tension specimens. From these results $C_2 = 1.06 \times 10^{-15}$ and $m = 5.6$ for stress intensity factors in $MPa\sqrt{m}$ and crack growth rates in $m/cycle$.

In order to correlate the test results of Tagahani and Powell with those obtained in the present study the stress intensity range $\triangle K_I$ had to be modified to suit the bending specimen geometry. The stress intensity factor for a semi-elliptical surface crack under bending is given by Newman and Raju [105] as:

$$\triangle K_I = 0.502\triangle\sigma\sqrt{\pi b} \tag{5.13}$$

where $\triangle\sigma$ is the applied stress range and b is the crack depth. The calibration given for $\triangle K_I$ corresponds to a mean aspect ratio $b/a = 0.8$, and an approximate crack depth/specimen thickness $b/t = 0.25$.

SEM examinations of the fracture surfaces revealed that the initial semicircular shape of microstructuraly short cracks gradually changes as cracks grow giving place to a slightly semi-elliptical crack shape. This change in crack shape in bending specimens appears to be due to two factors, namely, (i) the decreasing stress field to which the cracks are subjected as they grow away from the surface, and (ii) the coalescence of two or more cracks which can take place as

cracks grow longer. Measurements of the aspect ratio (ratio between the crack depth and half surface crack length) of these cracks were performed on some of the four point bend specimens tested. Fractographs (see e.g figures 5.12(a) and (b)) showed that the aspect ratios of the dominant cracks are approximately in the range of 0.75 to 0.84. In view of this observation a mean value of 0.8 aspect ratio was adopted in the long crack calculations. The stress intensity range $\triangle K_I$ can be then expressed as:

$$\triangle K_I = 0.502 \triangle \sigma \sqrt{\pi 0.8a} \tag{5.14}$$

where a is the half surface crack length.

After substitution of the stress intensity range (equation 5.14) and the long crack coefficients C_2 and m in equation 5.2, and a convenient transformation of units the final expression for Stage II crack growth rate in bending specimens can be written as:

$$\frac{da}{dN} = 4.677 \times 10^{-27} (\triangle \sigma \sqrt{a})^{5.6} \tag{5.15}$$

where a is the half crack length measured in μm and da/dN is the growth rate in $\mu m/cycle$.

In order to express growth rate in terms of strain range a further modification was done in equation 5.15. Substituting the stress range $\triangle \sigma$ by $E \triangle \epsilon_e$ for linear elastic conditions, with $E = 215000 MPa$, the following strain range based formula was obtained:

$$\frac{da}{dN} = 3400 (\triangle \epsilon_e \sqrt{a})^{5.6} \tag{5.16}$$

where a is the half crack length measured in μm and da/dN is the growth rate in $\mu m/cycle$.

Unlike equations 5.11 and 5.12, which describe microstructurally short crack growth in each material treatment condition, equations 5.15 and 5.16 were used to describe long crack growth in both as-received and stress relieved conditions. Although their formulation was based on test results obtained from Waspaloy in as-received condition, 'Paris' type equations 5.15 and 5.16 appeared to give a fair correlation with test results obtained from stress relieved material.

The Stage I to Stage II transition point was assumed by Yates and Grabowski [81] to occur when the long crack growth rate exceeded the short crack growth

rate, with the additional requirement that the short crack growth rate would never exceed the long crack growth rate as the crack grew.

The transitional crack length a_{tr} in four point bend was estimated by equating the growth rate in Stage I, represented by equations 5.11 and 5.12, with the growth rate in Stage II, represented by equation 5.16, as shown below:
Material in As-Received Condition

$$1.16 \times 10^{28}(\triangle\epsilon_e)^{13.25}(d_i - a_{tr}) = 3400(\triangle\epsilon_e\sqrt{a_{tr}})^{5.6} \tag{5.17}$$

Material in Stress Relieved Condition

$$2.44 \times 10^{19}(\triangle\epsilon_e)^{9.79}(d_i - a_{tr}) = 3400(\triangle\epsilon_e\sqrt{a_{tr}})^{5.6} \tag{5.18}$$

5.4.3 Fatigue Lifetime Predictions

Fatigue lifetimes of four point bend specimens were estimated by adding individual lifetimes N_s and N_l spent in both Stage I and Stage II crack growth regimes. Individual fatigue lifetimes were calculated by integrating the short and long crack growth equations, e.g. 5.1 and 5.2.

Short crack growth equation 5.1 was integrated from some initial crack length a_0, such as the surface roughness, to the transitional crack length a_{tr}, which was obtained by expressions 5.17 and 5.18. As equation 5.1 describes crack growth in a series of successive grains, integration was done separately for each interval corresponding to the microstructural distances d_1, d_2, ..., d_i, as expressed below:

$$N_s = \frac{1}{C_1}\left[\int_{a_0}^{0.95d_1}\frac{da}{(d_1-a)} + \int_{0.95d_1}^{0.95d_2}\frac{da}{(d_2-a)} + ... + \int_{0.95d_{i-1}}^{a_{tr}}\frac{da}{(d_i-a)}\right] \tag{5.19}$$

where the value of a_0 was taken from table 4.1 as the surface texture parameter $R_v = 0.42\mu m$ representing the maximum depth of the surface profile below the mean line of the assessment length for a polished surface.

It should be noted that the values of $0.95d_1$, $0.95d_2$, etc., of the integration limits were assumed by Yates and Grabowski [81] as a critical distance from which a crack would unlock a dislocation source to produce slip in the following grain.

In the long crack growth regime, fatigue lifetimes were estimated by integrating equation 5.2 from a transitional crack length a_{tr} to a value of crack length a_f

corresponding to the failure of the specimen, as in the expression given below:

$$N_l = \frac{1}{C_2'(\triangle\epsilon_e)^m} \int_{a_{tr}}^{a_f} a^{-\frac{m}{2}} da \tag{5.20}$$

where $C_2' = 3400$ and $m = 5.6$. The final crack length a_f was taken as $5mm$.

Predictions of fatigue lifetimes to failure N_f were made by simply adding the number of cycles N_s and N_l obtained from expressions 5.19 and 5.20.

Fatigue lifetimes of polished specimens were estimated and compared with the mean number of cycles observed from the experiments. Results of the predictions and experiments are compared in tables 1 to 6, Appendix C, and plotted in figures 5.13 to 5.18(a) and (b).

5.5 Application of the Model to Fatigue Crack Growth in Ground Surface Condition

The Yates and Grabowski model [81] was originally based on short crack data from tension/tension fatigue tests (see reference [82]) and although it was successfully used to predict fatigue lives under four point bend loading (see reference [29]), it has not yet been used to predict the effect of surface finish such as that produced by the grinding process on short fatigue crack growth.

Moreover, it cannot model the process of linking of cracks which, according to the present study, takes place in coarse ground surfaces, e.g. those developing pattern 'B' cracks. As observed in section 5.2.2, coalescence of individual subcracks did take place in the case of ground specimens (grinding condition 2) and it caused specimens to fail comparatively quickly. Therefore application of this model overstimates the fatigue lifetimes.

It was also said in section 5.2.2 that the majority of the individual subcracks were observed to initiate, coalesce and grow along individual grinding marks.

It is apparent that this process should be more severe in the case of surfaces having longer and deeper grinding marks. It is, therefore, essential to incorporate this process of linkage of subcracks into the existing short crack model so that realistic fatigue lifetime predictions are made for specimens and components, without excessive overestimation.

Experimental observation also indicated that the conventional surface texture parameters, shown in table 4.1, do not always bear a consistent relationship with the growth rates observed in ground surfaces, and therefore are not suitable to correlate short crack growth in machined surfaces.

A consistent relationship was observed between R_v parameter and the short crack growth rates in stress relieved specimens, however this relationship does not hold in the case of ground specimens in the as-received condition (conditions 3 and 4). Analysis of the mean crack growth results (see for example figure 4.12(b)) showed that despite the finer surface finish obtained by polishing (see figure 4.2), some of the ground surfaces (grinding condition 4) can produce longer lifetimes in the range of short crack lengths investigated. These results appear to indicate that, for the range of surface roughnesses obtained by polishing and fine grinding (conditions 3 and 4), no direct correlation exists between the conventional surface texture parameters, e.g. R_v, and the fatigue lifetime results. It was noted however that these fatigue lifetime results can be directly related to the residual stress measurements, suggesting that despite the fine finishes of the ground surfaces residual stress patterns may have played some role in the early stages of short fatigue crack growth.

It is therefore important to incorporate the effect of these residual stresses into the present crack growth model in order to make fatigue lifetime predictions more accurate and realistic.

5.5.1 Stage I Crack Growth Equation

Short crack growth in ground surfaces followed the same discontinuous pattern of behaviour observed in polished surfaces, indicating that crack growth in ground surfaces is also strongly affected by the material microstructure.

Accordingly, in order to describe microstructural short crack growth in ground surfaces the same equations as those described in section 5.4.1 were adopted (i.e. eq. 5.3 and 5.4). Since the effect of microstructure in the ground surfaces is the same as in the polished surfaces the values of the constants C_1 and d_i were assumed to be the same as in a polished surface, and short crack parameter C_1 was

taken from expressions 5.7 or 5.8 according to the material treatment condition.

5.5.2 Stage II Crack Growth Equation

Since Stage II crack growth is not influenced by microstructure and surface effects, such as surface roughness and residual stresses, the same equations (5.15 or 5.16) can be used to describe long crack growth in ground specimens. As in the case of polished specimens equations 5.15 and 5.16 were used to describe long crack growth regardless of the material treatment condition. Although the formulation of these equations was based on test results obtained from Waspaloy in the as-received condition they appeared to give a fair correlation with test results obtained from tests on ground specimens in both material treatment conditions.

As in the case of the polished surface condition the Stage I to Stage II transition point was assumed to occur when the long crack growth rate exceeded the short crack growth rate, with the additional requirement that the short crack growth rate would never exceed the long crack growth rate as the crack grew.

The transitional crack length a_{tr} in four point bend was estimated by equating the growth rate in Stage I, represented by equations 5.11 and 5.12, with the growth rate in Stage II, represented by equation 5.16, as shown in expressions 5.17 and 5.18.

5.5.3 Fatigue Lifetime Predictions in Ground Stress Relieved Condition

Fatigue lifetime predictions for ground specimens (grinding conditions 1 and 2) were made in a similar way to that described for polished surfaces in section 5.4.3.

Individual fatigue lifetimes $(N_s)_g$ and $(N_l)_g$, spent in Stage I and Stage II crack growth regimes, were calculated by integrating equations 5.1 and 5.2. Short crack growth equation 5.1 was integrated from some initial crack length a_0, which was taken from table 4.1 as the deepest surface irregularity R_v, to the transitional crack length a_{tr}, which was obtained by expressions 5.17 and 5.18.

In order to incorporate the process of crack coalescence observed in surfaces

ground in condition 2, into the fatigue lifetime predictions the following assumptions have been made:

- Multiple crack initiation occurs along grinding marks
- Cracks join at once on reaching a given length
- During the coalescence process crack growth rates will vary according to a linear process without interacting with grain boundaries

Regarding the second assumption, it is apparent that cracks growing along grinding marks (pattern 'B' cracks) did not join at once, and that some of them joined earlier than others. However, the moment or length with which cracks joined could not be established accurately from replica observations. Crack measurements in the very early stages of fatigue lifetime could not be performed due to the difficulty in locating accurately the tips of the cracks that grew along individual grinding marks. Estimates of these lengths had to rely on SEM observations. Observation of the fracture surfaces of the specimens indicated that a number of crack initiation sites are located at distances (D) as close as $90\mu m$ apart from each others. A conservative approach was then used, and cracks were assumed to join on reaching a length corresponding approximately to half that distance, namely, $D/2 = 45\mu m$, as shown in figure 5.19.

The number of initiation sites was assumed to be proportional to the length of the grinding marks, as shown for example in figure 5.20, and it was estimated simply by dividing the average length of the grinding marks by the length at which cracks were observed to coalesce. In the present study measurements of these grinding marks were performed indicating an average length L_a of $450\mu m$. The number of initiation sites was therefore calculated by dividing half this length ($225\mu m$) by half the distance between crack initiation sites ($45\mu m$), giving a number n_i of 5 initiation sites.

Integration of equation 5.1 was performed for the same intervals corresponding to the microstructural distances d_1, d_2, ..., d_i, found in polished surfaces. However, as assumed before, on reaching a length of $45\mu m$ the five initiated

cracks will join and their length will rapidly increase to $225\mu m$ making ineffective the three next microstructural barriers d_2, d_3 and d_4 for this particular case. Accordingly, the description of short crack growth will be given by the following integration limits:

$$(N_s)_g = \frac{1}{C_1}\left[\int_{a_0}^{D/2}\frac{da}{(d_1-a_i)} + \int_{n_iD/2}^{0.95d_n}\frac{da}{(d_n-a)} + \int_{0.95d_n}^{0.95d_{n+1}}\frac{da}{(d_{n+1}-a)} + \ldots + \int_{0.95d_{i-1}}^{a_{tr}}\frac{da}{(d_i-a)}\right] \quad (5.21)$$

where the value of a_0 was taken from table 4.1 as the surface texture parameter $R_v = 1.49\mu m$, $D/2$ was given the value of $45\mu m$ corresponding to half the distance between crack initiation sites, n_i was estimated as 5 and corresponds to the number of crack initiation sites along a grinding mark of average length L_a, and d_n designates the distance between the crack initiation site and the microstructural barrier ahead of the tip of the crack after the coalescence process has occurred. Values of other constants which appear in this expression, i.e. C_1 and a_{tr}, were assumed to be the same as in the case of polished surface condition, explained in section 5.4.3.

It is apparent that the process of crack coalescence in a ground surface is strongly dependent on the orientation of the grinding marks, and must be more severe in the case of surfaces having longer and deeper grinding marks. However, the role of these three parameters is still not fully understood and further investigation will be necessary for its physical understanding and mathematical quantification.

As in the case of polished specimens described in section 5.4.3, fatigue lifetimes in the long crack growth regime were estimated by integrating equation 5.15 (or 5.16) from a transitional crack length a_{tr} to a value of crack length a_f corresponding to the failure of the specimen, as shown by expression 5.20. Predictions of fatigue lifetimes to failure for ground specimens N_f were made by simply adding the number of cycles $(N_s)_g$ and $(N_l)_g$ obtained from the apropriate expressions.

Fatigue lifetimes of ground stress relieved specimens (grinding conditions 1 and 2) were estimated and compared with the mean number of cycles observed from the experiments. Results of the predictions and experiments are compared

in tables 7 and 8, Appendix C, and plotted in figures 5.21 and 5.22, (a) and (b).

5.5.4 Fatigue Lifetime Predictions in Ground As-Received Condition

As mentioned in section 5.5, a consistent relationship was observed between the surface texture parameter R_v and the short crack growth rates in stress relieved specimens, however this relationship did not appear to hold in the case of ground specimens in as-received condition (conditions 3 and 4). Crack growth results (see figure 4.12(b)) showed that despite the finer surface finish obtained by polishing, fatigue lifetimes for ground surfaces (grinding condition 4) were longer in the whole range of short crack lengths investigated. These results indicate that, for the range of finishes obtained by polishing and fine grinding (conditions 3 and 4), conventional surface texture parameters, e.g. R_v, have no relevance in terms of short fatigue crack growth, and that fatigue lifetimes are directly related to the residual stress patterns induced by the finishing process (see figure 5.23).

It was said in chapter 2 that whatever the nature of the residual stresses introduced in the surface of a metal, their effect on fatigue crack growth is the same as if mean stresses of the same magnitude were superimposed on the cyclic operating stresses.

In order to incorporate the effect of residual stresses into the fatigue lifetime predictions of ground as-received specimens the variation in depth of combined mean stresses (superposition of cyclic operating stresses and residual stresses) had to be taken into account. As the X-ray diffraction measurements were only applied to the surface of the specimens, assumptions had to be made regarding the depth and profile of the residual stress layers.

Data available in the literature (see e.g. references [2][71][108]) indicate that the depth of residual stresses introduced by low stress and conventional grinding procedures are in the range of $15\mu m$, according to Almen and Black [71], $25\mu m$ to $50\mu m$, according to Greenfield and Allen [2], and $25\mu m$ to $75\mu m$, according to Koster [108]. As surface grinding procedures adopted in the present work were

very gentle and produced much finer finishes than those of conventional practice, a lower average limit of the range indicated in the literature ($20\mu m$) was deemed to be more appropriate and was adopted as an approximate value for depth of the residual layer in the calculations.

Residual stress gradients across the cross section of the specimen or component usually vary from case to case. However, in order to simplify calculations it is common to assume residual stress profiles to be constant or linear over the depth of the residual layer (see e.g. figure 2.14). In the present work residual stresses were assumed to be maximum at the surface and to decrease linearly to a depth of $20\mu m$ where residual stress magnitude was assumed to be zero. It is quite evident that the minimum magnitude of these internal stresses does not decrease to zero but they change sign in order to balance the stresses generated at or near the surface. However, since these reversed stresses are balanced over a much larger area their magnitudes are usually much lower than those developed at or near the surface and therefore their effect on fatigue crack growth will be much more reduced compared with the effect of the stress due to the applied load.

In order to account for the effect of residual stress gradients on short fatigue crack growth an approach proposed by Wang and Miller [109] has been adopted and modified in the present work. This approach was developed to predict fatigue crack growth under the combination of mean and alternating stresses. As residual stress gradients are superimposed on the applied mean stress, values of the combined mean stresses had to be described as a function of the depth for each surface finish condition.

Combined mean stresses at any depth were estimated by algebraically adding the residual stress and the mean stress due to the applied load at that depth. Variation in depth of combined mean stresses are shown in figure 5.24 for the three different surface conditions, namely polished, ground in conditions 3 and 4.

Application of Wang and Miller's approach involved a simple transformation of equation 5.7 which can be rewritten as:

$$C_1' = 2.71 \times 10^{-43}(f_2(\sigma_m)\triangle\sigma)^{13.25} \tag{5.22}$$

where the value of C_1' incorporates the effect of the mean stress σ_m as proposed

by Wang and Miller [109]; values of $f_2(\sigma_m)$ were experimentally determined by the same workers as a function of the applied mean stress σ_m; and $\triangle\sigma$ is the stress range applied in the test.

In order to extend the applicability of Wang and Miller's approach, which is limited to a NiCrMo steel, to let us say Waspaloy, it would be more reasonable to make $f = f(\sigma_m/\sigma_a)$ instead of $f_2 = f(\sigma_m)$ as proposed by Wang and Miller. Values of $f = f(\sigma_m/\sigma_a)$ were derived from Wang and Miller's results [109] and are plotted in figure 5.25. It is to be noted from this plot that $f(\sigma_m/\sigma_a) = f_2(\sigma_m) - 1$. Equation 5.22 can then be rewritten as:

$$C_1'' = 2.71 \times 10^{-43} \left(\triangle\sigma \left(\frac{1 + f(\sigma_m/\sigma_a)}{1 + f_{pol}} \right) \right)^{13.25} \tag{5.23}$$

where the value of C_1'' incorporates the effect of the mean stress and stress amplitude ratio (σ_m/σ_a); values of $f = f(\sigma_m/\sigma_a)$ are plotted in figure 5.25 as a function of the mean stress and stress amplitude ratio (σ_m/σ_a) and relate basically to crack opening, i.e. to the effects of frictional interference or oxide debris for a Stage I crystallographic crack subject to lower stress levels; and $\triangle\sigma$ is the stress range applied in the test. The term f_{pol} was introduced in this equation as a correction term for C_1' in equation 5.22 to represent the effect of the mean stress and stress amplitude ratio (σ_m/σ_a) on the short crack growth rate in polished as-received surface condition.

Integration of short crack growth equation 5.1 was basically performed as described earlier in this section. Initial crack length, a_0, was taken from table 4.1 as the deepest surface irregularity R_v, and the transitional crack length, a_{tr}, was obtained by expressions 5.17. However, unlike fatigue lifetime calculations of stress relieved and polished specimens, where the applied stress and consequently C_1 were assumed to be constant with depth, integration of short crack growth equation 5.1 for the as-received material condition had to take into account the variation with depth of the combined mean stress. Because of the variation in depth of the combined mean stress and consequent variation of C_1'', integration of the first term of equation 5.19, corresponding to the first microstructural barrier d_1, had to be performed numerically. The first step of this numerical integration starting at a crack size of a_0 is shown below:

- $a = a_0 = R_v$; $N = 0$ *cycles*
- $\triangle a = 0.5\mu m$
- $da/dN = C_1''(d_1 - a)$
- $\triangle N = \triangle a/(da/dN)$
- $(N_{s_1})_g = N + \triangle N$
- $a = a_0 + \triangle a$

The numerical integration procedure described above was continued up to a crack length $a = 0.95d_1$. Account was taken in the integration procedure of the variation of the combined mean stress with the crack depth a (shown in figure 5.24) by recalculating C_1'' as expressed by equation 5.23 before calculating (da/dN) in every step of the integration procedure.

Integration of the other terms corresponding to the microstructural barriers d_2, d_3, ..., d_i, shown in equation 5.19, was performed analytically as in the case of polished specimens.

As described in section 5.5.3, fatigue lifetimes in the long crack growth regime were estimated by integrating equation 5.15 (or 5.16) from a transitional crack length a_{tr} to a value of crack length a_f corresponding to the failure of the specimen, as shown by expression 5.20. Predictions of fatigue lifetimes to failure for ground as-received specimens N_f were made by simply adding the number of cycles $(N_s)_g$ and $(N_l)_g$ as in the case of polished specimens.

Fatigue lifetimes of ground as received specimens (grinding conditions 3 and 4) were estimated and compared with the mean number of cycles observed from the experiments. Results of the predictions and experiments are compared in tables 9 and 10, Appendix C, and plotted in figures 5.26 and 5.27, (a) and (b).

Chapter 6

Discussion

6.1 Introduction

This chapter is concerned with the discussion of the short crack growth results obtained from four point bend fatigue tests on Waspaloy.

Fatigue crack growth results obtained from polished and ground surfaces are compared for both material treatment conditions, and the various effects affecting the behaviour of short cracks are discussed in detail.

The application of an existing short crack growth model (Yates-Grabowski model) which was used in this study to describe short fatigue crack growth, is discussed in this chapter. Furthermore, the extension of this model to describe both the effect of residual stress layers and the process of short crack coalescence observed in ground surfaces, is also discussed in this chapter.

Predictions of fatigue lifetimes to failure for polished surface specimens are presented in form of 'theoretical' S-N curves and compared with the fatigue endurance results obtained in both material treatment conditions.

6.2 Fatigue Crack Growth Results

6.2.1 Short Crack Growth in Polished Surfaces

Fatigue lifetime results from polished surface specimens, tested in the as-received condition are shown in tables B.1, B.2 and B.3, Appendix B. Fatigue life-

times at different applied stress levels can be compared by means of figure 6.1(a) in which cracks are shown to grow faster at increasing stress levels.

Fatigue lifetime results from polished specimens, tested in stress relieved condition (tables B.4, B.5 and B.6, Appendix B), show the same type of dependence with the applied stress range (see figure 6.1(b)).

Comparison of fatigue lifetime results from as-received (tables B.1, B.2 and B.3, Appendix B) and stress relieved conditions (B.4, B.5 and B.6, Appendix B) shows that, under the same stress range condition, stress relieved specimens gave much longer fatigue lifetimes than as-received specimens. Results obtained from the stress relieved specimens showed that the mean lifetime for cracks to reach a length of $100\mu m$ at a stress range of 750 MPa was 497426 *cycles* (see table B.6, Appendix B), against 189109 *cycles* (see table B.3, Appendix B) for the as-received condition; a mean lifetime of 363927 *cycles* (see table B.5, Appendix B) at 792 MPa, against 138748 *cycles* (see table B.2, Appendix B) for the as-received condition; and a mean lifetime of 265330 *cycles* (see table B.4, Appendix B) at 850 MPa, against 46498 *cycles* (see table B.1, Appendix B) to reach the same depth.

Although the increase in the fatigue lifetimes of heat treated specimens occurred over the whole range of crack lengths observed, it can be noted that the observed differences in lifetime between the stress relieved and the as-received conditions were more significant in the early stages of fatigue crack growth; As an example, at a stress range of 850 MPa, the fatigue lifetime to reach $100\mu m$ was 5.7 times longer in the stress relieved condition than in the as-received condition. In comparison, the fatigue lifetime to reach $400\mu m$ was 3.5 times longer and the fatigue lifetime to failure was 3.1 times longer in the stress relieved condition. Differences in fatigue lifetime between the two treatment conditions were observed regardless of the applied stress range (see e.g. differences in lifetime at 792 MPa and 750 MPa).

It is apparent from these results that the observed increase in the fatigue lifetimes of stress relieved specimens was due to a stronger retardation in the early phase of short crack growth. The increased resistance to the initiation and

growth of short cracks in the annealed material can be ascribed to metallurgical alterations which were produced by the heat treatment process. Changes in the size and distribution of precipitates are known to occur at intermediate temperatures during stress relieving and annealing of this superalloy (see reference [90]).

Although the heat treatment did not produce any significant change in the grain size of the material it may well have caused particle coarsening and also changes in the degree of coherence between precipitates and the matrix. These metallurgical alterations are known to strongly affect the crack growth response of nickel base alloys (see reference [52]).

6.2.2 Short Crack Growth in Ground Surfaces

6.2.2.1 Stress Relieved Material Condition

Analysis of the crack growth results shown in tables B.5, B.7 and B.8, Appendix B, for material in stress relieved condition indicated that, although short crack growth takes the most significant proportion of the fatigue lifetime of both polished and ground specimens, this proportion tends to be significantly reduced as a consequence of deeper grinding marks found in coarse ground surfaces (grinding condition 2). Figures 4.10(a) and (b) show that cracks growing from coarse ground surfaces, termed pattern 'B' cracks (see definition in section 5.2.2), grow much faster than cracks growing from polished and fine ground surfaces, termed pattern 'A' cracks.

Pattern 'A' cracks (shown in tables B.5 and B.7) developed in polished and fine ground surfaces can be seen to take longer to reach the same length. As an example, cracks growing from a polished surface take 363927 *cycles* to reach a length of 100μm which is 69% of the mean lifetime to failure of the specimens. In a fine ground surface cracks take 320164 *cycles* to reach the same length, which is 61% of the total life of the specimen. In comparison cracks take only 94657 *cycles* to reach the same length in a coarse ground surface, or 28% of the total life of the specimens. Differences between the mean lifetimes observed to grow pattern 'A' and pattern 'B' cracks in surfaces ground in condition 1 and 2 (stress

relieved material condition) can be better appreciated by means of figure 4.12(a).

Results obtained for each grade of surface finish, i.e. polished and grinding conditions 1 and 2, were compared. A Student's t statistics described in reference [103] was used to assess the level of significance of the differences observed in mean fatigue lifetimes. This procedure (see reference [103]) consisted in testing the hypothesis that the two samples had equal mean number of cycles by estimating the probability of this occurrence. The means and the standard deviations of each sample of data were found through a log-normal distribution. Fatigue lifetimes observed in polished surface condition were used as a base of comparison and the t-value was computed as:

$$t = \frac{\mid log(N_{mean_1}) - log(N_{mean_2}) \mid}{\sqrt{\frac{(n_1-1)\sigma_1^2+(n_2-1)\sigma_2^2}{(n_1+n_2-2)}}\sqrt{\frac{1}{n_1}+\frac{1}{n_2}}} \tag{6.1}$$

Comparison of the computed value of t with its tabulated values gives the probability that the observed differences have arisen by chance. Results of this statistics are shown in table 6.1.

In spite of the differences between the mean lifetimes observed for cracks growing from polished and fine ground surfaces (grinding condition 1), table 6.1 shows that these differences are not highly significant. The Student's t statistics shows that the probability of these differences arising by chance are in the range of 20% to 50% for cracks shorter than 100μm. It also shows that these differences are more significant for crack lengths in the range of 12μm to 75μm.

Differences between the mean lifetimes observed to grow cracks from polished and coarse ground surfaces (grinding condition 2) are highly significant. Table 6.1 shows that the probability of these differences arising by chance are less than 0.1% for the whole range of crack lengths observed. It should be pointed out that none of the cracks described as pattern 'B' could be measured when their length was shorter than 60μm (surface crack length of 120μm). Since the cracks grew along the grinding marks the accurate location of the crack tips in earlier stages of growth was not possible.

It can be noted from figure 4.12(a) that, although fatigue lifetimes observed for polished and fine ground surfaces (grinding condition 1) are not much different,

the fatigue lifetimes of coarse ground surfaces (grinding condition 2) are much shorter. Differences in fatigue lifetimes are much greater than would be expected by considering only the small difference in depth of the machining marks (see table 4.1), 1.14μm for fine ground (grinding condition 1) surfaces and 1.49μm for coarse ground (grinding condition 2) surface. Effects that have contributed to these differences in fatigue lifetimes are discussed in detail in section 6.4.

6.2.2.2 Non Relieved Material Condition

Analysis of the crack growth results shown in tables B.2, B.9 and B.10, Appendix B, for material in non relieved condition indicated that, although grinding in condition 4 was the most severe, i.e. higher downfeed rate has been employed (see table 3.3), fatigue lifetimes from specimens ground in condition 4 were longer than those obtained from both condition 3 and polished condition (see figure 4.12(b)). The higher downfeed rate employed in grinding condition 4 would be expected to produce surfaces of much poorer quality regarding fatigue. Surface roughness measurements (e.g. R_a and R_v) shown in table 4.1 did not indicate, however, any considerable differences in roughness between surfaces ground in condition 3 and 4.

In spite of the apparent inconsistency of these observations they are in agreement with some of the results presented in the literature (see e.g. references [2][7][90]). Reference [90] shows, for example, that for a number of high temperature alloys, e.g. Grade 300 maraging steel, Ti-6Al-4V, René 95, high stress (or abusive) grinding procedures can give rise to the same fatigue response, and in some instances to higher fatigue strength than that obtained by conventional (or low stress) grinding procedures.

It must be pointed out that despite the higher downfeed rate employed in grinding condition 4 grinding procedures are still gentle if compared with those employed by other workers (see e.g. reference [7]).

Fatigue lifetime results from ground non relieved specimens were found to be related to the magnitude of the residual stresses introduced by the grinding operation. In spite of a poorer condition, compared for example with the pol-

ished surface, grinding in condition 4 induced residual compressive stresses (see section 4.4).

Effects of residual compressive stresses were also observed in previous works and were reviewed in section 2.4.2. SN results presented by Greenfield [2], for example, indicate a similar effect in a low alloy engineering steel (see figure 2.13). Effects of residual stresses induced by grinding operations are discussed in detail in section 6.4.3.

Fatigue lifetime results obtained from non relieved specimens, i.e. polished and grinding conditions 3 and 4 were compared. A Student's t statistics, described in the previous section, was used to assess the level of significance of the differences observed in mean fatigue lifetimes. Fatigue lifetimes observed in specimens ground in condition 4 were used as a base of comparison. Results of this statistics are shown in table 6.2.

Comparison of these results shows that fatigue lifetimes of specimens ground in conditions 3 and 4 are significantly different at the levels of 1% to 30% over the whole range of crack lengths observed. Differences in fatigue lifetime are most significant (1%) for crack lengths in the range of 12 and 25μm.

Differences in fatigue lifetime between the ground (condition 4) and polished specimens do not appear to be highly significant. The probability of the differences arising by chance are higher than 30% for crack lengths greater than 75μm. However, it can be noted from table 6.2 that the highest levels of significance, 5%, appear to arise for crack lengths in the range of 12 and 25μm, which coincides with the approximate depth of residual layer (20μm) found in this study.

Since the surface finish and the microstructure of specimens ground in conditions 3 and 4 were approximately the same it can be concluded that the differences observed in fatigue lifetime are mainly to be ascribed to the different residual stress patterns introduced by surface finishing operations (see section 4.4).

6.3 Fatigue Crack Initiation

6.3.1 Crack Initiation in Polished Surfaces

Short fatigue crack growth behaviour has been particularly emphasized in a number of recent experimental works. Most have been concerned with the natural initiation of cracks, i.e. from smooth surfaces such as those produced by mechanical and electrolytical polishing, their early propagation and interaction with metallurgical and microstructural features of the material.

In the present work, natural initiation of cracks was observed to occur in Waspaloy according to each one of the following mechanisms:

1. Initiation along slip bands, as shown in figure 5.1.

2. Initiation along twin boundaries, as shown in figure 5.2.

3. Initiation from grains showing no signs of slip bands, as shown in figure 5.3.

4. Initiation at grain boundaries, as shown in figures 5.4(a) and (b).

As observed by a number of previous workers [26][27][28][29], fatigue crack initiation in this nickel base superalloy appears to be predominantly associated with the mechanism described as (1), although other mechanisms of crack initiation, such as (2) and (4) observed in this study, were also referred in the literature, see e.g. references [29][82][83].

In the present work, the first two mechanisms of crack initiation, described as (1) and (2) were observed to occur more frequently in polished specimens in as-received condition, whereas initiation by the third mechanism (3) was predominant in polished specimens in stress relieved condition. The reason why the first two mechanisms of crack initiation could not be observed in stress relieved specimens may be related to the fact that some degree of surface oxidation could have been caused by the heat treating process. This may have impaired the initial mirror finish of the surface, thus preventing the observation of visible slip bands.

Exceptions to the rule of slip band cracking are fairly well understood and can be attributed to subsidiary effects, some of them have been discussed in

section 2.2.1. Zhang [83], in a study of the short crack growth in this superalloy, found that crack initiation and growth along grain boundaries might be attributed to different degrees of etching used by different workers. Deeper etching would make the microstructure clearer but it would severely reduce the strength of grain or twin boundaries, making them more prone to crack initiation.

It was clear in the present work that, irrespective of the mechanism and initiation site in the microstructure, cracks showed an initial orientation of approximately 45° with the principal axis of the specimen. This initial orientation suggests that crack initiation in bending specimens is a Mode II (shear mode) controlled process.

6.3.2 Crack Initiation in Ground Surfaces

The process of crack initiation has long been a major object of investigation. However, as described in the previous section, most of these studies have only been concerned with the natural initiation of cracks, e.g. from intrusions and extrusions caused by cyclic slip, observed in smooth surfaces of laboratory specimens.

From the results and observations made in the present work it appears that, despite the academic interest these studies may raise they are of little relevance to the understanding of the crack initiation process in engineering surfaces.

Extensive research in metal fatigue has shown that crack initiation in the surface of a real component is due to some type of stress raising feature. Stress concentration can result in the surface of a component due to (*i*) manufacturing defects, e.g. machining marks and scratches, (*ii*) notch-like discontinuities, introduced as a design feature of the component, and (*iii*) microstructural and metallurgical inhomogenities, e.g. inclusions, voids and triple points.

Moreover, observations made in the present study indicate that, although single deep and short grinding marks may be very effective as initiation sites cracks will propagate much faster as a result of the multiple initiation and subsequent coalescence which were observed to take place along longer grinding marks.

It appears therefore from the present study that much more investigation needs to be done in order to fully describe the role of engineering surface features

and their relationship with both fatigue crack initiation and propagation process.

Present techniques, such as optical and acoustic microscopy, though extremely valuable for the study of crack initiation in smooth surfaces (of laboratory specimens) do not appear to be totally suitable to observe this process in engineering surfaces.

6.4 The Metal Surface Condition - Effect of Surface Finishing Operations on Short Fatigue Crack Growth

6.4.1 Effect of Microstructure

It was evident in the present work that the growth of short cracks is strongly affected by microstructural features and that grain boundaries and twin boundaries act as microstructural barriers giving rise to an intermittent pattern of crack behaviour. Acceleration and deceleration periods are observed at crack lengths approximately multiples of the grain size. As observed by previous workers [14][26][28][29][41], cracks show a decreasing growth rate on approaching grain boundaries, slowing down to a minimum and even arresting (see e.g. figure 5.6(a), (b) and (c)) at or near grain boundaries. As shown in the replicas, after reaching the first grain boundary, cracks change their initial path and experience a period of increasing growth rate. Crack speed continues to rise until the crack tip approaches the next grain, when a further retardation and change of direction takes place.

It must be noted that this intermittent pattern of behaviour was observed in both polished and ground surfaces, indicating that the microstructural effect is present regardless of the grade of surface finish.

In a previous work, Zhang [83] noted that the grain boundary blocking effect occurred over a distance of several grain diameters, though the first boundary was the strongest barrier to crack growth. In the present work, however, this did not appear to be always the case. Stronger retardation effects were noted in

some instances after the crack had overcome the first or even the second grain boundary.

A measure of resistance to crack growth of a particular grain appears to be the change of path that cracks experience on reaching the nearest grain boundary. Small retardations in growth are usually followed by a slight change of direction, whereas strong retardations are usually followed by a steep change of direction, e.g. 90°.

An explanation of the 'zig-zag' type patterns of crack path observed in the short crack growth regime is provided by Boyd-Lee and King [106]. It is observed by these workers that both mode I and mode II components are operative in this regime. The mode I component tries to orientate the crack perpendicular to the tensile axis due to crack opening but the mode II component drives crack growth at 45° to the tensile axis. The attempt to satisfy both of these conditions results in this 'zig-zag' type pattern.

This discontinuous pattern of behaviour can be noted for crack lengths equivalent to several grain diameters, but eventually mode I predominates. The 'zig-zag' type pattern of crack path ceases to be evident and the crack path orientates itself approximately perpendicular to the tensile axis.

6.4.2 Effect of Surface Finish

The role of surface finish in metal fatigue has been given a lot of attention in the past only to include the effect of surface roughness. Surface roughness has often been regarded as an index of surface quality in fatigue design and one of the most critical factors in the fatigue performance of highly stressed components. It is widely accepted that exceedingly smooth surfaces, such as those produced by mechanical and electrolytical polishing, will provide the maximum fatigue strength for most engineering components. A logical explanation that has frequently been put forward is that the surface irregularities of a machined component have the same effect of a series of overlapping micro-notches. These micro-notches cause stress concentration and act as crack initiation sites making fatigue failure occur faster or at a lower nominal stress than it would occur in a

highly polished specimen. Accordingly, the greater the roughness of the surface of a machined component, the lower will be its fatigue strength.

In spite of the apparent support for this idea by a number of experimental studies (see section 2.4.2) it is to be noted that most of the present studies on the effect of surface finish still ignore the fact that any metal removal process will always introduce additional residual stresses, whose effects on fatigue crack growth will invariably interfere with those of the surface roughness produced by a particular finishing operation.

Observations made in the present study on a range of fine ground surfaces suggest that, if variations in surface roughness have any consistent relationship with the growth of short cracks this can only be applied to fatigue crack growth in specimens subject to prior annealing for stress relief.

As shown in tables B.5, B.7 and B.8, Appendix B, fatigue lifetime results for stress relieved material indicate that the mean number of cycles required for cracks to reach lengths in the range of 12μm to 800μm is reduced in a direct proportion with the grade of surface finish (shown in table 4.1).

Fatigue lifetimes for any given crack lengths were observed to be the longest in polished surfaces, which showed a surface roughness value $R_v = 0.15\mu m$. In comparison with the polished surfaces, fatigue lifetimes were observed to decrease in fine ground surfaces (grinding condition 1), having $R_v = 1.14\mu m$, and in coarse ground surfaces (grinding condition 2), having $R_v = 1.49\mu m$.

In spite of the consistent relationship between mean number of cycles and roughness values observed for all grades of surface finish in stress relieved specimens it is apparent that the faster growth rates observed in coarse ground surfaces (grinding condition 2) are not only related to the depth of the grinding marks of the surface but also to their length and orientation. It was observed from the present study that longer and deeper grinding marks give rise to multiple crack initiation sites. Due to the close proximity of these initiation sites (less than $100\mu m$ in this particular case) cracks will coalesce very early, and as a result much faster growth rates will take place. A detailed discussion of this process is presented in section 6.4.4.

Unlike the results obtained from stress relieved specimens, fatigue lifetime results from non-relieved specimens showed no consistent relationship with any of the surface roughness parameters shown in table 4.1.

Analysis of the results obtained from non-relieved specimens, shown in tables B.2, B.9 and B.10, Appendix B, indicates that longer fatigue lifetimes for any given crack lengths can be observed to occur in surfaces ground in condition 4, although the roughness value of this surface, $R_v = 0.46\mu m$, appears to be practically the same as in surfaces ground in condition 3 ($R_v = 0.52\mu m$), and greater than in polished surface condition ($R_v = 0.15\mu m$).

It follows from the discussion above that topographic features, such as the length and orientation of grinding marks, can strongly influence short crack growth response in a ground surface and give rise to different patterns of crack behaviour, as discussed in section 6.2.2. Since conventional surface texture parameters, such as R_a and R_v (shown in table 4.1), can not describe the physical aspect of an engineering surface it can be concluded that they have little relevance to the fatigue crack growth response of a ground surface.

Moreover, the initiation and early growth of short cracks in ground surfaces were observed to be controlled by residual stress patterns. In such cases it appears that gentle grinding operations can actually increase the crack growth resistance by producing a compressive residual stress layer, although it may give a rougher grade of finish than the polished or electropolished condition.

Support of this view is given by a number of studies which were reviewed in sections 2.4.2 and 2.4.3. Although none of these former studies were concerned with the direct observation of short crack growth behaviour, results available in form of SN-data appear to be consistent with those obtained in the present work.

El-Helieby and Rowe [7], for example, observed (see S-N results in figure 2.12) fatigue limits of 461 and $196 MNm^{-2}$ for conventional and abusive grinding, respectively, although the surface finish was practically the same, 0.56 and $0.55\mu m$. They also observed that the fatigue strengths of 883 and $196 MNm^{-2}$, exhibited by gentle and abusive grinding were in reverse order of the surface finishes, 1.0 and $0.55\mu m$, respectively.

As expressed by El-Helieby and Rowe [7], it appears that the effect of surface finish has been overemphasized in its general relationship to fatigue properties of materials, which can be completely dominated by residual stress patterns. It is also their view that surface roughness measurements as an index of surface quality for fatigue design purposes can be misleading and dangerous.

It follows that attempts to improve fatigue lifetimes of machine components by finely finishing their surfaces (through surface polishing and/or electropolishing operations) may in fact have the opposite effect. Since these operations can remove beneficial compressive residual layers introduced by previous operations, such as grinding, they can actually give rise to faster crack growth and result in earlier fatigue failure of the component.

6.4.3 Effect of Residual Stresses

Residual stresses induced by manufacturing procedures can result from a combination of mechanical, thermal and chemical effects. Residual stresses introduced by surface grinding procedures are mainly due to mechanical and thermal factors, although high temperatures generated by a particular grinding process may also cause phase transformation, such as rehardening and overtempering, producing residual stresses in the surface and subsurface layers.

Grinding forces can produce elastic and plastic deformation in the surface of a specimen or component (see reference [7]). In gentle grinding processes, such as those employed in the present work, high tensile grinding stresses can be expected to develop in the surface of the specimen during the grinding operation. The surface metal will yield, becoming more elongated than the subsurface layers and the core. As soon as the grinding force is removed, the surface layer will tend to return to its original form or length, but due to the constraint of the skin layer, which experienced elastic and plastic deformation, it can recover only the elastic part of its total elongation. As a consequence, the skin layer will continue to exert tension on the subsurface layer while experiencing compression itself. The magnitude and in-depth distribution of these residual stresses can be expected to vary with changes in the grinding conditions, shown for example in table 3.4 for

grinding conditions 3 and 4.

In the present work a direct correlation was found to exist between the residual stress magnitudes induced by the grinding process and the mean fatigue lifetimes of as-received (not relieved) specimens. The dependence of fatigue lifetimes with the magnitudes of surface residual stresses of ground specimens is represented in figure 5.23. This figure shows that as surface residual stress shifts from compression to increasing tension fatigue lifetimes (N/N_f) required for the crack to grow deeper, for example to $12\mu m$, $25\mu m$ and $50\mu m$, are progressively reduced.

Similar relationship to that presented in figure 5.23 was proposed by Koster [72] to express the effect of peak residual stress on fatigue strength of ground parts. Results of his study for a ground steel AISI 4340 (RC50) were shown in figure 2.17 and appear to be consistent with those presented in this work.

As it was said in section 2.4.3, whatever the nature of the residual stresses their effect on the fatigue properties are the same as if mean stresses of the same magnitude were superimposed on the applied stresses.

Based on the fatigue crack growth results obtained in this study from ground as-received (not relieved) specimens the effect of residual stress on short crack growth behaviour was illustrated by means of a da/dN versus a plot, which is presented in figure 6.2. Crack growth rates are shown in this plot to be not only affected by successive microstructural barriers but also by the residual stress fields induced by different grinding operations. Three distinct situations are shown in this plot according to the pattern of residual stresses developed by the grinding process:

1. For a surface in which residual stresses are non-existent, $\sigma_r = 0$, or of very low magnitude, such as that of highly polished, electropolished, or stress relieved specimens, short crack growth (represented in the figure by the thick solid line) will be strongly affected by microstructural barriers. As observed by a number of previous workers [14][63][27][29][60], cracks will initially exhibit high rates of growth which will decrease on approaching the first microstructural barrier (see figure). Cracks will show an intermit-

tent pattern of behaviour with acceleration and deceleration periods over a distance equivalent to several grain diameters.

2. For a surface in which residual stresses are tensile, $\sigma_r > 0$, short crack growth (represented in the figure by the dashed line) will also be strongly affected by microstructural barriers. However, because residual stresses and applied stresses have the same sign and direction, the magnitude of the combined mean stresses (see figure 5.24) in and near the surface will be higher than in the case of a stress-free surface. As a consequence the crack will initially grow faster than in the first case, but as it grows deeper and away from the residual stress field the effect of the superimposed mean stresses disappears, and its growth rate will progessively reduce to the same as in the stress-free surface.

3. For a surface in which residual stresses are compressive, $\sigma_r < 0$, short crack growth (represented in the figure by the dotted line) will also be strongly affected by microstructural barriers. However, because surface residual stresses (compressive stresses) are of opposite sign to the applied stresses (tensile stresses), the magnitude of the combined mean stresses (see figure 5.24) in and near the surface will be lower than in the case of a stress-free surface. As a consequence the crack will initially grow slower than in the first case, but as it grows deeper and away from the residual stress field the effect of the superimposed mean stresses disappears, and its growth rate will progressively increase to the same as in the stress-free surface.

It can be observed that the effect of residual stresses induced by grinding operations can be either beneficial or detrimental depending on their magnitude, sign and direction with respect to the applied stresses.

One question that can be raised regards the effect of such a thin residual layer on the fatigue lifetimes to propagate cracks in this superalloy. This can be appreciated by looking at the proportion of lifetime (see e.g. reference [110]) which is spent to propagate a crack to depths of $12\mu m$, $25\mu m$ and $50\mu m$, corresponding to the distance from a crack initiation site in the surface to the first

microstructural barrier in this nickel alloy. It was shown in this work that short crack growth can take a large proportion, which can be in excess of 40% of the total fatigue lifetime of a polished or fine ground specimen. A large proportion of the fatigue lifetime to failure for this superalloy can be spent with the crack growing within the first or second grain near the surface.

It can be appreciated that a lower mean stress near the surface or subsurface layer of a component will produce a delay in the early fatigue crack growth process. Such a lower mean stress, caused for example by a thin compressive residual layer of $20\mu m$, as shown in figure 6.2, will make cracks slower in reaching a depth of $12\mu m$, $25\mu m$ or $50\mu m$, and can be therefore regarded as highly beneficial in high cycle fatigue.

6.4.4 Effects of Crack Coalescence

As described in the previous sections, short crack growth in a ground surface cannot be related to any single surface texture parameter like R_a or R_v. Short crack growth in the present study has been shown to be affected not only by the depth of grinding marks but their length (see e.g. in the coarse ground surfaces 200 to 300μm) and orientation.

These three parameters appear, therefore, to control the short crack response in a ground surface. The depth of the grinding marks R_v appears to determine the crack initiation site or sites. Accordingly, it would appear that the deepest grinding marks of the surface would be the most favourable initiation sites, however, as shown by a number of workers, in some alloys cracks can initiate either from inclusions [14][33][34] or from particles of the grinding wheel becoming detached and embedded in the ground surface [1]. Such inclusions and particles may have an overriding effect as initiation sites, particularly if they are large enough.

In the absence of these defects, however, the depth of the grinding marks R_v will prevail in the control of the initiation site. On the other hand the length of the grinding marks appear to be related to the number of initiation sites and therefore with the number of cracks which will coalesce. Accordingly, the longer the grinding marks the greater the number of crack coalescence events that will

take place.

It follows that the two different crack growth responses observed in fine ground and coarse ground surfaces are related to two different patterns of crack coalescence: in a fine ground surface cracks will not coalesce within a single grinding mark, i.e. crack coalescence will not be collinear, whereas in a coarse ground surface coalescence will be collinear, i.e. along a single grinding mark.

It must be noted that multiple crack initiation and coalescence are common processes in many fatigue situations, and their effects have been observed in a number of recent studies, related particularly to high strain fatigue, high temperature conditions and environmental fatigue, see e.g. references [32] [107]. In most of these situations the severity of this process will be determined by the crack density, stress or strain range, number and location of corrosion pits, etc.. Individual subcracks have to change their original path decelerating at times before joining (see reference [107]). Although multiple initiation may occur, the coalescence of initiated cracks can be delayed depending upon the location of these subcracks. Such a delay will make the coalescence process less critical.

Unlike all these situations, in a ground surface having long and deep transverse marks the probability of cracks coalescing will be much higher. Since initiation sites are collinear crack growth will be assisted by the direction and depth of grinding marks. Closer initiation sites will make cracks join much earlier causing faster growth and failure of the component.

The begining of this process (colinear coalescence) appears to mark the transition between the two patterns of response observed in ground surfaces (patterns 'A' and 'B').

The roles of the depth, length and orientation of the grinding marks in the process of short crack coalescence appear to be of a much more complex nature. Their understanding and quantification is complicated by practical difficulties in controlling directly the physical character of engineering surfaces, i.e. depths and lengths of grinding marks, by simply acting on the machining or grinding parameters, i.e. downfeed, wheel speed, wheel hardness and coolant.

It is clear from what was previously said that further work is necessary in

order to understand the role of the physical character of engineering surfaces in the short crack behaviour.

6.5 Fatigue Crack Growth Modelling

The model adopted in this study (Yates and Grabowski model [81]) was based on detailed experimental studies of short crack growth in Waspaloy. The model in its original form was based on short crack growth results obtained from tension/tension fatigue tests (see reference [82]), and it was later developed to predict fatigue lives under four point bend loading (see reference [29]). Although it has been validated using a wide range of crack growth data the Yates and Grabowski model had not been previously used to simulate short fatigue crack growth in engineering surfaces, such as the ones obtained in the present study by grinding operations.

As observed in the present study, physical features such as the depth, length and orientation of grinding marks, can influence the short crack growth response in an engineering surface. Early coalescence of individual subcracks can take place in some instances, such as the case of specimens ground in condition 2, and cause specimens to fail much quicker than it would otherwise, i.e. without coalescence processes taking place. Moreover crack growth results obtained from ground surfaces in this study appear to indicate that, short fatigue crack growth in ground non-relieved specimens (grinding conditions 3 and 4) can be dominated by residual stress patterns.

As previously observed, application of this or other current short crack growth models would overstimate the fatigue lifetimes of specimens and engineering components. An extension of Yates and Grabowski model was therefore necessary in order to incorporate these unaccounted effects of surface topography and residual stress.

Predictions of fatigue lifetimes were made in the present study using both the four-point-bend version and the extended version, which is proposed in this work. Fatigue crack growth in polished surfaces was described by the four-point-bend version of the model [29] whereas the short crack growth in ground surfaces was

described by the extended version.

Results of the lifetime predictions are compared with the mean number of cycles observed from the experiments in Appendix C, and plotted in figures 5.13 to 5.18, 5.21 and 5.22, 5.26 and 5.27(a) and (b).

Fatigue lifetime predictions using the model have been shown to be satisfactory in most cases for the whole range of crack lengths investigated. Predictions of fatigue lifetimes to failure have also been made and showed good agreement with the endurance results obtained from the experiments.

Regarding the predictions of lifetimes to failure it must be noted that although in some cases predictions were not conservative they did not exceed too much the upper limit of the scatter band (N_{+1sd}).

It was observed that there was only one case (set of tests corresponding to grinding condition 3) in which predictions can be considered dangerously unsafe (see table C.9, Appendix C and figures 5.26(a) and (b)). Table C.9 shows, however, that these predictions are in good agreement with the experimental results for crack lengths within the range of 12 to $600\mu m$. In looking for an explanation for the increasing disagreement between N_{model} and N_{mean} for cracks longer than $600\mu m$ it was observed from the replicas that one of the dominant cracks investigated propagated towards the edge of the specimen at a very early stage. Although crack initiation from the edges was successfully avoided in most specimens by polishing their edges this measure was not effective in preventing any crack from propagating towards the edge as it happened in this specific case.

It is appropriate to point out that, to the knowledge of the author, the model in its extended version represents the first attempt to describe short fatigue crack growth in engineering surfaces, such as those produced by grinding operations. Although based on a detailed experimental study the model is in an early stage of development and further experimental work is necessary to test it.

6.5.1 Comparison of Theoretical and Experimental S-N Curves for Polished Surfaces

Predicted lifetimes to failure were plotted in figures 6.3(a) and (b) together with the endurance results of the 14 polished surface specimens which were tested.

Power regression curves were fitted to the endurance results obtained from the tests and are represented in the plots by the solid lines. These regression curves can be expressed by the 'Basquin' type equations 4.1 and 4.2, which were described in chapter 4.

A best-fit analysis was applied to the data points corresponding to the theoretical (calculated) number of cycles to failure (see tables C.1 to C.6, Appendix C). The best-fit curves obtained from this analysis are represented in the plots by the dotted lines.

Comparison of the presented theoretical and experimental S-N curves indicates that satisfactory predictions have been achieved in all ranges of applied stress for both treatment conditions. It also shows that the assumptions made in the calculations, i.e. (a) fatigue as a two stage crack growth process, (b) no crack initiation period, and (c) the change from Stage I to Stage II is accomplished with no delay, are valid for design purposes and give good agreement with the experimental results.

It follows that theoretical S-N curves can be predicted by integrating fracture mechanics based equations such as 5.1 and 5.2 and that fracture mechanics equations, which were used in the present work to describe Stage I and Stage II crack growth, can provide a basis for the physical understanding of the conventional S-N diagrams.

Chapter 7

Conclusions and Future Work

7.1 Conclusions

Based on the experimental observations and theoretical analysis carried out in the present work with regard to the effect of manufacturing operations on short fatigue crack growth of Waspaloy at room temperature the following conclusions can be presented:

1. Fatigue crack growth was observed to follow two distinct patterns of behaviour, namely patterns 'A' and 'B', which appear to be related with the surface topography produced by the finishing operations.

2. Cracks developing pattern 'A' of behaviour appeared to be deflected from their initial path as a result of the surface microstructure and not to be affected by the depth and orientation of the grinding marks produced in the surface of the specimens.

3. Cracks developing pattern 'B' of behaviour initiated and propagated along the grinding marks, showing to be strongly affected by the depth and orientation of surface defects.

4. Faster growth rates observed in pattern 'B' are due to coalescence processes. Such coalescence processes result from multiple and collinear crack initiation along grinding marks.

5. Short fatigue crack growth behaviour in ground surfaces cannot be related to any conventional surface texture parameters, such as R_a or R_v.

6. Short crack growth is affected not only by the depth of grinding marks but also by their length and orientation.

7. Since conventional surface texture parameters, such as R_a and R_v, cannot describe the physical character of a engineering surface they appear to be of little relevance to the short fatigue crack growth response of a ground surface.

8. Although single deep and short grinding marks may be very effective as initiation sites cracks will propagate much faster as a result of the multiple initiation and subsequent coalescence which take place along longer grinding marks.

9. The initiation and early growth of short cracks in ground surfaces can be controlled by residual stress patterns. In such cases it appears that fine grinding operations can actually increase the crack growth resistance by producing a compressive residual stress layer, although it may give a rougher grade of finish than the polished or electropolished condition.

10. Since fatigue crack initiation occurs predominantly at the surface of the specimen and at regions of maximum tensile stresses, an intentionally produced thin surface layer of residual compressive stress can greatly improve fatigue lifetimes of components.

11. Attempts to improve fatigue lifetimes of machine components by finely finishing their surfaces (through surface polishing and/or electropolishing operations) may have the opposite effect. These finishing operations can remove beneficial compressive residual layers introduced by previous operations, such as grinding, giving rise to faster crack growth rates and shorter fatigue lifetimes.

12. Natural crack initiation in this nickel base alloy occurs predominantly along persistent slip bands (PSB) and twin boundaries, although initiation from

grain boundaries and from grains showing no signs of slip bands can also be observed.

13. Irrespective of the initiation site cracks show an initial orientation of approximately 45° with the principal axis of the specimen. This initial orientation indicates that natural crack initiation in bending specimens occurs by a Stage I Mode II (shear mode) process.

14. Short crack growth in this alloy was observed to be of intermittent nature. Cracks experience a succession of acceleration and deceleration periods over a distance equivalent to several grain diameters.

15. Cracks experience a decreasing growth rate on approaching grain boundaries, slowing down to a minimum and even arresting at or near grain boundaries.

16. Microstructural short crack growth rates in Waspaloy are faster than the corresponding growth rates for long cracks at equivalent stress intensity ranges below the transition crack length.

17. A short crack growth model (Yates-Grabowski model) was used in the present study to simulate fatigue crack behaviour and predict fatigue crack growth rates and fatigue lifetimes to failure. The model gives satisfactory predictions when compared with experimental data.

7.2 Future Work

1. In the present work the effect of the grinding marks was investigated in a single transverse direction, however it was apparent that the direction of these marks will play an important role on the coalescence process. It is therefore necessary to investigate the effect of the orientation of the grinding marks on short crack growth.

2. Significant improvement in fatigue crack growth results (resistance) was obtained by heat treating this alloy at 1010°C. Comparison of the fatigue

lifetime results in the as-received and heat treated conditions indicates that the increased lifetimes obtained under room temperature high cycle fatigue in the heat treated condition may be associated with important changes in the metallurgical condition of this alloy, such as distribution and sizes of precipitates. These alterations in metallurgical condition may have produced substantial changes in the thermomechanical properties of this alloy. It is therefore necessary to investigate the creep and creep-fatigue properties in the heat treated condition and compare them with the previous condition.

References

[1] Suhr, R.W., 1986, *The Effect of Surface Finish on High Cycle Fatigue of a Low Alloy Steel*, The Behaviour of Short Fatigue Cracks, EGF Pub.1, Eds. K. J. Miller and E. R. de Los Rios, Mechanical Engineering Publications, London, pp. 69-86.

[2] Greenfield, P. and Allen, D.H., 1987, *The Effect of Surface Finish on High Cycle Fatigue Strength of Materials*, GEC J. Res., Vol. 5, pp. 5-12.

[3] Greenfield, P., Allen, D.H., Byrne, P. and Taylor, D., 1990, *Surface Roughness Effects on Fatigue: A Fracture Mechanics Approach*, Fatigue 90, Fourth International Conference on Fatigue and Fatigue Thresholds, Hawaii, Eds. H. Kitagawa and T. Tanaka, EMAS, Warley, UK, 1990, Vol. 1, pp. 391-396.

[4] Wagner, L. and Lütjering, G., 1990, *Influence of Surface Condition on Fatigue Strength*, Fatigue 90, Fourth International Conference on Fatigue and Fatigue Thresholds, Hawaii, Eds. H. Kitagawa and T. Tanaka, EMAS, Warley, UK, Vol. 1, pp.323-328.

[5] Taylor, D. and Clancy, O.M., 1991, *The Fatigue Performance of Machined Surfaces*, Fatigue Fract. Engng. Mater. Struct., Vol.14, No.213, pp.329-336.

[6] Hyler, W.S., 1958, *Extra Fatigue Strength Is Now Available*, SAE Journal, pp. 40-41.

[7] El-Helieby, S.O.A. and Rowe, G.W., 1980, *Influences of Surface Roughness and Residual Stress on Fatigue Life of Ground Steel Components*, Met. Tech., Vol. 7, pp. 221-225.

[8] Metals Handbook, Desk Edition, 1983, *Surface Texture and Integrity*, Chap. 27, pp. 20-26, American Society for Metals.

[9] Dieter, G.E., 1986, *Mechanical Metallurgy*, 3rd Edition, McGraw-Hill Book Company, New York.

[10] Miller, K.J., 1987, *The Behaviour of Short Fatigue Cracks and Their Initiation: Part II - A General Summary*, Fatigue Fract. Engng. Mater. Struct., Vol. 10, No. 2, pp. 93-113.

[11] Pook, L.P., 1983, *The Role of Crack Growth in Metal Fatigue*, 1st Edition, Metal Society, London.

[12] Irwin, G.R., 1957, *Fracture Mechanics*, J. App. Phys., Vol. 24, pp. 361-364.

[13] Pearson, S., 1975, *Initiation of Fatigue Cracks in Commercial Aluminum Alloys and Subsequent Propagation of Very Short Fatigue Cracks*, Eng. Fract. Mechanics, Vol. 7, pp. 235-247.

[14] Lankford, J., 1982, *The Growth of Small Fatigue Cracks in 7075-T6 Aluminum*, Fatigue Engng. Mater. Struct., Vol. 5, pp. 233-248.

[15] Miller K.J., 1982, *The Short Crack Problem*, Fatigue Engng. Mater. Struct., Vol. 5, pp. 223-232.

[16] Suresh, S. and Ritchie, R.O., 1984, *Propagation of Short Fatigue Cracks*, Int. Met. Rev., Vol. 29, pp. 445-476.

[17] Davidson, D.L. and Lankford, J., 1985, *Experimental Mechanics of Fatigue Crack Growth: The Effect of Crack Size*, Fundamentals of Deformation and Fracture, IUTAM Eshelby Memorial Symposium, Eds. B.A. Bilby, K.J. Miller and J.R. Willis, pp. 559-572, Cambridge University Press.

[18] Brown. M.W., 1986, *Interfaces Between Short, Long and Non-propagating Cracks*, The Behaviour of Short Fatigue Cracks, EGF Pub.1, Eds. K.J. Miller and E.R. de los Rios, Mech. Eng. Publications Ltd., London, pp. 423-439.

[19] Schijve, J., 1979, *Four Lectures on Fatigue Crack Growth*, Engng. Fract. Mechanics, Vol. 11, pp. 167-221.

[20] Miller, K.J., 1982, *The Short-Crack Problem*, Proc. Mech. & Thermal Behaviour of Metallic Materials, LXXXII Corso, pp. 165-175, Soc. Italiana di Fisica, Bologna, Italy.

[21] Forsyth, P.J.E., 1961, *A Two Stage Process of Fatigue Crack Growth*, Proc. Crack Propagation Symposium, Cranfield, Vol. 1, pp. 76-94.

[22] Brown, M.W. and Miller, K.J., 1973, *A Theory for Fatigue Failure Under Multiaxial Stress-Strain Conditions*, Proc. Inst. Mech. Engrs., Vol. 187, Inst. Mech. Engrs., London, pp. 745-755.

[23] Thomson, N., Wadsworth, N.J. and Louat, N., 1956, *The Origin of Fatigue Fracture in Copper*, Phil. Mag., Vol. 1, pp. 113-126.

[24] Forsyth, P.J.E., 1951, *Some Metallographic Observations on the Fatigue of Metals*, J. Inst. Metals, Vol. 80, pp. 181-186.

[25] Cottrell, A.H. and Hull, D., 1957, *Extrusion and Intrusion by Cyclic Slip in Copper*, Proc. Roy. Soc., Vol. A242, pp. 211-213.

[26] Brown, C.W., King, J.E. and Hicks, M.A., 1984, *Effects of Microstructure on Long and Short Crack Growth in Nickel Base Superalloys*, Metal Science, Vol. 18, pp. 374-380.

[27] Grabowski, L. and King, J.E., 1992, *Modelling Short Crack Growth Behaviour in Nickel-Base Superalloys*, Fatigue Fract. Engng. Mater. Struct., Vol. 15, No. 6, pp. 595-606.

[28] Stephens, R.R., Grabowski, L. and Hoeppner, D.W., 1993, *The Effect of Temperature on the Behaviour of Short Fatigue Cracks in Waspaloy Using an In Situ SEM Fatigue Apparatus*, Int. J. Fatigue, Vol. 15, No. 4, pp. 273-282.

[29] Yates, J.R., Zhang, W. and Miller, K.J., 1993, *The Initiation and Propagation Behaviour of Short Fatigue Cracks in Waspaloy Subjected to Bending*, Fatigue Fract. Engng. Mater. Struct., Vol. 16, No. 3, pp. 351-362.

[30] De los Rios, E.R., Tang, Z. and Miller, K.J., 1984, *Short Crack Fatigue Behaviour in a Medium Carbon Steel*, Fatigue Fract. Engng. Mater. Struct. Vol. 7, pp. 97-108.

[31] Klesnil, M. and Lukas, P., 1992, *Fatigue of Metallic Materials*, 2nd Rev. Edition, Elsevier Scientific Publishing Company, Oxford, pp 65-91.

[32] Shaikh, Z., 1991, *Initiation, Propagation and Coalescence of Short Fatigue Cracks in AISI Stainless Steel at 20 and* $550°C$, Ph.D. Thesis, University of Sheffield.

[33] Fine, M.E., 1980, *Fatigue Resistance of Metals*, Metall. Trans., Vol. 11A, pp. 365-379.

[34] Khalifa, T.A., 1988, *Effect of Inclusion on the Fatigue Limit of a Heat Treated Carbon Steel*, Mat. Sc. Eng., 102A, pp. 175-180.

[35] Murtaza, G., 1992, *Corrosion Fatigue Short Crack Growth Behaviour in a High Strength Steel*, Ph.D. Thesis, University of Sheffield.

[36] Tomkins, B., 1981, *High Strain Fatigue*, In Subcritical Crack Growth Due to Fatigue, Stress Corrosion and Creep: Lectures from a course held at the Joint Research Centre, ISPRA (Italy) October 19th - 23rd, 1981 in collaboration with the European Group on Fracture, Ed. L.H. Larsson, Elsevier Applied Science Publishers.

[37] Laird, C. and Smith, C.G, 1963, *Initial Stages of Damage in High Stress Fatigue in Some Pure Metals*, Phil. Mag., Vol. 8, pp. 1945-1963.

[38] McMillan, J.C. and Pelloux, R.M.N., 1967, *Fatigue Crack Propagation under Program and Random Loads*, Fatigue Crack Propagation, ASTM STP415, pp 505-532.

[39] Duggan, T.V. and Byrne, J., 1977, *Metallurgical Aspects of Fatigue*, Fatigue as a Design Criterion, The MacMillan Press Ltd., London.

[40] Morris, W.L., 1980, *The Non-Continuum Crack Tip Deformation Behaviour of Surface Microcracks*, Metall. Trans. 11A, pp. 1117-1123.

[41] Taylor, D. and Knott, J.F., 1981, *Fatigue Crack Propagation Behaviour of Short Cracks; The Effects of Microstructure*, Fatigue Engng. Mater. Struct., Vol. 4, pp. 147-155.

[42] Knott, J.F., 1981, *Fundamentals of Fracture Mechanics*, Butterworths, London.

[43] Broek, D., 1989, *The Practical Use of Fracture Mechanics*, 1st Edition, Kluwer Academic Publishers, Dordrecht, The Netherlands.

[44] Rooke, D.P. and Cartwright, D.J., 1976, *A Compendium of Stress Intensity Factors Handbook*, HMSO, London.

[45] Tada, H., Paris, P.C. and Irwin, G.R., 1985, *The Stress Intensity of Cracks Handbook*, Del Research Corporation, Hellertown, PA, USA.

[46] Murakami, Y., 1987, *Stress Intensity Factors Handbook*, Pergamon Press, Oxford.

[47] Smith, R.A., 1978, *An Introduction to Fracture Mechanics for Engineers; Part I: Stresses Due to Notches and Cracks*, Mat. in Eng. Appl., Vol. 1, pp. 121-128.

[48] Frost, N.E., Marsh, K.J. and Pook, L.P., 1974, *Metal Fatigue*, Oxford Engineering Science Series.

[49] Smith, R.A., 1978, *An Introduction to Fracture Mechanics for Engineers; Part II: Using the Stress Intensity Factor to Characterise Fracture and Fatigue Crack Growth*, Mat. in Eng. Appl., Vol. 1, pp. 227-235.

[50] Paris, P.C. and Erdogan, F., 1963, *A Critical Analysis of Crack Propagation Laws*, J. Basic Engineering, Trans. ASME, Vol. 85, pp. 528-534.

[51] LeMay, I., 1981, *Principles of Mechanical Metallurgy*, Edward Arnold Publishers, London.

[52] Campbell, J.E, Gerberich, W.W. and Underwood, J.H., 1982, *Application of Fracture Mechanics for Selection of Metallic Structural Materials*, American Society for Metals, Metals Park, Ohio.

[53] Ritchie, R.O., 1979, *Near Threshold Fatigue-Crack Propagation in Steels*, Int. Met. Rev., Vol. 24, No. 5 and 6, pp. 205-230.

[54] Richards, C.E. and Lindley, T.C., 1972, *The Influence of Stress Intensity and Microstructure on Fatigue Crack Propagation in Ferritic Materials*, Engng. Fract. Mechanics, Vol. 4, pp. 951-978.

[55] Miller, K.J., 1987, *The Behaviour of Short Fatigue Cracks and Their Initiation: A Review of Two Recent Books*, Part-1, Fatigue Fract. Engng. Mater. Struct., Vol. 10, pp. 75-91.

[56] Kitagawa, H. and Takahashi, S., 1976, *Applicability of Fracture Mechanics to Very Small Cracks or the Cracks in the Early Stage*, Proc. 2nd Int. Conf. Mech. Behaviour of Materials, ICM2 American Society for Metals, Ohio, pp. 627-631.

[57] Smith, R.A., 1977, *On the Short Crack Limitations of Fracture Mechanics*, Int. J. Fracture., Vol. 13, pp. 717-720.

[58] Taylor, D., 1986, *Fatigue of Short Cracks: the Limitation of Fracture Mechanics*, The Behaviour of Short Fatigue Cracks, EGF Pub.1, Eds. K.J. Miller and E.R. de los Rios, pp. 479-490.

[59] Tarasov, L.P., Hyler, W.S. and Letner, H.R., 1958, *Effect of Grinding Direction and of Abrasive Tumbling on the Fatigue Limit of Hardened Steel*, Proc. Am. Soc. Mater., 58, pp. 528-539.

[60] Sheldon, E.P., Cook, T.S., Jones, J.W. and Lankford, J., 1981 *Some Observation on Small Fatigue Cracks in a Superalloy*, Fatigue Engng. Mater. Struct., Vol. 3, pp. 219-228.

[61] De los Rios, E.R., Mohamed, H.J. and Miller, K.J., 1985, *A Micro-mechanics Analysis for Short Fatigue Crack Growth*, Fatigue Fract. Engng. Mater. Struct. Vol. 8, pp. 49-63.

[62] Brown, C.W. and Hicks, M.A., 1983, *A Study of Short Fatigue Crack Growth Behaviour in Titanium Alloy IMI685*, Fatigue Engng. Mater. Struct., Vol. 6, pp. 67-76.

[63] Navarro, A. and de los Rios, E.R., 1988, *Short and Long Fatigue Crack Growth. A Unified Model*, Phil. Mag., Vol. 57, pp. 15-36.

[64] Miller, K.J., 1991, *Metal Fatigue - Past, Current and Future*, 27th John Player Lecture, Proc. Instn. Mech. Engrs., Vol. 205, Inst. Mech. Engrs., London, pp. 1-14. .

[65] McCarver, J.F. and Ritchie, R.O., 1982, *Fatigue Crack Propagation Thresholds for Long and Short Cracks in René 95 Nickel-Base Superalloy*, Mater. Sci. Eng., Vol. 55, pp. 63-67.

[66] Ritchie, R.O. and Suresh, S., 1982, *A Geometric Model for Fatigue Crack Closure Induced by Fracture Surface Roughness*, Metall. Trans., Vol. 13A, pp. 1627-1631.

[67] James, M.R. and Morris, W.L., 1983, *Effect of Fracture Surface Roughness on Growth of Short Fatigue Cracks*, Metall. Trans., Vol. 14A, pp. 153-155.

[68] Sherrington, I. and Smith, E.H., 1987, *Parameters for Characterizing the Surface Topography of Engineering Components*, Proc. Instn. Mech. Engnrs., Vol. 201, No. C4, pp. 297-306.

[69] Rosenthal, D., 1959, *Influence of Residual Stress on Fatigue*, Metal Fatigue, Eds. G. Sines and J.L. Waisman, pp. 170-196, McGraw-Hill, New York.

[70] Fuchs, H.O., 1972, *Regional Tensile Stress as a Measure of the Fatigue Strength of Notched Parts*, in Proceedings 1971 International Conference on Mechanical Behaviour of Materials, Society of Materials Science, Kyoto, Japan, Vol. II, pp. 478-488.

[71] Almen, J.O. and Black, P.H., 1963, *Residual Stresses and Fatigue in Metals*, McGraw-Hill, New York.

[72] Koster, W.P., 1974, *Surface Integrity of Machined Materials*, Technical Report AFML-TR-74-60.

[73] Forsyth, P.J.E., 1969, *The Physical Basis of Metal Fatigue*, Chap. 10, pp. 165-177, Ist Edition, Blackie & Son Limited, London.

[74] Winholtz, R.A. and Cohen, J.B., 1992, *Changes in the Macrostresses and Microstresses in Steel with Fatigue*, Mat. Sci. and Eng., A154, pp. 155-163.

[75] Morris, W.L., James, M.R. and Buck, O., 1981, *Growth Rate Models for Short Surface Cracks in Aluminum 2219-T851*, Metall. Trans., Vol. 12A, pp. 57-64.

[76] Chan, K.S. and Lankford, J., 1983 *A Crack-tip Strain Model for the Growth of Small Fatigue Cracks*, Scripta Metal., Vol. 17, pp. 529-532.

[77] Zurek, A.K., James, M.R. and Morris, W.L., 1983, *The Effect of Grain Size on Fatigue Growth of Short Cracks*, Metallurgical Trans., Vol. 14A, pp. 1697-1705.

[78] Hobson, P.D., 1985, *The Growth of Short Fatigue Cracks in a Medium Carbon Steel*, Ph.D. Thesis, University of Sheffield.

[79] Hobson, P.B., Brown, M.W. and de los Rios, E.R., 1986, *Two Phases of Short Crack Growth in a Medium Carbon Steel*, The Behaviour of Short Fatigue Cracks, EGF Pub.1, Eds. K.J. Miller and E.R. de los Rios, Mech. Eng. Publications Ltd., London, pp. 441-459.

[80] Navarro, A. and de los Rios, E.R., 1988, *A Microstruturally-Short Fatigue Crack Growth Equation*, Fatigue Fract. Engng. Mater. Struct., Vol. 11, pp. 383-396.

[81] Yates, J.R. and Grabowski, L., 1990, *Fatigue Life Assessment Using a Short Crack Growth Model*, Proceedings of the Fourth International Conference

on Fatigue and Fatigue Thresholds, Fatigue'90, Hawaii, 1990, Vol. 4, pp. 2369-2376, Eds. H. Kitagawa and T. Tanaka, EMAS, Warley, UK.

[82] Wang, S.Z., Miller, K.J., Brown, M.W. and de los Rios, E.R., 1990, *A Statistical Analysis of Short Fatigue Crack Growth*, Fatigue Fract. Engng. Mater. Struct., Vol. 14, pp. 351-368.

[83] Zhang, W., 1991, *Short Fatigue Crack Growth Under Different Loading Systems*, Ph.D. Thesis, University of Sheffield.

[84] Navarro, A. and de los Rios, E.R., 1988, *A Model for Short Fatigue Crack Propagation with an Interpretation of the Short-Long Crack Transition*, Fatigue Fract. Engng. Mater. Struct., Vol. 10, pp. 169-186.

[85] Taira, S., Tanaka, K. and Hoshina, M., 1979, *Grain Size Effect on Crack Nucleation and Growth in Long-Life Fatigue of Low Carbon Steel*, Fatigue Mechanisms, Ed. J.T. Fong, ASTM STP 675, pp. 135-173.

[86] Navarro, A. and de los Rios, E.R., 1988, *An Alternative Model of the Blocking of Dislocations at Grain Boundaries*, Phil. Mag. A, Vol. 57, pp. 37-42.

[87] Hourlier, F. and Pineau, A., 1981, *Fatigue Crack Propagation Behaviour under Complex Mode Loading*, Advances in Fracture Research, ICF5, Ed. D. François, pp. 1833-1840.

[88] Yates, J.R., 1990, *An Investigation of Test Geometry and Data Analysis Procedures for Short Crack Growth in Waspaloy at* $19°C$, Report to Rolls-Royce plc., Department of Mechanical & Process Engineering, University of Sheffield.

[89] Forsyth, P.J.E., 1969, *The Physical Basis of Metal Fatigue*, Chap. 2, pp. 27-33, Ist Edition, Blackie & Son Limited, London.

[90] Metals Handbook, Ninth Edition, 1981, *Heat Treating*, Vol. 4, pp. 650-671, American Society for Metals.

[91] Lankford, J., 1977, *Initiation and Early Growth of Fatigue Cracks in High Strength Steel*, Eng. Fract. Mechanics, Vol. 9, No. 3, pp. 617-624.

[92] Brown, C.W. and Smith, G.C., 1982, *A Two Stage Plastic Replication Technique for Monitoring Fatigue Crack Initiation and Early Crack Growth*, Advances in Crack Length Measurement, Ed. C.J. Beevers, Engineering Materials Advisory Services Ltd., pp. 41-52.

[93] Newman, J.C.,Jr. Swain, M.H. and Phillips, E.P., 1987, *An Assessment of the Small Crack Effect for 2024-T3 Aluminium Alloy*, Small Fatigue Cracks, Eds. R.O. Ritchie and J. Lankford, The Metallurgical Society, pp. 427-452.

[94] Birt, M.J. and Beevers, C.J., 1989, *The Fatigue Response of the Aluminun-Lithium Alloy, 8090*, Proceedings of the Fifth International Aluminium Lithium Conference, Eds. T.H. Sander and E.A. Starke, pp. 893-992.

[95] Rao, K.T.V. and Ritchie, R.O., 1989, *Mechanical Properties of Al-Li Alloys, Part 2 - Fatigue Crack Propagation*, Material Science and Technology, Vol. 5, pp. 896-907.

[96] Swain, M.H., 1992, *Monitoring Small-Crack Growth by the Replication Method*, Small Crack Test Methods, ASTM STP 1149, Eds. J.M. Larsen and J.E. Allison, American Society for Testing and Materials, pp. 34-56.

[97] Engineering Sciences Data , 1991, *Fatigue - Endurance Data Volume 2, Statistical methods*, Engineering Sciences Data Unit.

[98] Miller, K.J., 1985, *Initiation and Growth Rates of Short Fatigue Cracks*, Fundamentals of Deformation and Fracture, IUTAM Eshelby Memorial Symposium, Eds. B.A. Bilby, K.J. Miller and J.R. Willis, pp. 477-500, Cambridge University Press.

[99] Hobson, P.D., 1982, *The Formulation of a Crack Growth Equation for Short Cracks*, Fatigue Engng. Mater. Struct. Vol. 5, No. 4, pp. 323-327.

[100] Wang, C.H. and Miller, K.J., 1992, *The Effect of Mean and Alternating Shear Stress on Short Fatigue Crack Growth Rates*, Fatigue Fract. Engng. Mater. Struct., Vol. 15, No. 12, pp. 1223-1236.

[101] Healy, J.C., 1989, *Short Fatigue Crack Growth at Elevated Temperature*, PhD Thesis, University of Birmingham.

[102] Chatfield, C., 1983 *Statistics for Technology - A Course in Applied Statistics*, 3rd Edn., Chapman and Hall.

[103] Lee, J.D. and Lee, T.D., 1982, *Statistics and Computer Methods in BASIC*, Van Nostrand Reinhold Company, Wokingham, England.

[104] Tagahani, N. and Powell, B.E., 1988, *Threshold Testing for Vibration Assessment of Turbine Disc and Blade Materials*, Report of Dept. of Mech. Eng., Portsmouth Polytechnic, UK.

[105] Newman, J.C., Jr. and Raju, I.S., 1987, *Stress Intensity Factors Handbook*, Ed. Y. Murakami, Pergamon Press, Oxford, pp. 42-45.

[106] Boyd-Lee, A.D. and King, J.E., 1990, *Crack Initiation and the Short-To-Long Crack Growth Transition in a Ni-Base Superalloy*, Fatigue 90, Fourth International Conference on Fatigue and Fatigue Thresholds, Hawaii, Eds. H. Kitagawa and T. Tanaka, EMAS, Warley, UK, Vol. 1, pp. 1205-1210.

[107] Rehman, H.U., 1991, *The Influence of Microstructural Variables on the Growth of Short Fatigue Cracks in a High Strength Steel*, Ph.D. Thesis, University of Sheffield.

[108] Koster, W.P., 1970, *Surface Integrity of Machined Structural Components*, Technical Report AFML-TR-70-11.

[109] Wang, C.H. and Miller, K.J., 1993, *Short Fatigue Crack Growth under Mean Stress, Uniaxial Loading*, Fatigue Fract. Engng. Mater. Struct., Vol. 16, No. 2, pp. 181-198.

[110] Boabaid, J.S. and Yates, J.R., 1993, *The Effect of the Grinding Condition on Short Fatigue Crack Growth in Waspaloy at* $19°C$, Durability and Structural Reliability of Airframes, Proceedings of the 17th International Committee on Aeronautical Fatigue Symposium, Ed. E.F. Blom, EMAS, Warley, West Midlands, pp. 883-898.

Tables

Cr	Co	Mo	Ti	Al	Fe	C	Ni
19.5	13.5	4.2	3.0	1.4	1.0	0.06	balance

Table 3.1 - Nominal chemical composition in weight % of Waspaloy.

0.2% Proof Strength	880MPa
Ultimate Tensile Strength	1250MPa
Young's Modulus	215GPa
Poisson's Ratio	0.3

Table 3.2 - Mechanical properties of Waspaloy.

Grinding parameters	Condition 1	Condition 2	Condition 3	Condition 4
Grinding wheel	GC46LV[a]	GC46LV[a]	GC60-17V[b]	GC60-17V[b]
Wheel speed	2570rpm	2570rpm	2570rpm	2570rpm
Table speed	*[c]	*[c]	14m/min	14m/min
Crossfeed per pass	1mm	1mm	1mm	1mm
Infeed rate (roughening)	10μm	10μm	10μm	10μm
Infeed rate (finishing)	5μm	*[d]	4μm	20μm
Grinding fluid	Soluble oil	Soluble oil	Soluble oil	Soluble oil

(a) No wheel dressing performed.

(b) Wheel dressing performed after the roughening operation.

(c) Table speed not measured.

(d) No finishing operation performed.

Table 3.3 - Surface grinding parameters for four-point-bend specimens.

$\Delta\sigma$ [MPa]	σ_{max} [MPa]	$\sigma_{min}/\sigma_{max}$
750	833	0.1
792	880	0.1
850	880	0.03

Table 3.4 - Applied stress ranges, maximum stress and stress ratios in four point bend tests.

Surface Condition	$R_a[\mu m]$	$R_p[\mu m]$	$R_v[\mu m]$	$R_y[\mu m]$	$R_{zDIN}[\mu m]$
Polished	0.05	0.22	0.15	0.35	0.29
Ground (Condition 1)	0.40	4.12	1.14	5.27	2.60
Ground (Condition 2)	0.51	1.99	1.49	3.22	2.59
Ground (Condition 3)	0.11	0.51	0.52	0.84	0.77
Ground (Condition 4)	0.12	0.62	0.46	1.00	0.78

Table 4.1 - Measurements of Surface Texture Parameters.

Specimen	Final Surface and Treatment Condition	$\Delta\sigma$ [MPa]	N_f [cycles]
F5	Ground (cond.1)/Stress relieved	792	528000
Mean			528000
F6	Ground (cond.2)/Stress relieved	792	351650
F9	Ground (cond.2)/Stress relieved	792	295000
F10	Ground (cond.2)/Stress relieved	792	368000
Mean			338217
F22	Ground (cond.3)/As-received	792	298374
F23	Ground (cond.3)/As-received	792	268020
Mean			283197
F27	Ground (cond.4)/As-received	792	356718
F28	Ground (cond.4)/As-received	792	378568
Mean			367643

Table 4.3 - Fatigue lifetimes to failure for ground surface specimens in stress relieved and as-received condition.

Specimen	Final Treatment Condition	$\Delta\sigma$ [MPa]	N_f [cycles]
F1	As-received	850	135000
F2	As-received	850	135000
F3	As-received	850	135000
Mean			135000
F33	As-received	792	324872
F34	As-received	792	375950
Mean			350411
F4	As-received	750	600000
F32	As-received	750	616634
Mean			608317
F15	Stress relieved	850	425957
F18	Stress relieved	850	417724
Mean			421841
F12	Stress relieved	792	598000
F13	Stress relieved	792	502000
F14	Stress relieved	792	497000
Mean			532333
F19	Stress relieved	750	897101
F20	Stress relieved	750	733229
Mean			815165

Table 4.2 - Fatigue lifetimes to failure for polished surface specimens in as received and stress relieved conditions.

	Polished vs. Ground (cond.1)			Polished vs. Ground (cond.2)		
a [μm]	degrees of freedom	Student's t	Significance	degrees of freedom	Student's t	Significance
12	11	1.484	<20%	-	-	-
25	11	1.527	<20%	-	-	-
50	11	1.573	<20%	-	-	-
75	11	1.416	<20%	10	5.726	<0.1%
100	11	0.739	<50%	13	7.434	<0.1%
125	11	0.671	<60%	15	6.085	<0.1%
150	11	0.616	<60%	15	5.797	<0.1%
175	11	0.519	<70%	16	6.471	<0.1%
200	11	0.334	<80%	16	6.670	<0.1%
250	10	0.452	<70%	16	7.364	<0.1%
300	8	0.291	<80%	13	7.637	<0.1%
350	7	0.142	<90%	13	8.323	<0.1%
400	6	0.005	<100%	12	8.444	<0.1%
500	5	0.047	<100%	11	8.131	<0.1%
600	5	0.060	<100%	11	7.812	<0.1%
700	5	0.061	<100%	11	7.653	<0.1%
800	4	0.220	<90%	10	7.649	<0.1%
failure	2	0.037	<100%	4	5.032	<1%

Table 6. 1 - Student's t statistics for comparison of fatigue lifetime results from ground and polished specimens tested in stress relieved condition.

	Ground (cond.4) vs. (cond.3)			Ground (cond.4) vs. Polished		
a [μm]	degrees of freedom	Student's t	Significance	degrees of freedom	Student's t	Significance
12	9	3.284	<1%	14	2.456	<5%
25	9	3.517	<1%	14	2.250	<5%
50	9	2.496	<5%	14	2.033	<10%
75	9	1.856	<10%	14	1.254	<30%
100	8	1.328	<30%	13	0.615	<60%
125	8	1.305	<30%	13	0.073	<100%
150	8	1.399	<20%	13	0.136	<90%
175	8	1.307	<30%	13	0.193	<90%
200	8	1.381	<30%	13	0.455	<70%
250	8	1.265	<30%	13	0.320	<80%
300	8	1.675	<20%	13	0.941	<40%
350	8	1.584	<20%	13	1.038	<40%
400	8	1.690	<20%	11	0.819	<50%
500	8	1.957	<10%	10	0.808	<50%
600	8	2.169	<10%	9	0.306	<80%
700	8	2.371	<5%	9	0.308	<80%
800	7	2.145	<10%	9	0.213	<90%
failure	2	4.272	<20%	2	0.637	<90%

Table 6.2 - Student's t statistics for comparison of fatigue lifetime results from ground and polished specimens tested in as-received condition.

Figures

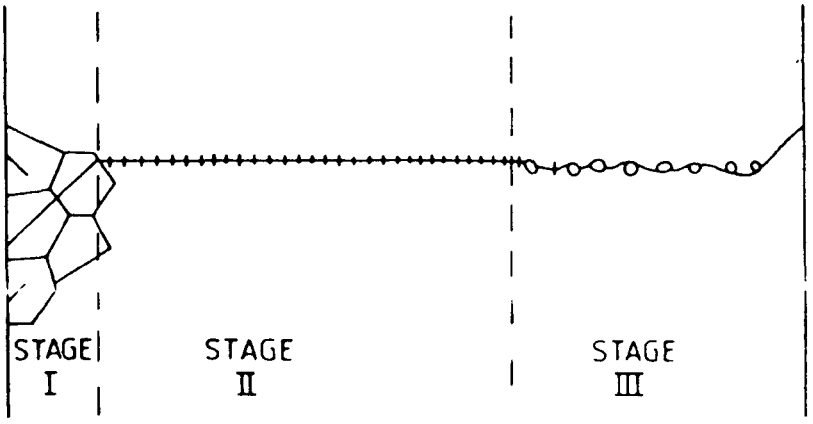

Fig. 2.1 Schematic representation of three stages of fatigue crack growth (from ref. [36]).

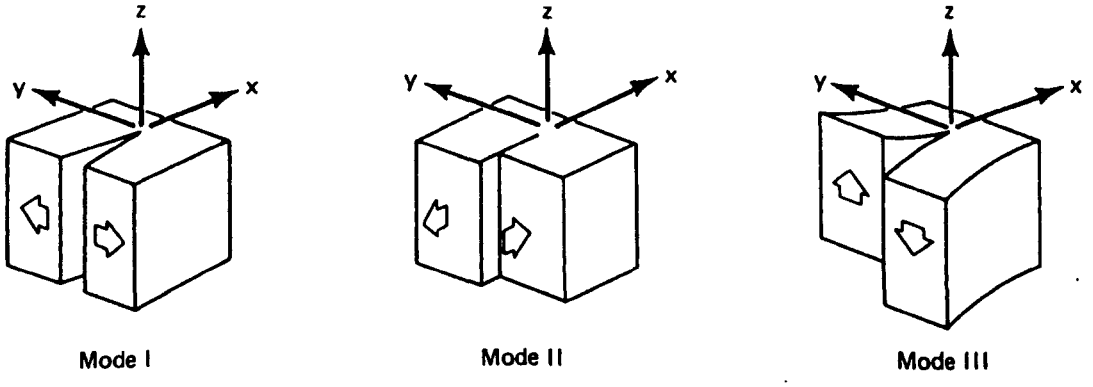

Fig. 2.2 Three modes of crack tip deformation: Mode I (opening mode), Mode II (in-plane shear mode), Mode III (antiplane shear mode) (from ref. [52]).

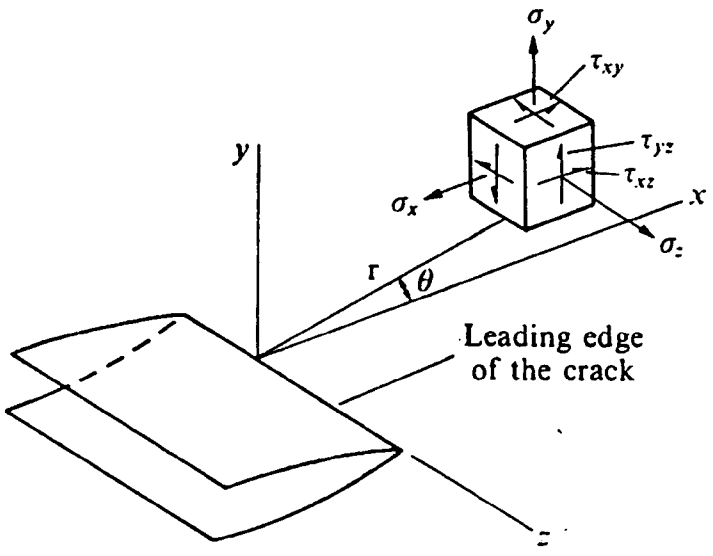

Fig. 2.3 Stress components in the crack-tip stress field (from ref. [48]).

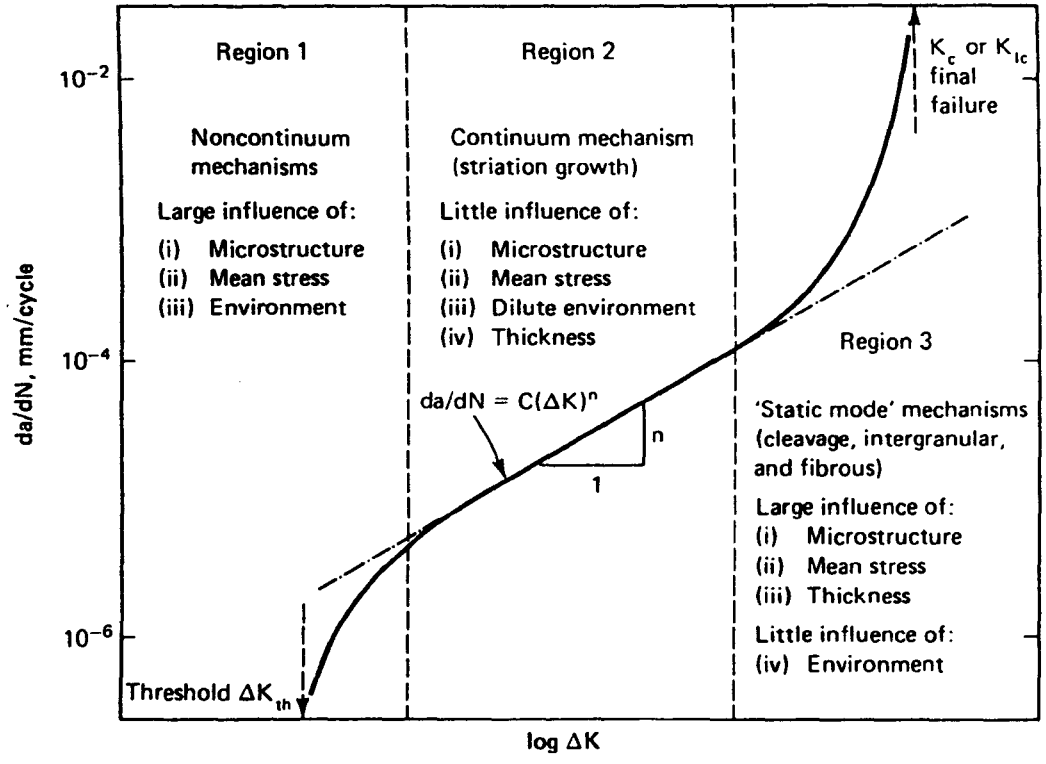

Fig. 2.4 Schematic variation of fatigue crack growth rate, da/dN, with stress intensity range, ΔK, in steels, showing three regions of primary crack growth mechanisms (from ref. [52]).

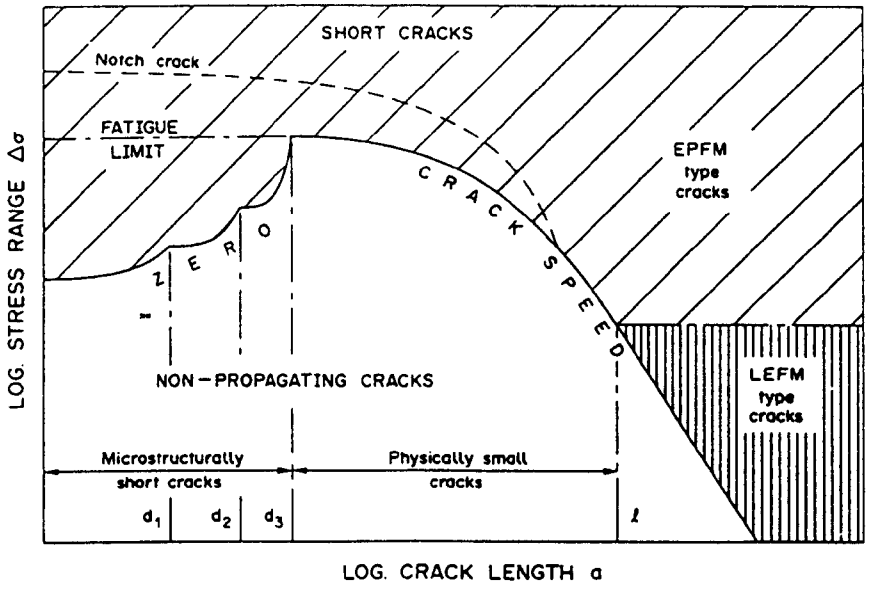

Fig. 2.5 Three regimes of short crack growth: (*i*) microstructurally short cracks (MSC), (*ii*) physically small cracks (PSC), (*iii*) highly stressed cracks (from ref. [55]).

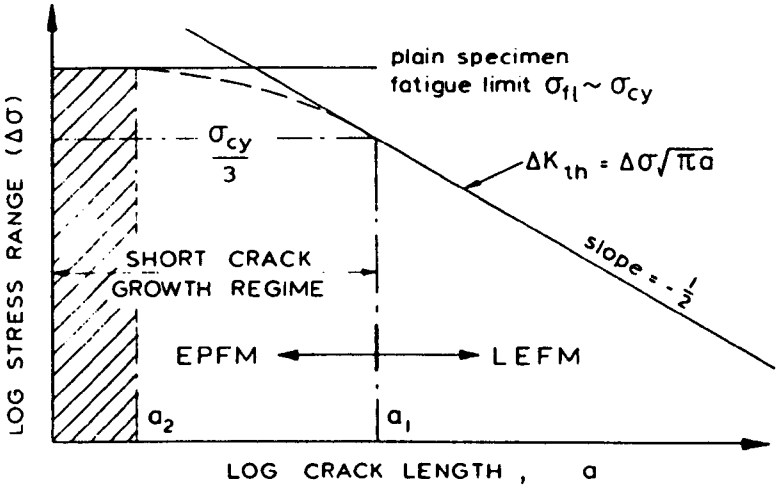

Fig. 2.6 Kitagawa-Takahashi type diagram showing the change in the threshold stress range with crack length (from ref. [20]).

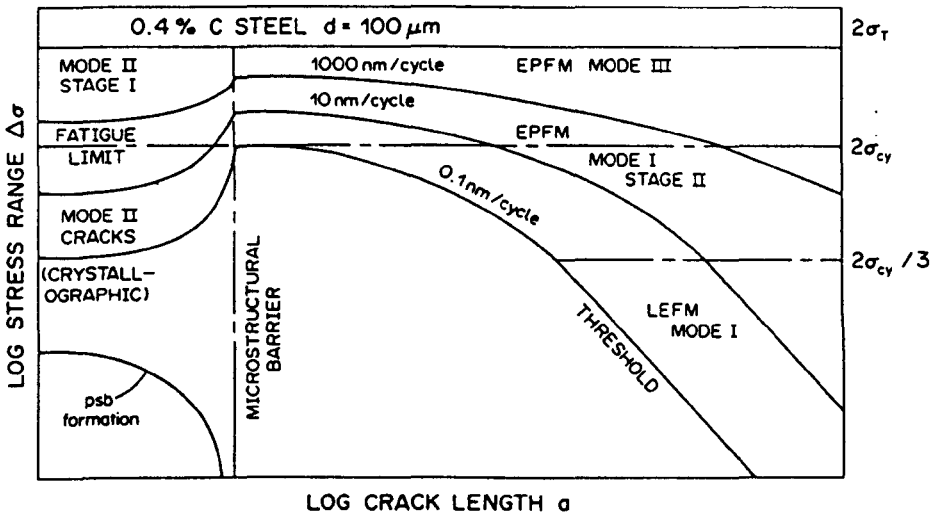

Fig. 2.7 Brown fatigue fracture-mode map showing contours of constant crack growth rate (from ref. [18]).

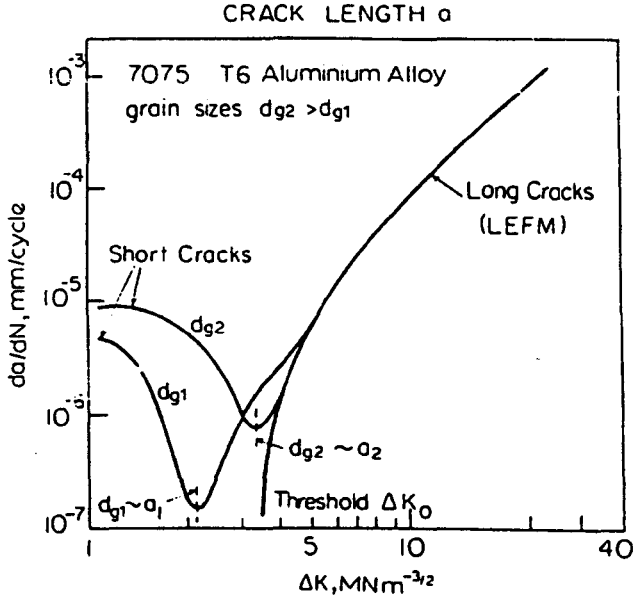

Fig. 2.8 Effect of grain size, d_g, on the growth of microstructurally short cracks (from ref. [16]).

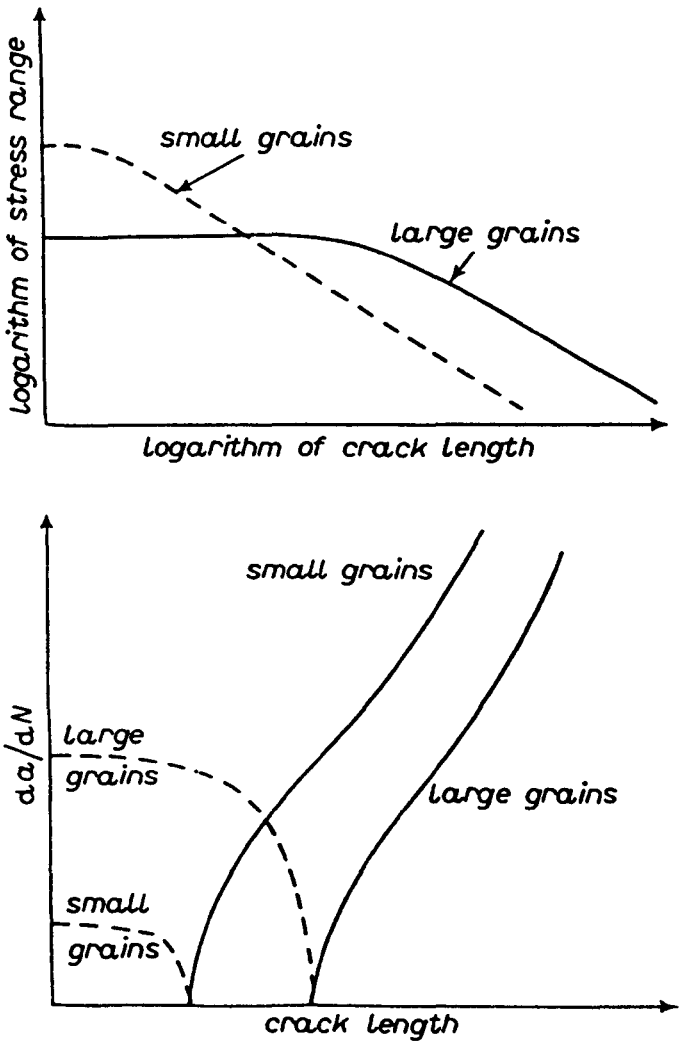

Fig. 2.9 Schematic representation of the behaviour of short and long cracks in small and large-grained materials (from ref. [20]).

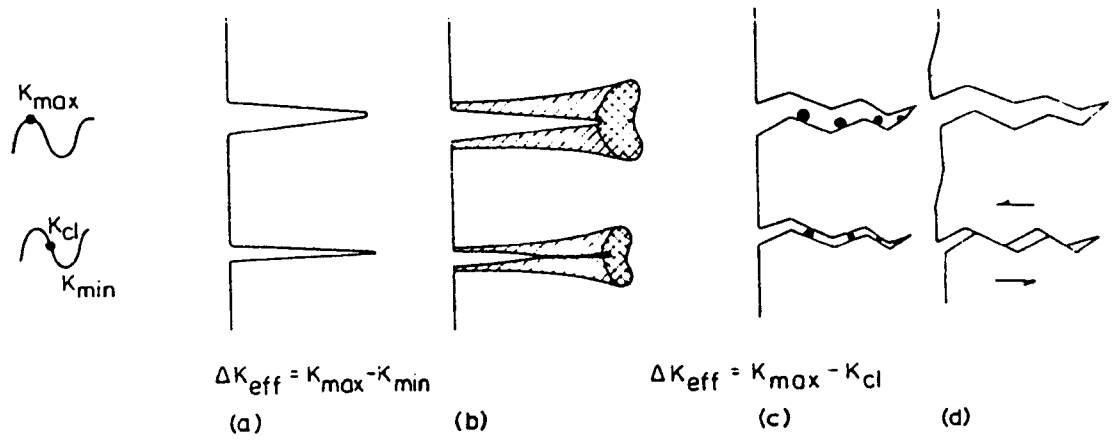

Fig. 2.10 Mechanics of fatigue crack closure (after Ritchie and Suresh [66]): (*a*) no closure; closure induced by (*b*) cyclic plasticity, (*c*) corrosion deposits, and *(d)* rough fracture surfaces.

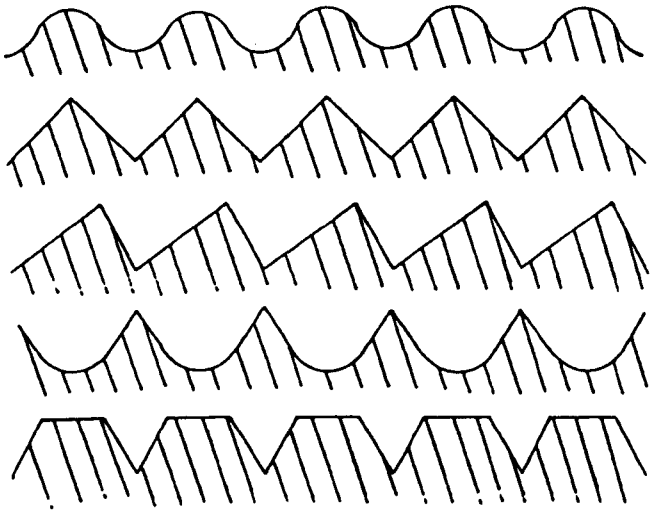

Fig. 2.11 Profiles of different geometries having identical R_a values (from ref. [68]).

Grinding Condition	Surface finish, R_a μm	Fatigue limit MPa
Gentle	1.00	883
Conventional	0.56	461
Abusive	0.55	196

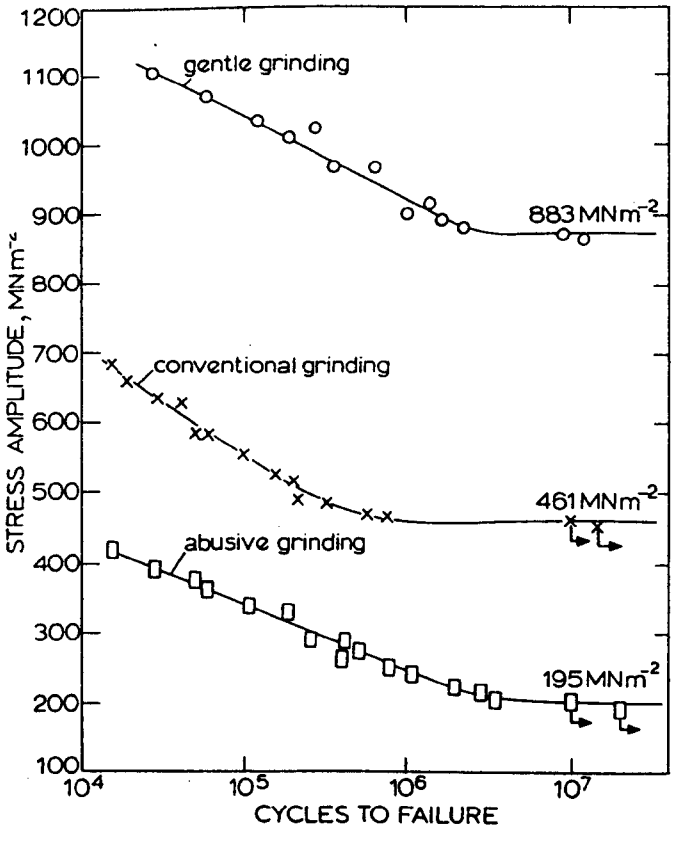

Fig. 2.12 Effect of grinding conditions on the fatigue strength of EN31 steel at room temperature (from ref. [7]).

Surface finish	Residual stress, MPa	Talysurf. μm
Fine ground	-199	0.26
Coarse ground	-236	1.00

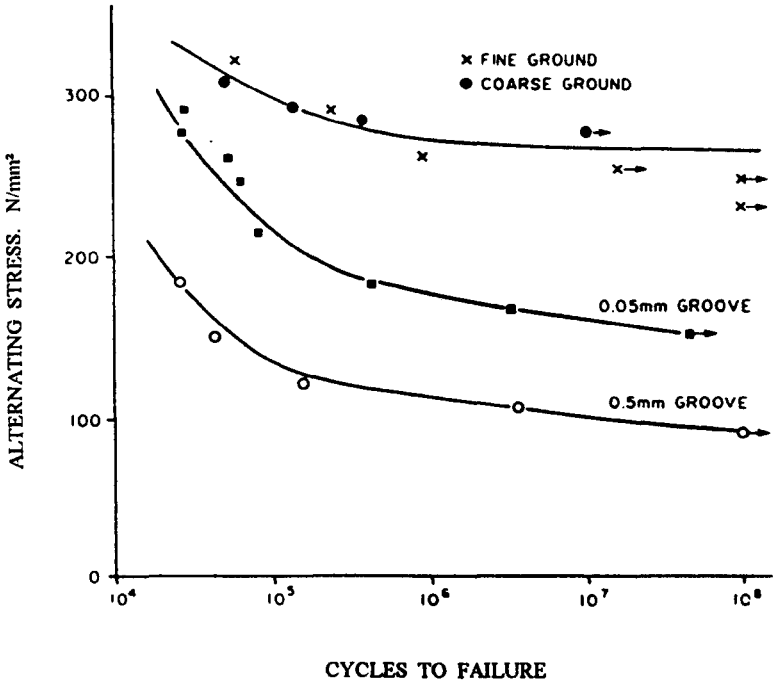

Fig. 2.13 Effect of surface finish on the fatigue strength of EN19 steel (from ref. [2]).

Fig. 2.14 Superposition of residual stresses and stresses due to the applied load (from ref. [70]).

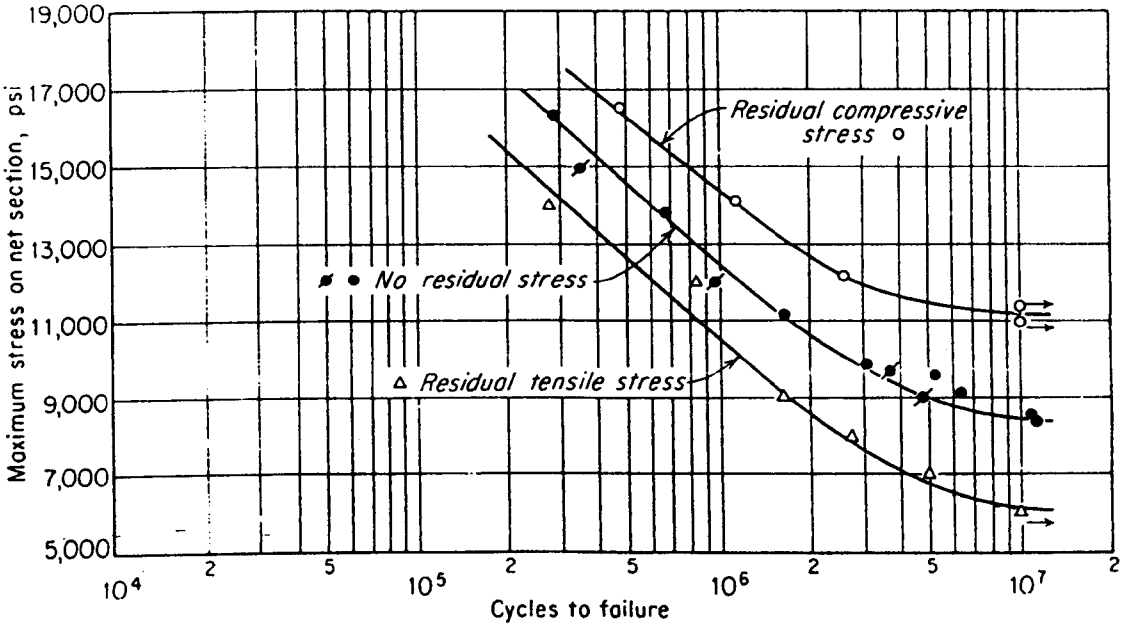

Fig. 2.15 Influence of residual stress on the fatigue strength of 61S-T6 aluminium alloy (from ref. [69]).

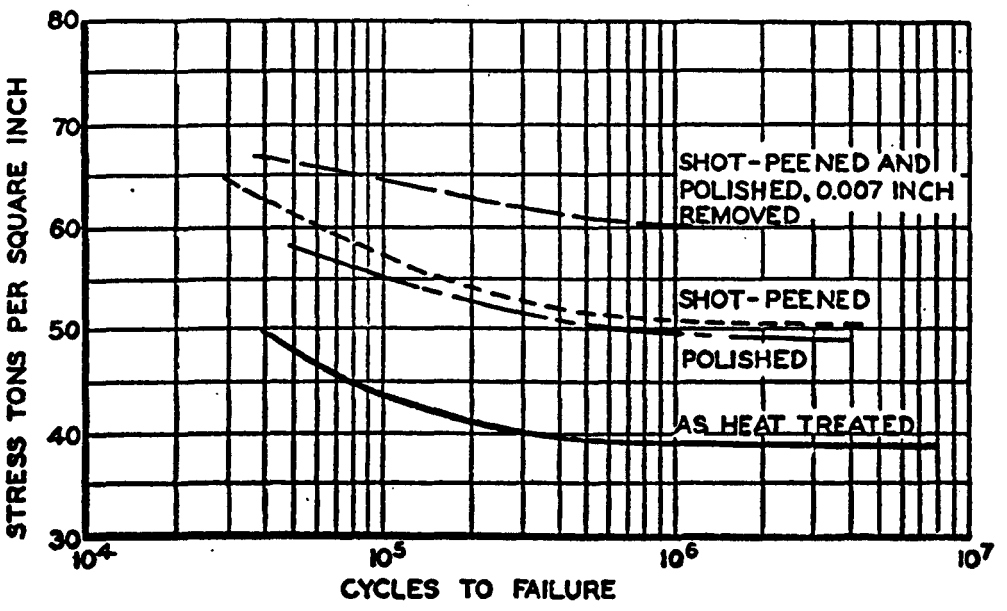

Fig. 2.16 Effect of surface finishing operations on the fatigue strength of a Cr-V steel: (*i*) heat treating, (*ii*) polishing, (*iii*) shot peening, and (*iv*) shot peening followed by polishing (from ref. [6]).

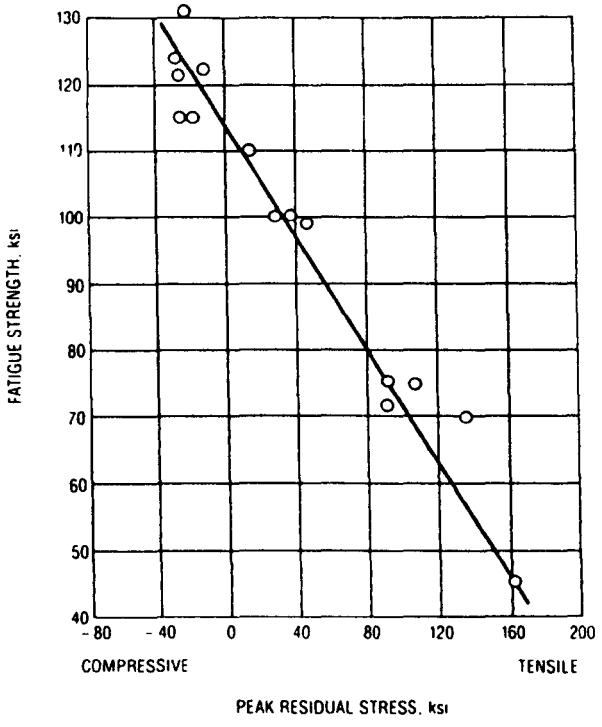

Fig. 2.17 Effect of peak residual stress on fatigue strength in ground AISI 4340 (from ref. [72]).

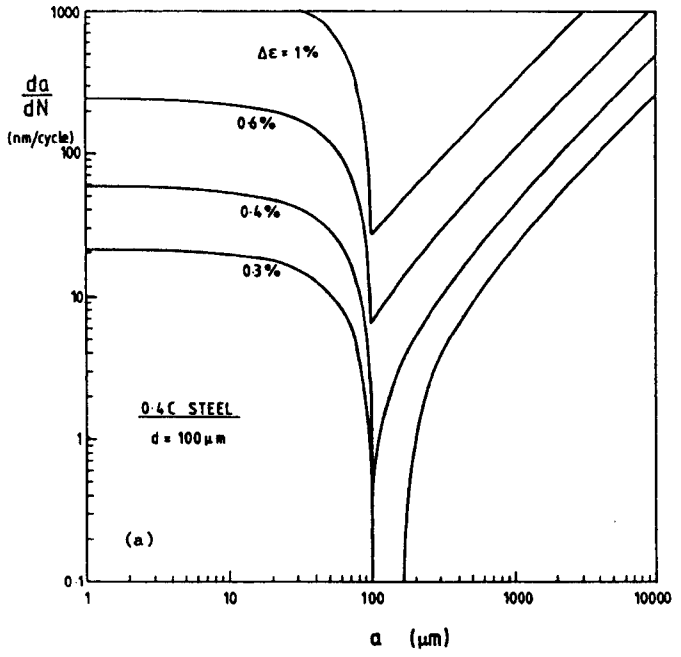

Fig. 2.18 Typical fatigue diagram to represent short crack growth (after Brown [18]).

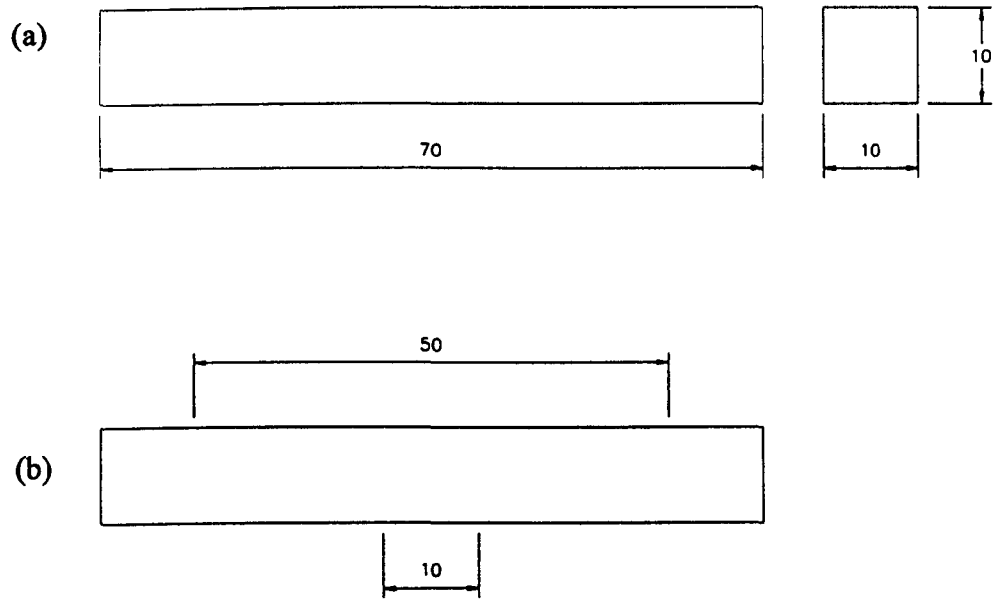

Fig. 3.1 Four-point-bend fatigue specimens with (*a*) dimensions, and (*b*) loading points.

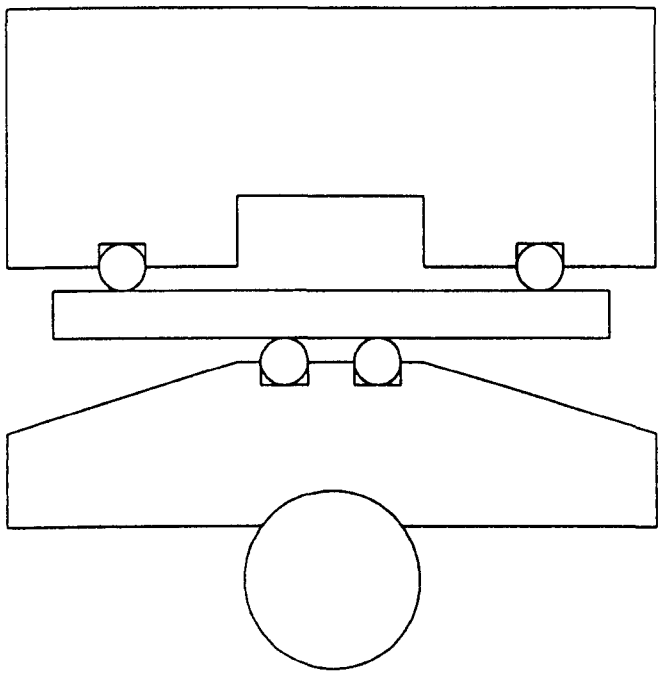

Fig. 3.2 Four-point-bend loading fixture (schematic illustration).

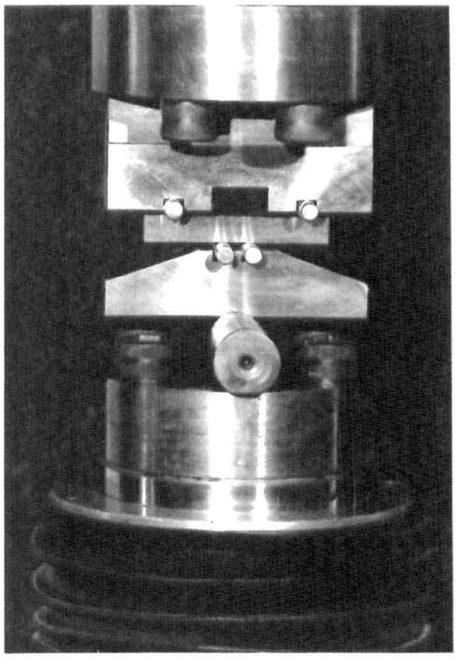

Fig. 3.3 Four-point-bend loading fixture (photograph).

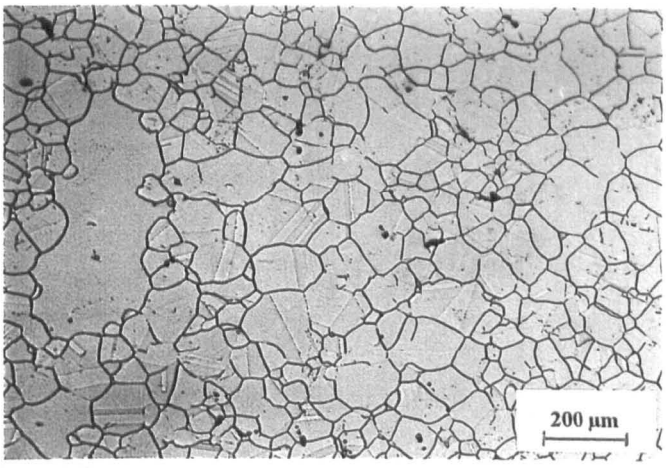

Fig. 4.1 Microstructure of Waspaloy (micrograph).

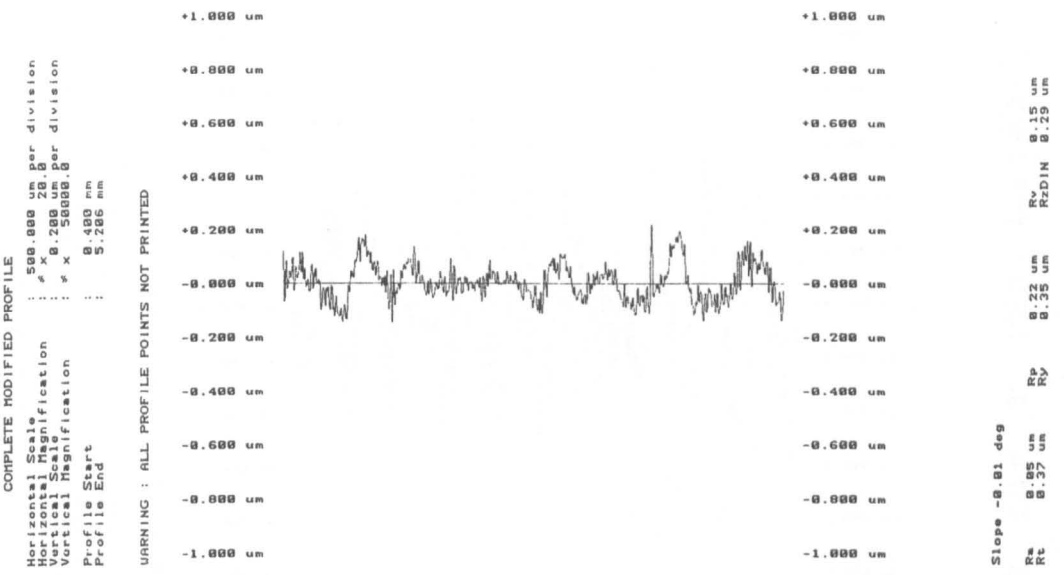

Fig. 4.2 Typical surface profile and surface texture parameters for polished finish.

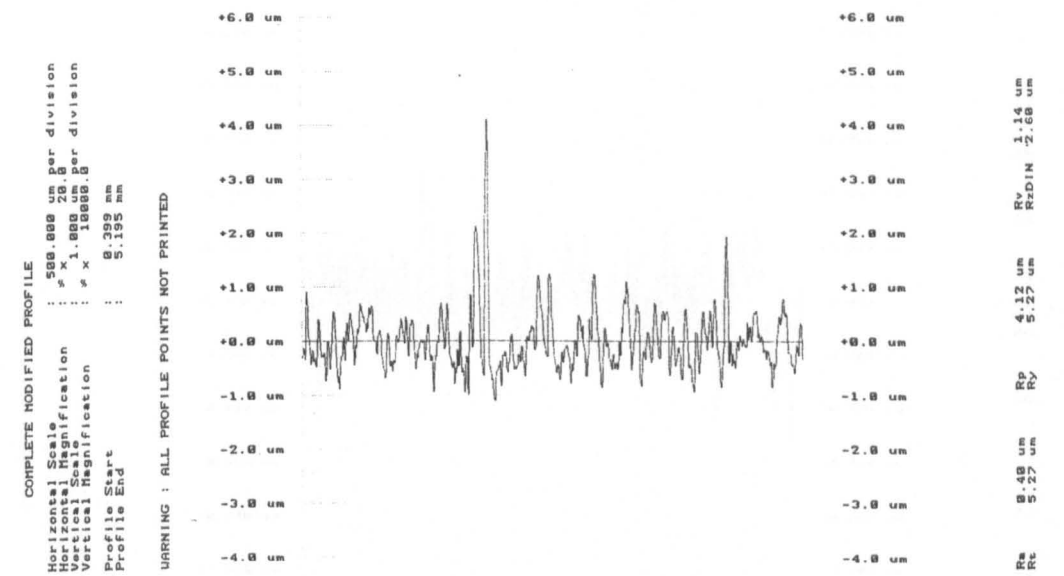

Fig. 4.3 Typical surface profile and surface texture parameters for ground (condition 1) finish.

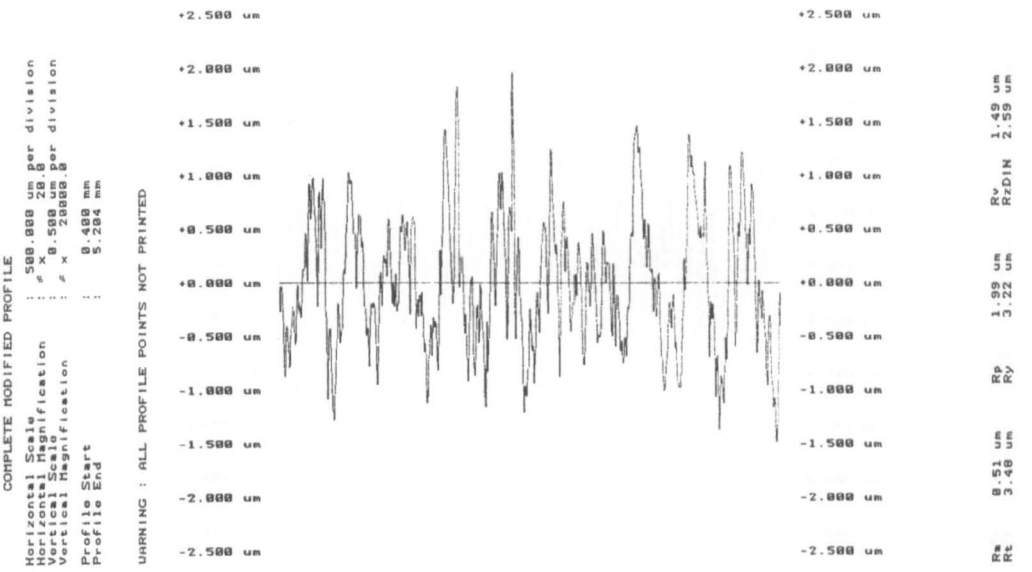

Fig. 4.4 Typical surface profile and surface texture parameters for ground (condition 2) finish.

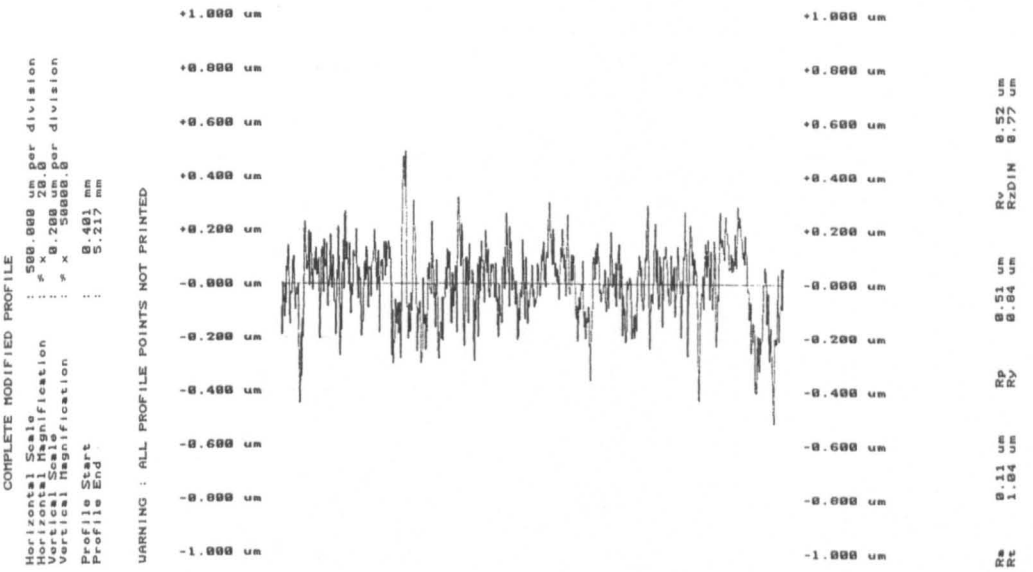

Fig. 4.5 Typical surface profile and surface texture parameters for ground (condition 3) finish.

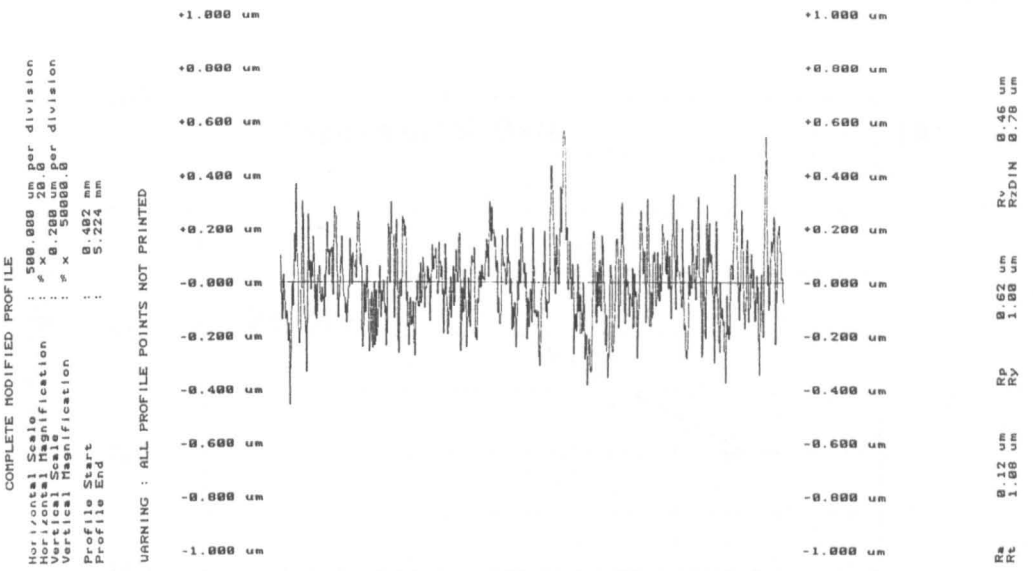

Fig. 4.6 Typical surface profile and surface texture parameters for ground (condition 4) finish.

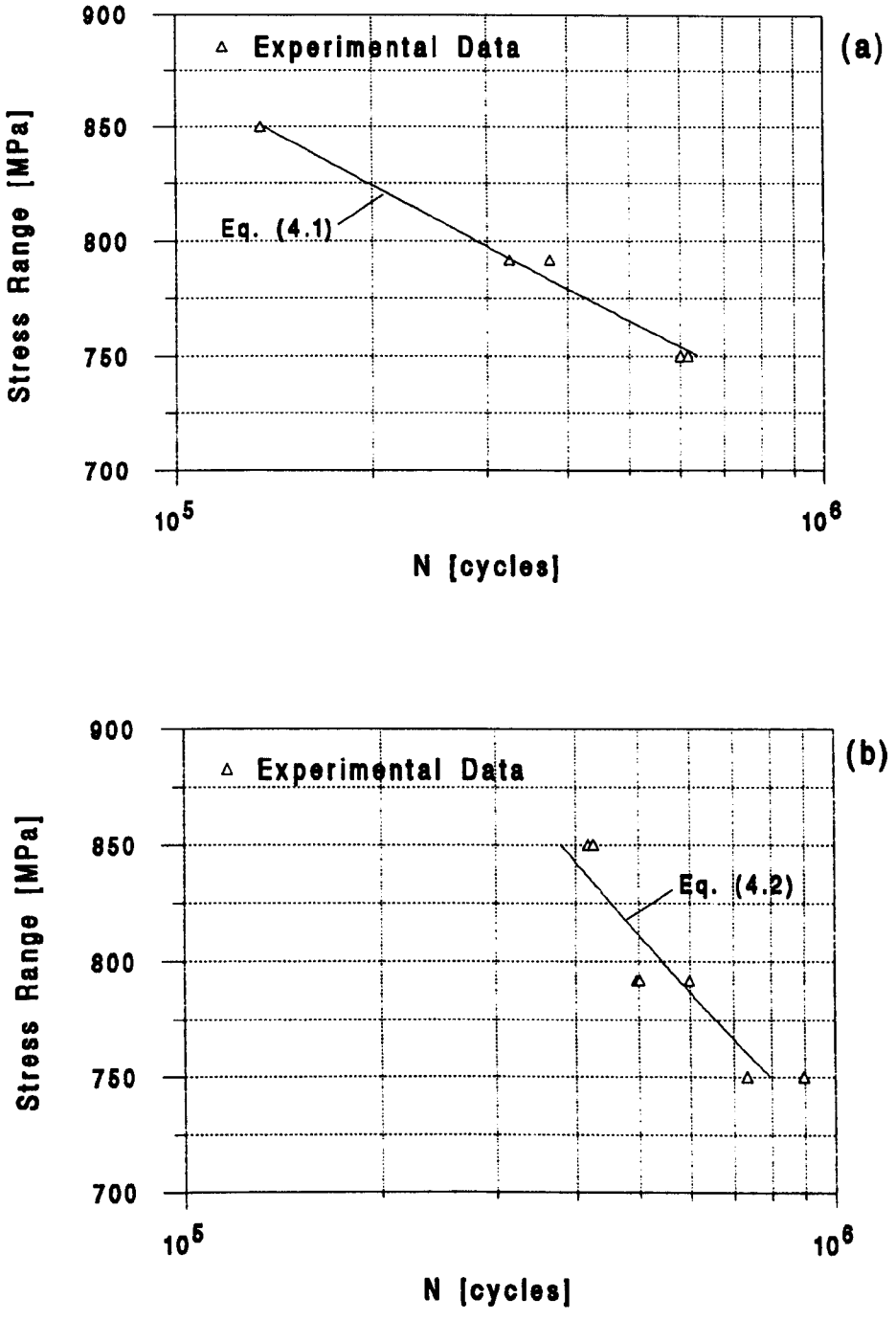

Fig. 4.7 Fatigue endurance (SN-data) for Waspaloy, polished surface finish; (*a*) Material in as-received condition, and (*b*) in stress relieved condition.

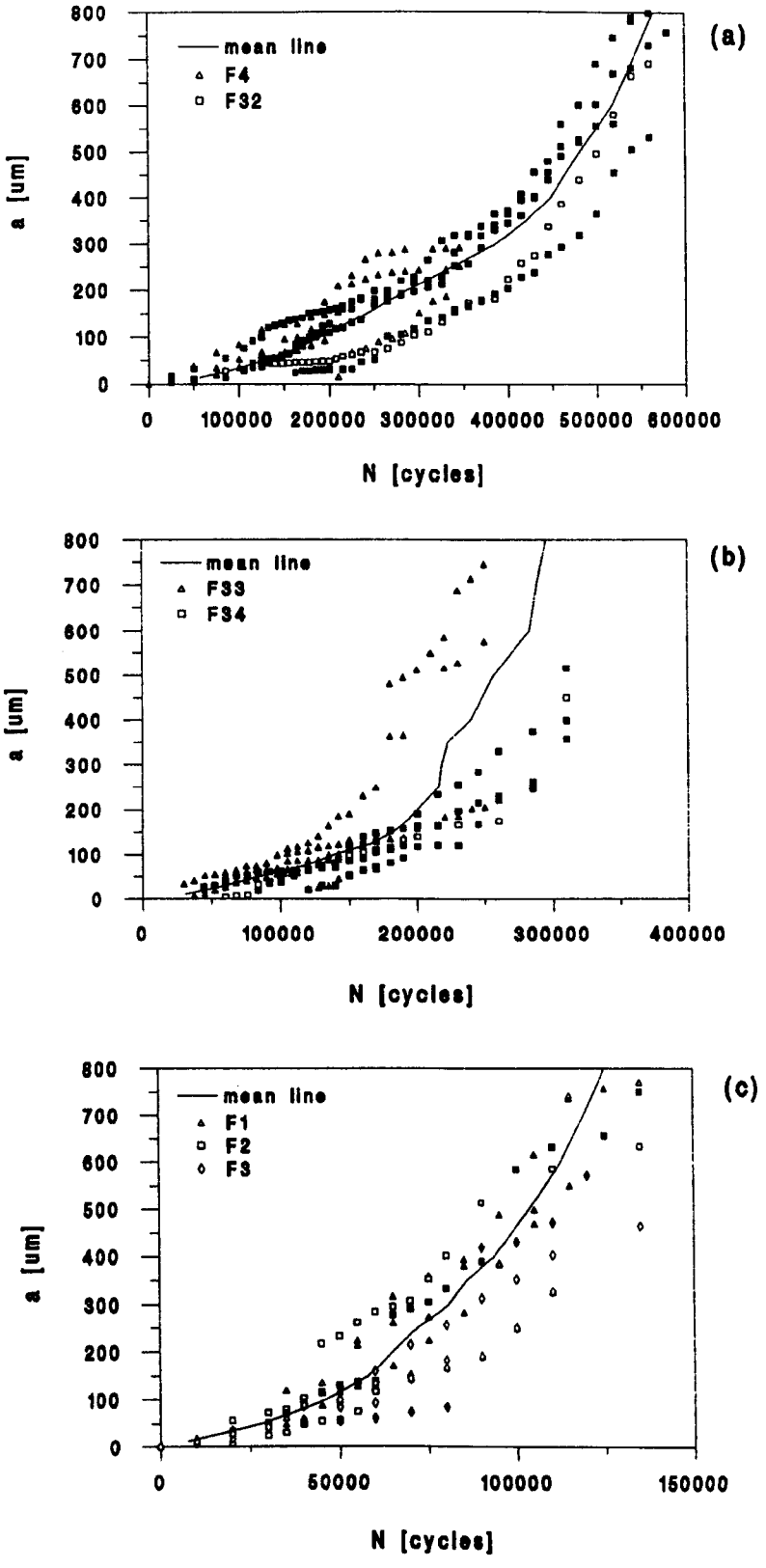

Fig. 4.8 Half crack length against number of cycles results and mean fatigue lifetimes for polished/as-received specimens, (*a*) Stress range 750MPa, (*b*) Stress range 792MPa, and (*c*) Stress range 850MPa.

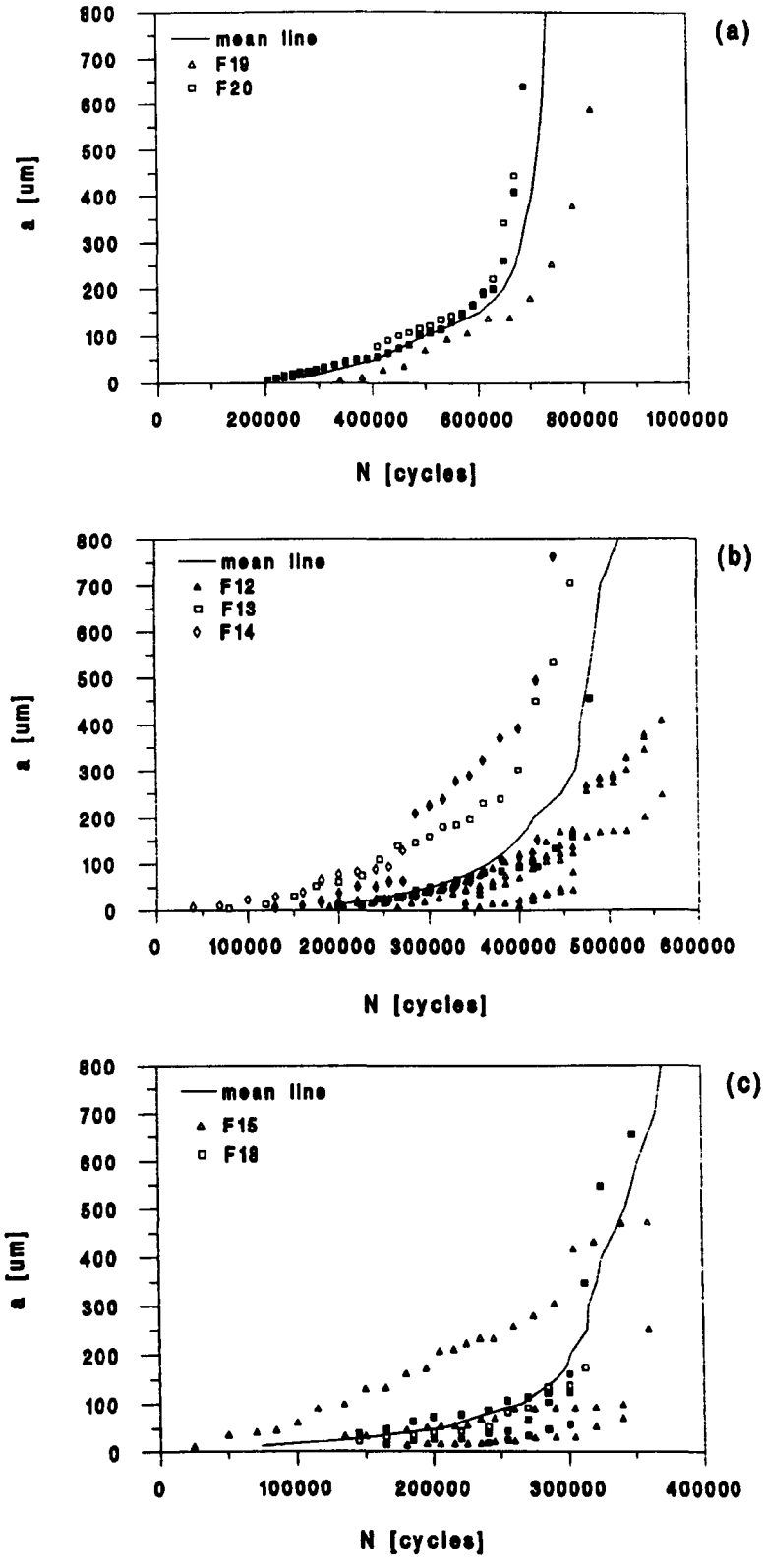

Fig. 4.9 Half crack length against number of cycles results and mean fatigue lifetimes for polished/stress relieved specimens, (*a*) Stress range 750MPa, (*b*) Stress range 792MPa, and (*c*) Stress range 850MPa.

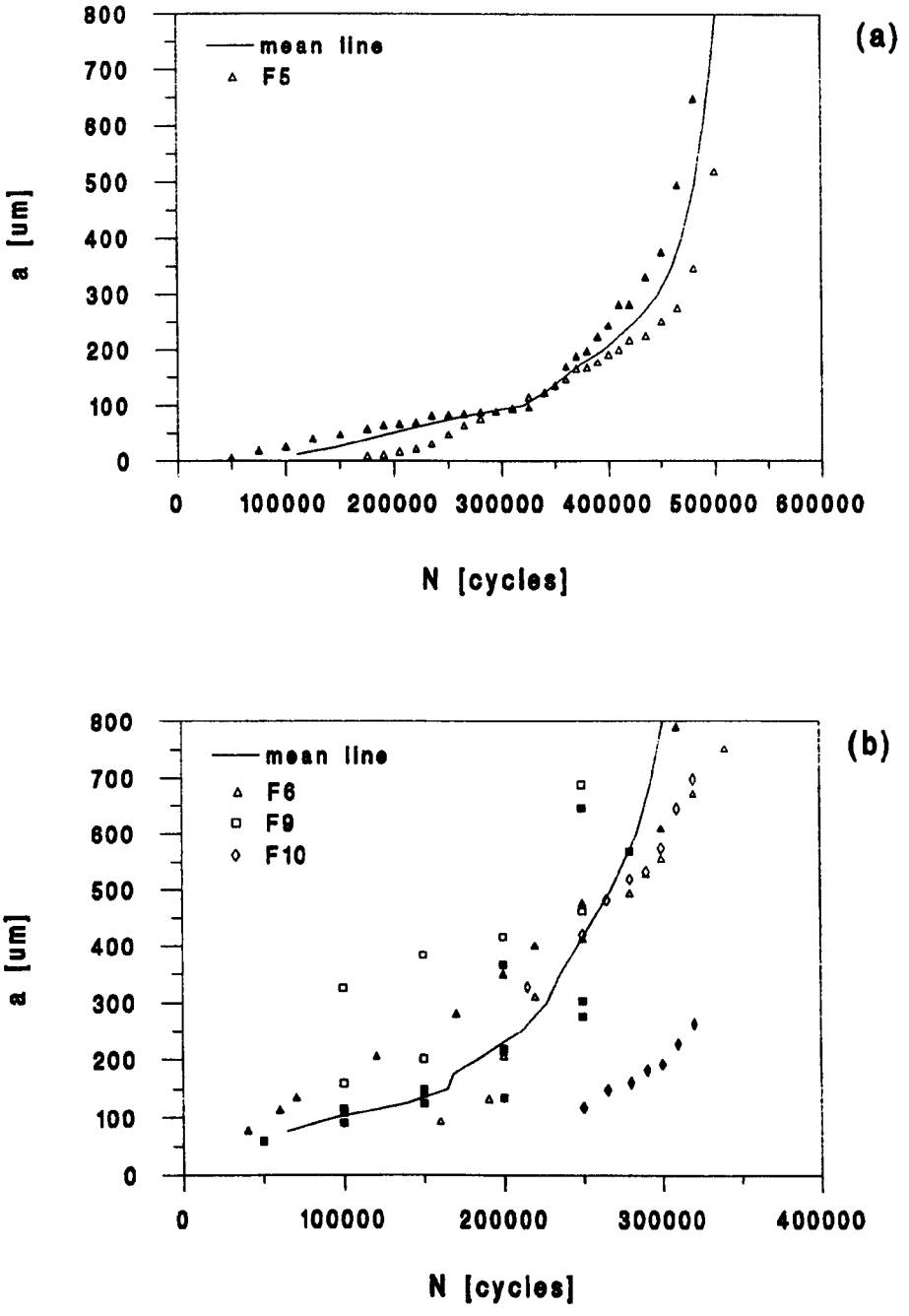

Fig. 4.10 Half crack length against number of cycles results and mean fatigue lifetime for ground/stress relieved specimens, stress range 792 MPa, (*a*) Grinding condition 1, and (*b*) Grinding condition 2.

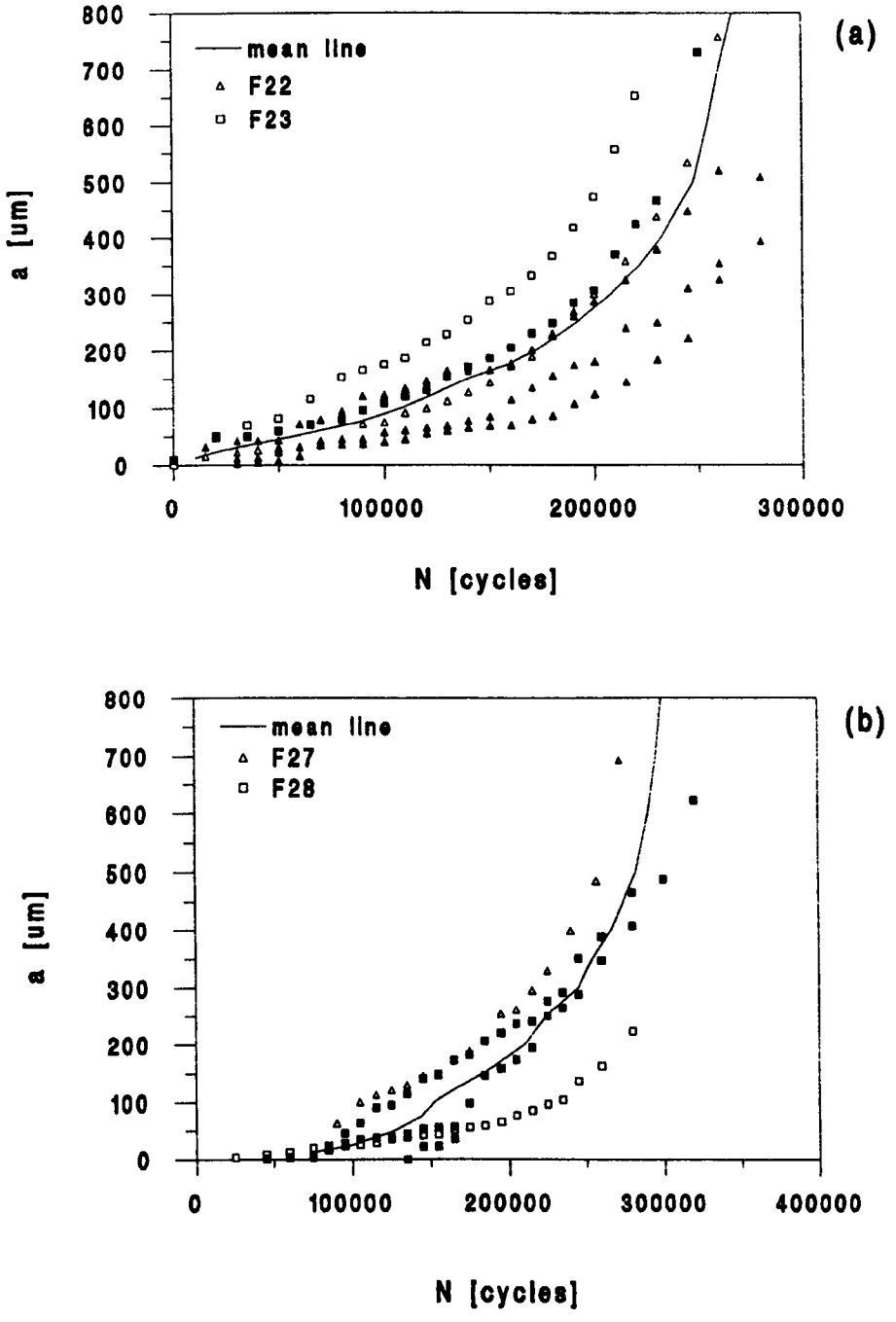

Fig. 4.11 Half crack length against number of cycles results and mean fatigue lifetime for ground/as-received, stress range 792 MPa, (*a*) Grinding condition 3, and (*b*) Grinding condition 4.

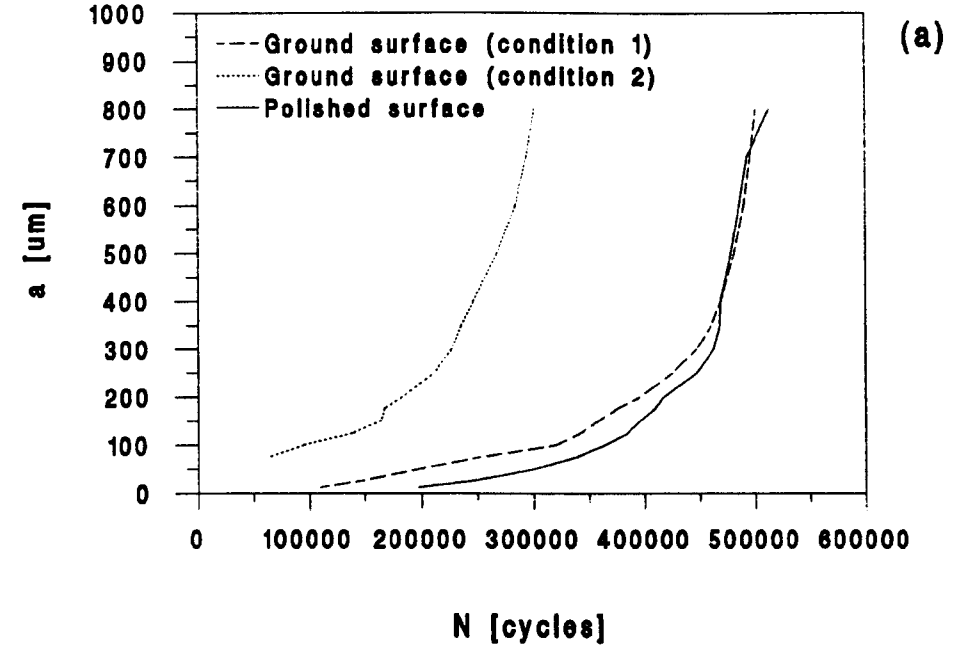

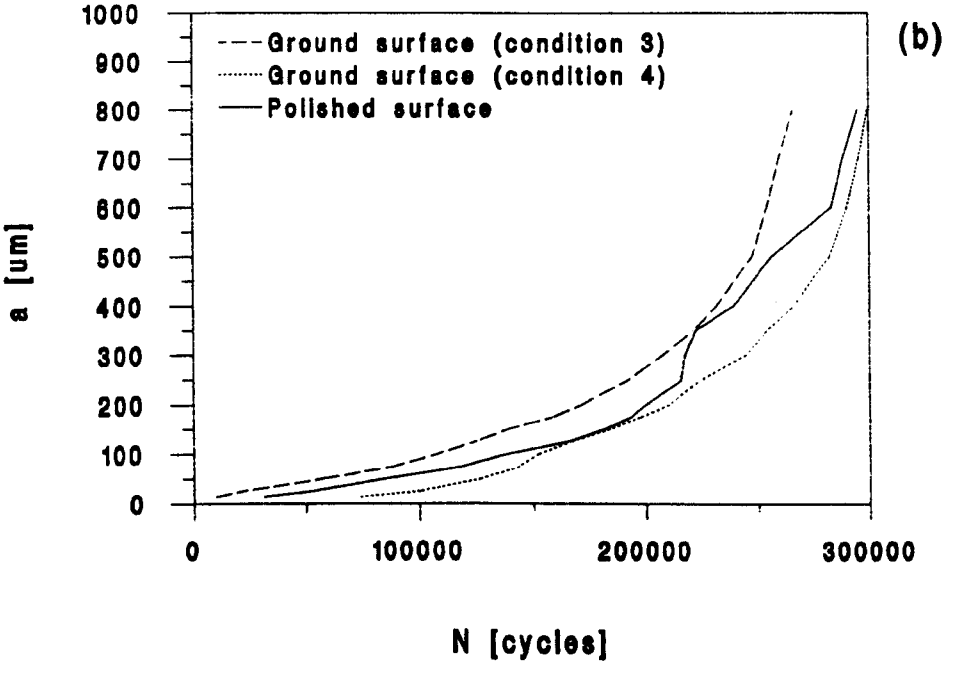

Fig. 4.12 Comparison of mean fatigue lifetimes for polished and ground surfaces, stress range 792 MPa, (*a*) Material in stress relieved condition, (*b*) Material in as-received condition.

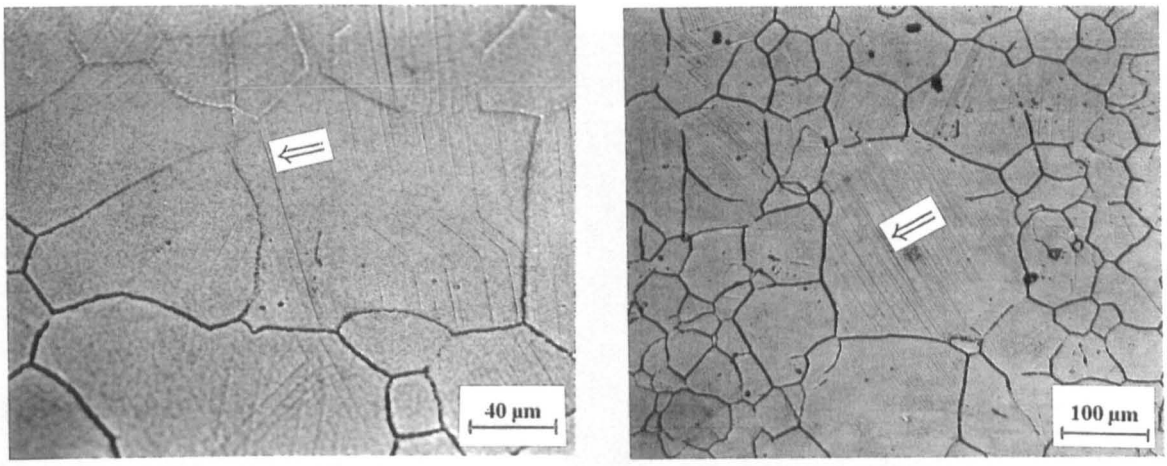

Fig. 5.1 Crack initiation along slip bands (PSB).

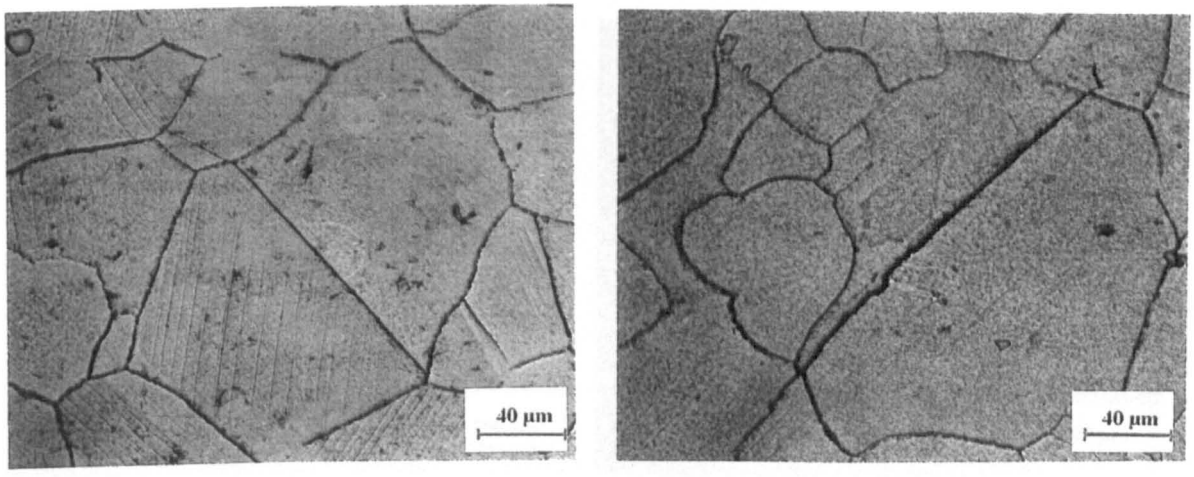

Fig. 5.2 Crack initiation along twin boundaries.

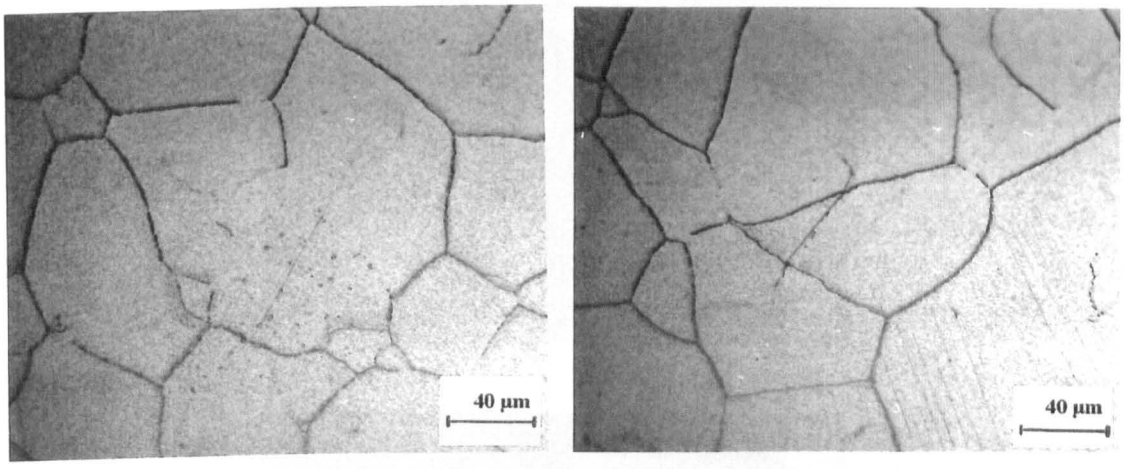

Fig. 5.3 Crack initiation in grains showing no signs of slip bands.

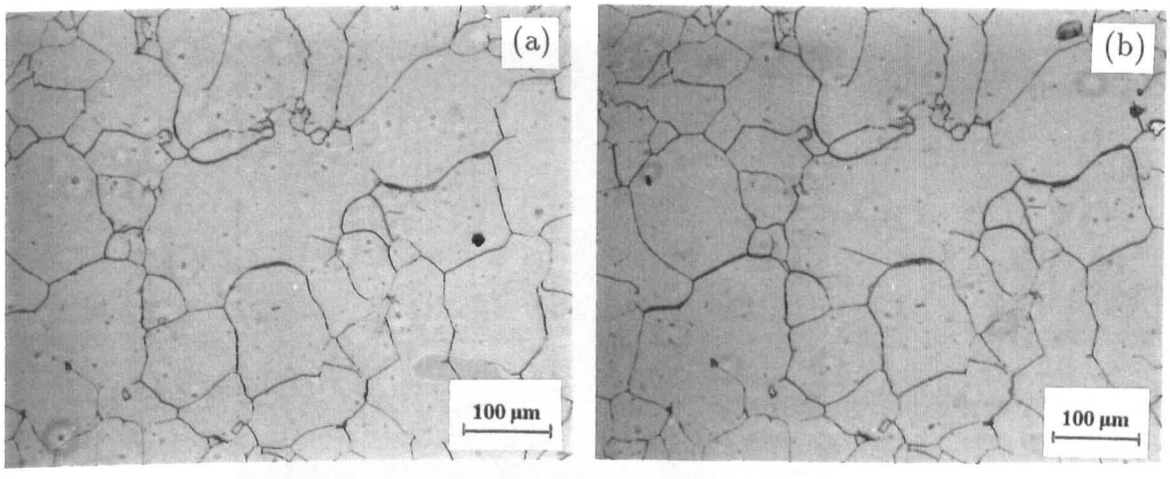

Fig. 5.4 Crack initiation at a grain boundary, stress range 792MPa, (*a*) $N = 100000$ *cycles*, (*b*) $N = 180000$ *cycles*.

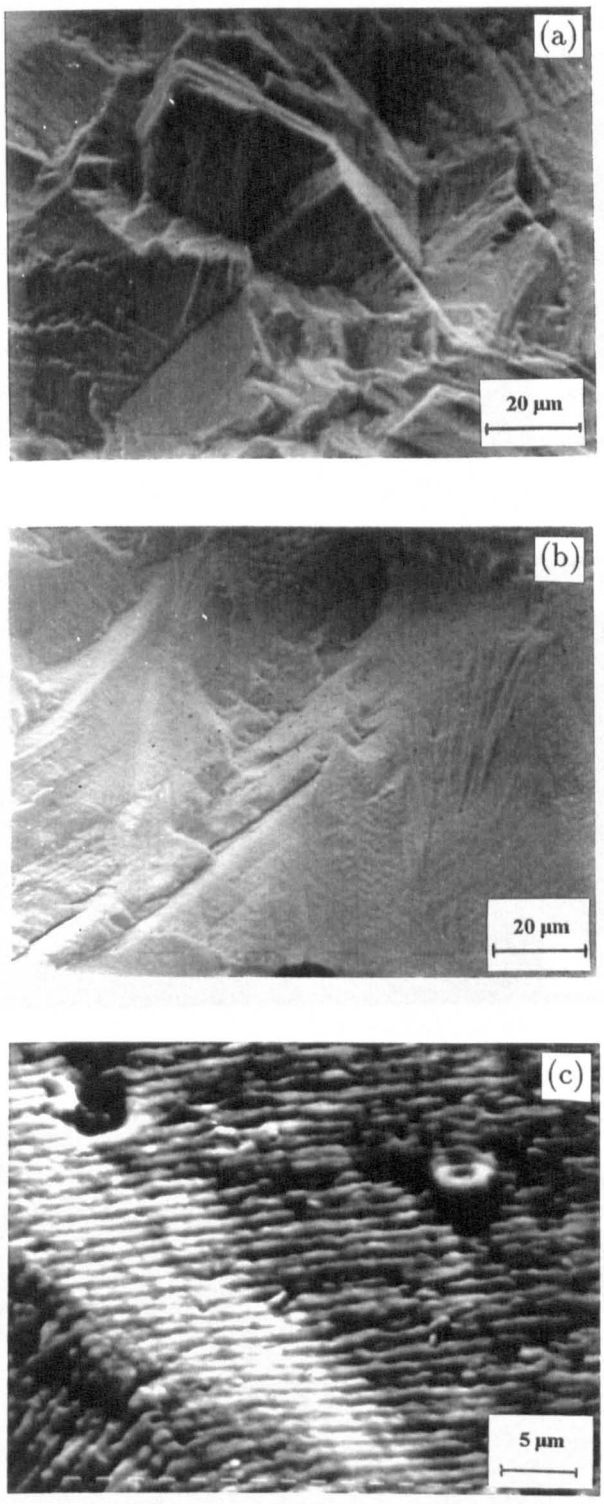

Fig. 5.5 Fatigue fracture surfaces: (*a*) Stage I (crystallographic), (*b*) Stage II (earlier growth), and (*c*) Stage II (striation mode).

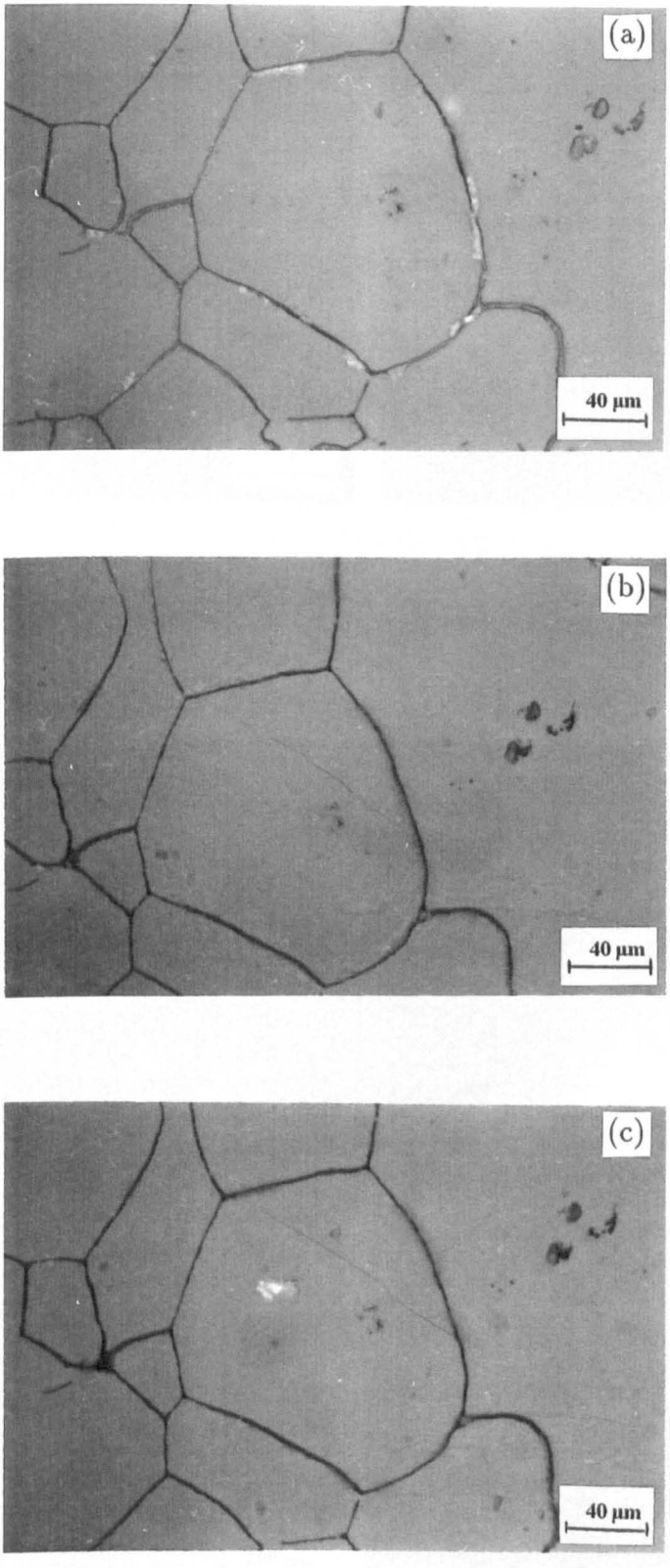

Fig. 5.6 Arrest of a crack on reaching grain boundary, stress range 792MPa, (a) $N = 100000$ *cycles*, (b) $N = 260000$ *cycles*, (c) $N = 360000$ *cycles*; $(N_f = 375950$ *cycles*$)$.

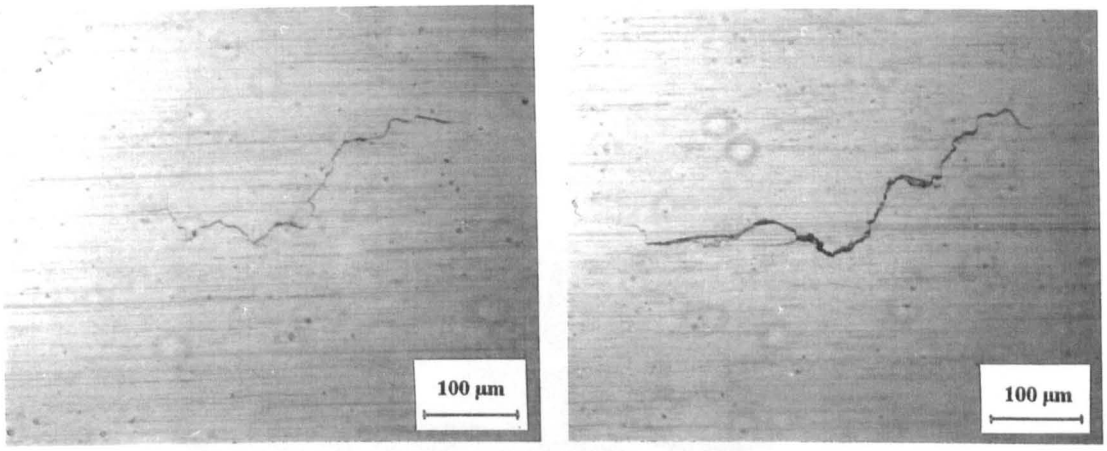

Fig. 5.7 Pattern 'A' of crack behaviour developed in fine ground surfaces.

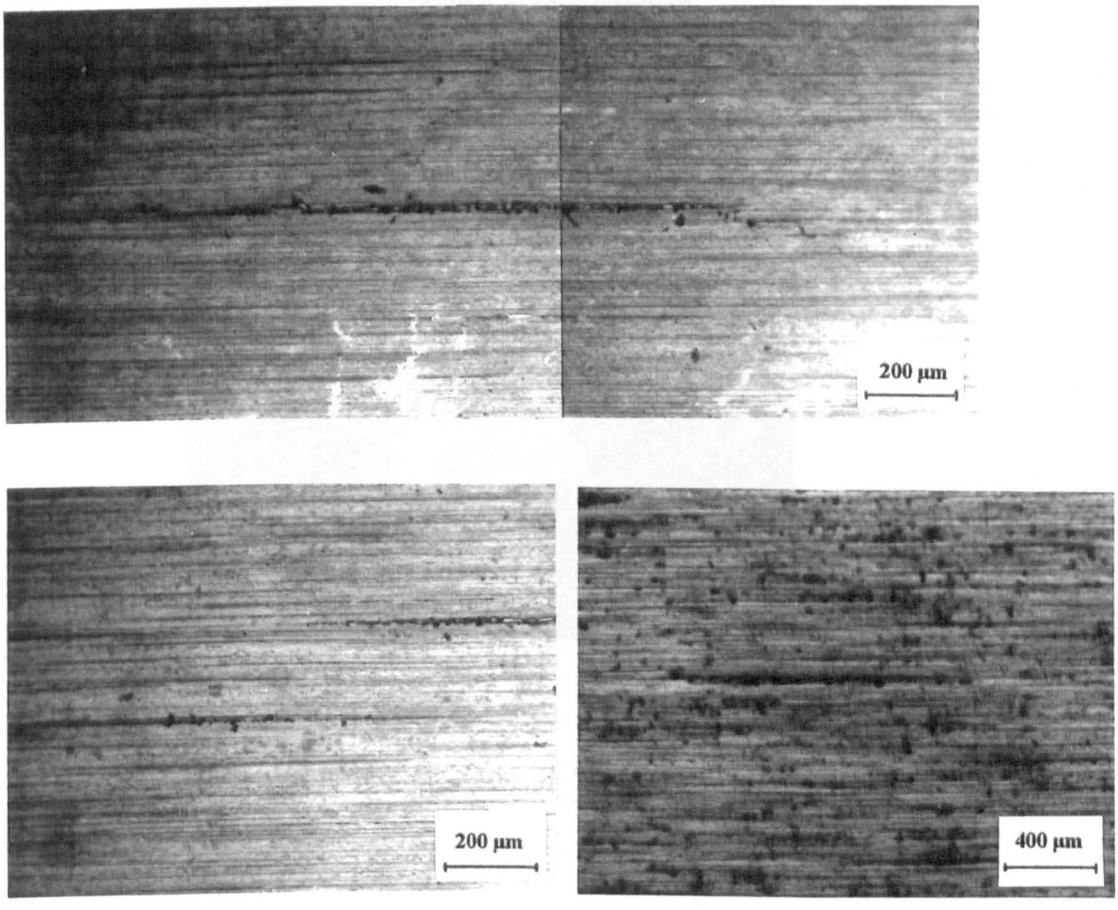

Fig. 5.8 Pattern 'B' of crack behaviour developed in coarse ground surfaces.

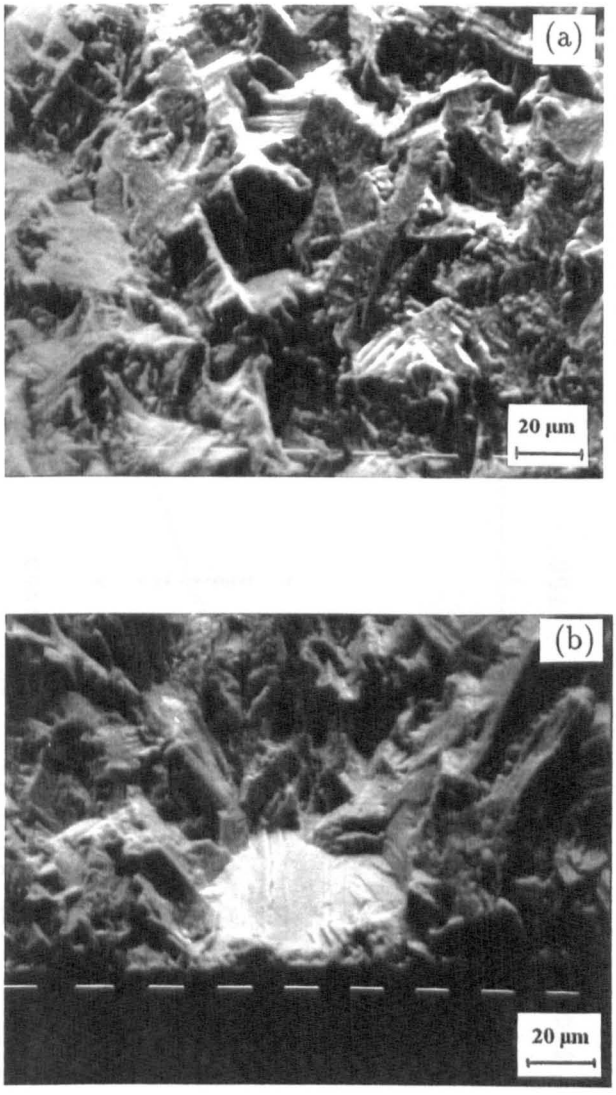

Fig. 5.9 Fatigue fracture surfaces of (*a*) fine ground surface, and (*b*) coarse ground surface.

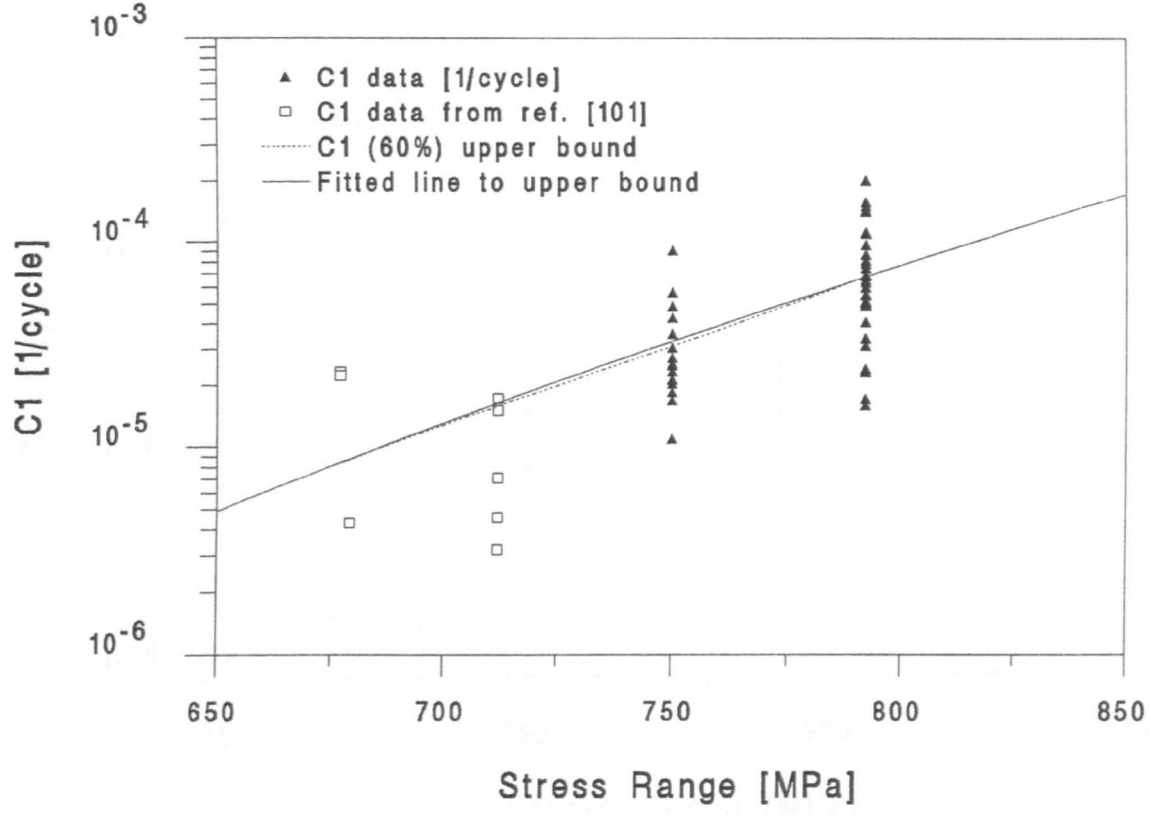

Fig. 5.10 Short crack growth parameter C_1 versus stress range for Waspaloy in as-received condition.

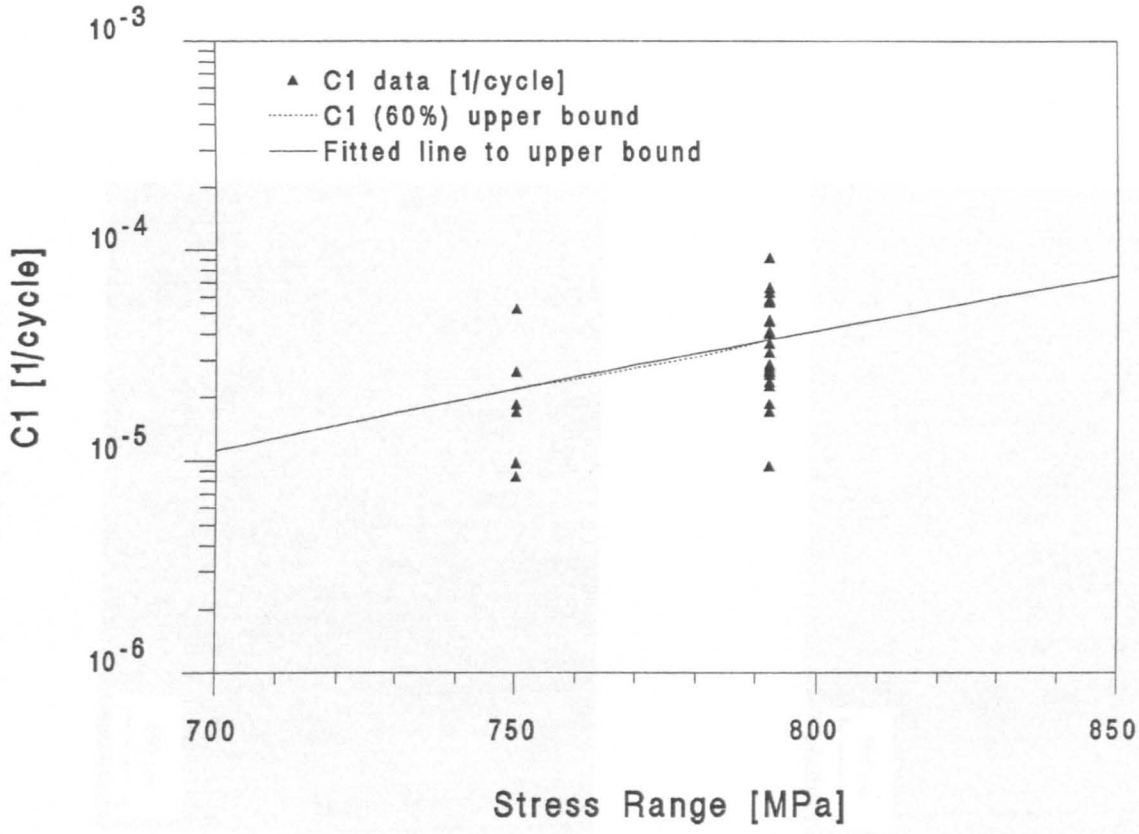

Fig. 5.11 Short crack growth parameter C_1 versus stress range for Waspaloy in stress relieved condition.

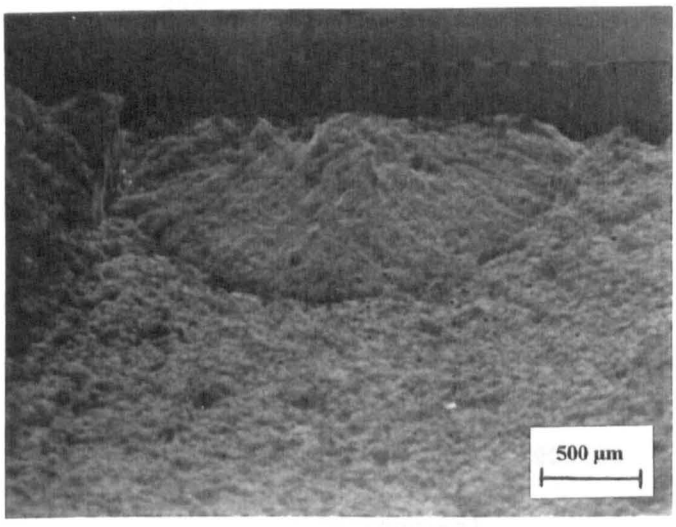

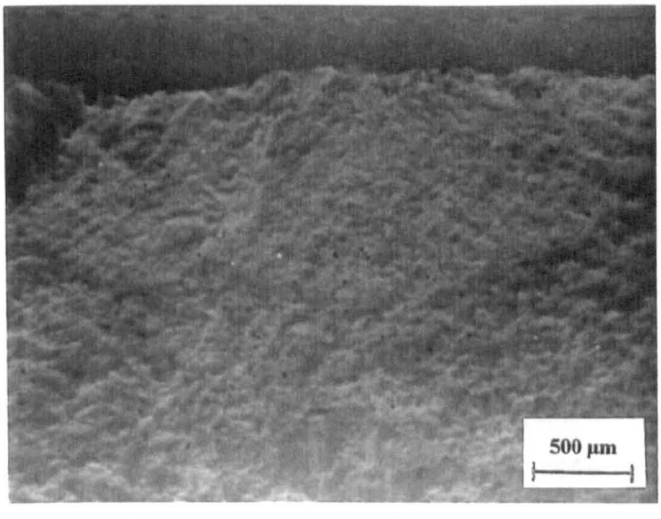

Fig. 5.12 Fatigue crack shapes.

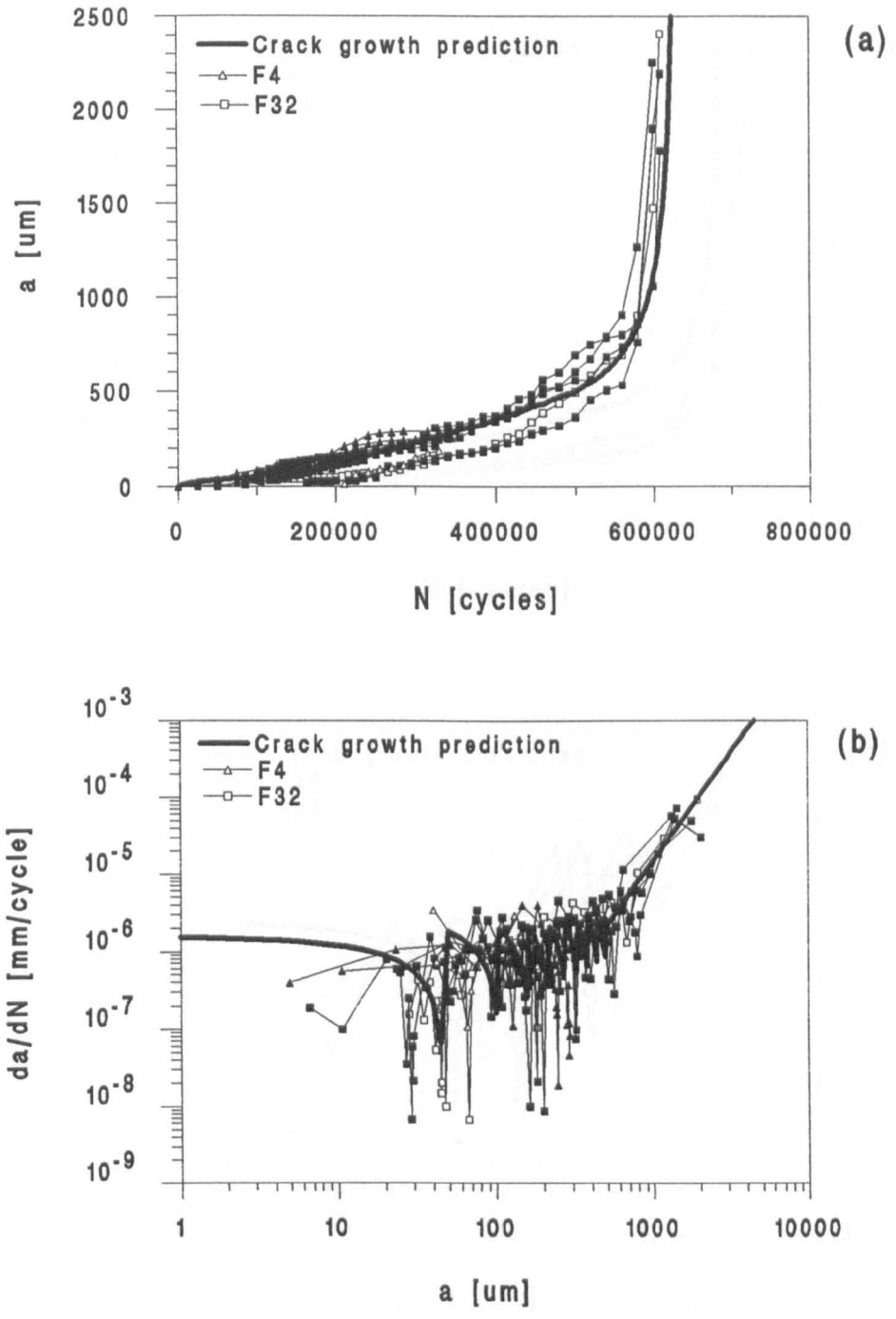

Fig. 5.13 Crack growth prediction and results for polished/as-received specimens, stress range 750MPa; (*a*) Half crack length versus number of cycles, and (*b*) Crack growth rate versus mean crack length.

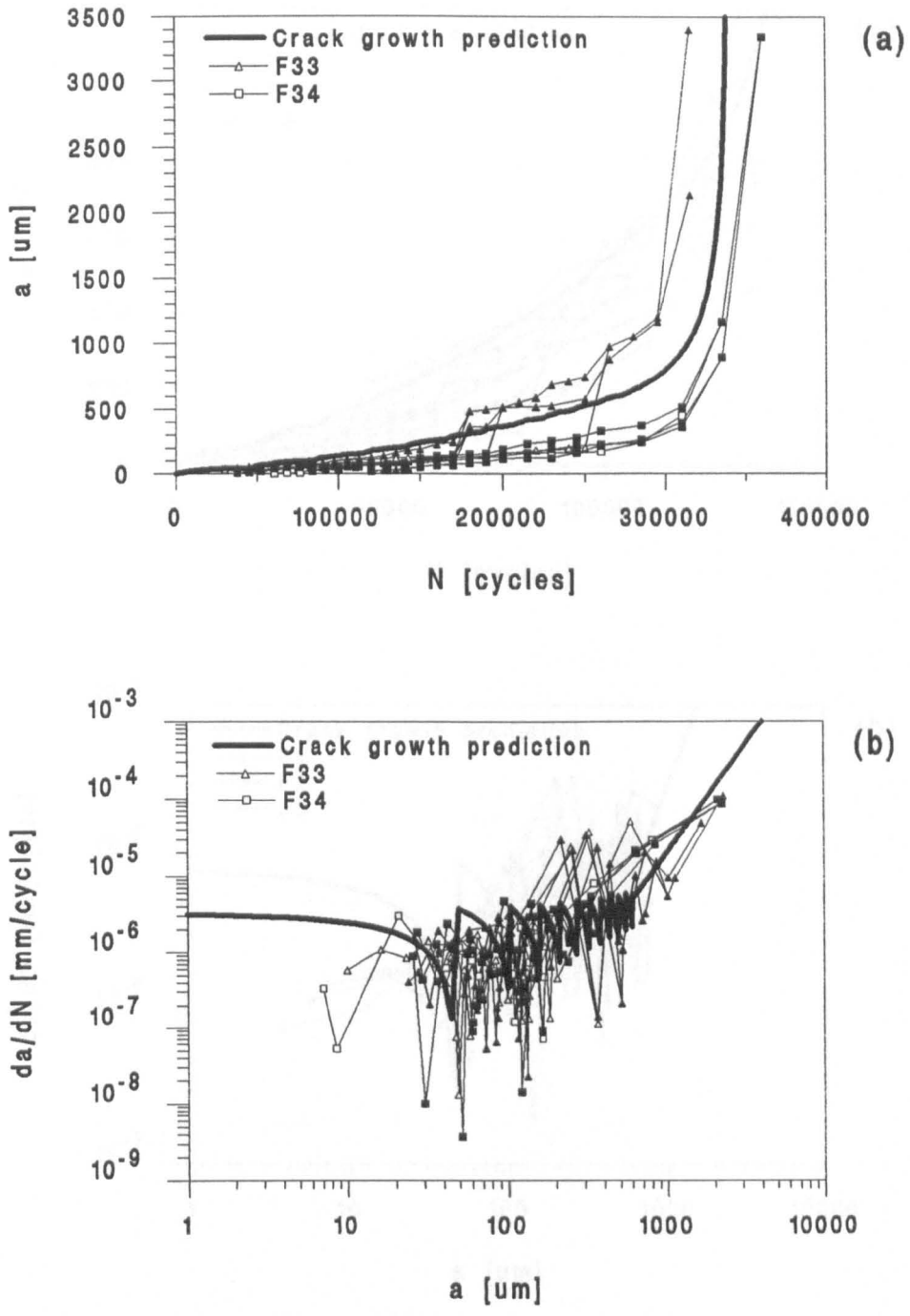

Fig. 5.14 Crack growth prediction and results for polished/as-received specimens, stress range 792MPa; (*a*) Half crack length versus number of cycles, and (*b*) Crack growth rate versus mean crack length.

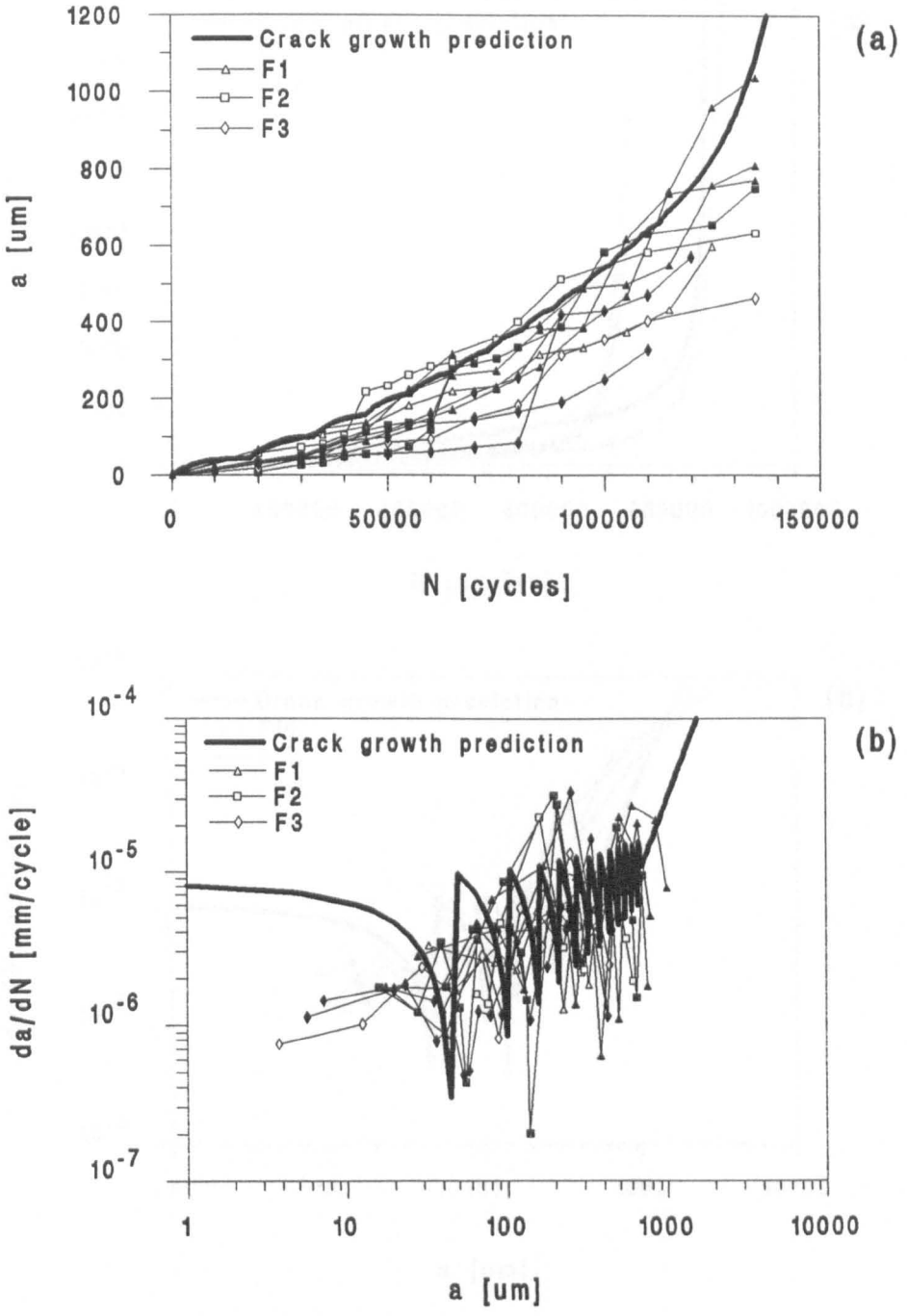

Fig. 5.15 Crack growth prediction and results for polished/as received specimens, stress range 850MPa; (*a*) Half crack length versus number of cycles, and (*b*) Crack growth rate versus mean crack length.

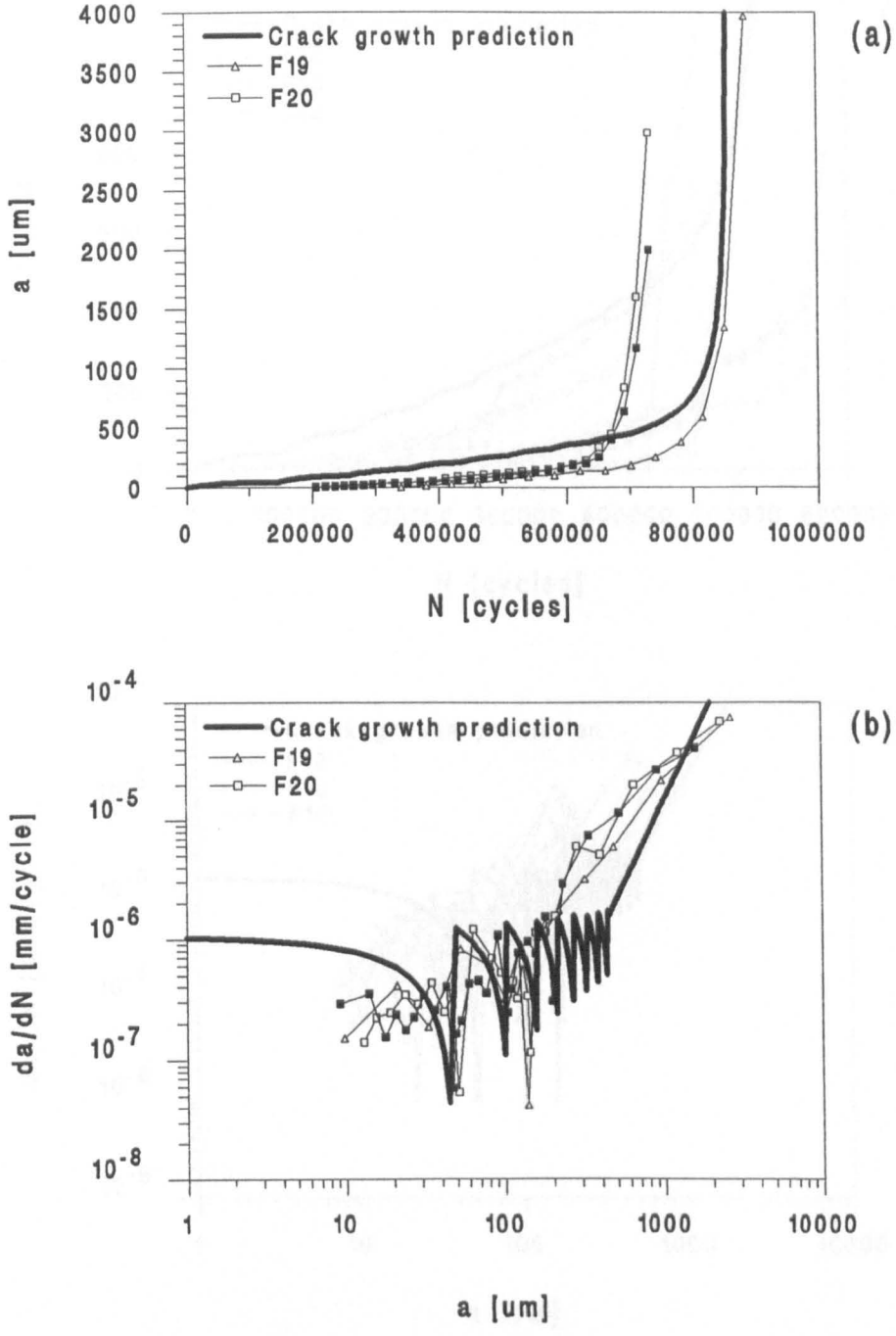

Fig. 5.16 Crack growth prediction and results for polished/stress relieved specimens, stress range 750MPa; (*a*) Half crack length versus number of cycles, and (*b*) Crack growth rate versus mean crack length.

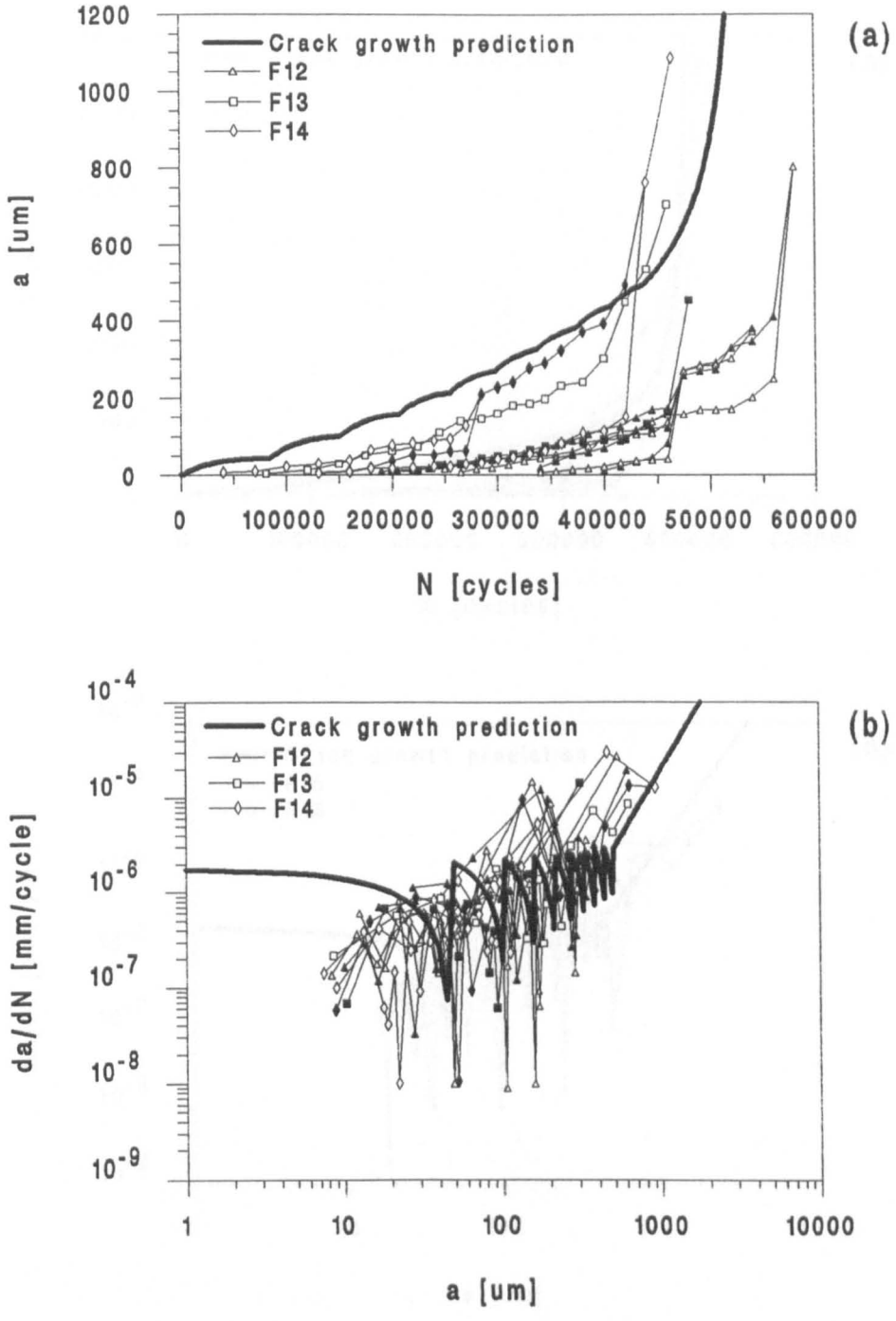

Fig. 5.17 Crack growth prediction and results for polished/stress relieved specimens, stress range 792MPa; (*a*) Half crack length versus number of cycles, and (*b*) Crack growth rate versus mean crack length.

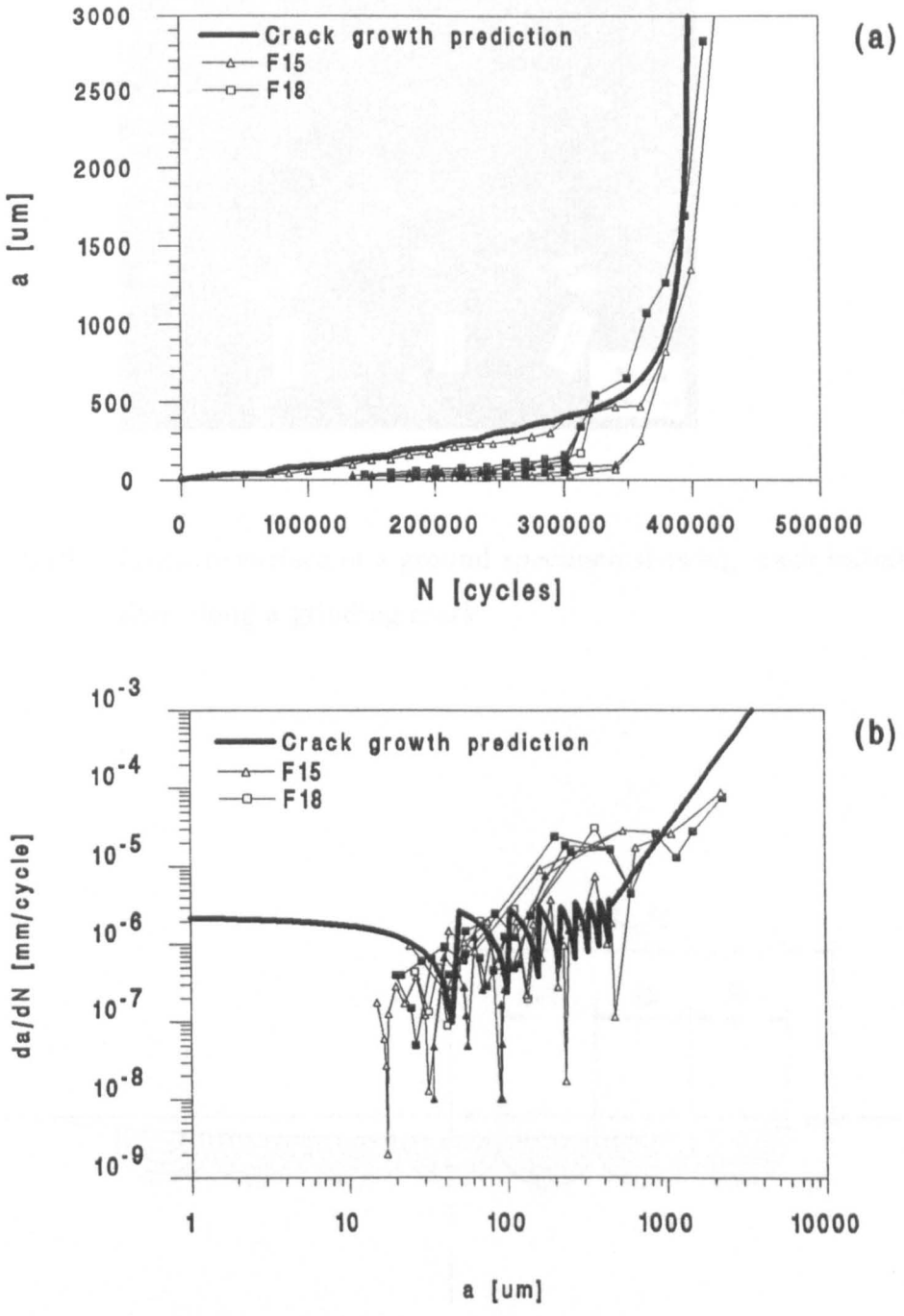

Fig. 5.18 Crack growth prediction and results for polished/stress relieved specimens, stress range 850MPa; (*a*) Half crack length versus number of cycles, and (*b*) Crack growth rate versus mean crack length.

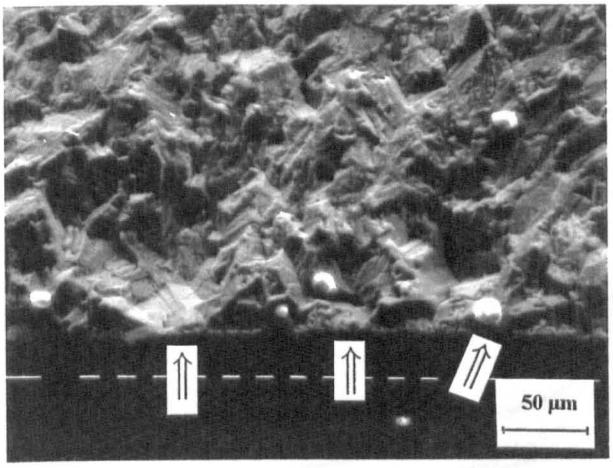

Fig. 5.19 Fracture surface of a ground specimen showing crack initiation sites along a grinding mark.

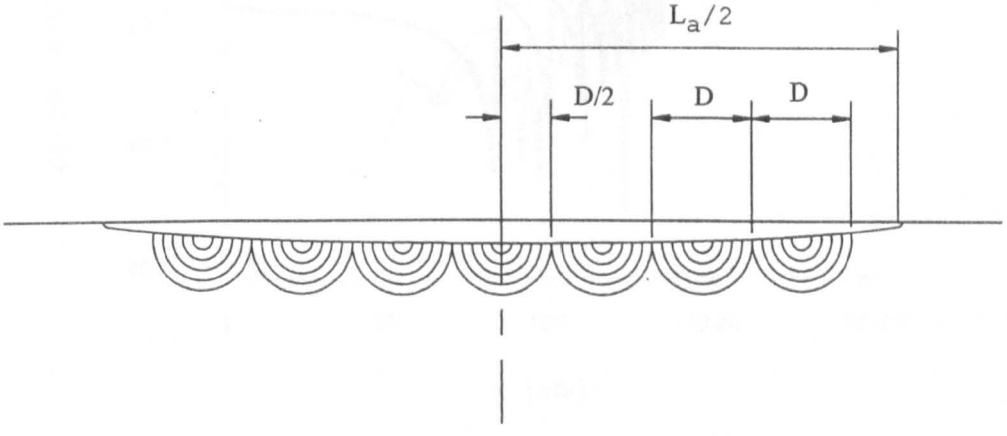

Fig. 5.20 Schematic representation of multiple initiation and coalescence of cracks along a grinding mark.

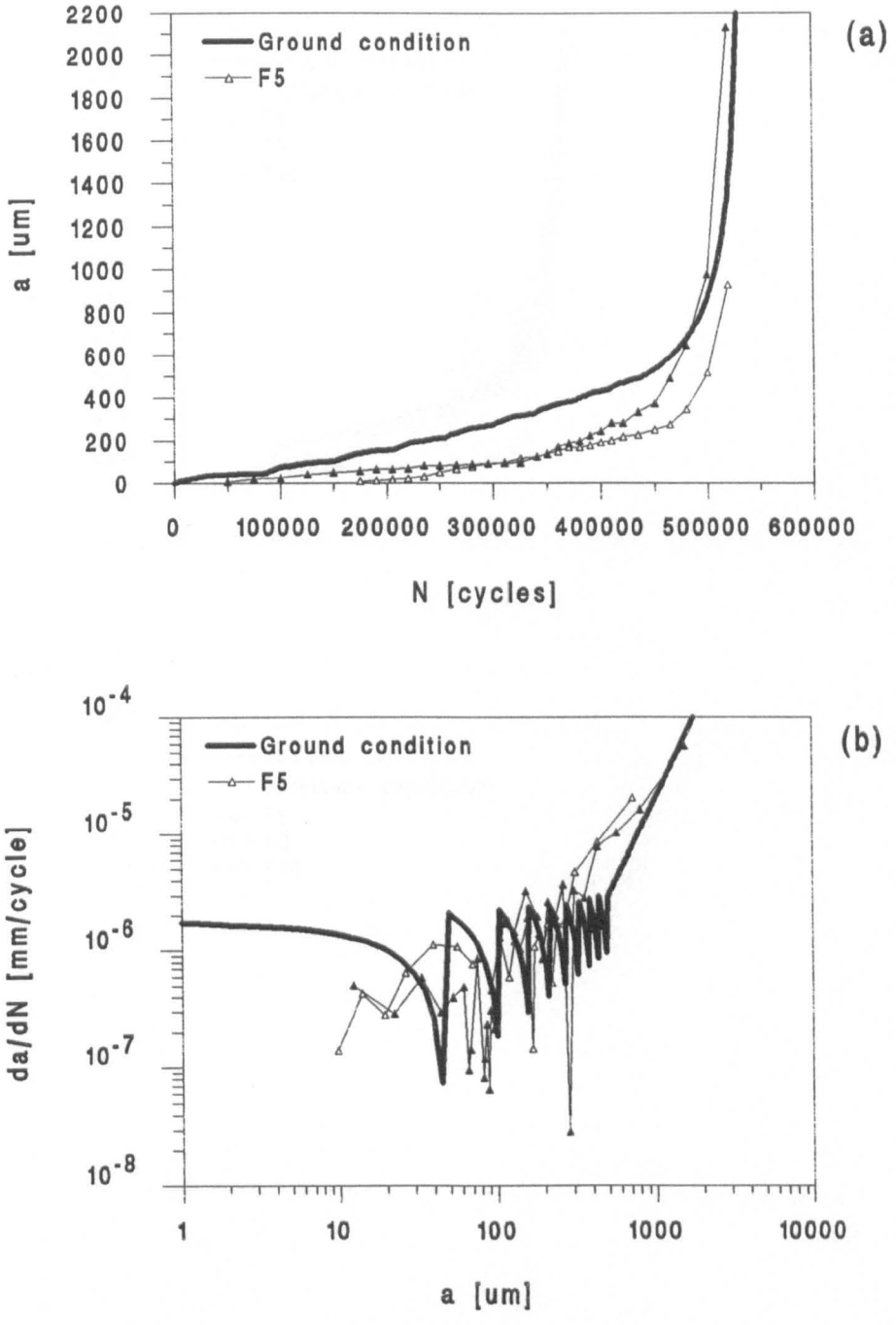

Fig. 5.21 Crack growth prediction and results for ground/stress relieved (condition 1) specimens, stress range 792MPa; (*a*) Half crack length versus number of cycles, and (*b*) Crack growth rate versus mean crack length.

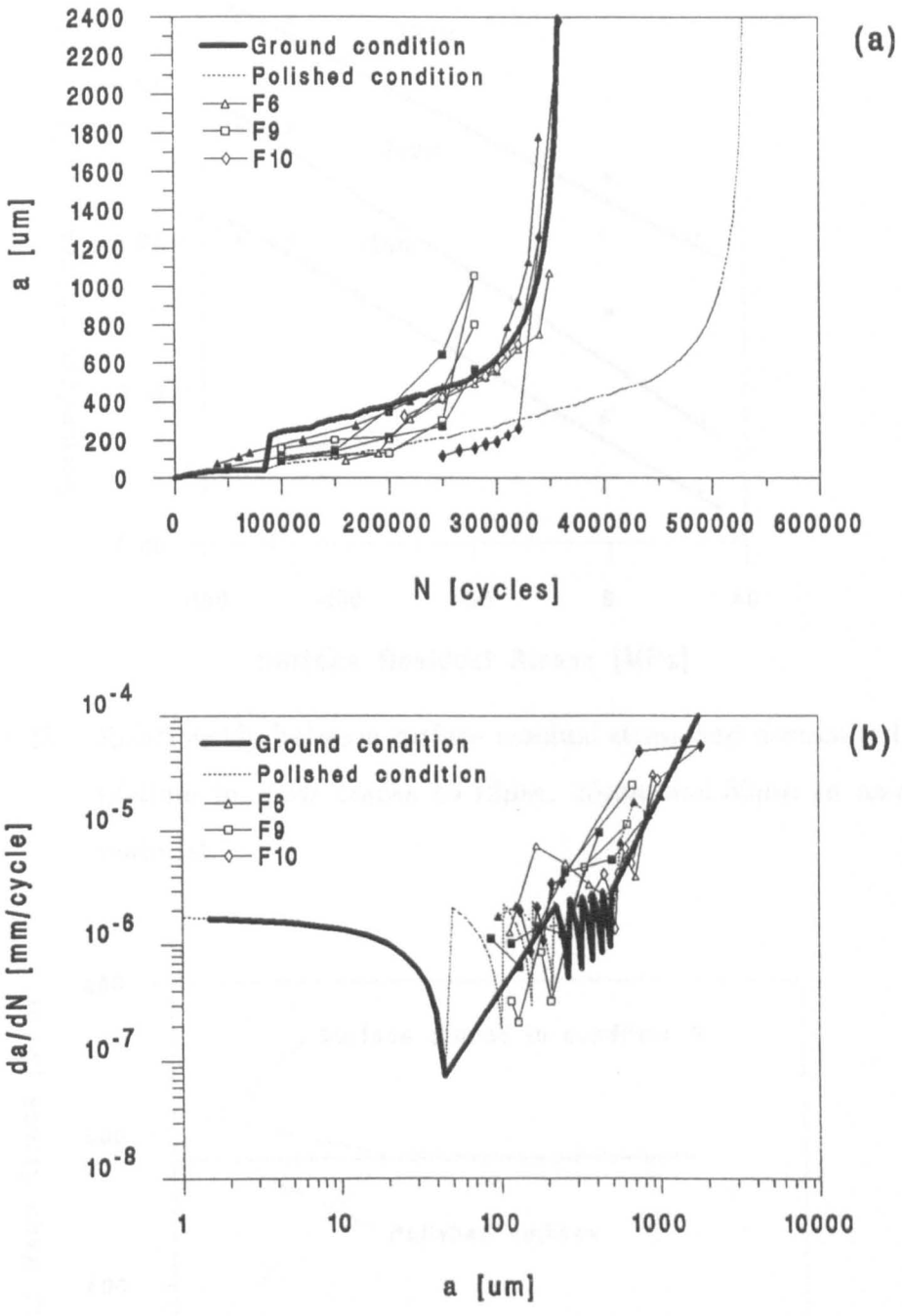

Fig. 5.22 Crack growth prediction and results for ground/stress relieved (condition 2) specimens, stress range 792MPa; (*a*) Half crack length versus number of cycles, and (*b*) Crack growth rate versus mean crack length.

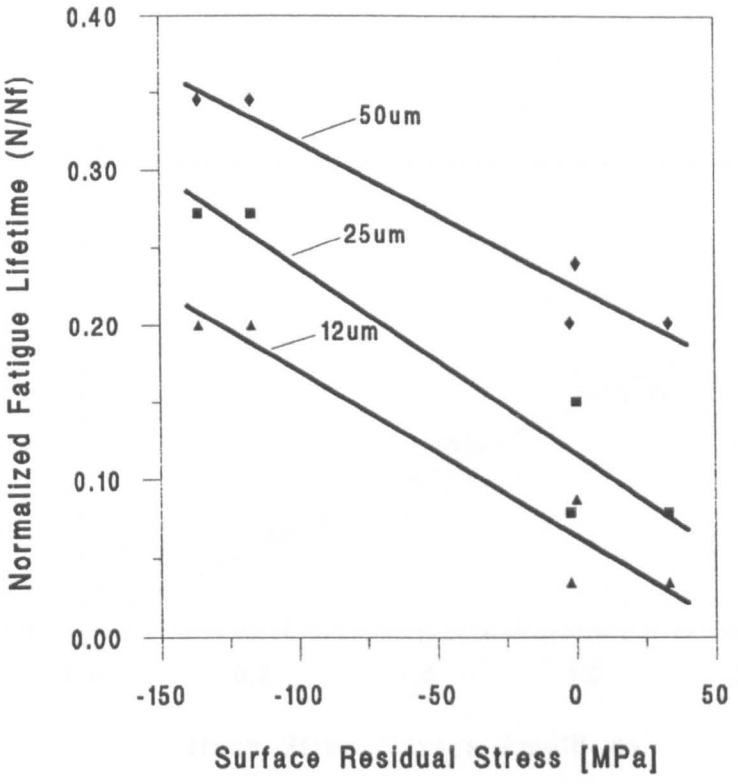

Fig. 5.23 Relationship between surface residual stress and normalized fatigue lifetime to grow cracks to $12\mu m$, $25\mu m$ and $50\mu m$ in as-received material.

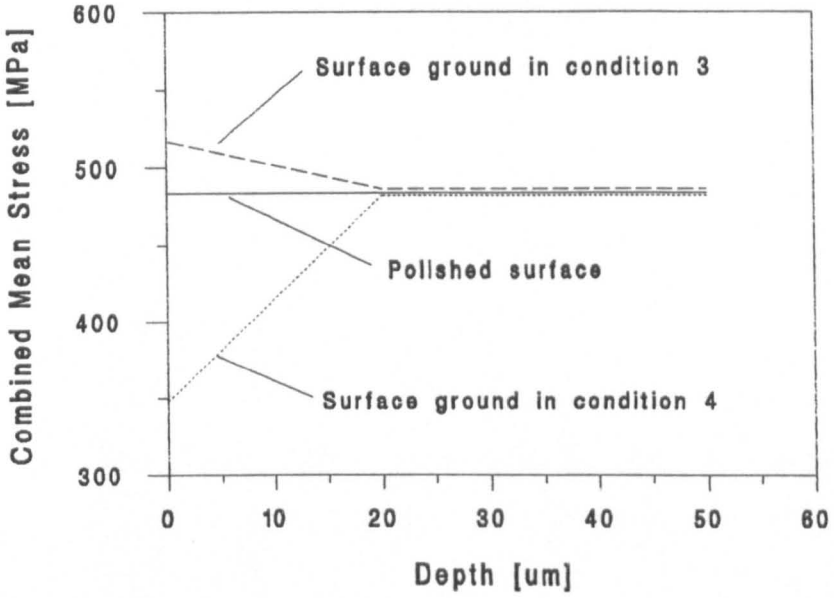

Fig. 5.24 Variation of combined mean stress with depth in ground/as-received specimens.

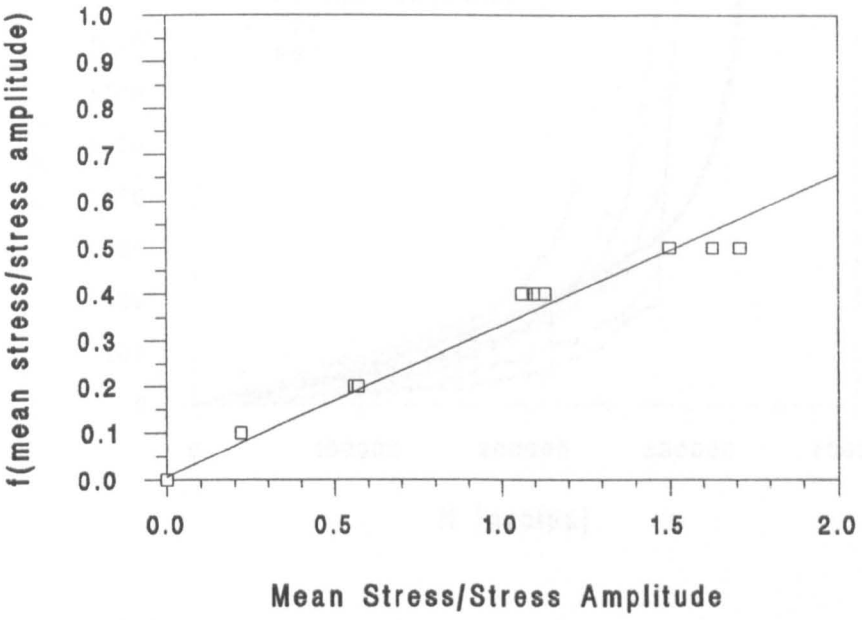

Fig. 5.25 Function $f(\sigma_m/\sigma_a)$ versus mean stress and stress amplitude ratio as derived from Wang and Miller [109].

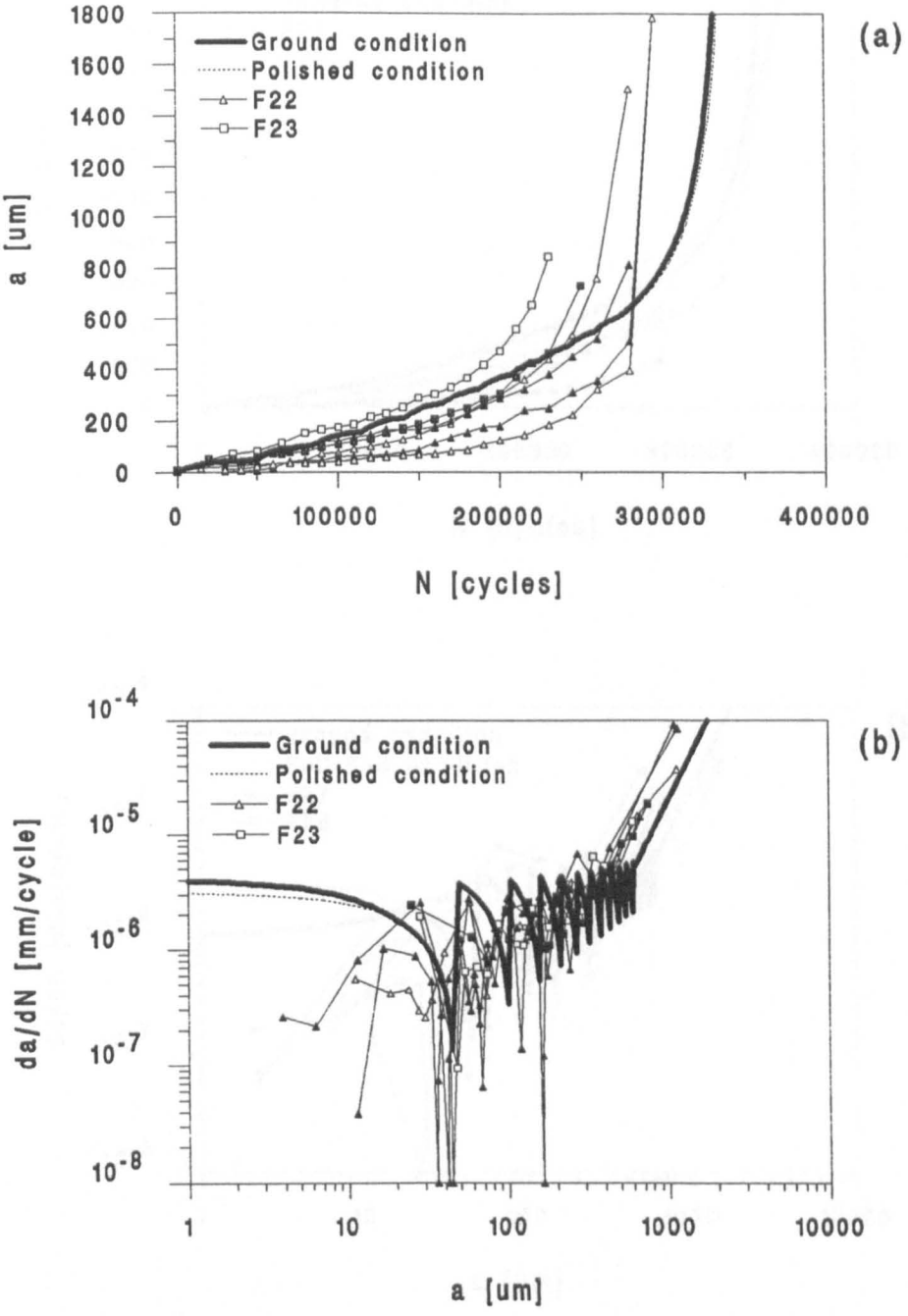

Fig. 5.26 Crack growth prediction and results for ground/as-received (condition 3) specimens, stress range 792MPa; (*a*) Half crack length versus number of cycles, and (*b*) Crack growth rate versus mean crack length.

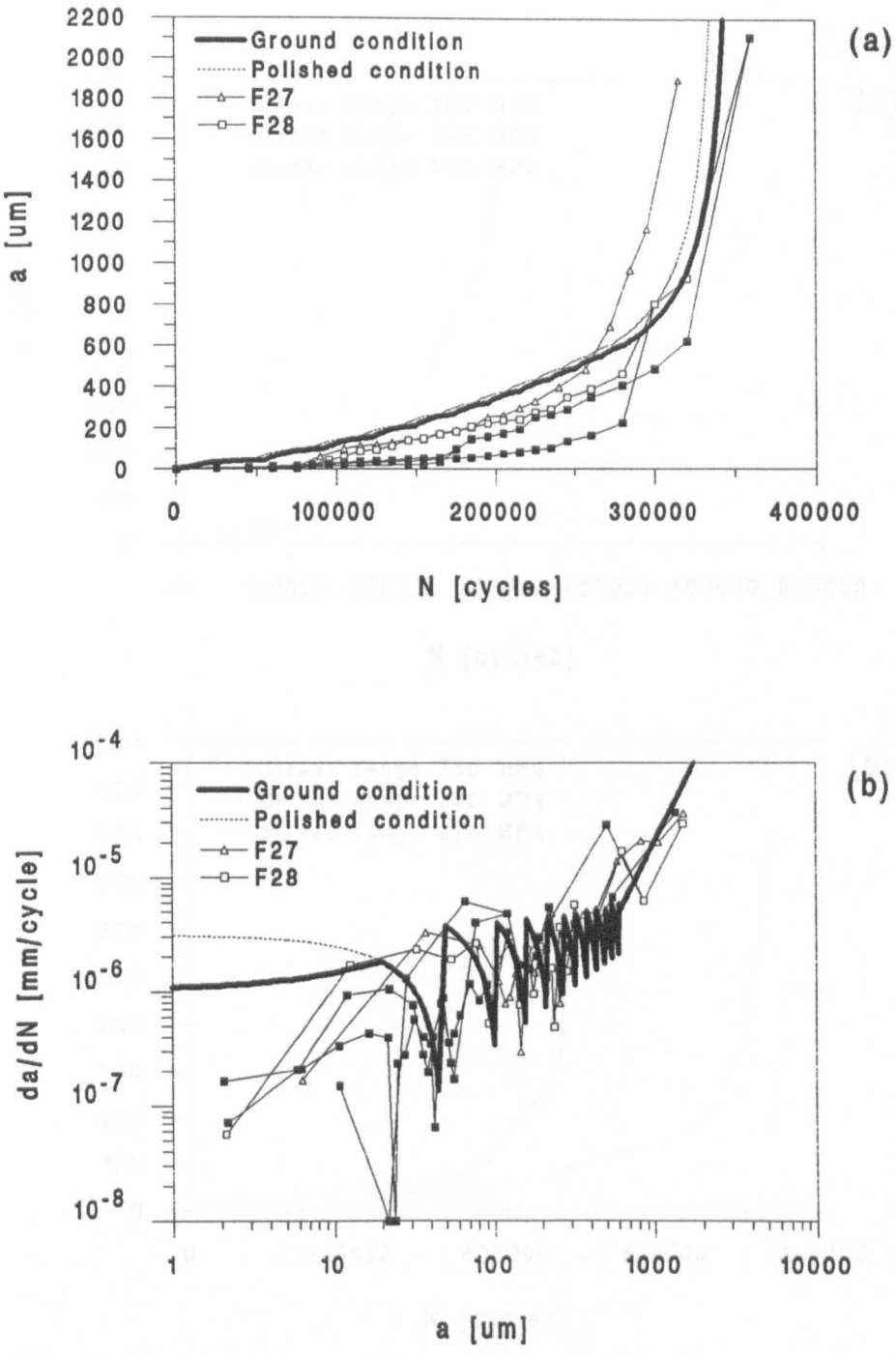

Fig. 5.27 Crack growth prediction and results for ground/as-received (condition 4) specimens, stress range 792MPa; (*a*) Half crack length versus number of cycles, and (*b*) Crack growth rate versus mean crack length.

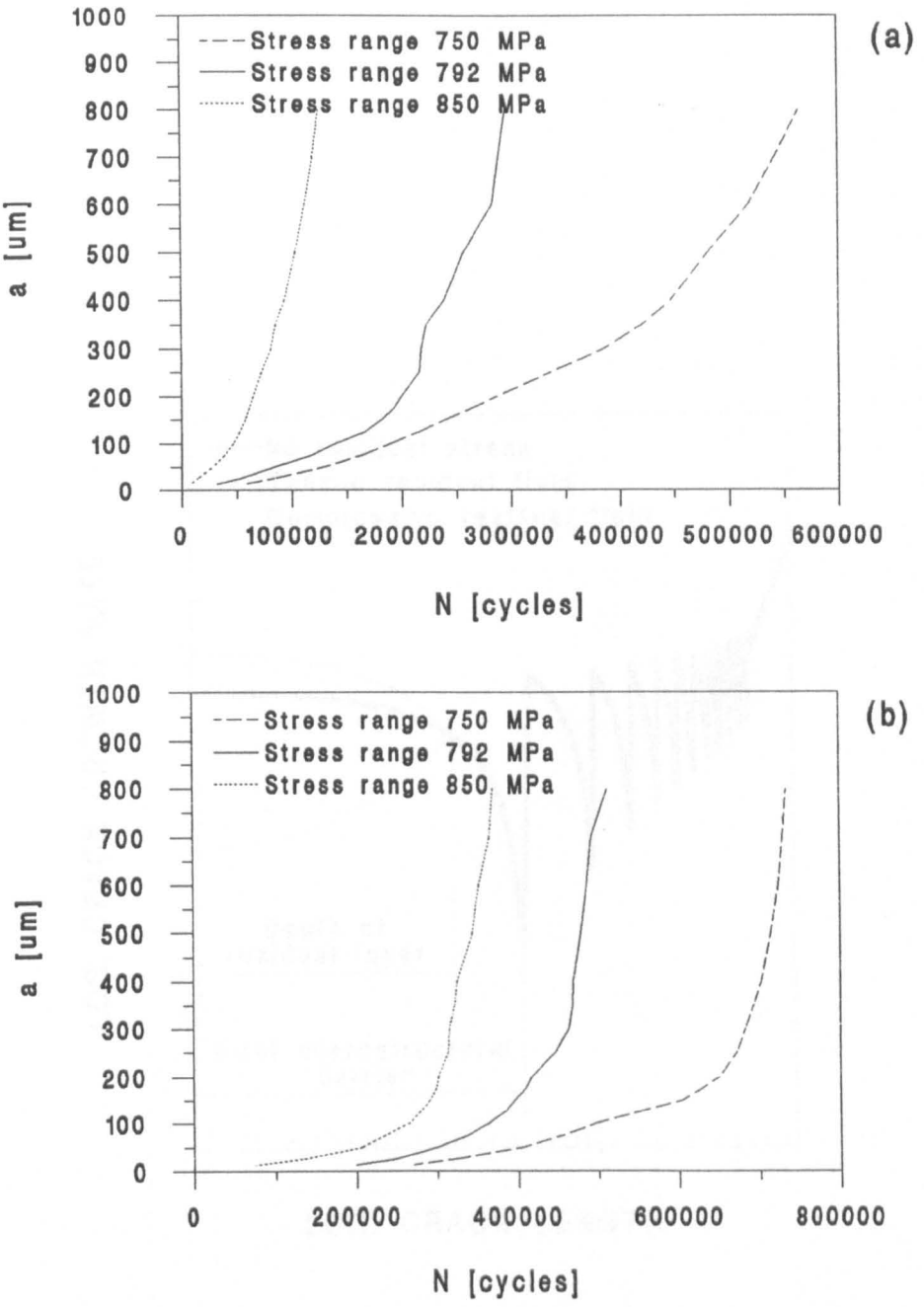

Fig. 6.1 Mean fatigue lifetimes for polished/electropolished specimens at different stress levels; (*a*) Material in as-received condition, (*b*) Material in stress relieved condition.

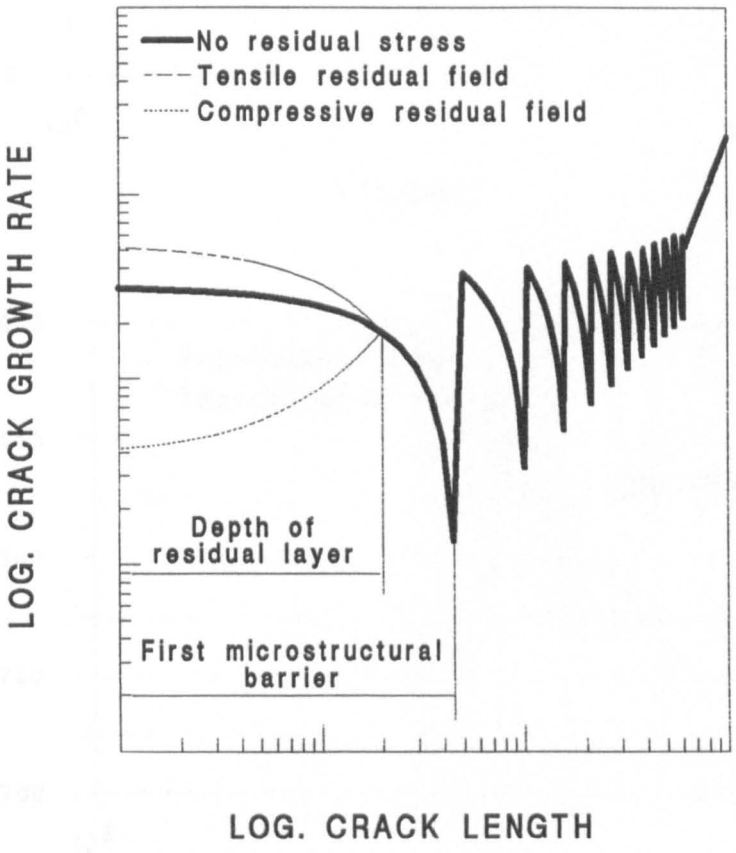

Fig. 6.2 Effect of residual stress fields induced by grinding operations on short fatigue crack growth.

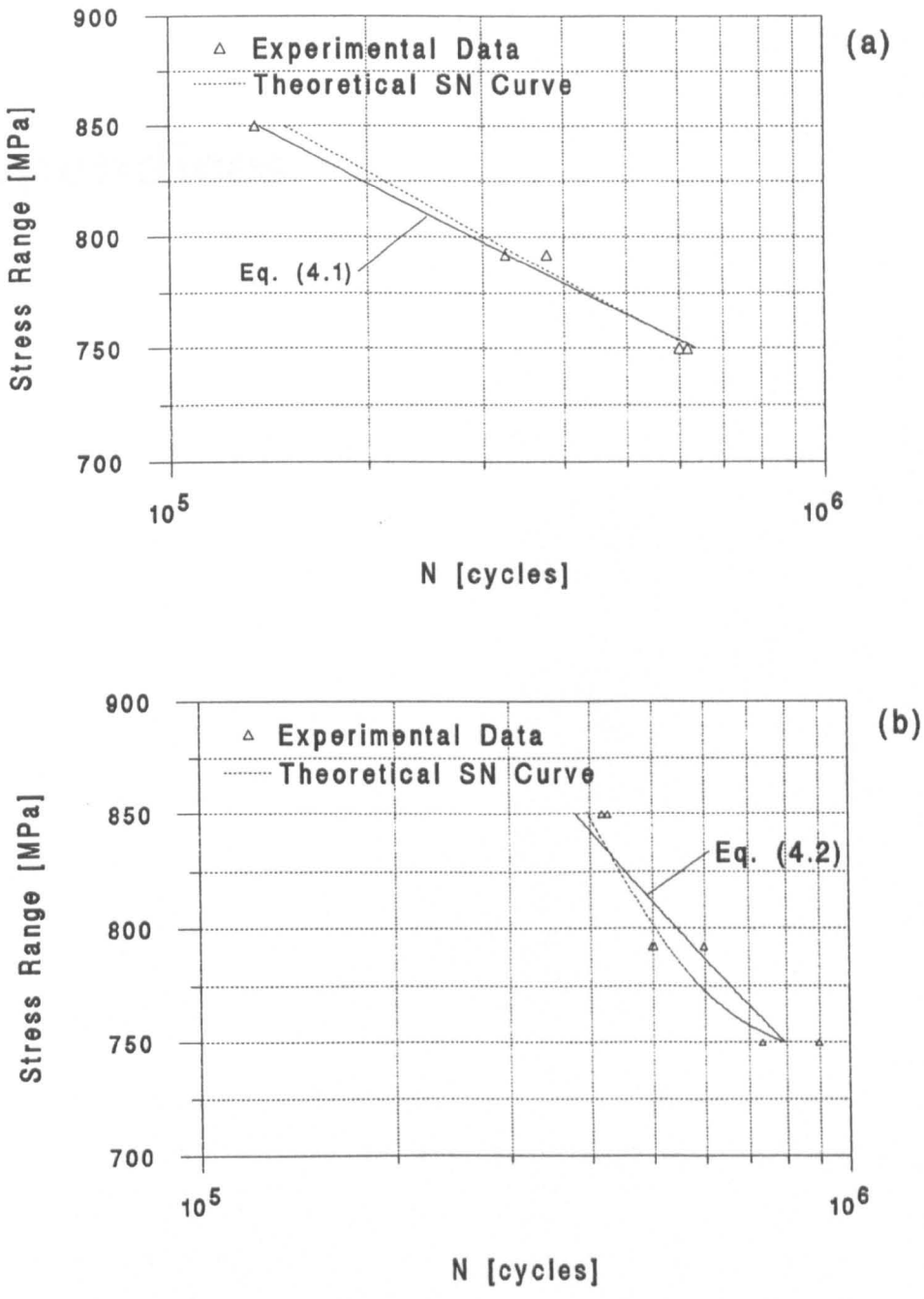

Fig. 6.3 Theoretical and experimental fatigue endurance (SN-data) for Waspaloy, polished surface finish; (*a*) Material in as-received condition, and (*b*) in stress relieved condition.

Appendices

Appendix A - Experimental Crack Growth Data

Table A1 - Experimental crack growth results for test F1 on polished surface/as-received material condition, Stress range 850MPa.

Number of Cycles	Half Surface Crack Length	Crack Growth Rate	Mean Crack Length
N	a	da/dN	a_{mean}
[cycles]	[μm]	[mm/cycle]	[μm]
Crack Number F1/1			
0	0.00	-	-
20000	65.42	3.2710E-06	32.71
35000	103.41	2.5327E-06	84.42
45000	126.11	2.2700E-06	114.76
55000	182.01	5.5900E-06	154.06
65000	218.87	3.6860E-06	200.44
75000	231.52	1.2650E-06	225.20
85000	315.09	8.3570E-06	273.31
95000	333.38	1.8290E-06	324.24
105000	374.04	4.0660E-06	353.71
115000	432.80	5.8760E-06	403.42
125000	599.85	1.6705E-05	516.33
Crack Number F1/2			
0	0.00	-	-
20000	56.17	2.8085E-06	28.09
35000	119.30	4.2087E-06	87.74
45000	136.42	1.7120E-06	127.86
55000	214.05	7.7630E-06	175.24
65000	259.90	4.5850E-06	236.98
75000	273.49	1.3590E-06	266.70
85000	380.96	1.0747E-05	327.23
95000	387.26	6.3000E-07	384.11
105000	616.87	2.2961E-05	502.07
115000	736.26	1.1939E-05	676.57
135000	771.87	1.7805E-06	754.07

continued on the next page

N	a	da/dN	a_{mean}
[cycles]	[μm]	[mm/cycle]	[μm]
Crack Number F1/3			
0	0.00	-	-
20000	35.37	1.7685E-06	17.69
35000	48.36	8.6600E-07	41.87
45000	114.15	6.5790E-06	81.26
55000	223.52	1.0937E-05	168.84
65000	316.40	9.2880E-06	269.96
75000	359.50	4.3100E-06	337.95
85000	392.71	3.3210E-06	376.11
95000	488.72	9.6010E-06	440.72
105000	499.64	1.0920E-06	494.18
115000	549.68	5.0040E-06	524.66
125000	758.76	2.0908E-05	654.22
135000	809.91	5.1150E-06	784.34
Crack Number F1/4			
0	0.00	-	-
20000	34.96	1.7480E-06	17.48
35000	61.05	1.7393E-06	48.01
45000	88.71	2.7660E-06	74.88
55000	128.95	4.0240E-06	108.83
65000	170.70	4.1750E-06	149.83
75000	224.23	5.3530E-06	197.47
85000	282.60	5.8370E-06	253.42
95000	385.49	1.0289E-05	334.05
105000	468.84	8.3350E-06	427.17
115000	742.13	2.7329E-05	605.49
125000	960.72	2.1859E-05	851.43
135000	1038.19	7.7470E-06	999.46

Table A2 - Experimental crack growth results for test F2 on polished surface/as-received material condition, Stress range 850MPa.

Number of Cycles	Half Surface Crack Length	Crack Growth Rate	Mean Crack Length
N	a	da/dN	a_{mean}
[cycles]	[μm]	[mm/cycle]	[μm]
Crack Number F2/1			
0	0.00	-	-
20000	57.03	2.8515E-06	28.52
30000	72.79	1.5760E-06	64.91
35000	79.64	1.3700E-06	76.22
40000	102.70	4.6120E-06	91.17
45000	217.58	2.2976E-05	160.14
50000	233.46	3.1760E-06	225.52
55000	262.33	5.7740E-06	247.90
60000	284.13	4.3600E-06	273.23
65000	295.10	2.1940E-06	289.62
70000	306.39	2.2580E-06	300.75
75000	353.69	9.4600E-06	330.04
80000	401.40	9.5420E-06	377.55
90000	512.81	1.1141E-05	457.11
110000	585.13	3.6160E-06	548.97
135000	633.19	1.9224E-06	609.16
Crack Number F2/2A			
0.00	0.00	-	-
20000	7.26	3.6300E-07	3.63
30000	24.74	1.7480E-06	16.00
35000	30.82	1.2160E-06	27.78
40000	47.93	3.4220E-06	39.38
45000	54.43	1.3000E-06	51.18
50000	56.58	4.3000E-07	55.51
55000	74.57	3.5980E-06	65.58
60000	117.49	8.5840E-06	96.03
65000	277.81	3.2064E-05	197.65
70000	290.73	2.5840E-06	284.27
75000	304.25	2.7040E-06	297.49

continued on the next page

N	a	da/dN	a_{mean}
[cycles]	[μm]	[mm/cycle]	[μm]
Crack Number F2/2A (continuation)			
80000	332.35	5.6200E-06	318.30
90000	388.62	5.6270E-06	360.49
100000	585.03	1.9641E-05	486.83
110000	632.65	4.7620E-06	608.84
125000	655.25	1.5067E-06	643.95
135000	749.93	9.4680E-06	702.59
Crack Number F2/2B			
0	0.00	-	-
20000	33.27	1.6635E-06	16.64
30000	50.96	1.7690E-06	42.12
35000	71.81	4.1700E-06	61.39
40000	93.56	4.3500E-06	82.69
45000	114.84	4.2560E-06	104.20
50000	129.57	2.9460E-06	122.21
55000	136.81	1.4480E-06	133.19
60000	137.83	2.0400E-07	137.32
65000	277.81	2.7996E-05	207.82
70000	290.73	2.5840E-06	284.27
75000	304.25	2.7040E-06	297.49
80000	332.35	5.6200E-06	318.30
90000	388.62	5.6270E-06	360.49
100000	585.03	1.9641E-05	486.83
110000	632.65	4.7620E-06	608.84
125000	655.25	1.5067E-06	643.95
135000	749.93	9.4680E-06	702.59

Table A3 - Experimental crack growth results for test F3 on polished surface/as-received material condition, Stress range 850MPa.

Number of Cycles	Half Surface Crack Length	Crack Growth Rate	Mean Crack Length
N	a	da/dN	a_{mean}
[cycles]	[μm]	[mm/cycle]	[μm]
Crack Number F3/1			
0	0.00	-	-
10000	7.58	7.5800E-07	3.79
20000	17.78	1.0200E-06	12.68
30000	41.33	2.3550E-06	29.56
40000	56.45	1.5120E-06	48.89
50000	84.46	2.8010E-06	70.46
60000	92.70	8.2400E-07	88.58
70000	150.09	5.7390E-06	121.40
80000	182.22	3.2130E-06	166.16
90000	313.05	1.3083E-05	247.64
100000	353.52	4.0470E-06	333.29
110000	403.27	4.9750E-06	378.40
135000	464.26	2.4396E-06	433.77
Crack Number F3/2A			
0	0.00	-	-
20000	34.07	1.7035E-06	17.04
30000	46.17	1.2100E-06	40.12
40000	88.63	4.2460E-06	67.40
50000	113.84	2.5210E-06	101.24
60000	159.69	4.5850E-06	136.77
70000	214.18	5.4490E-06	186.94
80000	255.74	4.1560E-06	234.96
90000	419.05	1.6331E-05	337.40
100000	430.44	1.1390E-06	424.75
110000	471.73	4.1290E-06	451.09
120000	572.03	1.0030E-05	521.88

continued on the next page

N	a	da/dN	a_{mean}
[cycles]	[μm]	[mm/cycle]	[μm]
Crack Number F3/2B			
0	0.00	-	-
10000	14.37	1.4370E-06	7.19
20000	32.67	1.8300E-06	23.52
30000	40.56	7.8900E-07	36.62
40000	50.98	1.0420E-06	45.77
50000	55.74	4.7600E-07	53.36
60000	60.82	5.0800E-07	58.28
70000	73.06	1.2240E-06	66.94
80000	84.62	1.1560E-06	78.84
90000	419.05	3.3443E-05	251.84
100000	430.44	1.1390E-06	424.75
110000	471.73	4.1290E-06	451.09
120000	572.03	1.0030E-05	521.88
Crack Number F3/3			
0	0.00	-	-
10000	11.31	1.1310E-06	5.66
20000	28.29	1.6980E-06	19.80
30000	42.58	1.4290E-06	35.44
40000	87.07	4.4490E-06	64.83
50000	98.80	1.1730E-06	92.94
60000	133.50	3.4700E-06	116.15
70000	144.36	1.0860E-06	138.93
80000	166.99	2.2630E-06	155.68
90000	190.81	2.3820E-06	178.90
100000	249.69	5.8880E-06	220.25
110000	326.97	7.7280E-06	288.33

Table A4 - Experimental crack growth results for test F33 on polished surface/as-received material condition, Stress range 792MPa.

Number of Cycles	Half Surface Crack Length	Crack Growth Rate	Mean Crack Length
N	a	da/dN	a_{mean}
[cycles]	[μm]	[mm/cycle]	[μm]
Crack Number F33/1A			
0	0.00	-	-
60000	37.33	6.2208E-07	18.66
67500	40.26	3.9133E-07	38.79
75000	43.23	3.9600E-07	41.75
82500	48.85	7.4933E-07	46.04
90000	48.95	1.3333E-08	48.90
105000	57.88	5.9533E-07	53.42
112500	58.47	7.8000E-08	58.17
120000	71.46	1.7327E-06	64.96
127500	77.17	7.6067E-07	74.31
135000	99.16	2.9327E-06	88.16
142500	100.98	2.4200E-07	100.07
150000	107.04	8.0800E-07	104.01
160000	109.81	2.7700E-07	108.42
170000	131.76	2.1950E-06	120.78
180000	134.55	2.7950E-07	133.15
190000	137.21	2.6600E-07	135.88
200000	511.70	3.7449E-05	324.46
220000	515.90	2.0975E-07	513.80
230000	526.92	1.1020E-06	521.41
250000	575.67	2.4378E-06	551.29
265000	881.51	2.0389E-05	728.59
295000	1169.84	9.6108E-06	1025.67
315000	2134.92	4.8254E-05	1652.38
Crack Number F33/1B1			
0	0.00	-	-
120000	22.75	1.8958E-07	11.38
127500	25.81	4.0800E-07	24.28
135000	29.92	5.4733E-07	27.86
142500	44.45	1.9380E-06	37.18
150000	51.56	9.4733E-07	48.00
160000	63.66	1.2105E-06	57.61

continued on the next page

N [cycles]	a [μm]	da/dN [mm/cycle]	a_{mean} [μm]
Crack Number F33/1B1 (continuation)			
170000	66.38	2.7200E-07	65.02
180000	365.30	2.9892E-05	215.84
190000	366.42	1.1250E-07	365.86
200000	511.70	1.4528E-05	439.06
220000	515.90	2.0975E-07	513.80
230000	526.92	1.1020E-06	521.41
250000	575.67	2.4378E-06	551.29
265000	881.51	2.0389E-05	728.59
295000	1169.84	9.6108E-06	1025.67
315000	2134.92	4.8254E-05	1652.38
Crack Number F33/1B2			
0	0.00	-	-
37500	7.77	2.0707E-07	3.88
45000	12.20	5.9133E-07	9.98
52500	20.34	1.0853E-06	16.27
60000	26.65	8.4133E-07	23.50
67500	37.39	1.4320E-06	32.02
75000	41.04	4.8667E-07	39.22
82500	47.64	8.7933E-07	44.34
90000	48.20	7.4667E-08	47.92
97500	56.06	1.0480E-06	52.13
105000	66.02	1.3287E-06	61.04
112500	67.98	2.6133E-07	67.00
120000	76.28	1.1067E-06	72.13
127500	81.54	7.0067E-07	78.91
135000	87.58	8.0533E-07	84.56
142500	89.25	2.2267E-07	88.41
150000	112.66	3.1220E-06	100.95
160000	117.25	4.5900E-07	114.96
170000	128.95	1.1700E-06	123.10
180000	365.30	2.3635E-05	247.12
190000	366.42	1.1250E-07	365.86
200000	511.70	1.4528E-05	439.06
220000	515.90	2.0975E-07	513.80
230000	526.92	1.1020E-06	521.41
250000	575.67	2.4378E-06	551.29
265000	881.51	2.0389E-05	728.59
295000	1169.84	9.6108E-06	1025.67
315000	2134.92	4.8254E-05	1652.38

continued on the next page

N	a	da/dN	a_{mean}
[cycles]	[μm]	[mm/cycle]	[μm]
Crack Number F33/1B3			
0	0.00	-	-
75000	60.96	8.1280E-07	30.48
82500	63.73	3.6933E-07	62.35
90000	65.06	1.7733E-07	64.40
97500	68.86	5.0600E-07	66.96
105000	84.82	2.1287E-06	76.84
112500	85.31	6.4667E-08	85.06
120000	86.72	1.8867E-07	86.01
127500	87.76	1.3867E-07	87.24
135000	90.35	3.4533E-07	89.06
142500	94.54	5.5867E-07	92.45
150000	115.91	2.8487E-06	105.22
160000	116.64	7.3000E-08	116.27
170000	146.38	2.9740E-06	131.51
180000	365.30	2.1892E-05	255.84
190000	366.42	1.1250E-07	365.86
200000	511.70	1.4528E-05	439.06
220000	515.90	2.0975E-07	513.80
230000	526.92	1.1020E-06	521.41
250000	575.67	2.4378E-06	551.29
265000	881.51	2.0389E-05	728.59
295000	1169.84	9.6108E-06	1025.67
315000	2134.92	4.8254E-05	1652.38
Crack Number F33/2A			
0	0.00	-	-
127500	118.20	9.2706E-07	59.10
135000	119.60	1.8600E-07	118.90
142500	121.88	3.0467E-07	120.74
150000	122.83	1.2667E-07	122.36
160000	127.77	4.9400E-07	125.30
170000	129.25	1.4750E-07	128.51
180000	134.80	5.5500E-07	132.02
190000	136.12	1.3200E-07	135.46
200000	158.01	2.1895E-06	147.06
220000	182.41	1.2200E-06	170.21
230000	183.76	1.3500E-07	183.09
240000	201.16	1.7400E-06	192.46

continued on the next page

N [cycles]	a [μm]	da/dN [mm/cycle]	a_{mean} [μm]
Crack Number F33/2A (continuation)			
250000	205.77	4.6050E-07	203.46
265000	975.47	5.1313E-05	590.62
280000	1056.85	5.4257E-06	1016.16
295000	1199.35	9.5000E-06	1128.10
315000	3399.79	1.1002E-04	2299.57
Crack Number F33/2B1			
0	0.00	-	-
30000	33.86	1.1285E-06	16.93
37500	41.28	9.9000E-07	37.57
45000	52.78	1.5333E-06	47.03
52500	54.98	2.9333E-07	53.88
60000	58.76	5.0400E-07	56.87
67500	65.22	8.6067E-07	61.99
75000	73.58	1.1153E-06	69.40
82500	73.98	5.3333E-08	73.78
90000	78.71	6.3000E-07	76.34
97500	100.18	2.8633E-06	89.44
105000	103.04	3.8067E-07	101.61
112500	106.28	4.3200E-07	104.66
120000	109.20	3.9000E-07	107.74
127500	115.62	8.5600E-07	112.41
135000	120.03	5.8733E-07	117.82
142500	122.76	3.6467E-07	121.39
150000	132.89	1.3500E-06	127.82
160000	133.11	2.2500E-08	133.00
170000	137.91	4.8000E-07	135.51
180000	480.99	3.4308E-05	309.45
190000	495.04	1.4050E-06	488.02
200000	511.50	1.6455E-06	503.27
210000	549.14	3.7645E-06	530.32
220000	584.11	3.6308E-06	547.80
230000	686.82	1.0271E-05	635.47
240000	712.74	2.5915E-06	699.78
250000	745.00	3.2265E-06	728.87
265000	975.47	1.5364E-05	860.23
280000	1056.85	5.4257E-06	1016.16
295000	1199.35	9.5000E-06	1128.10
315000	3399.79	1.1002E-04	2299.57

continued on the next page

N	a	da/dN	a_{mean}
[cycles]	[μm]	[mm/cycle]	[μm]
Crack Number F33/2B2			
0	0.00	-	-
45000	20.21	4.4911E-07	10.11
52500	31.98	1.5693E-06	26.10
60000	33.53	2.0667E-07	32.76
67500	41.65	1.0827E-06	37.59
75000	49.98	1.1100E-06	45.81
82500	64.88	1.9867E-06	57.43
90000	81.18	2.1733E-06	73.03
97500	99.09	2.3880E-06	90.13
105000	112.97	1.8513E-06	106.03
112500	117.24	5.6867E-07	115.10
120000	125.61	1.1160E-06	121.42
127500	140.77	2.0213E-06	133.19
135000	164.07	3.1067E-06	152.42
142500	184.29	2.6960E-06	174.18
150000	189.14	6.4667E-07	186.71
160000	229.56	4.0420E-06	209.35
170000	248.65	1.9095E-06	239.10
180000	480.99	2.3234E-05	364.82
190000	495.04	1.4050E-06	488.02
200000	511.50	1.6455E-06	503.27
210000	549.14	3.7645E-06	530.32
220000	584.11	3.4970E-06	566.63
230000	686.82	1.0271E-05	635.47
240000	712.74	2.5915E-06	699.78
250000	745.00	3.2265E-06	728.87
265000	975.47	1.5364E-05	860.23
280000	1056.85	5.4257E-06	1016.16
295000	1199.35	9.5000E-06	1128.10
315000	3399.79	1.1002E-04	2299.57

Table A5 - Experimental crack growth results for test F34 on polished surface/as-received material condition, Stress range 792MPa.

Number of Cycles	Half Surface Crack Length	Crack Growth Rate	Mean Crack Length
N	a	da/dN	a_{mean}
[cycles]	[μm]	[mm/cycle]	[μm]
Crack Number F34/1A1			
0	0.00	-	-
60000	5.71	9.5083E-08	2.85
68000	8.37	3.3313E-07	7.04
76000	8.79	5.2500E-08	8.58
84000	33.19	3.0500E-06	20.99
92000	38.88	7.1125E-07	36.04
100000	43.92	6.2938E-07	41.40
110000	55.80	1.1885E-06	49.86
120000	63.66	7.8600E-07	59.73
130000	68.62	4.9550E-07	66.14
140000	78.45	9.8350E-07	73.53
150000	98.84	2.0390E-06	88.65
160000	104.26	5.4150E-07	101.55
170000	109.51	5.2500E-07	106.88
180000	110.71	1.2050E-07	110.11
190000	132.22	2.1510E-06	121.47
200000	139.68	7.4600E-07	135.95
215000	163.84	1.6107E-06	151.76
230000	165.22	9.2000E-08	164.53
245000	166.29	7.1000E-08	165.75
260000	173.47	4.7867E-07	169.88
285000	246.30	2.9132E-06	209.88
310000	449.40	8.1240E-06	347.85
335000	1168.84	2.8778E-05	809.12
360000	3340.45	8.6864E-05	2254.65
Crack Number F34/1A2			
0	0.00	-	-
44000	27.54	6.2591E-07	13.77
52000	31.04	4.3688E-07	29.29
60000	41.45	1.3013E-06	36.24
68000	51.93	1.3100E-06	46.69
76000	51.96	3.7500E-09	51.94

continued on the next page

N	a	da/dN	a_{mean}
[cycles]	[μm]	[mm/cycle]	[μm]
Crack Number F34/1A2 (continuation)			
84000	59.74	9.7250E-07	55.85
92000	60.47	9.1250E-08	60.10
100000	61.42	1.1938E-07	60.94
110000	63.47	2.0450E-07	62.44
120000	65.46	1.9950E-07	64.46
130000	68.66	3.2000E-07	67.06
140000	71.09	2.4300E-07	69.88
150000	119.68	4.8585E-06	95.38
160000	139.25	1.9570E-06	129.46
170000	147.71	8.4650E-07	143.48
180000	152.34	4.6250E-07	150.02
190000	157.92	5.5800E-07	155.13
200000	189.33	3.1410E-06	173.62
215000	233.68	2.9570E-06	211.50
230000	254.13	1.3633E-06	243.91
245000	283.93	1.9867E-06	269.03
260000	330.47	3.1027E-06	307.20
285000	374.63	1.7662E-06	352.55
310000	515.94	5.6524E-06	445.28
335000	1168.84	2.6116E-05	842.39
360000	3340.45	8.6864E-05	2254.65
Crack Number F34/1B1			
0	0.00	-	-
84000	20.42	2.4304E-07	10.21
92000	34.91	1.8119E-06	27.66
100000	38.24	4.1625E-07	36.58
110000	50.80	1.2555E-06	44.52
120000	66.07	1.5275E-06	58.43
130000	75.49	9.4150E-07	70.78
140000	80.58	5.0900E-07	78.03
150000	85.88	5.3050E-07	83.23
160000	91.55	5.6650E-07	88.71
170000	104.45	1.2900E-06	98.00
180000	115.26	1.0810E-06	109.85
190000	118.36	3.1050E-07	116.81
200000	162.76	4.4395E-06	140.56
215000	164.12	9.0667E-08	163.44

continued on the next page

N	a	da/dN	a_{mean}
[cycles]	[μm]	[mm/cycle]	[μm]
Crack Number F34/1B1 (continuation)			
230000	195.30	2.0787E-06	179.71
245000	214.81	1.3007E-06	205.05
260000	229.09	9.5200E-07	221.95
285000	248.20	7.6440E-07	238.64
310000	357.90	4.3880E-06	303.05
335000	898.06	2.1607E-05	627.98
360000	3340.45	9.7696E-05	2119.26
Crack Number F34/1B2			
0	0.00	-	-
120000	21.44	1.7863E-07	10.72
130000	30.37	8.9350E-07	25.90
140000	30.37	1.0000E-08	30.37
150000	54.17	2.3800E-06	42.27
160000	64.90	1.0730E-06	59.54
170000	72.47	7.5650E-07	68.68
180000	81.91	9.4400E-07	77.19
190000	93.05	1.1140E-06	87.48
200000	117.59	2.4545E-06	105.32
215000	120.98	2.2567E-07	119.28
230000	121.19	1.4333E-08	121.08
245000	166.33	3.0093E-06	143.76
260000	221.73	3.6933E-06	194.03
285000	262.45	1.6286E-06	242.09
310000	399.31	5.4744E-06	330.88
335000	898.06	1.9950E-05	648.68
360000	3340.45	9.7696E-05	2119.26

Table A6 - Experimental crack growth results for test F4 on polished surface/as-received material condition, Stress range 750MPa.

Number of Cycles	Half Surface Crack Length	Crack Growth Rate	Mean Crack Length
N	a	da/dN	a_{mean}
[cycles]	[μm]	[mm/cycle]	[μm]
Crack Number F4/1			
0	0.0	-	-
210000	14.70	7.0000E-08	7.35
225000	66.27	3.4380E-06	40.49
240000	75.88	6.4067E-07	71.08
255000	89.46	9.0533E-07	82.67
270000	96.94	4.9867E-07	93.20
285000	108.42	7.6533E-07	102.68
300000	152.15	2.9153E-06	130.29
315000	177.20	1.6700E-06	164.68
330000	187.08	6.5867E-07	182.14
Crack Number F4/2			
0	0.00	-	-
75000	33.04	4.4053E-07	16.52
100000	51.50	7.3840E-07	42.27
125000	64.00	5.0000E-07	57.75
150000	66.76	1.1040E-07	65.38
165000	71.54	3.1867E-07	69.15
180000	81.17	6.4200E-07	76.36
195000	92.75	7.7200E-07	86.96
Crack Number F4/3			
0	0.0	-	-
50000	3.64	7.2800E-08	1.82
75000	17.53	5.5560E-07	10.59
100000	33.60	6.4280E-07	25.57
125000	67.55	1.3580E-06	50.58
150000	94.99	1.0976E-06	81.27
165000	99.74	3.1667E-07	97.37
180000	116.53	1.1193E-06	108.14
195000	175.70	3.9447E-06	146.12
210000	210.11	2.2940E-06	192.91
225000	232.74	1.5087E-06	221.43

continued on the next page

N	a	da/dN	a_{mean}
[cycles]	[μm]	[mm/cycle]	[μm]
Crack Number F4/3 (continuation)			
240000	266.78	2.2693E-06	249.76
255000	279.92	8.7600E-07	273.35
270000	281.68	1.1733E-07	280.80
285000	287.27	3.7267E-07	284.48
315000	288.65	4.6000E-08	287.96
330000	290.49	1.2267E-07	289.57
345000	291.72	8.2000E-08	291.11
Crack Number F4/4			
0	0.00	-	-
25000	9.83	3.9320E-07	4.92
50000	36.55	1.0688E-06	23.19
75000	67.00	1.2180E-06	51.78
100000	82.88	6.3520E-07	74.94
125000	115.51	1.3052E-06	99.20
150000	126.66	4.4600E-07	121.09
165000	128.34	1.1200E-07	127.50
180000	141.89	9.0333E-07	135.12
195000	147.91	4.0133E-07	144.90
210000	154.52	4.4067E-07	151.22
225000	214.13	3.9740E-06	184.33
240000	223.43	6.2000E-07	218.78
255000	233.58	6.7667E-07	228.51
270000	238.52	3.2933E-07	236.05
285000	241.40	1.9200E-07	239.96
300000	243.76	1.5733E-07	242.58
330000	244.32	1.8667E-08	244.04
345000	252.60	5.5200E-07	248.46

Table A7 - Experimental crack growth results for test F32 on polished surface/as-received material condition, Stress range 750MPa.

Number of Cycles	Half Surface Crack Length	Crack Growth Rate	Mean Crack Length
N	a	da/dN	a_{mean}
[cycles]	[μm]	[mm/cycle]	[μm]
Crack Number F32/1			
0	0.00	-	-
85000	26.76	3.1476E-07	13.38
105000	29.87	1.5550E-07	28.31
115000	34.19	4.3250E-07	32.03
125000	35.52	1.3250E-07	34.85
140000	41.61	4.0633E-07	38.56
147500	42.01	5.3333E-08	41.81
155000	43.74	2.3000E-07	42.87
162500	44.84	1.4667E-07	44.29
170000	44.95	1.4667E-08	44.89
177500	45.10	2.0000E-08	45.02
185000	46.84	2.3200E-07	45.97
192500	47.89	1.4067E-07	47.36
200000	47.89	1.0000E-08	47.89
207500	52.80	6.5467E-07	50.35
215000	58.49	7.5800E-07	55.64
225000	61.27	2.7800E-07	59.88
235000	66.47	5.2000E-07	63.87
250000	66.57	6.6667E-09	66.52
265000	74.34	5.1833E-07	70.45
280000	87.42	8.7167E-07	80.88
295000	104.74	1.1550E-06	96.08
310000	110.80	4.0367E-07	107.77
325000	131.98	1.4123E-06	121.39
340000	154.44	1.4970E-06	143.21
355000	173.28	1.2560E-06	163.86
370000	180.50	4.8167E-07	176.89
385000	182.10	1.0667E-07	181.30
400000	223.77	2.7777E-06	202.93
415000	258.48	2.3140E-06	241.12
430000	274.55	1.0717E-06	266.51

continued on the next page

N [cycles]	a [μm]	da/dN [mm/cycle]	a_{mean} [μm]
Crack Number F32/1 (continuation)			
445000	338.29	4.2493E-06	306.42
460000	386.80	3.2337E-06	362.54
480000	438.33	2.5765E-06	412.56
500000	496.59	2.9130E-06	467.46
520000	580.94	4.2175E-06	538.76
540000	664.96	4.2013E-06	622.95
560000	691.30	1.3170E-06	678.13
580000	900.55	1.0463E-05	795.93
600000	1473.74	2.8660E-05	1187.15
610000	2407.84	9.3410E-05	1940.79
Crack Number F32/2			
0	0.00	-	-
115000	43.33	3.7674E-07	21.66
125000	50.70	7.3700E-07	47.01
132500	52.43	2.3067E-07	51.56
140000	54.75	3.1000E-07	53.59
147500	60.99	8.3200E-07	57.87
155000	64.78	5.0467E-07	62.88
162500	84.07	2.5727E-06	74.42
170000	92.76	1.1580E-06	88.41
177500	93.85	1.4600E-07	93.30
185000	99.67	7.7533E-07	96.76
192500	107.83	1.0880E-06	103.75
200000	109.29	1.9533E-07	108.56
207500	117.39	1.0800E-06	113.34
215000	120.28	3.8533E-07	118.84
225000	130.46	1.0175E-06	125.37
235000	137.52	7.0600E-07	133.99
250000	168.21	2.0460E-06	152.86
265000	176.82	5.7433E-07	172.51
280000	189.83	8.6733E-07	183.33
295000	215.84	1.7340E-06	202.84
310000	221.51	3.7800E-07	218.68
325000	228.22	4.4700E-07	224.86
340000	252.35	1.6090E-06	240.28
355000	257.07	3.1433E-07	254.71
370000	291.18	2.2743E-06	274.12
385000	331.83	2.7097E-06	311.50

continued on the next page

N	a	da/dN	a_{mean}
[cycles]	[μm]	[mm/cycle]	[μm]
Crack Number F32/2 (continuation)			
400000	344.96	8.7567E-07	338.39
415000	361.99	1.1350E-06	353.47
430000	403.49	2.7667E-06	382.74
445000	438.57	2.3387E-06	421.03
460000	511.30	4.8487E-06	474.93
480000	520.10	4.4000E-07	515.70
500000	556.76	1.8333E-06	538.43
520000	562.51	2.8750E-07	559.64
540000	682.05	5.9768E-06	622.28
560000	731.57	2.4760E-06	706.81
580000	855.65	6.2043E-06	793.61
600000	1059.64	1.0199E-05	957.64
610000	1788.28	7.2864E-05	1423.96
Crack Number F32/3A			
0	0.00	-	-
25000	4.24	1.6960E-07	2.12
50000	8.95	1.8820E-07	6.59
85000	12.47	1.0057E-07	10.71
105000	28.10	7.8150E-07	20.28
115000	34.55	6.4550E-07	31.32
125000	37.96	3.4050E-07	36.25
132500	44.03	8.1000E-07	40.99
140000	52.71	1.1567E-06	48.37
147500	57.77	6.7467E-07	55.24
155000	63.50	7.6467E-07	60.63
162500	71.51	1.0673E-06	67.50
170000	79.69	1.0907E-06	75.60
177500	98.63	2.5260E-06	89.16
185000	108.00	1.2493E-06	103.32
192500	122.54	1.9387E-06	115.27
200000	128.34	7.7333E-07	125.44
215000	161.38	2.2027E-06	144.86
225000	161.38	1.0000E-08	161.38
235000	181.20	1.9815E-06	171.29
250000	181.51	2.0667E-08	181.35
265000	188.97	4.9733E-07	185.24
280000	193.13	2.7767E-07	191.05
295000	198.41	3.5200E-07	195.77

continued on the next page

N	a	da/dN	a_{mean}
[cycles]	[μm]	[mm/cycle]	[μm]
Crack Number F32/3A (continuation)			
310000	207.36	5.9667E-07	202.89
325000	213.46	4.0633E-07	210.41
340000	280.69	4.4820E-06	247.07
355000	316.69	2.4003E-06	298.69
370000	317.82	7.5333E-08	317.26
385000	341.07	1.5497E-06	329.44
400000	364.84	1.5847E-06	352.95
415000	408.86	2.9350E-06	386.85
430000	457.17	3.2203E-06	433.01
445000	479.77	1.5070E-06	468.47
460000	559.92	5.3430E-06	519.84
480000	601.69	2.0885E-06	580.80
500000	690.78	4.4545E-06	646.23
520000	746.87	2.8048E-06	718.82
540000	781.82	1.7473E-06	764.34
560000	799.26	8.7200E-07	790.54
580000	858.49	2.9615E-06	828.87
600000	1901.08	5.2130E-05	1379.78
610000	2196.99	2.9592E-05	2049.03
Crack Number F32/3B			
0	0.00	-	-
162500	22.80	1.4028E-07	11.40
170000	26.88	5.4400E-07	24.84
177500	27.14	3.4667E-08	27.01
185000	29.02	2.5067E-07	28.08
192500	29.07	6.6667E-09	29.04
200000	29.51	5.8667E-08	29.29
215000	29.82	2.1000E-08	29.66
225000	30.63	8.1000E-08	30.23
235000	46.34	1.5710E-06	38.49
250000	50.63	2.8600E-07	48.49
265000	101.97	3.4223E-06	76.30
280000	105.61	2.4300E-07	103.79
295000	116.97	7.5700E-07	111.29
310000	134.12	1.1433E-06	125.54
325000	142.43	5.5433E-07	138.27
340000	160.42	1.1993E-06	151.43
355000	166.63	4.1367E-07	163.52

continued on the next page

N [cycles]	a [μm]	da/dN [mm/cycle]	a_{mean} [μm]
Crack Number F32/3B (continuation)			
370000	176.04	6.2767E-07	171.33
385000	192.61	1.1043E-06	184.32
400000	203.66	7.3700E-07	198.13
415000	229.06	1.6933E-06	216.36
430000	239.15	6.7233E-07	234.10
445000	276.45	2.4870E-06	257.80
460000	292.82	1.0913E-06	284.64
480000	319.81	1.3495E-06	306.32
500000	365.12	2.2655E-06	342.47
520000	454.65	4.4763E-06	409.88
540000	505.08	2.5215E-06	479.86
560000	531.77	1.3345E-06	518.42
580000	758.19	1.1321E-05	644.98
600000	1901.08	5.7145E-05	1329.63
610000	2196.99	2.9592E-05	2049.03
Crack Number F32/4			
0	0.00	-	-
25000	16.07	6.4260E-07	8.03
50000	30.74	5.8700E-07	23.40
85000	54.01	6.6471E-07	42.37
105000	75.27	1.0633E-06	64.64
115000	90.16	1.4885E-06	82.71
125000	98.74	8.5800E-07	94.45
132500	119.27	2.7373E-06	109.00
140000	124.55	7.0467E-07	121.91
147500	127.36	3.7467E-07	125.96
155000	134.55	9.5800E-07	130.95
162500	137.51	3.9533E-07	136.03
170000	140.55	4.0533E-07	139.03
177500	150.48	1.3233E-06	145.51
185000	152.45	2.6333E-07	151.46
192500	153.79	1.7800E-07	153.12
200000	158.26	5.9667E-07	156.02
207500	161.01	3.6667E-07	159.64
215000	166.63	7.4933E-07	163.82
225000	175.04	8.4050E-07	170.83
235000	182.90	7.8600E-07	178.97
250000	199.29	1.0927E-06	191.09

continued on the next page

N	a	da/dN	a_{mean}
[cycles]	[μm]	[mm/cycle]	[μm]
Crack Number F32/4 (continuation)			
265000	199.42	8.6667E-09	199.35
280000	220.96	1.4363E-06	210.19
295000	227.88	4.6133E-07	224.42
310000	265.12	2.4827E-06	246.50
325000	307.55	2.8287E-06	286.34
340000	319.83	8.1867E-07	313.69
355000	321.32	9.9333E-08	320.58
370000	339.40	1.2050E-06	330.36
385000	365.00	1.7067E-06	352.20
400000	371.95	4.6367E-07	368.47
415000	394.53	1.5053E-06	383.24
430000	401.22	4.4567E-07	397.87
445000	456.18	3.6643E-06	428.70
460000	490.64	2.2970E-06	473.41
480000	526.82	1.8093E-06	508.73
500000	603.09	3.8135E-06	564.96
520000	671.06	3.3983E-06	637.07
540000	788.75	5.8848E-06	729.90
560000	904.14	5.7693E-06	846.44
580000	1268.33	1.8210E-05	1086.23
600000	2254.24	4.9296E-05	1761.28

Table A.8 - Experimental crack growth results for test F15 on polished surface/stress relieved material condition, Stress range 850MPa.

Number of Cycles	Half Surface Crack Length	Crack Growth Rate	Mean Crack Length
N	a	da/dN	a_{mean}
[cycles]	[μm]	[mm/cycle]	[μm]
Crack Number F15/1A			
0	0.00	-	-
25000	12.40	4.9600E-07	6.20
50000	36.71	9.7220E-07	24.55
70000	42.05	2.6700E-07	39.38
85000	45.65	2.4033E-07	43.85
100000	61.37	1.0480E-06	53.51
115000	90.96	1.9727E-06	76.17
135000	100.00	4.5175E-07	95.48
150000	130.05	2.0037E-06	115.02
165000	133.33	2.1833E-07	131.69
180000	160.47	1.8093E-06	146.90
195000	170.48	6.6767E-07	165.47
205000	207.74	3.7260E-06	189.11
215000	210.51	2.7650E-07	209.12
225000	223.50	1.2990E-06	217.00
235000	233.13	9.6300E-07	228.31
245000	233.30	1.7000E-08	233.21
260000	256.66	1.5573E-06	244.98
275000	278.83	1.4780E-06	267.74
290000	304.23	1.6937E-06	291.53
305000	416.43	7.4797E-06	360.33
320000	431.38	9.9700E-07	423.90
340000	469.38	1.8998E-06	450.38
360000	471.63	1.1275E-07	470.50
380000	823.59	1.7598E-05	647.61
400000	1351.21	2.6381E-05	1087.40
420000	3092.85	8.7082E-05	2222.03
Crack Number F15/1B1			
0	0.00	-	-
135000	34.31	2.5415E-07	17.16
150000	34.31	1.0000E-08	34.31

continued on the next page

N [cycles]	a [μm]	da/dN [mm/cycle]	a_{mean} [μm]
Crack Number F15/1B1 (continuation)			
165000	35.03	4.8000E-08	34.67
180000	45.39	6.9067E-07	40.21
195000	51.68	4.1933E-07	48.54
205000	54.43	2.7500E-07	53.06
215000	55.63	1.2000E-07	55.03
225000	56.13	5.0000E-08	55.88
235000	68.60	1.2465E-06	62.36
245000	71.19	2.5950E-07	69.89
260000	89.96	1.2510E-06	80.57
275000	89.96	1.0000E-08	89.96
290000	92.45	1.6600E-07	91.20
305000	92.45	1.0000E-08	92.45
320000	93.23	5.2333E-08	92.84
340000	98.51	2.6400E-07	95.87
360000	251.86	7.6673E-06	175.18
380000	823.59	2.8587E-05	537.72
400000	1351.21	2.6381E-05	1087.40
420000	3092.85	8.7082E-05	2222.03
Crack Number F15/1B2			
0	0.00	-	-
180000	13.84	7.6861E-08	6.92
195000	16.45	1.7433E-07	15.14
205000	17.05	6.0000E-08	16.75
215000	17.32	2.7000E-08	17.19
225000	17.34	2.0000E-09	17.33
235000	18.57	1.2300E-07	17.96
245000	21.40	2.8300E-07	19.99
260000	23.99	1.7233E-07	22.69
275000	29.62	3.7567E-07	26.80
290000	31.43	1.2033E-07	30.52
305000	31.61	1.2333E-08	31.52
320000	54.28	1.5110E-06	42.94
340000	70.56	8.1400E-07	62.42
360000	251.86	9.0650E-06	161.21
380000	823.59	2.8587E-05	537.72
400000	1351.21	2.6381E-05	1087.40
420000	3092.85	8.7082E-05	2222.03

Table A.9 - Experimental crack growth results for test F18 on polished surface/stress relieved material condition, Stress range 850MPa.

Number of Cycles	Half Surface Crack Length	Crack Growth Rate	Mean Crack Length
N	a	da/dN	a_{mean}
[cycles]	[μm]	[mm/cycle]	[μm]
Crack Number F18/1A			
0	0.00	-	-
145000	21.87	1.5083E-07	10.94
165000	30.84	4.4825E-07	26.35
185000	33.49	1.3275E-07	32.16
200000	40.97	4.9867E-07	37.23
220000	42.74	8.8500E-08	41.86
240000	52.70	4.9775E-07	47.72
255000	82.86	2.0110E-06	67.78
270000	90.85	5.3267E-07	86.86
285000	133.39	2.8357E-06	112.12
301000	136.54	1.9688E-07	134.96
313000	173.02	3.0404E-06	154.78
325000	546.90	3.1156E-05	359.96
349000	655.09	4.5081E-06	600.99
365000	1071.41	2.6020E-05	863.25
380000	1268.20	1.3119E-05	1169.81
395000	1690.57	2.8158E-05	1479.38
410000	2832.14	7.6105E-05	2261.35
Crack Number F18/1B1			
0	0.00	-	-
165000	16.01	9.7030E-08	8.01
185000	23.97	3.9775E-07	19.99
200000	26.22	1.5033E-07	25.09
220000	27.21	4.9500E-08	26.72
240000	40.14	6.4650E-07	33.68
255000	43.88	2.4933E-07	42.01
270000	66.04	1.4770E-06	54.96
285000	102.98	2.4627E-06	84.51
301000	123.08	1.2566E-06	113.03
313000	346.49	1.8617E-05	234.78
325000	546.50	1.6668E-05	446.49
349000	655.09	4.5246E-06	600.80

continued on the next page

N	a	da/dN	a_{mean}
[cycles]	[μm]	[mm/cycle]	[μm]
Crack Number F18/1B1 (continuation)			
365000	1071.41	2.6020E-05	863.25
380000	1268.20	1.3119E-05	1169.81
395000	1690.57	2.8158E-05	1479.38
410000	2832.14	7.6105E-05	2261.35
Crack Number F18/1B2			
0.00	0.00	-	-
145000	38.83	2.6776E-07	19.41
165000	46.93	4.0525E-07	42.88
185000	62.07	7.5675E-07	54.50
200000	72.06	6.6600E-07	67.06
220000	77.80	2.8700E-07	74.93
240000	87.06	4.6325E-07	82.43
255000	106.22	1.2773E-06	96.64
270000	113.62	4.9333E-07	109.92
285000	122.04	5.6100E-07	117.83
301000	159.82	2.3613E-06	140.93
313000	346.49	1.5556E-05	253.15
325000	546.90	1.6701E-05	446.69
349000	655.09	4.5081E-06	600.99
365000	1071.41	2.6020E-05	863.25
380000	1268.20	1.3119E-05	1169.81
395000	1690.57	2.8158E-05	1479.38
410000	2832.14	7.6105E-05	2261.35
Crack Number F18/1B3			
0	0.00	-	-
240000	18.69	7.7854E-08	9.34
255000	24.66	3.9833E-07	21.67
270000	33.85	6.1233E-07	29.25
285000	47.64	9.1967E-07	40.74
301000	57.47	6.1438E-07	52.56
313000	346.49	2.4085E-05	201.98
325000	546.90	1.6701E-05	446.69
349000	655.09	4.5081E-06	600.99
365000	1071.41	2.6020E-05	863.25
380000	1268.20	1.3119E-05	1169.81
395000	1690.57	2.8158E-05	1479.38
410000	2832.14	7.6105E-05	2261.35

Table A.10 - Experimental crack growth results for test F12 on polished surface/stress relieved material condition, Stress range 792MPa.

Number of Cycles	Half Surface Crack Length	Crack Growth Rate	Mean Crack Length
N	a	da/dN	a_{mean}
[cycles]	[μm]	[mm/cycle]	[μm]
Crack Number F12/1A1			
0	0.00	-	-
250000	16.02	6.4080E-08	8.01
265000	28.24	8.1433E-07	22.13
280000	33.05	3.2067E-07	30.64
295000	43.01	6.6400E-07	38.03
310000	44.84	1.2200E-07	43.92
325000	49.18	2.8967E-07	47.01
340000	49.18	1.0000E-08	49.18
355000	54.49	3.5367E-07	51.83
370000	63.11	5.7500E-07	58.80
385000	76.29	8.7867E-07	69.70
400000	92.79	1.0997E-06	84.54
415000	105.84	8.7033E-07	99.31
430000	105.98	9.0000E-09	105.91
445000	108.50	1.6800E-07	107.24
460000	136.91	1.8943E-06	122.70
475000	269.92	8.8670E-06	203.41
490000	285.68	1.0510E-06	277.80
505000	290.99	3.5400E-07	288.34
520000	328.22	2.4820E-06	309.61
540000	346.32	9.0500E-07	337.27
560000	409.89	3.1785E-06	378.11
580000	804.87	1.9749E-05	607.38
Crack Number F12/1A2			
0	0.00	-	-
400000	11.40	2.8488E-08	5.70
415000	22.00	7.0700E-07	16.70
430000	34.43	8.2867E-07	28.22
445000	48.03	9.0667E-07	41.23
460000	83.28	2.3500E-06	65.66
475000	269.92	1.2442E-05	176.60
490000	285.68	1.0510E-06	277.80
505000	290.99	3.5400E-07	288.34

continued on the next page

N	a	da/dN	a_{mean}
[cycles]	[μm]	[mm/cycle]	[μm]
Crack Number F12/1A2 (continuation)			
520000	328.22	2.4820E-06	309.61
540000	346.32	9.0500E-07	337.27
560000	409.89	3.1785E-06	378.11
580000	804.87	1.9749E-05	607.38
Crack Number F12/1B			
0	0.00	-	-
265000	8.04	3.0321E-08	4.02
280000	17.01	5.9833E-07	12.52
295000	19.44	1.6167E-07	18.22
310000	27.27	5.2200E-07	23.35
325000	36.69	6.2833E-07	31.98
340000	44.32	5.0867E-07	40.51
355000	46.00	1.1200E-07	45.16
370000	53.80	5.1967E-07	49.90
385000	59.32	3.6833E-07	56.56
400000	101.47	2.8097E-06	80.39
415000	112.80	7.5567E-07	107.13
430000	116.68	2.5833E-07	114.74
445000	139.40	1.5150E-06	128.04
460000	158.12	1.2477E-06	148.76
475000	158.12	1.0000E-08	158.12
490000	168.87	7.1700E-07	163.49
505000	170.26	9.2333E-08	169.56
520000	171.22	6.4000E-08	170.74
540000	200.53	1.4655E-06	185.87
560000	248.70	2.4088E-06	224.61
580000	804.87	2.7809E-05	526.79
Crack Number F12/2A1			
0	0.00	-	-
340000	19.00	5.5882E-08	9.50
355000	35.80	1.1200E-06	27.40
370000	54.55	1.2497E-06	45.17
385000	61.33	4.5233E-07	57.94
400000	70.69	6.2367E-07	66.01
415000	91.22	1.3690E-06	80.95
430000	115.50	1.6183E-06	103.36
445000	121.22	3.8133E-07	118.36
460000	123.04	1.2133E-07	122.13

continued on the next page

N	a	da/dN	a_{mean}
[cycles]	[μm]	[mm/cycle]	[μm]
Crack Number F12/2A1 (continuation)			
475000	268.97	9.7287E-06	196.00
490000	270.00	6.9000E-08	269.48
505000	290.00	1.3333E-06	280.00
520000	350.00	4.0000E-06	320.00
540000	373.30	1.1648E-06	361.65
Crack Number F12/2A2			
0	0.00	-	-
340000	7.27	2.1382E-08	3.64
355000	9.31	1.3600E-07	8.29
370000	14.77	3.6400E-07	12.04
385000	17.42	1.7633E-07	16.09
400000	22.71	3.5267E-07	20.06
415000	32.41	6.4700E-07	27.56
430000	38.37	3.9733E-07	35.39
445000	40.53	1.4367E-07	39.45
460000	43.70	2.1167E-07	42.11
475000	268.97	1.5018E-05	156.33
490000	282.99	9.3467E-07	275.98
505000	285.16	1.4500E-07	284.07
520000	301.81	1.1100E-06	293.49
540000	373.30	3.5743E-06	337.55
Crack Number F12/3			
0	0.00	-	-
190000	8.74	4.5974E-08	4.37
205000	11.20	1.6433E-07	9.97
220000	15.55	2.8967E-07	13.37
235000	17.31	1.1767E-07	16.43
250000	27.63	6.8767E-07	22.47
265000	28.11	3.2333E-08	27.87
280000	37.06	5.9667E-07	32.59
295000	39.42	1.5700E-07	38.24
310000	44.97	3.7000E-07	42.19
325000	56.97	8.0000E-07	50.97
340000	64.51	5.0300E-07	60.74
355000	77.10	8.3933E-07	70.81
370000	91.34	9.4933E-07	84.22

continued on the next page

N	a	da/dN	a_{mean}
[cycles]	[μm]	[mm/cycle]	[μm]
Crack Number F12/3 (continuation)			
385000	105.06	9.1467E-07	98.20
400000	120.81	1.0497E-06	112.93
415000	126.21	3.6000E-07	123.51
430000	149.03	1.5213E-06	137.62
445000	169.87	1.3893E-06	159.45
460000	174.18	2.8733E-07	172.02
475000	257.72	5.5693E-06	215.95
490000	269.03	7.5433E-07	263.37
505000	273.03	2.6633E-07	271.03
520000	329.96	3.7957E-06	301.49
540000	379.96	2.4998E-06	354.96

Table A.11 - Experimental crack growth results for test F13 on polished surface/stress relieved material condition, Stress range 792MPa.

Number of Cycles	Half Surface Crack Length	Crack Growth Rate	Mean Crack Length
N	a	da/dN	a_{mean}
[cycles]	[μm]	[mm/cycle]	[μm]
Crack Number F13/1			
0	0.00	-	-
80000	4.27	5.3313E-08	2.13
120000	12.93	2.1650E-07	8.60
150000	29.96	5.6783E-07	21.44
175000	51.87	8.7640E-07	40.92
200000	62.28	4.1640E-07	57.08
225000	74.28	4.8000E-07	68.28
245000	109.99	1.7855E-06	92.14
265000	139.81	1.4908E-06	124.90
285000	146.43	3.3100E-07	143.12
300000	159.83	8.9367E-07	153.13
315000	180.50	1.3780E-06	170.17
330000	184.87	2.9133E-07	182.69
345000	196.45	7.7200E-07	190.66
360000	230.32	2.2580E-06	213.39
380000	239.06	4.3675E-07	234.69
400000	301.59	3.1265E-06	270.32
420000	449.10	7.3755E-06	375.34
440000	534.87	4.2888E-06	491.98
460000	705.42	8.5275E-06	620.15
480000	998.33	1.4646E-05	851.88
Crack Number F13/2			
0	0.00	-	-
200000	9.52	4.7575E-08	4.76
225000	11.20	6.7200E-08	10.36
245000	24.94	6.8725E-07	18.07
265000	30.08	2.5700E-07	27.51
285000	43.52	6.7200E-07	36.80
300000	51.27	5.1667E-07	47.40
315000	54.45	2.1167E-07	52.86
330000	65.91	7.6433E-07	60.18

continued on the next page

N	a	da/dN	a_{mean}
[cycles]	[μm]	[mm/cycle]	[μm]
Crack Number F13/2 (continuation)			
345000	75.15	6.1600E-07	70.53
360000	81.59	4.2900E-07	78.37
380000	84.47	1.4400E-07	83.03
400000	92.27	3.9025E-07	88.37
420000	93.50	6.1500E-08	92.89
440000	132.89	1.9693E-06	113.19
460000	164.07	1.5590E-06	148.48
480000	454.86	1.4540E-05	309.46

Table A.12 - Experimental crack growth results for test F14 on polished surface/stress relieved material condition, Stress range 792MPa.

Number of Cycles	Half Surface Crack Length	Crack Growth Rate	Mean Crack Length
N	a	da/dN	a_{mean}
[cycles]	[μm]	[mm/cycle]	[μm]
Crack Number F14/1A1			
0	0.00	-	-
40000	7.43	1.8563E-07	3.71
70000	10.41	9.9500E-08	8.92
100000	22.86	4.1500E-07	16.64
130000	30.25	2.4617E-07	26.55
160000	39.37	3.0417E-07	34.81
180000	66.11	1.3368E-06	52.74
200000	77.76	5.8250E-07	71.93
220000	82.56	2.4000E-07	80.16
240000	88.92	3.1800E-07	85.74
255000	93.34	2.9467E-07	91.13
270000	128.50	2.3443E-06	110.92
285000	208.79	5.3527E-06	168.65
300000	225.83	1.1360E-06	217.31
315000	239.90	9.3800E-07	232.87
330000	276.98	2.4717E-06	258.44
345000	289.41	8.2900E-07	283.19
360000	323.24	2.2553E-06	306.33
380000	371.53	2.4143E-06	347.38
400000	392.27	1.0373E-06	381.90
420000	493.95	5.0840E-06	443.11
440000	763.15	1.3460E-05	628.55
465000	1086.71	1.2943E-05	924.93
Crack Number F14/1A2			
0	0.00	-	-
130000	7.95	6.1154E-08	3.98
160000	9.68	5.7667E-08	8.82
180000	19.47	4.8950E-07	14.58
200000	37.29	8.9100E-07	28.38
220000	52.05	7.3775E-07	44.67
240000	52.26	1.0500E-08	52.15
255000	62.65	6.9300E-07	57.45

continued on the next page

N	a	da/dN	a_{mean}
[cycles]	[μm]	[mm/cycle]	[μm]
Crack Number F14/1A2 (continuation)			
270000	64.07	9.4333E-08	63.36
285000	208.79	9.6483E-06	136.43
300000	225.83	1.1360E-06	217.31
315000	239.90	9.3800E-07	232.87
330000	276.98	2.4717E-06	258.44
345000	289.41	8.2900E-07	283.19
360000	323.24	2.2553E-06	306.33
380000	371.53	2.4143E-06	347.38
400000	392.27	1.0373E-06	381.90
420000	493.95	5.0840E-06	443.11
440000	763.15	1.3460E-05	628.55
465000	1086.71	1.2943E-05	924.93
Crack Number F14/1B			
0	0.00	-	-
130000	5.27	4.0500E-08	2.63
160000	9.51	1.4150E-07	7.39
180000	17.21	3.8475E-07	13.36
200000	18.43	6.1000E-08	17.82
220000	19.24	4.0500E-08	18.83
240000	22.16	1.4625E-07	20.70
255000	22.16	1.0000E-08	22.16
270000	29.44	4.8500E-07	25.80
285000	30.80	9.1000E-08	30.12
300000	43.29	8.3233E-07	37.04
315000	47.71	2.9500E-07	45.50
330000	57.19	6.3200E-07	52.45
345000	63.41	4.1433E-07	60.30
360000	83.74	1.3553E-06	73.57
380000	109.85	1.3058E-06	96.79
400000	114.46	2.3025E-07	112.15
420000	151.94	1.8740E-06	133.20
440000	763.15	3.0561E-05	457.54
465000	1086.71	1.2943E-05	924.93

Table A.13 - Experimental crack growth results for test F19 on polished surface/stress relieved material condition, Stress range 750MPa.

Number of Cycles	Half Surface Crack Length	Crack Growth Rate	Mean Crack Length
N	a	da/dN	a_{mean}
[cycles]	[μm]	[mm/cycle]	[μm]
Crack Number F19/1			
0	0	-	-
340000	6.85	2.0132E-08	3.42
380000	12.88	1.5075E-07	9.86
420000	29.28	4.1013E-07	21.08
460000	36.85	1.8925E-07	33.07
500000	69.77	8.2300E-07	53.31
540000	93.23	5.8638E-07	81.50
580000	106.15	3.2300E-07	99.69
620000	137.82	7.9188E-07	121.98
660000	139.49	4.1750E-08	138.66
700000	181.58	1.0523E-06	160.54
740000	252.63	1.7763E-06	217.11
780000	379.26	3.1656E-06	315.94
815000	588.32	5.9733E-06	483.79
850000	1350.43	2.1774E-05	969.37
885000	3971.82	7.4897E-05	2661.12

Table A.14 - Experimental crack growth results for test F20 on polished surface/stress relieved material condition, Stress range 750MPa.

Number of Cycles	Half Surface Crack Length	Crack Growth Rate	Mean Crack Length
N	a	da/dN	a_{mean}
[cycles]	[μm]	[mm/cycle]	[μm]
Crack Number F20/1			
0.00	0.00	-	-
235000	11.88	5.0535E-08	5.94
250000	13.98	1.4037E-07	12.93
265000	17.33	2.2340E-07	15.66
280000	21.03	2.4658E-07	19.18
295000	26.24	3.4720E-07	23.64
310000	30.57	2.8861E-07	28.40
330000	39.12	4.2764E-07	34.84
350000	44.10	2.4876E-07	41.61
370000	51.10	3.5000E-07	47.60
390000	52.16	5.3276E-08	51.63
410000	76.19	1.2012E-06	64.17
430000	90.03	6.9224E-07	83.11
450000	100.47	5.2189E-07	95.25
470000	107.45	3.4891E-07	103.96
490000	116.37	4.4627E-07	111.91
510000	122.84	3.2314E-07	119.60
530000	135.48	6.3230E-07	129.16
550000	142.20	3.3618E-07	138.84
570000	144.51	1.1522E-07	143.36
590000	167.26	1.1377E-06	155.89
610000	190.13	1.1435E-06	178.70
630000	221.83	1.5848E-06	205.98
650000	342.02	6.0093E-06	281.92
670000	445.00	5.1492E-06	393.51
690000	844.91	1.9996E-05	644.96
710000	1602.73	3.7891E-05	1223.82
730000	2986.66	6.9196E-05	2294.70

continued on the next page

N	a	da/dN	a_{mean}
[cycles]	[μm]	[mm/cycle]	[μm]
Crack Number F20/2			
0.00	0.00	-	-
205000	7.03	3.4301E-08	3.52
220000	11.41	2.9195E-07	9.22
235000	16.70	3.5268E-07	14.06
250000	19.01	1.5364E-07	17.85
265000	22.58	2.3831E-07	20.79
280000	25.23	1.7682E-07	23.91
295000	28.62	2.2605E-07	26.93
310000	33.78	3.4349E-07	31.20
330000	38.90	2.5606E-07	36.34
350000	46.95	4.0257E-07	42.92
370000	48.11	5.7898E-08	47.53
390000	51.41	1.6494E-07	49.76
410000	55.60	2.0963E-07	53.50
430000	64.05	4.2284E-07	59.83
450000	73.08	4.5144E-07	68.57
470000	80.21	3.5632E-07	76.65
490000	101.56	1.0677E-06	90.89
510000	106.45	2.4440E-07	104.01
530000	114.23	3.8879E-07	110.34
550000	129.58	7.6782E-07	121.91
570000	148.64	9.5259E-07	139.11
590000	163.86	7.6106E-07	156.25
610000	195.05	1.5595E-06	179.45
630000	201.16	3.0575E-07	198.10
650000	259.21	2.9023E-06	230.18
670000	408.82	7.4807E-06	334.01
690000	638.66	1.1492E-05	523.74
710000	1176.60	2.6897E-05	907.63
730000	2003.18	4.1329E-05	1589.89

Table A.15 - Experimental crack growth results for test F5 on ground surface (grinding condition 1), stress relieved material condition, Stress range 792MPa.

Number of Cycles	Half Surface Crack Length	Crack Growth Rate	Mean Crack Length
N	a	da/dN	a_{mean}
[cycles]	[μm]	[mm/cycle]	[μm]
Crack Number F5/1			
0	0.00	-	-
175000	8.76	5.0057E-08	4.38
190000	10.88	1.4133E-07	9.82
205000	17.30	4.2800E-07	14.09
220000	21.50	2.8000E-07	19.40
235000	31.24	6.4933E-07	26.37
250000	48.06	1.1213E-06	39.65
265000	64.08	1.0680E-06	56.07
280000	75.47	7.5933E-07	69.78
295000	88.60	8.7533E-07	82.04
310000	95.41	4.5400E-07	92.01
325000	115.00	1.3060E-06	105.21
340000	123.83	5.8867E-07	119.42
350000	135.77	1.1940E-06	129.80
360000	146.05	1.0280E-06	140.91
370000	165.27	1.9220E-06	155.66
380000	166.72	1.4500E-07	166.00
390000	177.41	1.0690E-06	172.07
400000	191.38	1.3970E-06	184.40
410000	200.29	8.9100E-07	195.84
420000	217.13	1.6840E-06	208.71
435000	225.00	5.2467E-07	221.07
450000	250.63	1.7087E-06	237.82
465000	275.97	1.6893E-06	263.30
480000	347.32	4.7567E-06	311.65
500000	518.60	8.5640E-06	432.96
520000	929.59	2.0550E-05	724.10

continued on the next page

N	a	da/dN	a_{mean}
[cycles]	[μm]	[mm/cycle]	[μm]
Crack Number F5/2			
0	0.00	-	-
50000	6.09	1.2180E-07	3.05
75000	18.69	5.0400E-07	12.39
100000	25.85	2.8640E-07	22.27
125000	40.38	5.8120E-07	33.12
150000	47.81	2.9720E-07	44.10
175000	57.77	3.9840E-07	52.79
190000	65.07	4.8667E-07	61.42
205000	66.49	9.4667E-08	65.78
220000	68.65	1.4400E-07	67.57
235000	81.47	8.5467E-07	75.06
250000	82.70	8.2000E-08	82.09
265000	84.48	1.1867E-07	83.59
280000	87.94	2.3067E-07	86.21
295000	88.92	6.5333E-08	88.43
310000	93.54	3.0800E-07	91.23
325000	96.71	2.1133E-07	95.13
340000	121.96	1.6833E-06	109.34
350000	136.39	1.4430E-06	129.18
360000	169.31	3.2920E-06	152.85
370000	189.03	1.9720E-06	179.17
380000	197.58	8.5500E-07	193.31
390000	223.97	2.6390E-06	210.78
400000	243.80	1.9830E-06	233.89
410000	281.15	3.7350E-06	262.48
420000	281.44	2.9000E-08	281.30
435000	331.34	3.3267E-06	306.39
450000	374.80	2.8973E-06	353.07
465000	494.07	7.9513E-06	434.44
480000	648.00	1.0262E-05	571.04
500000	977.63	1.6482E-05	812.82
520000	2131.31	5.7684E-05	1554.47

Table A.16 - Experimental crack growth results for test F6 on ground surface (grinding condition 2), stress relieved material condition, Stress range 792MPa.

Number of Cycles	Half Surface Crack Length	Crack Growth Rate	Mean Crack Length
N	a	da/dN	a_{mean}
[cycles]	[μm]	[mm/cycle]	[μm]
Crack Number F6/1			
160000	94.22	-	-
190000	132.60	1.2793E-06	113.41
200000	207.25	7.4650E-06	169.93
220000	311.13	5.1940E-06	259.19
250000	413.01	3.3960E-06	362.07
280000	494.50	2.7163E-06	453.76
300000	557.26	3.1380E-06	525.88
320000	672.54	5.7640E-06	614.90
340000	752.46	3.9960E-06	712.50
350000	1070.11	3.1765E-05	911.29
Crack Number F6/2			
40000	78.72	-	-
60000	114.20	1.7740E-06	96.46
70000	135.91	2.1710E-06	125.06
120000	206.38	1.4094E-06	171.15
170000	280.72	1.4868E-06	243.55
200000	349.89	2.3057E-06	315.31
220000	400.53	2.5320E-06	375.21
250000	476.37	2.5280E-06	438.45
290000	529.04	1.3168E-06	502.71
300000	609.99	8.0950E-06	569.52
310000	790.23	1.8024E-05	700.11
320000	928.68	1.3845E-05	859.46
330000	1129.49	2.0081E-05	1029.09
340000	1782.09	6.5260E-05	1455.79

Table A.17 - Experimental crack growth results for test F9 on ground surface (grinding condition 2), stress relieved material condition, Stress range 792MPa.

Number of Cycles	Half Surface Crack Length	Crack Growth Rate	Mean Crack Length
N	a	da/dN	a_{mean}
[cycles]	[μm]	[mm/cycle]	[μm]
Crack Number F9/1			
100000	158.50	-	-
150000	201.76	8.6520E-07	180.13
200000	218.14	3.2760E-07	209.95
250000	461.08	4.8588E-06	339.61
280000	803.46	1.1413E-05	632.27
Crack Number F9/2A			
50000	59.20	-	-
100000	115.68	1.1296E-06	87.44
150000	148.00	6.4640E-07	131.84
200000	366.26	4.3652E-06	257.13
250000	645.75	5.5898E-06	506.01
280000	1,059.07	1.3777E-05	852.41
Crack Number F9/2B			
100000	108.32	-	-
150000	124.63	3.2620E-07	116.48
200000	135.26	2.1260E-07	129.95
250000	302.81	3.3510E-06	219.04
280000	1,059.07	2.5209E-05	680.94
Crack Number F9/3			
100000	90.80	-	-
150000	142.05	1.0250E-06	116.43
200000	214.68	1.4526E-06	178.37
250000	276.29	1.2322E-06	245.49
280000	569.07	9.7593E-06	422.68

Table A.18 - Experimental crack growth results for test F10 on ground surface (grinding condition 2), stress relieved material condition, Stress range 792MPa.

Number of Cycles	Half Surface Crack Length	Crack Growth Rate	Mean Crack Length
N	a	da/dN	a_{mean}
[cycles]	[μm]	[mm/cycle]	[μm]
Crack Number F10/1A			
215000	327.30	-	-
250000	419.07	2.6220E-06	373.18
265000	481.88	4.1877E-06	450.47
280000	519.11	2.4820E-06	500.50
290000	532.82	1.3710E-06	525.97
300000	575.14	4.2320E-06	553.98
310000	645.43	7.0290E-06	610.29
320000	697.44	5.2010E-06	671.44
340000	1257.56	2.8006E-05	977.50
360000	2376.79	5.5962E-05	1817.17
Crack Number F10/1B			
250000	118.23	-	-
265000	147.87	1.9763E-06	133.05
280000	160.90	8.6833E-07	154.38
290000	181.97	2.1070E-06	171.43
300000	192.86	1.0890E-06	187.41
310000	227.61	3.4750E-06	210.23
320000	264.01	3.6400E-06	245.81
340000	1257.56	4.9678E-05	760.78
360000	2376.79	5.5962E-05	1817.17

Table A.19 - Experimental crack growth results for test F22 on ground surface (grinding condition 3), as-received material condition, Stress range 792MPa.

Number of Cycles	Half Surface Crack Length	Crack Growth Rate	Mean Crack Length
N	a	da/dN	a_{mean}
[cycles]	[μm]	[mm/cycle]	[μm]
Crack Number F22/1			
0	6.97	-	-
15000	15.31	5.5600E-07	11.14
30000	21.56	4.1700E-07	18.43
40000	26.05	4.4900E-07	23.81
50000	29.03	2.9750E-07	27.54
60000	31.63	2.6000E-07	30.33
70000	35.27	3.6450E-07	33.45
80000	44.69	9.4150E-07	39.98
90000	70.80	2.6110E-06	57.74
100000	74.79	3.9950E-07	72.79
110000	90.22	1.5425E-06	82.50
120000	98.03	7.8150E-07	94.12
130000	110.47	1.2435E-06	104.25
140000	126.78	1.6310E-06	118.62
150000	143.04	1.6260E-06	134.91
160000	172.27	2.9230E-06	157.65
170000	188.56	1.6290E-06	180.41
180000	230.22	4.1665E-06	209.39
190000	268.59	3.8365E-06	249.40
200000	300.95	3.2365E-06	284.77
215000	359.35	3.8930E-06	330.15
230000	438.75	5.2937E-06	399.05
245000	534.78	6.4017E-06	486.76
260000	758.20	1.4895E-05	646.49
280000	1507.76	3.7478E-05	1132.98
Crack Number F22/2A			
0	0.00	-	-
30000	2.55	8.5000E-08	1.28
40000	5.19	2.6400E-07	3.87
50000	7.36	2.1650E-07	6.27
60000	15.54	8.1800E-07	11.45
70000	41.38	2.5840E-06	28.46

continued on the next page

N	a	da/dN	a_{mean}
[cycles]	[μm]	[mm/cycle]	[μm]
Crack Number F22/2A (continuation)			
80000	44.58	3.2000E-07	42.98
90000	44.58	1.0000E-08	44.58
100000	57.11	1.2530E-06	50.84
110000	60.09	2.9800E-07	58.60
120000	65.13	5.0400E-07	62.61
130000	67.40	2.2700E-07	66.26
140000	76.14	8.7400E-07	71.77
150000	84.84	8.7000E-07	80.49
160000	113.16	2.8325E-06	99.00
170000	134.25	2.1090E-06	123.71
180000	155.02	2.0765E-06	144.63
190000	173.68	1.8665E-06	164.35
200000	179.66	5.9800E-07	176.67
215000	239.35	3.9793E-06	209.51
230000	249.48	6.7533E-07	244.42
245000	310.39	4.0607E-06	279.94
260000	355.12	2.9820E-06	332.76
280000	510.34	7.7608E-06	432.73
295000	1784.09	8.4917E-05	1147.21
Crack Number F22/2B			
0	0.00	-	-
30000	11.21	3.7350E-07	5.60
40000	11.59	3.8500E-08	11.40
50000	21.83	1.0235E-06	16.71
60000	30.65	8.8200E-07	26.24
70000	35.91	5.2650E-07	33.28
80000	35.91	1.0000E-08	35.91
90000	36.65	7.3500E-08	36.28
100000	39.38	2.7300E-07	38.01
110000	45.05	5.6700E-07	42.21
120000	54.87	9.8250E-07	49.96
130000	58.42	3.5500E-07	56.65
140000	64.64	6.2200E-07	61.53
150000	67.90	3.2600E-07	66.27
160000	68.55	6.5000E-08	68.23
170000	79.92	1.1365E-06	74.23
180000	85.08	5.1650E-07	82.50
190000	106.50	2.1415E-06	95.79

continued on the next page

N	a	da/dN	a_{mean}
[cycles]	[μm]	[mm/cycle]	[μm]
Crack Number F22/2B (continuation)			
200000	122.11	1.5610E-06	114.30
215000	143.91	1.4537E-06	133.01
230000	183.51	2.6400E-06	163.71
245000	221.66	2.5430E-06	202.58
260000	325.05	6.8930E-06	273.35
280000	395.30	3.5123E-06	360.17
295000	1784.09	9.2586E-05	1089.69
Crack Number F22/3			
0	0.00	-	-
15000	31.18	2.0783E-06	15.59
30000	41.91	7.1567E-07	36.54
40000	41.91	1.0000E-08	41.91
50000	43.07	1.1600E-07	42.49
60000	71.08	2.8005E-06	57.07
70000	78.78	7.7000E-07	74.93
80000	93.99	1.5210E-06	86.38
90000	119.82	2.5835E-06	106.90
100000	121.22	1.3950E-07	120.52
110000	133.35	1.2130E-06	127.28
120000	146.46	1.3110E-06	139.90
130000	164.66	1.8200E-06	155.56
140000	164.63	1.0000E-08	164.64
150000	165.85	1.2150E-07	165.24
160000	176.85	1.1000E-06	171.35
170000	201.07	2.4220E-06	188.96
180000	226.51	2.5440E-06	213.79
190000	260.44	3.3930E-06	243.47
200000	287.22	2.6785E-06	273.83
215000	324.75	2.5020E-06	305.99
230000	380.04	3.6860E-06	352.40
245000	449.08	4.6027E-06	414.56
260000	521.34	4.8173E-06	485.21
280000	813.37	1.4601E-05	667.35

Table A.20 - Experimental crack growth results for test F23 on ground surface (grinding condition 3), as-received material condition, Stress range 792MPa.

Number of Cycles	Half Surface Crack Length	Crack Growth Rate	Mean Crack Length
N	a	da/dN	a_{mean}
[cycles]	[μm]	[mm/cycle]	[μm]
Crack Number F23/1			
0	0.00	-	-
20000	49.48	2.4738E-06	24.74
35000	69.07	1.3060E-06	59.27
50000	80.71	7.7600E-07	74.89
65000	114.10	2.2260E-06	97.40
80000	152.63	2.5690E-06	133.36
90000	165.15	1.2520E-06	158.89
100000	175.34	1.0190E-06	170.25
110000	186.27	1.0930E-06	180.81
120000	215.35	2.9075E-06	200.81
130000	229.18	1.3830E-06	222.26
140000	253.65	2.4470E-06	241.41
150000	288.24	3.4595E-06	270.94
160000	305.33	1.7085E-06	296.78
170000	332.33	2.7000E-06	318.83
180000	368.24	3.5910E-06	350.28
190000	418.61	5.0375E-06	393.42
200000	473.40	5.4790E-06	446.01
210000	556.98	8.3581E-06	515.19
220000	654.06	9.7079E-06	605.52
230000	843.19	1.8913E-05	748.63
Crack Number F23/2			
0	8.92	-	-
20000	47.64	1.9358E-06	28.28
35000	49.05	9.4333E-08	48.34
50000	58.79	6.4933E-07	53.92
65000	69.42	7.0867E-07	64.11
80000	78.68	6.1700E-07	74.05
90000	95.37	1.6690E-06	87.02
100000	107.84	1.2475E-06	101.60
110000	119.08	1.1240E-06	113.46
120000	130.09	1.1005E-06	124.58
130000	152.80	2.2715E-06	141.44
140000	170.63	1.7830E-06	161.72

continued on the next page

N	a	da/dN	a_{mean}
[cycles]	[μm]	[mm/cycle]	[μm]
Crack Number F23/2 (continuation)			
150000	186.50	1.5870E-06	178.57
160000	205.00	1.8500E-06	195.75
170000	230.35	2.5345E-06	217.67
180000	248.26	1.7910E-06	239.30
190000	284.36	3.6100E-06	266.31
200000	306.23	2.1875E-06	295.29
210000	371.64	6.5410E-06	338.94
220000	425.04	5.3395E-06	398.34
230000	466.68	4.1645E-06	445.86
250000	730.77	1.3204E-05	598.72

Table A.21 - Experimental crack growth results for test F27 on ground surface (grinding condition 4), as-received material condition, Stress range 792MPa.

Number of Cycles	Half Surface Crack Length	Crack Growth Rate	Mean Crack Length
N	a	da/dN	a_{mean}
[cycles]	[μm]	[mm/cycle]	[μm]
Crack Number F27/1			
0	0.00	-	-
75000	12.65	1.6860E-07	6.32
90000	62.19	3.3030E-06	37.42
105000	100.65	2.5640E-06	81.42
115000	113.15	1.2495E-06	106.90
125000	121.11	7.9600E-07	117.13
135000	130.02	8.9100E-07	125.56
145000	144.49	1.4475E-06	137.25
155000	147.46	2.9700E-07	145.98
165000	173.34	2.5875E-06	160.40
175000	187.87	1.4535E-06	180.60
185000	205.08	1.7205E-06	196.47
195000	254.15	4.9070E-06	229.61
205000	261.99	7.8400E-07	258.07
215000	295.99	3.4005E-06	278.99
225000	328.60	3.2610E-06	312.30
240000	399.02	4.6947E-06	363.81
257000	485.29	5.0747E-06	442.16
272000	692.98	1.3846E-05	589.13
285000	963.88	2.0839E-05	828.43
295000	1165.23	2.0135E-05	1064.56
315000	1891.56	3.6316E-05	1528.39

Table A.22 - Experimental crack growth results for test F28 on ground surface (grinding condition 4), as-received material condition, Stress range 792MPa.

Number of Cycles	Half Surface Crack Length	Crack Growth Rate	Mean Crack Length
N	a	da/dN	a_{mean}
[cycles]	[μm]	[mm/cycle]	[μm]
Crack Number F28/1A			
0	0.00	-	-
25000	4.11	1.6440E-07	2.06
45000	8.28	2.0850E-07	6.20
60000	13.26	3.3200E-07	10.77
75000	19.75	4.3267E-07	16.51
85000	23.74	3.9850E-07	21.74
95000	23.74	1.0000E-08	23.74
105000	26.08	2.3450E-07	24.91
115000	28.85	2.7650E-07	27.46
125000	34.54	5.6900E-07	31.69
135000	38.56	4.0250E-07	36.55
145000	42.06	3.5000E-07	40.31
155000	42.71	6.5000E-08	42.39
165000	50.57	7.8600E-07	46.64
175000	54.15	3.5750E-07	52.36
185000	58.48	4.3300E-07	56.31
195000	64.75	6.2750E-07	61.61
205000	76.48	1.1730E-06	70.62
215000	84.88	8.4000E-07	80.68
225000	96.29	1.1405E-06	90.58
235000	104.27	7.9850E-07	100.28
245000	137.31	3.3035E-06	120.79
260000	163.07	1.7177E-06	150.19
280000	223.25	3.0090E-06	193.16
300000	800.59	2.8867E-05	511.92
320000	924.82	6.2113E-06	862.70
360000	2107.37	2.9564E-05	1516.09
Crack Number F28/1B			
0	0.00	-	-
75000	4.25	5.6667E-08	2.13
85000	21.08	1.6825E-06	12.66
95000	44.53	2.3455E-06	32.80

continued on the next page

N	a	da/dN	a_{mean}
[cycles]	[μm]	[mm/cycle]	[μm]
Crack Number F28/1B (continuation)			
105000	63.82	1.9290E-06	54.18
115000	90.45	2.6630E-06	77.14
125000	95.71	5.2550E-07	93.08
135000	114.62	1.8910E-06	105.16
145000	141.39	2.6775E-06	128.00
155000	149.11	7.7150E-07	145.25
165000	172.47	2.3360E-06	160.79
175000	182.06	9.5950E-07	177.26
185000	206.75	2.4690E-06	194.41
195000	219.86	1.3105E-06	213.30
205000	235.85	1.5995E-06	227.85
215000	240.77	4.9200E-07	238.31
225000	277.00	3.6225E-06	258.88
235000	291.88	1.4885E-06	284.44
245000	349.92	5.8040E-06	320.90
260000	387.80	2.5250E-06	368.86
280000	464.68	3.8443E-06	426.24
300000	800.59	1.6796E-05	632.64
320000	924.82	6.2113E-06	862.70
360000	2107.37	2.9564E-05	1516.09
Crack Number F28/2A			
0	0.00	-	-
145000	21.66	1.4938E-07	10.83
155000	21.66	1.0000E-08	21.66
165000	34.74	1.3080E-06	28.20
175000	97.14	6.2395E-06	65.94
185000	146.32	4.9180E-06	121.73
195000	158.00	1.1680E-06	152.16
205000	173.77	1.5770E-06	165.88
215000	194.39	2.0620E-06	184.08
225000	250.19	5.5805E-06	222.29
235000	264.64	1.4445E-06	257.41
245000	289.08	2.4440E-06	276.86
260000	347.80	3.9150E-06	318.44
280000	406.84	2.9518E-06	377.32
300000	487.73	4.0448E-06	447.28
320000	622.43	6.7348E-06	555.08
360000	2107.37	3.7124E-05	1364.90

continued on the next page

N	a	da/dN	a_{mean}
[cycles]	[μm]	[mm/cycle]	[μm]
Crack Number F28/2B			
0	0.00	-	-
60000	4.34	7.2333E-08	2.17
75000	7.45	2.0700E-07	5.89
85000	16.81	9.3600E-07	12.13
95000	27.36	1.0550E-06	22.08
105000	34.95	7.5950E-07	31.15
115000	37.75	2.8000E-07	36.35
125000	39.72	1.9700E-07	38.74
135000	43.71	3.9900E-07	41.72
145000	52.57	8.8600E-07	48.14
155000	54.94	2.3700E-07	53.76
165000	56.66	1.7150E-07	55.80
175000	97.14	4.0480E-06	76.90
185000	146.32	4.9180E-06	121.73
195000	158.00	1.1680E-06	152.16
205000	173.77	1.5770E-06	165.88
215000	194.39	2.0620E-06	184.08
225000	250.19	5.5805E-06	222.29
235000	264.64	1.4445E-06	257.41
245000	289.08	2.4440E-06	276.86
260000	347.80	3.9150E-06	318.44
280000	406.84	2.9518E-06	377.32
300000	487.73	4.0448E-06	447.28
320000	622.43	6.7348E-06	555.08
360000	2107.37	3.7124E-05	1364.90

Appendix B - Mean Crack Growth Results

Table B.1 - Fatigue lifetime results for polished surface specimens tested in as-received condition, Stress range 850MPa.

a [μm]	$log(N_{mean})$	σ	Number of data points	N_{mean} [cycles]
12	3.8768	0.2359	11	7531
25	4.1567	0.1797	11	14345
50	4.4478	0.1518	11	28045
75	4.5831	0.1399	11	38291
100	4.6674	0.1202	11	46498
125	4.7192	0.0951	11	52384
150	4.7633	0.0890	11	57987
175	4.7902	0.0937	11	61684
200	4.8120	0.0951	11	64870
250	4.8582	0.0841	11	72138
300	4.9072	0.0650	10	80765
350	4.9334	0.0475	9	85781
400	4.9707	0.0458	9	93479
500	5.0149	0.0429	7	103495
600	5.0516	0.0330	6	112625
700	5.0760	0.0298	4	119122
800	5.0973	0.0378	2	125118
failure	5.1303	0.0000	3	135000

Table B.2 - Fatigue lifetime results for polished surface specimens tested in as-received condition, Stress range 792MPa.

a [μm]	$log(N_{mean})$	σ	Number of data points	N_{mean} [cycles]
12	4.4889	0.3345	11	30825
25	4.7231	0.2597	11	52862
50	4.9257	0.1729	11	84269
75	5.0736	0.1164	11	118475
100	5.1422	0.0981	11	138748
125	5.2197	0.0735	11	165863
150	5.2593	0.0663	11	181680
175	5.2854	0.0801	11	192938
200	5.3008	0.0826	11	199908
250	5.3341	0.0919	11	215806
300	5.3378	0.1019	11	217651
350	5.3470	0.1070	11	222352
400	5.3788	0.1087	9	239220
500	5.4091	0.0991	8	256528
600	5.4519	0.0654	7	283051
700	5.4605	0.0602	7	288734
800	5.4701	0.0540	7	295175
failure	5.5434	0.0448	2	349479

Table B.3 - Fatigue lifetime results for polished surface specimens tested in as-received condition, Stress range 750MPa.

a [μm]	$log(N_{mean})$	σ	Number of data points	N_{mean} [cycles]
12	4.7414	0.3371	9	55128
25	4.9221	0.2502	9	83571
50	5.1112	0.2072	9	129194
75	5.2163	0.1696	9	164561
100	5.2767	0.1548	8	189109
125	5.3322	0.1399	8	214870
150	5.3815	0.1126	8	240721
175	5.4219	0.1053	8	264172
200	5.4573	0.1099	7	286642
250	5.5265	0.0891	7	336127
300	5.5858	0.0666	5	385332
350	5.6238	0.0481	5	420548
400	5.6502	0.0365	5	446896
500	5.6821	0.0326	5	480984
600	5.7145	0.0272	5	518227
700	5.7337	0.0230	5	541624
800	5.7518	0.0114	5	564716
failure	5.7841	0.0084	2	608260

Table B.4 - Fatigue lifetime results for polished surface specimens tested in stress relieved condition, Stress range 850MPa.

a [μm]	$log(N_{mean})$	σ	Number of data points	N_{mean} [cycles]
12	4.8691	0.3106	7	73975
25	5.1192	0.2982	7	131573
50	5.3150	0.1873	7	206536
75	5.3707	0.1647	7	234812
100	5.4238	0.1386	7	265330
125	5.4446	0.1266	7	278343
150	5.4637	0.1023	7	290857
175	5.4752	0.0853	7	298680
200	5.4793	0.0812	7	301526
250	5.4977	0.0503	7	314557
300	5.4991	0.0325	6	315553
350	5.5078	0.0376	4	321937
400	5.5123	0.0351	4	325309
500	5.5357	0.0311	4	343340
600	5.5476	0.0235	4	352882
700	5.5638	0.0164	3	366287
800	5.5689	0.0167	3	370621
failure	5.6251	0.0060	2	421820

Table B.5 - Fatigue lifetime results for polished surface specimens tested in stress relieved condition, Stress range 792MPa.

a [μm]	$log(N_{mean})$	σ	Number of data points	N_{mean} [cycles]
12	5.2948	0.2091	11	197132
25	5.3929	0.1816	11	247089
50	5.4770	0.1495	11	299913
75	5.5286	0.1208	11	337784
100	5.5610	0.1026	11	363927
125	5.5847	0.1043	11	384320
150	5.5980	0.0975	11	396271
175	5.6119	0.0990	11	409182
200	5.6198	0.0946	11	416725
250	5.6506	0.0662	10	447352
300	5.6656	0.0691	8	463039
350	5.6707	0.0698	7	468446
400	5.6713	0.0653	6	469092
500	5.6802	0.0671	5	478804
600	5.6868	0.0643	5	486153
700	5.6925	0.0623	5	492582
800	5.7104	0.0617	4	513336
failure	5.7246	0.0452	3	530380

Table B.6 - Fatigue lifetime results for polished surface specimens tested in stress relieved condition, Stress range 750MPa.

a [μm]	$log(N_{mean})$	σ	Number of data points	N_{mean} [cycles]
12	5.4305	0.1242	3	269465
25	5.5073	0.0914	3	321605
50	5.6079	0.0610	3	405375
75	5.6589	0.0475	3	455952
100	5.6967	0.0488	3	497426
125	5.7423	0.0357	3	552501
150	5.7809	0.0391	3	603876
175	5.7977	0.0377	3	627617
200	5.8126	0.0338	3	649601
250	5.8272	0.0359	3	671795
300	5.8342	0.0381	3	682697
350	5.8406	0.0403	3	692795
400	5.8466	0.0412	3	702375
500	5.8541	0.0426	3	714632
600	5.8597	0.0449	3	724014
700	5.8628	0.0443	3	729137
800	5.8654	0.0441	3	733584
failure	5.9090	0.0619	2	811037

Table B.7 - Fatigue lifetime results for ground surface specimens (grinding condition 1) tested in stress relieved condition, Stress range 792MPa.

a [μm]	$log(N_{mean})$	σ	Number of data points	N_{mean} [cycles]
12	5.0376	0.3495	2	109039
25	5.1699	0.2588	2	147885
50	5.2964	0.1480	2	197881
75	5.4015	0.0632	2	252071
100	5.5054	0.0129	2	320164
125	5.5334	0.0010	2	341543
150	5.5540	0.0068	2	358073
175	5.5742	0.0203	2	375110
200	5.5966	0.0224	2	395034
250	5.6284	0.0346	2	424969
300	5.6506	0.0305	2	447263
350	5.6632	0.0259	2	460467
400	5.6715	0.0216	2	469371
500	5.6825	0.0206	2	481433
600	5.6897	0.0180	2	489432
700	5.6953	0.0159	2	495825
800	5.7001	0.0150	2	501309
failure	5.7226		1	528000

Table B.8 - Fatigue lifetime results for ground surface specimens (grinding condition 2) tested in stress relieved condition, Stress range 792MPa.

a [μm]	$log(N_{mean})$	σ	Number of data points	N_{mean} [cycles]
75	4.8061		1	63987
100	4.9762	0.2088	4	94657
125	5.1410	0.2004	6	138367
150	5.2157	0.1779	6	164306
175	5.2245	0.1567	7	167702
200	5.2629	0.1332	7	183202
250	5.3251	0.1033	7	211382
300	5.3567	0.0875	7	227370
350	5.3730	0.0685	8	236038
400	5.3926	0.0579	8	246938
500	5.4282	0.0455	8	268056
600	5.4539	0.0440	8	284411
700	5.4689	0.0437	8	294353
800	5.4790	0.0430	8	301330
failure	5.5273	0.0507	3	336713

Table B.9 - Fatigue lifetime results for ground surface specimens (grinding condition 3) tested in as-received condition, Stress range 792MPa.

a [μm]	$log(N_{mean})$	σ	Number of data points	N_{mean} [cycles]
12	3.9930	0.5862	6	9840
25	4.3522	0.3945	6	22501
50	4.7568	0.2842	6	57126
75	4.9458	0.2188	6	88270
100	5.0340	0.1856	6	108132
125	5.0972	0.1640	6	125075
150	5.1438	0.1518	6	139256
175	5.2001	0.1216	6	158532
200	5.2348	0.1072	6	171718
250	5.2826	0.0897	6	191682
300	5.3173	0.0743	6	207622
350	5.3450	0.0676	6	221334
400	5.3654	0.0644	6	231950
500	5.3935	0.0530	6	247445
600	5.4053	0.0457	6	254271
700	5.4145	0.0403	6	259742
800	5.4253	0.0408	5	266228
failure	5.4515	0.0329	2	282790

Table B.10 - Fatigue lifetime results for ground surface specimens (grinding condition 4) tested in as-received condition, Stress range 792MPa.

a [μm]	$log(N_{mean})$	σ	Number of data points	N_{mean} [cycles]
12	4.8664	0.0664	5	73516
25	5.0001	0.1169	5	100029
50	5.1037	0.1325	5	126975
75	5.1577	0.1419	5	143773
100	5.1826	0.1507	4	152267
125	5.2235	0.1230	4	167288
150	5.2653	0.0991	4	184190
175	5.2949	0.0947	4	197179
200	5.3228	0.0825	4	210273
250	5.3504	0.0706	4	224068
300	5.3885	0.0485	4	244612
350	5.4051	0.0396	4	254133
400	5.4252	0.0334	4	266212
500	5.4509	0.0288	4	282433
600	5.4627	0.0315	4	290192
700	5.4705	0.0292	4	295475
800	5.4763	0.0268	4	299440
failure	5.5652	0.0183	2	367481

Appendix C - Fatigue Lifetime Predictions and Mean Crack Growth Results

Table C.1 - Observed and predicted fatigue lifetimes for polished surfaces in as-received condition, Stress range 750MPa.

a [μm]	$log(N_{mean})$	σ	N_{-1sd} [cycles]	N_{mean} [cycles]	N_{+1sd} [cycles]	N_{model} [cycles]
12	4.7414	0.3371	25367	55128	119807	9000
25	4.9221	0.2502	46978	83571	148670	23174
50	5.1112	0.2072	80177	129194	208178	98987
75	5.2163	0.1696	111352	164561	243195	117040
100	5.2767	0.1548	132398	189109	270110	167174
125	5.3322	0.1399	155684	214870	296555	187088
150	5.3815	0.1126	185758	240721	311946	217031
175	5.4219	0.1053	207317	264172	336618	245772
200	5.4573	0.1099	222545	286642	369200	267562
250	5.5265	0.0891	273788	336127	412659	314335
300	5.5858	0.0666	330546	385332	449198	357386
350	5.6238	0.0481	376473	420548	469784	397175
400	5.6502	0.0365	410862	446896	486092	434150
500	5.6821	0.0326	446184	480984	518499	501111
600	5.7145	0.0272	486755	518227	551734	537291
700	5.7337	0.0230	513663	541624	571108	560103
800	5.7518	0.0114	550070	564716	579751	575343
failure	5.7841	0.0084	596611	608260	620136	629364

Table C.2 - Observed and predicted fatigue lifetimes for polished surfaces in as-received condition, Stress range 792MPa.

a [μm]	$log(N_{mean})$	σ	N_{-1sd} [cycles]	N_{mean} [cycles]	N_{+1sd} [cycles]	N_{model} [cycles]
12	4.4889	0.3345	14269	30825	66591	4373
25	4.7231	0.2597	29067	52862	96137	11260
50	4.9257	0.1729	56596	84269	125475	48099
75	5.0736	0.1164	90620	118475	154893	56871
100	5.1422	0.0981	110696	138748	173908	81231
125	5.2197	0.0735	140051	165863	196431	90908
150	5.2593	0.0663	155941	181680	211667	105457
175	5.2854	0.0801	160424	192938	232041	119423
200	5.3008	0.0826	165294	199908	241772	130010
250	5.3341	0.0919	174650	215806	266661	152738
300	5.3378	0.1019	172144	217651	275189	173657
350	5.3470	0.1070	173789	222352	284485	192991
400	5.3788	0.1087	186250	239220	307255	210957
500	5.4091	0.0991	204181	256528	322294	243494
600	5.4519	0.0654	243484	283051	329048	270795
700	5.4605	0.0602	251389	288734	331626	288656
800	5.4701	0.0540	260675	295175	334240	299889
failure	5.5434	0.0448	315194	349479	387493	339703

Table C.3 - Observed and predicted fatigue lifetimes for polished surfaces in as-received condition, Stress range 850MPa.

a [μm]	$log(N_{mean})$	σ	N_{-1sd} [cycles]	N_{mean} [cycles]	N_{+1sd} [cycles]	N_{model} [cycles]
12	3.8768	0.2359	4374	7531	12964	1715
25	4.1567	0.1797	9484	14345	21698	4415
50	4.4478	0.1518	19773	28045	39777	18861
75	4.5831	0.1399	27749	38291	52839	22300
100	4.6674	0.1202	35257	46498	61324	31853
125	4.7192	0.0951	42079	52384	65212	35647
150	4.7633	0.0890	47241	57987	71176	41352
175	4.7902	0.0937	49714	61684	76536	46828
200	4.8120	0.0951	52115	64870	80745	50980
250	4.8582	0.0841	59437	72138	87552	59892
300	4.9072	0.0650	69535	80765	93809	68095
350	4.9334	0.0475	76887	85781	95705	75676
400	4.9707	0.0458	84130	93479	103866	82721
500	5.0149	0.0429	93760	103495	114240	95480
600	5.0516	0.0330	104373	112625	121528	106185
700	5.0760	0.0298	111220	119122	127586	115716
800	5.0973	0.0378	114685	125118	136499	123277
failure	5.1303	0.0000	135000	135000	135000	150079

Table C.4 - Observed and predicted fatigue lifetimes for polished surfaces in stress relieved condition, Stress range 750MPa.

a [μm]	$log(N_{mean})$	σ	N_{-1sd} [cycles]	N_{mean} [cycles]	N_{+1sd} [cycles]	N_{model} [cycles]
12	5.4305	0.1242	202430	269465	358699	13450
25	5.5073	0.0914	260540	321605	396983	34634
50	5.6079	0.0610	352270	405375	466485	147939
75	5.6589	0.0475	408753	455952	508602	174920
100	5.6967	0.0488	444585	497426	556547	249846
125	5.7423	0.0357	508914	552501	599822	280315
150	5.7809	0.0391	551894	603876	660753	325065
175	5.7977	0.0377	575463	627617	684499	368020
200	5.8126	0.0338	600940	649601	702201	400585
250	5.8272	0.0359	618564	671795	729607	470489
300	5.8342	0.0381	625398	682697	745247	534830
350	5.8406	0.0403	631457	692795	760092	594296
400	5.8466	0.0412	638848	702375	772219	649556
500	5.8541	0.0426	647900	714632	788238	727427
600	5.8597	0.0449	652961	724014	802799	763996
700	5.8628	0.0443	658380	729137	807499	786808
800	5.8654	0.0441	662719	733584	812025	802048
failure	5.9090	0.0619	703229	811037	935372	856069

Table C.5 - Observed and predicted fatigue lifetimes for polished surfaces in stress relieved condition, Stress range 792MPa.

a [μm]	$log(N_{mean})$	σ	N_{-1sd} [cycles]	N_{mean} [cycles]	N_{+1sd} [cycles]	N_{model} [cycles]
12	5.2948	0.2091	121807	197132	319036	7892
25	5.3929	0.1816	162639	247089	375387	20321
50	5.4770	0.1495	212568	299913	423148	86801
75	5.5286	0.1208	255751	337784	446129	102631
100	5.5610	0.1026	287350	363927	460912	146593
125	5.5847	0.1043	302296	384320	488599	164055
150	5.5980	0.0975	316574	396271	496032	190311
175	5.6119	0.0990	325761	409182	513964	215514
200	5.6198	0.0946	335158	416725	518144	234621
250	5.6506	0.0662	384120	447352	520992	275636
300	5.6656	0.0691	394909	463039	542924	313387
350	5.6707	0.0698	398852	468446	550183	348278
400	5.6713	0.0653	403587	469092	545231	380701
500	5.6802	0.0671	410299	478804	558747	439417
600	5.6868	0.0643	419292	486153	563676	466369
700	5.6925	0.0623	426741	492582	568581	483182
800	5.7104	0.0617	445311	513336	591752	494415
failure	5.7246	0.0452	477972	530380	588534	534229

Table C.6 - Observed and predicted fatigue lifetimes for polished surfaces in stress relieved condition, Stress range 850MPa.

a [μm]	$log(N_{mean})$	σ	N_{-1sd} [cycles]	N_{mean} [cycles]	N_{+1sd} [cycles]	N_{model} [cycles]
12	4.8691	0.3106	36185	73975	151231	6196
25	5.1192	0.2982	66212	131573	261456	15955
50	5.3150	0.1873	134175	206536	317922	68150
75	5.3707	0.1647	160694	234812	343115	80579
100	5.4238	0.1386	192849	265330	365051	115095
125	5.4446	0.1266	207966	278343	372537	128806
150	5.4637	0.1023	229804	290857	368129	149420
175	5.4752	0.0853	245426	298680	363490	169208
200	5.4793	0.0812	250078	301526	363558	184210
250	5.4977	0.0503	280178	314557	353155	216412
300	5.4991	0.0325	292768	315553	340112	246052
350	5.5078	0.0376	295204	321937	351091	273446
400	5.5123	0.0351	300077	325309	352662	298902
500	5.5357	0.0311	319647	343340	368790	336220
600	5.5476	0.0235	334291	352882	372506	354363
700	5.5638	0.0164	352711	366287	380386	365681
800	5.5689	0.0167	356677	370621	385110	373242
failure	5.6251	0.0060	416039	421820	427682	400043

Table C.7 - Observed and predicted fatigue lifetimes for ground surfaces (grinding condition 1) in stress relieved condition, Stress range 792MPa.

a [μm]	$log(N_{mean})$	σ	N_{-1sd} [cycles]	N_{mean} [cycles]	N_{+1sd} [cycles]	N_{model} [cycles]
12	5.0376	0.3495	48765	109039	243810	7892
25	5.1699	0.2588	81491	147885	268374	20321
50	5.2964	0.1480	140722	197881	278256	86801
75	5.4015	0.0632	217943	252071	291542	102631
100	5.5054	0.0129	310801	320164	329809	146593
125	5.5334	0.0010	340747	341543	342341	164055
150	5.5540	0.0068	352516	358073	363718	190311
175	5.5742	0.0203	357939	375110	393103	215514
200	5.5966	0.0224	375218	395034	415897	234621
250	5.6284	0.0346	392384	424969	460261	275636
300	5.6506	0.0305	416908	447263	479828	313387
350	5.6632	0.0259	433792	460467	488782	348278
400	5.6715	0.0216	446623	469371	493277	380701
500	5.6825	0.0206	459164	481433	504782	439417
600	5.6897	0.0180	469598	489432	510105	466369
700	5.6953	0.0159	478002	495825	514313	483182
800	5.7001	0.0150	484302	501309	518913	494415
failure	5.7226			528000		534229

Table C.8 - Observed and predicted fatigue lifetimes for ground surfaces (grinding condition 2) in stress relieved condition, Stress range 792MPa.

a [μm]	$log(N_{mean})$	σ	N_{-1sd} [cycles]	N_{mean} [cycles]	N_{+1sd} [cycles]	N_{model} [cycles]
12	-	-	-	-	-	7892
25	-	-	-	-	-	20321
50	-	-	-	-	-	84651
75	4.8061	-	-	63987	-	85350
100	4.9762	0.2088	58530	94657	153081	86049
125	5.1410	0.2004	87215	138367	219519	86749
150	5.2157	0.1779	109090	164306	247469	87448
175	5.2245	0.1567	116917	167702	240544	88147
200	5.2629	0.1332	134810	183202	248965	88846
250	5.3251	0.1033	166630	211382	268154	104642
300	5.3567	0.0875	185878	227370	278124	142393
350	5.3730	0.0685	201616	236038	276337	177283
400	5.3926	0.0579	216113	246938	282159	209706
500	5.4282	0.0455	241383	268056	297676	268423
600	5.4539	0.0440	257013	284411	314729	295375
700	5.4689	0.0437	266180	294353	325508	312188
800	5.4790	0.0430	272904	301330	332718	323420
failure	5.5273	0.0507	299604	336713	378419	363235

Table C.9 - Observed and predicted fatigue lifetimes for ground surfaces (grinding condition 3) in as-received condition, Stress range 792MPa.

a [μm]	$log(N_{mean})$	σ	N_{-1sd} [cycles]	N_{mean} [cycles]	N_{+1sd} [cycles]	N_{model} [cycles]
12	3.9930	0.5862	2551	9840	37950	3715
25	4.3522	0.3945	9071	22501	55812	10462
50	4.7568	0.2842	29690	57126	109914	47291
75	4.9458	0.2188	53333	88270	146094	56063
100	5.0340	0.1856	70520	108132	165804	80423
125	5.0972	0.1640	85739	125075	182458	90099
150	5.1438	0.1518	98184	139256	197511	104649
175	5.2001	0.1216	119813	158532	209763	118614
200	5.2348	0.1072	134162	171718	219787	129202
250	5.2826	0.0897	155927	191682	235635	151930
300	5.3173	0.0743	174965	207622	246374	172849
350	5.3450	0.0676	189431	221334	258611	192182
400	5.3654	0.0644	199989	231950	269019	210336
500	5.3935	0.0530	219002	247445	279580	242872
600	5.4053	0.0457	228858	254271	282506	270231
700	5.4145	0.0403	236699	259742	285028	288360
800	5.4253	0.0408	242365	266228	292439	299592
failure	5.4515	0.0329	262130	282790	305078	339407

Table C.10 - Observed and predicted fatigue lifetimes for ground surfaces (grinding condition 4) in as-received condition, Stress range 792MPa.

a [μm]	$log(N_{mean})$	σ	N_{-1sd} [cycles]	N_{mean} [cycles]	N_{+1sd} [cycles]	N_{model} [cycles]
12	4.8664	0.0664	63095	73516	85657	9284
25	5.0001	0.1169	76420	100029	130930	17089
50	5.1037	0.1325	93579	126975	172289	56455
75	5.1577	0.1419	103698	143773	199336	65227
100	5.1826	0.1507	107621	152267	215433	89587
125	5.2235	0.1230	126020	167288	222071	99264
150	5.2653	0.0991	146607	184190	231408	113813
175	5.2949	0.0947	158565	197179	245195	127779
200	5.3228	0.0825	173903	210273	254249	138367
250	5.3504	0.0706	190458	224068	263608	161094
300	5.3885	0.0485	218755	244612	273524	182013
350	5.4051	0.0396	231967	254133	278418	201347
400	5.4252	0.0334	246533	266212	287461	219500
500	5.4509	0.0288	264321	282433	301787	252037
600	5.4627	0.0315	269861	290192	312055	279565
700	5.4705	0.0292	276253	295475	316035	297223
800	5.4763	0.0268	281499	299440	318524	308456
failure	5.5652	0.0183	352353	367481	383258	348270